UNIVERSITÀ DEGLI STUDI DI PARMA

Dottorato di ricerca in Scienza e Tecnologia dei Materiali Innovativi

Ciclo XXVIII (2013-2015)

Molecular Approaches to Smart Materials *via* Interface Recognition and Conformationally Switchable Cavitands

Coordinatore:
Prof. Enrico Dalcanale

Tutor:
Prof. Enrico Dalcanale

Dottorando: Alessandro Pedrini

2016

Alla mia famiglia

"…vincere la materia è comprenderla,
e comprendere la materia è necessario per
comprendere l'universo e noi stessi…"

Primo Levi, Il sistema periodico

CONTENTS

CHAPTER 1

SUPRAMOLECULAR CHEMISTRY AT INTERFACES

1.1 Introduction

Supramolecular chemistry, defined by Jean-Marie Lehn as the "chemistry beyond the molecule", refers to the behavior of molecular assemblies formed through weak, non-covalent interactions.[1] Based on the principles of molecular recognition[2] and self-assembly,[3] supramolecular chemistry is intrinsically dynamic and deals with the formation of organized structures under equilibrium conditions.[4] Thanks to a constant and continuous development, this branch of chemistry has become transversal and has implications in various fields, ranging from the study of recognition phenomena in biological systems to the development of programmable and controllable soft materials. In Materials Science, supramolecular engineering has allowed the formation of complex, stimuli-responsive architectures through the self-assembly of designed and well-defined molecular units. As a result of non-covalent interactions involved, the formation of these assemblies usually arises from spontaneous processes and is thermodynamically driven. After an initial step that requires molecular recognition among structural subunits, the growth of a supramolecular architecture progresses through the formation of sequential interactions, according to a cooperative or linear behavior. The exact structure resulting from the self-assembly can be predicted only evaluating the thermodynamic state occupied by the vast majority of molecules. Regarding systems at the equilibrium, these states result form the difference between free energies of all possible configurations. However, the computation of free energy differences is still challenging and limits supramolecular engineering to a semi-quantitative approach that takes into account only enthalpic contributions.[5] Therefore, the choice of the weak interactions, as well as their spatial distribution in pre-organized binding motifs, highly affects the effectiveness of supramolecular complexation. Moreover the transfer of these molecular assemblies from solution, where are usually characterized and studied, to the final material preserving their functionality is crucial. Different interfaces, such as gas-solid, liquid-liquid or liquid-solid, have been used to control the formation of complex molecular assemblies.[6] As usually formed at the boundary between two phases, interfaces facilitate the formation of molecular assemblies. Molecular interactions are strongly influenced by the dielectric constant of the medium, and working at the interface leads to the formation of controlled structures and architectures over a broad surface range. In particular, supramolecular chemistry at interfaces has been used to construct various smart and soft surfaces able to adapt to external stimuli.[7]

In this thesis, supramolecular receptors, namely tetraphosphonate cavitands, are placed at liquid-liquid interfaces of complex dynamic emulsions. We expect their complexation abilities toward amino acids to affect interfacial tensions affording a detectable change of droplet morphology. A supramolecular protocol is then applied to surface functionalization with single-molecule magnets. Our aim is to reversibly anchor these relevant molecules on surface through the formation of a strong multiple hydrogen bond-based complex at liquid-solid interface.

1.2 Tetraphosphonate Cavitands as Molecular Receptors

Host-guest chemistry is aimed at studying the selective interactions that govern molecular recognition. As for biological systems, guest molecules are selectively complexed by receptors with both complementary shape and specific recognition functions. Extending the "lock and key" theory enunciated by Fischer in 1894,[8] Pedersen,[9] Lehn[1] and Cram[10] reported the synthesis of different pre-organized receptors able to bind specific substrates. Among these artificial receptors, cavitands are particularly attractive as they can complex complementary organic molecules or ions through pre-organized cavities.[11]
In particular resorcin[4]arene-based tetraphosphonate cavitands (Tiiii) have been successfully applied to the recognition of positively charged species such as alkaline-earth cations,[12] *N*-methylammonium[13] or *N*-methylpyridinium[14] species (Figure 1.1).

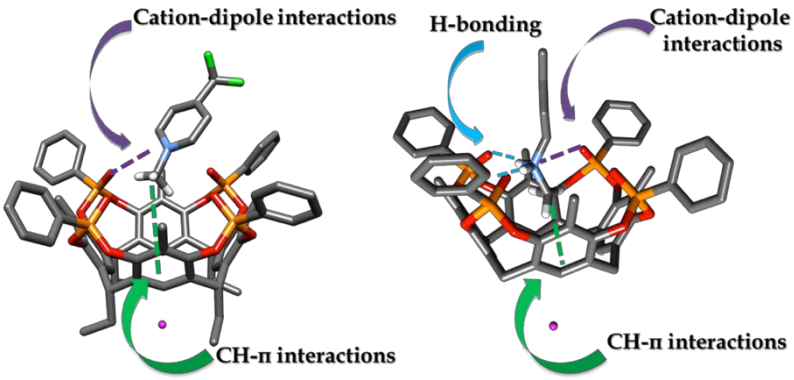

Figure 1.1 *Complexation mode of tetraphosphonate cavitands towards N-methylpyridinium (left) and N-methylammonium salts (right).*

These cavitand structures are characterized by the presence of four phosphonate groups at the upper rim, pointing inward the cavity. Complexation ability is influenced both by the number of P=O groups[15] and by their stereochemistry (orientation inward (i) or outward (o) the cavity).[16] The main specific interactions involved in guest complexation are: (i) multiple ion-dipole interactions between the inward facing P=O and the positive charge, (ii) single or double H-bonding involving the P=O groups and the nitrogen protons and (iii) CH_3-π interactions between an acidic *N*-methyl group of the guest and the π-basic cavity of the host.[17] As shown in Figure 1.1, in case of *N*-methylpyridinium salts recognition the process is driven by cation-dipole (purple) and CH-π interactions (green), while for *N*-methylammonium complexation all the three interactions operate in a synergistic fashion, causing a higher affinity towards the cavity.[18]

Tetraphosphonate cavitands can be conveniently synthesized in two steps (Figure 1.2), starting from properly functionalized resorcinols and aldehydes.

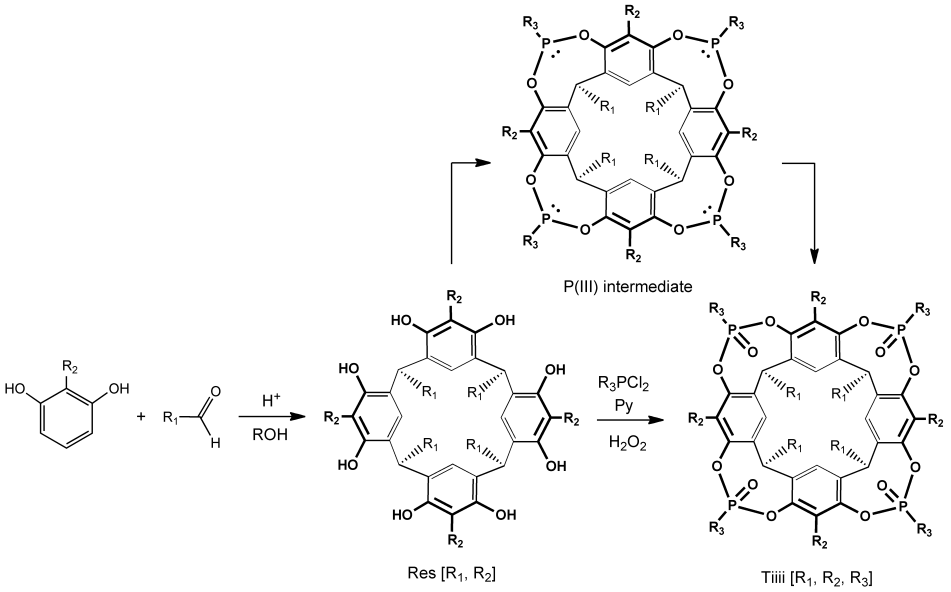

Figure 1.2 *Tiiii synthesis via P(III) intermediate*

The choice of different R_1, R_2 and R_3 allows a relatively easy derivatization of both the upper and the lower rim. In the first step, the acid-catalyzed condensation of resorcinols and aldehydes afforded resorcinarene scaffold,[19] which is too flexible to be used in host-guest chemistry. Bridging the phenolic groups with a proper functionality not only leads to a rigid cavity, but also

determines shape, dimensions and complexation properties of the final receptor. Reaction of resorcinarene with dichlorophosphines forms four P(III) units, which are subsequently oxidized in situ with hydrogen peroxide to give tetraphosphonate cavitand with all P=O groups oriented inward the cavity (Tiiii) as the major product in high yield (up to 90%).[20] The stereospecificity of the reaction is related to the formation of an P(III) intermediate with all the electrons lone pairs pointing inside the cavity.[21]

In our group we extensively studied the complexation properties of phosphonate cavitands toward organic guests in the solid state,[15b,25a] in solution,[22] and in the gas phase.[23] We focused our attention on the detection of sarcosine, a methylated form of glycine, as its abnormal concentration in urine has been correlated to aggressive prostate cancer forms,[24] both in water and urine. We initially grafted our receptor on a silicon wafer to detect sarcosine in urine with XPS and fluorescence measurements.[25] We functionalized single-walled carbon nanotubes (SWCNT's) with tetraphosphonate cavitand receptors to create a hybrid chemiresistive sensor for sarcosine with high selectivity and sensitivity in water (down to 0.02 mM).[26] Recently we exploited outstanding recognition properties of Tiiii in a nanomechanical device, based on cantilevers, to detect the whole class of methamphetamine drugs independently of the type of residue attached to the $^{+}N\text{-}CH_3$ moiety.[27]

In this thesis, a comprehensive study of tetraphosphonate recogniton properties towards amino acids is reported (Chapter 2). Amino acids complexation is investigated both in the solid state, through single crystal X-ray diffraction, and in solution, via NMR and ITC experiments.

As reported in Chapter 3, the complexation ability of these supramolecular receptors is then applied to the detection of biologically important *N*-methylated amino acids and peptides in complex dynamic emulsions-based sensing platform. Complexation at the liquid-liquid interface or in water solution is expected to modify tetraphosphonate cavitand-based surfactants effectiveness leading to a microscopic variation of droplet morphology.

1.3 Multiple Hydrogen Bond-based Molecular Architectures

Among supramolecular interactions, hydrogen bonds are suitable for the construction of complex architectures due to their directionality and strength.[28] The strength of this interaction highly depends on the hydrogen bond donor (D) and acceptor (A) couple, and can range from weak CH-π[29] to very strong FH-F^- interactions.[30] Simple systems based on double hydrogen bonds, such as

amides and carboxylic acids, or on triple interactions, such as purines and pyrimidines used by Nature to assemble DNA and RNA base pairs, can construct molecular aggregations.[31] Multiple (>3) hydrogen bonds, instead, can be arrayed to create powerful assembling tools, based on linear motifs, with an increased binding specificity.[32] For linear threefold hydrogen-bonding motifs, Jorgensen and co-workers, found a large difference in the association constants varying the spatial organization of donor and acceptor groups.[33] Although the ADA–DAD and DAA–ADD arrays exhibit an equal amount of hydrogen bonds, the association constant is highly affected by secondary cross-interactions (Figure 1.3), which contribute to the final binding energy (2.9 kJ mol^{-1} each).[34] This was confirmed by the study of complementary AAA–DDD array that revealed a significantly higher dimerization constant attributed to the presence of solely attractive secondary interactions.[35]

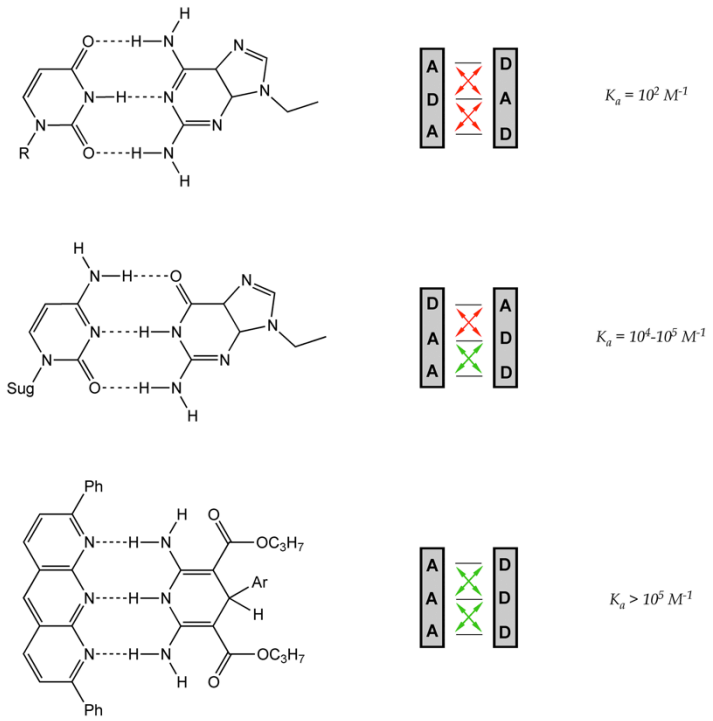

Figure 1.3 *Influence of attractive and repulsive secondary interactions on the association constant of threefold hydrogen-bonding motifs.*[37]

Self-complimentary ureidopyrimidinone-based quadruple hydrogen bonding AADD motif (UPy), reported by Mejier and co-workers,[36] has found extensive applications in self-assembly of polymeric supramolecular structures.[37]

An important aspect of the ureidopyrimidinone unit is the presence of three different tautomers in solution (Figure 1.4).[36] The formation of a stronger intramolecular hydrogen bond stabilizes the 4[1H]-pyrimidinone form forcing the carbonyl to be aligned to the aromatic ring.

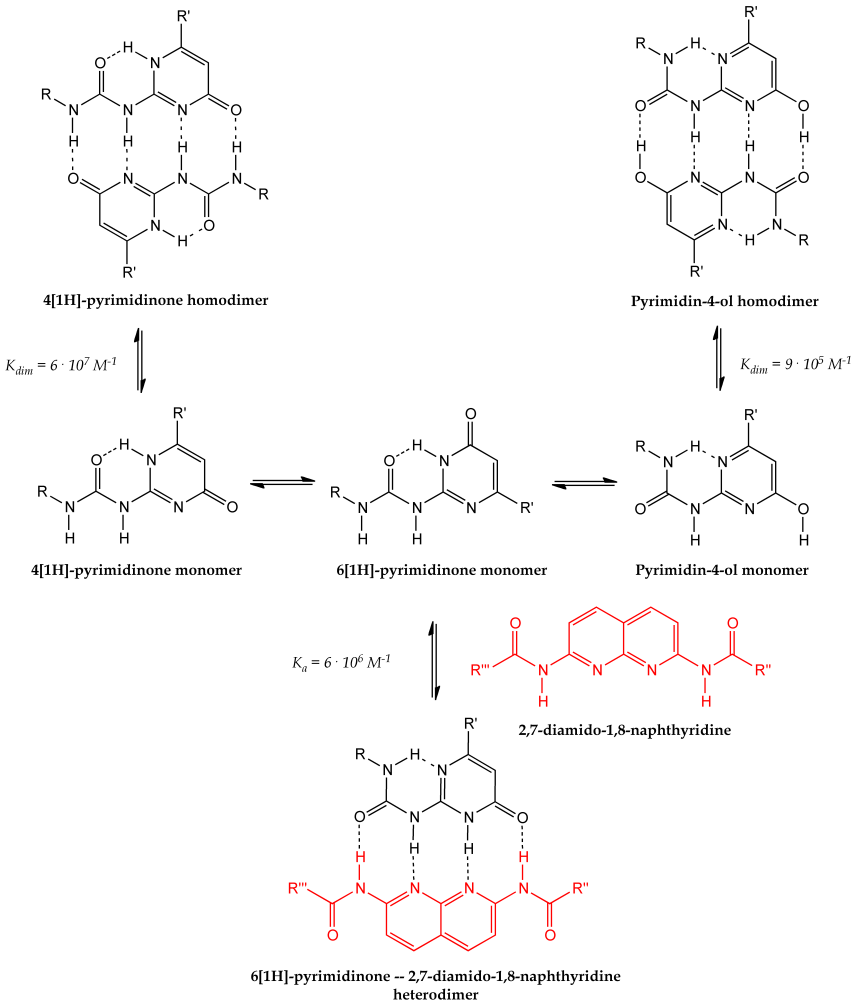

Figure 1.4 *Equilibria between the three tautomeric forms of ureidopyrimidinones and relative homodimers. NaPy (red) create an additional equilibrium for the heterocomplexation; dimerization and association constants in chloroform are reported.*

Thanks to the reduced number of repulsive secondary interactions, the dimerization constant (K_{dim}) was found to be $6 \cdot 10^7$ M^{-1} in chloroform, with a long lifetime of 0.1s.[38] The stabilization of the AADD motif, with respect to the DADA pyrimidin-4-ol tautomer, causes an increase in the association constant by two orders of magnitude. Equilibria completely change when a DAAD hydrogen bonding motif, for example a 2,7-diamido-1,8-naphthyridine (NaPy),[39] is added to a ureidopyrimidinone solution.[40] The 6[1H]-pyrimidinone tautomer, in fact, shows a complementary ADDA array and is able to form heterodimers with a high association constant ($K_a = 6 \cdot 10^6$ M^{-1} in chloroform).[41] The dual complexation modes of ureidopyrimidinones result in a concentration-dependent selectivity favoring UPy·NaPy heterocomplexes over UPy·UPy homodimers by a factor higher than 20:1 for concentration close to 0.1 M (1:1 ratio).[42] In fact, even if the dimerization constant for UPy·UPy is higher, the NaPy present a weak homodimerization capability ($K_{dim} = 10^1$-10^2 M^{-1} in chloroform)[43] so the formation of more stable heterocomplexes stabilize the system. As a consequence, NaPy motifs are powerful tools to desymmetrize ureidopyrimidinones-based assemblies.[44] In our group we successfully applied this concept to supramolecular polymer assembly/disassembly[45] and to reversible hierarchical self-assembly of complex architectures on silicon surface.[46]

In Chapter 5, the high selectivity between UPy and NaPy hydrogen bonding motif is exploited to reversibly decorate silicon and gold surfaces with single-molecule magnets preserving their outstanding magnetic properties.

1.4 References

[1] J. M. Lehn, *Angew. Chem. Int. Ed.* **1988**, *27*, 89-112.

[2] J. M. Lehn, *Science* **2002**, *295*, 2400-2403.

[3] a) G. M. Whitesides, J. P. Mathias, C. T. Seto, *Science* **1991**, *254*, 1312-1319; b) G. M. Whitesides, M. Boncheva, *PNAS* **2002**, *99*, 4796-4774.

[4] J. M. Lehn, *PNAS* **2002**, *99*, 4763–4768.

[5] A. Ciesielski, C.-A. Palma, M. Bonini, P. Samorì, *Adv. Mater.* **2010**, *22*, 3506–3520.

[6] H. Yang, B. Yuan, X. Zhang, O. A. Sherman, *Acc. Chem. Res.* **2014**, *47*, 2106-2115.

[7] X. Zhang, D. G. Whitten, *Langmuir* **2011**, *27*, 1245-1245.

[8] E. Fischer, *Ber. Dtsch. Chem. Ges.* **1894**, *27*, 2985-2993.

[9] a) C. J. Pedersen, *J. Am. Chem. Soc.* **1967**, *89*, 7017-7036; b) C. J. Pedersen, *Angew. Chem. Int. Ed.* **1988**, 1021-1027.

[10] D. J. Cram, *Angew. Chem. Int. Ed.* **1988**, *27*, 1009-1020.

[11] D. J. Cram, J. M. Cram, *Container Molecules and Their Guests* **1994**, The Royal Society of Chemistry, Cambridge, Chapter 5.

[12] a) P. Delangle, J.-C. Mulatier, B. Tinant, J.-P Declercq, J.-P. Dutasta, *Eur. J. Org. Chem.* **2001**, 3695-3704; b) J.-P. Dutasta, *Top. Curr. Chem.* **2004**, *232*, 55-91.

[13] D. Menozzi, R. Pinalli, C. Massera, F. Maffei, E. Dalcanale, *Molecules* **2015**, *20*, 4460-4472.

[14] D. Menozzi, E. Biavardi, C. Massera, F.-P. Schmidtchen, A. Cornia, E. Dalcanale, *Supramol. Chem.* **2010**, *22*, 768–775.

[15] a) R. Pinalli, F. F. Nachtigall, F. Ugozzoli, E. Dalcanale, *Angew. Chem., Int. Ed.* **1999**, *38*, 2377-2380; b) M. Melegari, M. Suman, L. Pirondini, D. Moiani, C. Massera, F. Ugozzoli, E. Kalenius, P. Vainiotalo, J.-C. Mulatier, J.-P. Dutasta, E. Dalcanale, *Chem. Eur. J.* **2008**, *14*, 5772-5779.

[16] R. Pinalli, M. Suman, E. Dalcanale, *Eur. J. Org. Chem.* **2004**, 451-462.

[17] R. Pinalli, E. Dalcanale, *Acc. Chem. Res.* **2013**, *46*, 399-411.

[18] D. Menozzi, E. Biavardi, C. Massera, F. P. Schmidtchen, A. Cornia, E. Dalcanale, *Supramol. Chem.* **2010**, *22*, 768-775

[19] L. M. Tunstad, J. A. Tucker, E. Dalcanale, J. Weiser, J. A. Bryant, J. C. Sherman, R. C. Helgeson, C. B. Knobler, D. J. Cram, *J. Org. Chem.* **1989**, *54*, 1305-1312.

[20] E. E. Nifantyev, V. I. Maslennikova, R. V. Merkulov, *Acc. Chem. Res.* **2005**, *38*, 108-116.

[21] W. Xu, J. P. Rourke, R. J. Puddephatt, *J. Chem. Soc., Chem. Commun.* **1993**, 145-147

[22] E. Biavardi, G. Battistini, M. Montalti, R. M. Yebeutchou, L. Prodi, E. Dalcanale, *Chem. Commun.* **2008**, 1638–1640.

[23] E. Kalenius, D. Moiani, E. Dalcanale, P. Vainiotalo, *Chem. Commun.* **2007**, 3865–3867.

[24] A. Sreekumar, L. M. Poisson, T. M. Rajendiran, A. P. Khan, Q. Cao, J. Yu, B. Laxman, R. Mehra, R. J. Lonigro, Y. Li, M. K. Nyati, A. Ahsan, S. Kalyana-Sundaram, B. Han, X. Cao, J. Byun, G. S. Omenn, D. Ghosh, S. Pennathur, D. C. Alexander, A. Berger, J. R. Shuster, J. T. Wei, S. Varambally, C. Beeche, A. M. Chinnaiyan, *Nature* **2009**, *457*, 910-914.

[25] a) E. Biavardi, M. Favazza, A. Motta, I. L. Fragalà, C. Massera, L. Prodi, M. Montalti, M. Melegari, G. C. Condorelli, E. Dalcanale, *J. Am. Chem. Soc.* **2009**, *131*, 7447-7455; b) E. Biavardi, C. Tudisco, F. Maffei, A. Motta, C. Massera, G. G. Condorelli, E. Dalcanale, *PNAS* **2012**, *109*, 2263-2268.

[26] M. Dionisio, J. M. Schnorr, V. K. Michaelis, R. G. Griffin, T. M. Swager, E. Dalcanale, *J. Am. Chem. Soc.* **2012**, *134*, 6540-6543.

[27] E. Biavardi, S. Federici, C. Tudisco, D. Menozzi, C. Massera, A. Sottini, G. G. Condorelli, P. Bergese, E. Dalcanale, *Angew. Chem. Int. Ed.* **2014**, *53*, 1–7.

[28] a) T. S. Moore, T. F. Winmill, *J. Chem. Soc. Trans.* **1912**, 101, 1635–1676, b) W. M. Latimer, W. H. Rodebush, *J. Am. Chem. Soc.* **1920**, 1419–1433.

[29] a) M. Nishio, Y. Umezawa, K. Honda, S. Tsuboyamad, H. Suezawa, *CrystEngComm* **2009**, *11*, 1757-1788; b) M. Nishio, *Phys. Chem. Chem. Phys.* **2011**, *13*, 13873–13900.

[30] a) P. G. Wenthold, R. R. Squires, *J. Phys. Chem.* **1995**, *99*, 2002–2005; b) C. Stein, R. Oswald, P. Sebald, P. Botschwina, H. Stoll, K. A. Peterson, *Mol. Phys*. **2013**, *111*, 2647–2652.

[31] Z.-T. Li, L.-Z. Wu, *Hydrogen Bonded Supramolecular Structures* **2015**, Springer, Berlin.

[32] a) R. P. Sijbesma, E. W. Meijer, *Chem. Comm.* **2003**, 5–16; b) F. Rodríguez-Llansola, E. W. Meijer, *J. Am. Chem. Soc.* **2013**, *135*, 6549−6553.

[33] a) W. L. Jorgensen, J. Pranata, *J. Am. Chem. Soc.* **1990**, *112*, 2008–2010; b) J. Pranata, S. G. Wierschke, W. L. Jorgensen, *J. Am. Chem. Soc.* **1991**, *113*, 2810–2819.

[34] a) D. A. Leigh, C. C. Robertson, A. M. Z. Slawin, P. I. T. Thomson, *J. Am. Chem. Soc.* **2013**, *135*, 9939−9943; b) B. A. Blight, C. A. Hunter, D. A. Leigh, H. McNab, P. I. T. Thomson, *Nat. Chem.* **2011**, *3*, 244–248.

[35] T. J. Murray, S. C. Zimmerman, *J. Am. Chem. Soc.* **1992**, *114*, 4010–4011.

[36] H. F. Beijer, R. P. Sijbesma, H. Kooijman, A. L. Spek, E. W. Meijer, *J. Am. Chem. Soc.* **1998**, *120*, 6761-6769.

[37] W. P.J. Appel, M. M.L. Nieuwenhuizen, E.W. Meijer, in *Supramolecular Polymer Chemistry, First Edition* **2012**, Wiley-VCH, Weinheim, Chapter 1.

[38] S. H. M. Söntjens, R. P. Sijbesma, M. H. P. van Genderen, E. W. and Meijer, *J. Am. Chem. Soc.* **2000**, *122*, 7487–7493.

[39] C. Alvarez-Rua, S. García-Granda, S. Goswami, R. Mukherjee, S. Dey, R. M. Claramunt, M. D. Santa María, I. Rozas, N. Jagerovic, I. Alkortae J. Elguero, *New. J. Chem.* **2004**, *28*, 700–707.

[40] T. F. A. de Greef, G. Ercolani, G. B. W. L. Ligthart, E. W. Meijer, R. P. Sijbesma, *J. Am. Chem. Soc.* **2008**, 130, 13755–13764.

[41] P. S. Corbin, S. C. Zimmerman, *J. Am. Chem. Soc.* **1998**, *120*, 9710-9711.

[42] G. B. W. L. Ligthart, H. Ohkawa, R. P. Sijbesma, E. W. Meijer, *J. Am. Chem. Soc.* **2005**, *127*, 810-811.

[43] X.-Q. Li, X.-K. Jiang, X.-Z. Wang, Z.-T. Li, *Tetrahedron* **2004**, *60*, 2063–2069.

[44] O. A. Scherman, G. B. W. L. Ligthart, R. P. Sijbesma, E. W. Meijer, *Angew. Chem. Int. Ed.* **2006**, *45*, 2072 –2076.

[45] F. Tancini, E. Rampazzo, E. Dalcanale, *Austr. J. Chem.* **2010**, *63*, 646-652.

[46] F. Tancini, D. Genovese, M. Montalti, L. Cristofolini, L. Nasi, L. Prodi, E. Dalcanale, *J. Am. Chem. Soc.* **2010**, *132*, 4781-4789.

CHAPTER 2

THE ORIGIN OF SELECTIVITY IN *N*-METHYL AMINO ACID COMPLEXATION BY TETRAPHOSPHONATE CAVITANDS *

* Part of this work has been carried out in the group of Prof. Pablo Ballester at Institute of Chemical Research of Catalonia (ICIQ), Tarragona, Spain.

2.1 Introduction

Amino acids, the building blocks of peptides, are appealing targets for molecular recognition. Their biological relevance and chemical diversity make them an ideal playground for testing the complexation ability and selectivity of abiotic receptors.[1] Since under physiological conditions the amino group is usually protonated, amino acids are mainly complexed either as zwitterions or as ammonium ions. In both cases the target is the ammonium cation, whose main interaction modes with a given receptor are H-bonds, cation-π and electrostatic interactions. The inset and strength of these interactions is dictated by the molecular complementarity of the interacting functional groups between host and guest. Amino acid binding has been achieved using many different receptors among which crown ethers,[2] calixarenes,[3] cucurbiturils,[4] molecular tweezers[5] are prominent.

A molecular host for amino acids zwitterions was proposed by Schmidtchen and co-workers.[2a] The authors connected covalently a chiral bicyclic guanidinium salt as an anchor function for the carboxylate to a triaza-crown ether as an ammonium binding moiety in combination with a strongly hydrophobic silyl ether. The so-designed synthetic host serves to complex and transfer amino acids from water into dichloromethane. Späth and König proposed the use of ditopic crown ether-guanidinium ion receptors for the complexation of zwitterionic amino acids and the neurotransmitter g-aminobutyric acid.[2d] More recently, the 18-crown-6 binding affinities for five different amino acids were determined using guided ion beam tandem mass spectrometry and structural information was obtained from theoretical calculations.[2e] The authors demonstrated that the ability of the *N*-terminal amino group to compete for 18C6 becomes less favorable as the size and proton affinity of the amino acid increases. Spectroscopic evidences of amino acids recognition by water-soluble uncharged porphyrin tweezers were reported by Villari et *al.*.[6] The binding between amino acids and porphyrins occurs *via* a coordination mechanism between the metal and the nitrogen of the amino group; the steric, hydrophobic and π–π interactions operate to stabilize the complexes. Nice examples are reported in literature using tetrasulphonatocalixarenes as suitable hosts for neutral and cationic amino acids.[7] The complexation event occurs with moderate affinity and it is both enthalpically and entropically driven, favored by charge-charge interactions involved in the formation of the complexes. As "aromatic cage" mimic (Figure 2.1), tetrasulfonatocalixarene is well suited to bind also post-translationally modified amino acids such as methylated lysines and arginines.[8]

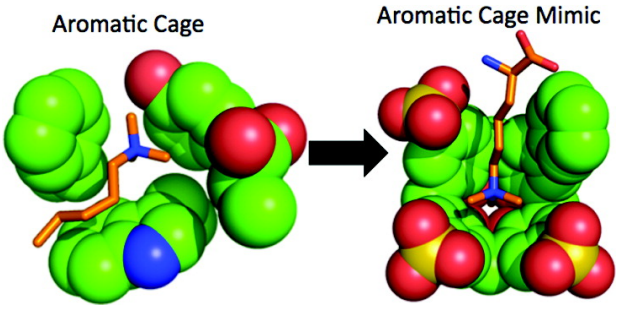

Figure 2.1 *Representation of the "aromatic cage" approach to the detection of trimethylated lysine with calixarenes.*[7e]

Cucurbiturils, among the most efficient synthetic hosts, have been also used for amino acids recognition in water due to their high affinities and selectivities in aqueous media and to the combination of electrostatic and hydrophobic interactions that govern binding.[9]

Tratraphosphonate (**Tiiii**) cavitands are powerful synthetic receptors presenting remarkable molecular recognition properties toward *N*-methylammonium salts. The origin of Tiiii selectivity toward these species, can be attributed to the presence of three interaction modes: (i) $N^{+}\bullet\bullet\bullet O{=}P$ cation–dipole interactions; (ii) CH–π interactions of the acidic $^{+}N–CH_3$ group with the π basic cavity; (iii) two simultaneous hydrogen bonds between two adjacent P=O bridges and the two nitrogen protons. Within the ammonium salt series, the bias toward the monomethylated species over di- and trimethylated ones is determined by the number of H-bonds formed with **Tiiii**, while non-methylated ammonium ions are less favored by the lack of CH_3–π interactions.[10] Tetraphosphonate cavitands were successfully used for the specific recognition of sarcosine in water and urine in presence of glycine as interferent.[11] In aqueous environment, the enhanced role played by the CH_3–π interactions leads to complete selectivity toward sarcosine versus glycine.

Herein, the study of tetraphosphonate cavitands eligibility for amino acids recognition is reported. We studied X-Ray crystal structure of thirteen complexes of the tetraphosphonate cavitand **1**, bearing no aliphatic chains at the lower rim, with amino acids. ^{1}H and ^{31}P NMR experiments and ITC analyses were performed on complexes between cavitand **2** or the water-soluble parent **3**, which possesses four positively charged pyridinium groups at the lower rim, and different amino acids. The reported studies allowed: (i) to highlight the non-covalent interactions involved in the binding event; (ii) to investigate tetraphosphonate cavitand ability to discriminate the different

amino acids; (iii) to calculate the K_a and evaluate the thermodynamic parameters of complexation, dissecting the entropic and enthalpic contributions.

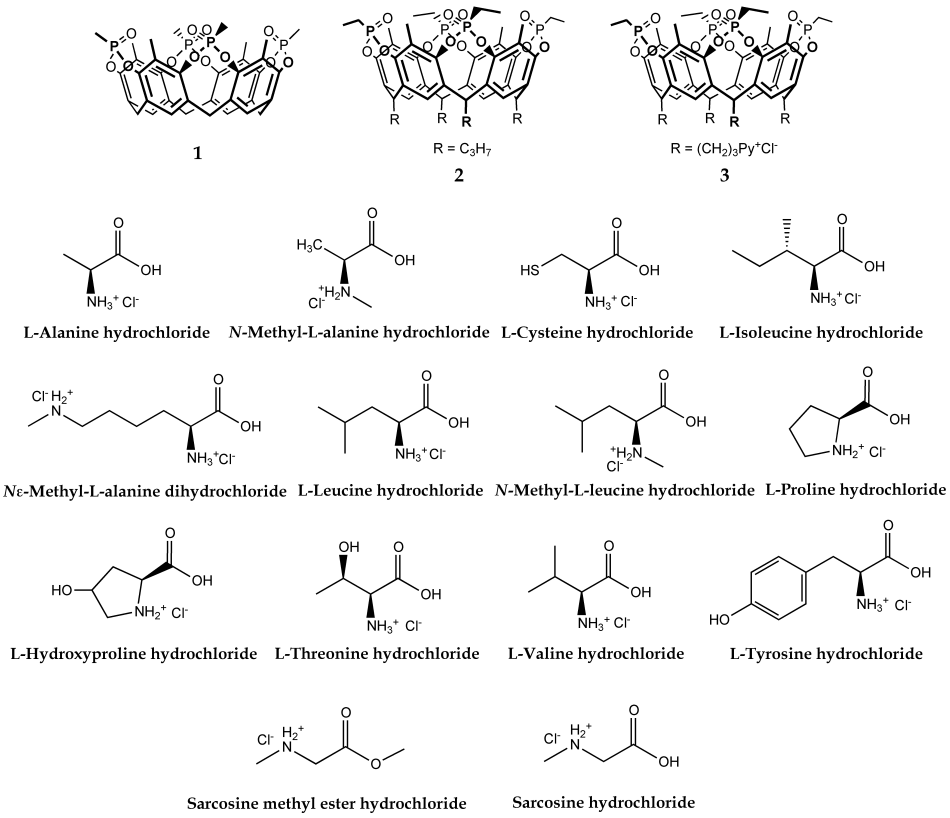

Figure 2.2 *Cavitands and amino acids involved in this study.*

2.2 Results and Discussion

2.2.1 Crystal Structures Determination

A systematic study was undertaken to assess the complexation properties of tetraphosphonate cavitands towards amino acids in the solid state. Both zwitterionic and cationic forms of proteinogenic amino acids and non-proteinogenic amino acids, such as 4-hydroxyproline and *N*-methylated amino acids have been tested. In this study, tetraphosphonate cavitand **1**, without

substituents at the lower rim, was chosen for its tendency to crystallize. The 1:1 host-guest complexes with the following amino acids were determined by single crystal X-ray diffraction: Ala, Ala·HCl, Cys, 4-Hyp, (D/L)-Ile·HCl, Leu·HCl, *N*-Me-Ala, *N*-Me-Leu·HCl, Pro, Ser, Thr, Tyr·HCl, Val. Crystallization trials were performed by the vapor diffusion method with sitting drops in Linbro multi-well plates containing trifluoroethanol (TFE) as solvent and PEG300 as precipitant (See Experimental Section).

Most of the crystals obtained by co-crystallization of the cavitand in the presence of the amino acids were triclinic and only three crystallized in the monoclinic $P2_1$ space group, Thr, *N*-Me-Leu·HCl and Ser, respectively. In the asymmetric unit of each crystal two crystallographically independent host-guest complexes were found, except for Thr and (D/L)-Ile·HCl, which present one independent complex, and *N*-Me-Ala and Ser, showing four independent complexes.

A single representative host-guest complex for each crystal structure is shown in Figure 2.3 (relevant geometric parameters describing the host–guest interaction are reported in Table S2.1). In all the structures containing the cationic forms of the amino acids (Ala·HCl, Leu·HCl, (D/L)-Ile·HCl, *N*-Me-Leu·HCl, Tyr·HCl,) the chloride anion has been detected at the bottom of the cavitand lower rim, forming weak C-H $\cdots$ Cl^- interactions with the aromatic CH fragments. The thirteen supramolecular complexes show different interaction patterns between host and guest, depending on the characteristic of amino acid side chain. It has been possible to distinguish four main groups of host-guests complexes, showing common interaction features:

- **not-hosted side chain**: the zwitterionic Ala establishes two hydrogen bonds between the amino acid ammonium group and two adjacent P=O units of the cavitand; the ammonium group completes its H-bond donor ability with a water molecule present inside the cavity of the receptor. The nitrogen atom is above the O mean plane, defined by the oxygen atoms of the P=O units, and the entire amino acid side chain is external to the cavity. Similar behavior is observed for the zwitterionic form of the hydrophobic Val and the hydrophilic Ser amino acids. Analogous weak interactions are observed also for the cationic Leu·HCl and the racemic (D/L)-Ile·HCl amino acids (Figure 2.3).
- **hosted side chain**: The protonated Ala·HCl establishes two hydrogen bonds between the amino acid ammonium group and two oxygen atoms of the adjacent P=O units. Conversely, the ammonium group is above the O mean plane, as shown in Figure 2.3. The side chain of Ala·HCl is inserted in the cavity of the receptor: thus the methyl group establishes CH $\cdots$ π

interactions with the aromatic walls of the cavitand. The protonated carboxylic group forms a supplementary H-bond with a third P=O group. The zwitterionic Thr shows analogous specific recognition of the side chain with a formation of CH $\cdots \pi$ interactions, by establishing a further hydrogen bond between the alcoholic group and an oxygen atom of a P=O unit. Also the zwitterionic Cys shows a cavitand-side chain amino acid interaction. In this case the thiol SH group is directed inwards the cavity and forms weak sulfur-arene interactions[12] with the aromatic rings (to the best of our knowledge the **1**·Cys is the first structures of an host-guest complex encapsulating a cysteine). The zwitterionic Pro establishes two H-bonds with both hydrogen atoms of the secondary ammonium group and two oxygen atoms of the adjacent P=O units. In this case the nitrogen atom is almost coplanar to the O mean plane as shown in Figure 2.3. The hydrophobic five-membered ring is deeply inserted into the cavity and forms CH $\cdots \pi$ interactions with the aromatic walls of the cavitand. In the zwitterionic 4-Hyp complex the additional H-bond formed between the OH group of 4-Hyp and a P=O unit produces a significant raising (about 1 Å) of the proline side chain from the bowl-shaped cavity.

- **hosted *N*-Me AA**: the secondary ammonium group of the zwitterionic *N*-Me-Ala establishes two hydrogen bonds with two oxygen atoms of the adjacent P=O units, with the nitrogen atom almost coplanar to the O mean plane as shown in Figure 2.3. Furthermore the *N*-methyl group is inserted in the cavity of the receptor and thus establishes CH $\cdots \pi$ interactions with the aromatic walls of the cavitand. In this case the methyl side chain of the modified alanine is oriented outwards the cavity. Similar behavior was observed for the cationic *N*-Me-Leu·HCl, with the *i*-butyl side chain protruding outside the cavity. Also for this complex the two crystallographic independent molecules show a different interactions for the protonated carboxylic group: H-bond with a P=O unit and H-bond with a solvent molecule.
- **Tyr complexation**: as special case of interaction, protonated Tyr·HCl forms three hydrogen bonds between ammonium group and three P=O units, but also the OH fragment of the carboxylic group is able to establish a hydrogen bond with a P=O unit. Since the aromatic side chain of Tyr is parallel to the top of the cavity it forms an interesting exo weak lone pair$\cdots\pi$[13] contact with an oxygen atom of a P=O unit.

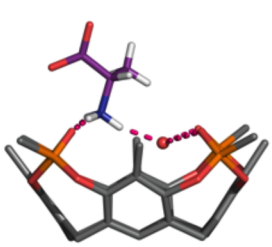

1·Ala

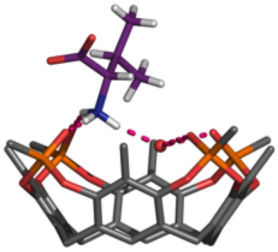

1·Val

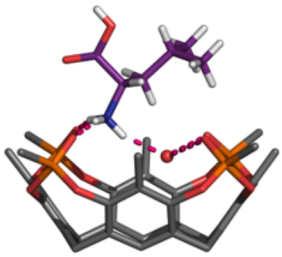

1·Leu·HCl

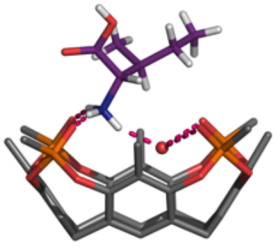

1·Ile·HCl

1·Ser

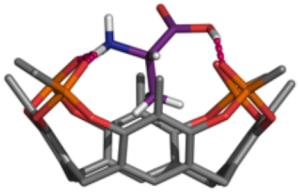

1·Ala·HCl

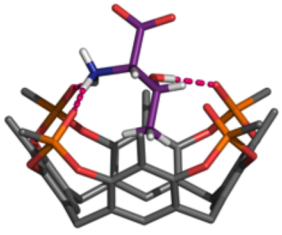

1·Thr

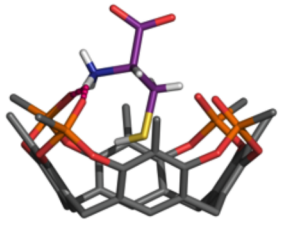

1·Cys

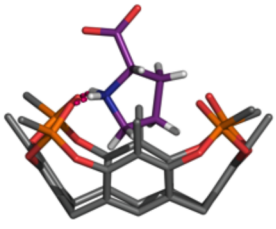

1·Pro

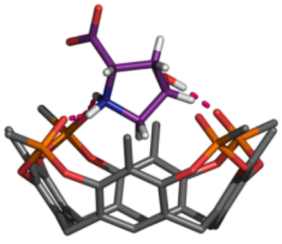

1·4Hyp

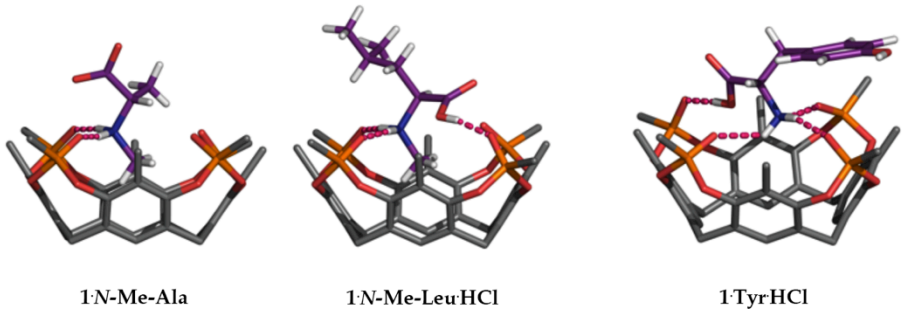

Figure 2.3 *Side views of the crystal structures of the thirteen* ***1****·amino acid complexes. The dashed lines depicted in magenta indicate hydrogen bonding interactions.*

2.2.2 ITC Measurements in Methanol

A comprehensive set of ITC complexation measurements was performed on seven different amino acids (guests) towards tetraphosphonate cavitand **2** (host), using methanol as solvent. The ITC experiments were carried out to quantify the thermodynamic parameters ΔH, K_a, ΔG and ΔS associated with the inclusion process. The thermodynamic parameters were extrapolated from the binding curves. The single-site (monovalent) model to fit the binding curve was adopted. For the ITC experiments, the novel cavitand **2** has been synthesized in one step starting from the corresponding resorcinarene (Scheme 2.1). Bridging reaction with dichloroethylphosphine in pyridine gave P(III) intermediate, which was oxidized *in situ* with hydrogen peroxide affording cavitand **2,** with the four phosphonate groups directed towards the cavity. The compound was characterized by mass spectrometry, ^{1}H NMR and ^{31}P NMR.

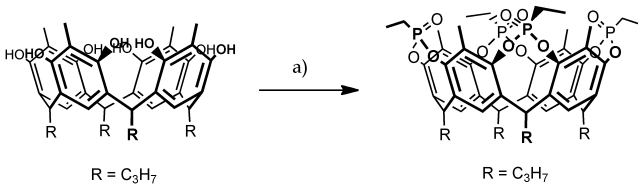

2

Scheme 2.1 *Synthesis of cavitand* **2***: a) (1) $EtPCl_2$, Py, 70°C, 3 h; (2) H_2O_2 35%, r.t, 30 min, 80% (over two steps).*

This cavitand, with respect to the one used in the X-Ray crystal structure studies, presents four propyl chains at the lower rim and ethyl substituents on

the P=O groups, which were introduced to impart solubility in the solvents used for both NMR and ITC studies. These changes in the cavitand structure do not affect the biding properties of the host.

In ITC experiments, the amino acids were used as hydrochloride salts in order to strength the complexation event. As shown in Table 2.1, the inclusion process is both enthalpy and entropy driven for all the analyzed guests and the enthalpy contribute is particular strong for entries **1**-**3**. The biggest K_a value is recorded for *N*-Me-Leu·HCl and *N*-Me-Ala·HCl, while the lowest is recorded for Cys·HCl. The other amino acids show K_a values very close to each other. Pro·HCl present a ΔH value comparable to the ones of *N*-Me-Leu·HCl and *N*-Me-Ala·HCl but a significant drop in the $T\Delta S$ value that is reflected in the loss of one order of magnitude in the K_a value.

	Guest	$K_a \pm \sigma_{Ka}$ (M^{-1})	$\Delta H \pm \sigma_{\Delta H}$ ($KJ \cdot mol^{-1}$)	$\Delta G \pm \sigma_{\Delta G}$ ($KJ \cdot mol^{-1}$)	$T\Delta S \pm \sigma_{T\Delta S}$ ($KJ \cdot mol^{-1}$)
I	***N*-Me-Leu·HCl**	$1.7 \pm 0.1 \cdot 10^5$	-15.9 ± 0,1	-29.8 ± 0.2	13.9 ± 0.2
II	***N*-Me-Ala·HCl**	$1.4 \pm 0.1 \cdot 10^5$	-20.1 ± 0.2	-29.4 ± 0.2	9.3 ± 0.3
III	**Pro·HCl**	$1.2 \pm 0.2 \cdot 10^4$	-19.8 ± 0.2	-23.3 ± 0.4	3.5 ± 0.5
IV	**Thr·HCl**	$2.0 \pm 0.3 \cdot 10^4$	-8.2 ± 0.2	-24.5 ± 0.4	16.3 ± 0.5
V	**Ala·HCl**	$1.1 \pm 0.1 \cdot 10^4$	-7.5 ± 0.7	-23.0 ± 0.2	15.5 ± 0.7
VI	**Tyr·HCl**	$1.1 \pm 0.1 \cdot 10^4$	-8.7 ± 0.3	-23.0 ± 0.2	14.3 ± 0.4
VII	**Cys·HCl**	$7.3 \pm 0.1 \cdot 10^3$	-9.07 ± 0.04	-22.04 ± 0.04	13.0 ± 0.1

Table 2.1 *ITC data for guests inclusion in cavitand* **2**.

The largest K_a obtained for entries **I** and **II** highlighted the pivotal role of the synergistic presence of multiple interactions. In the case of *N*-Me-Leu·HCl and *N*-Me-Ala·HCl the simultaneous presence of three different interactions between host and guest is possible: (i) $N^+ \cdots O{=}P$ cation–dipole interactions; (ii) CH–π interactions of the acidic $^+N{-}CH_3$ group with the π basic cavity; (iii) two simultaneous hydrogen bonds between two adjacent P=O bridges and the two nitrogen protons. In the case of Pro·HCl, the drop of the K_a value is ascribable entirely to a remarkable loss in the entropic contribution, possibly accountable

to an increase in solvent entropy associated with the desolvation of the guest upon complexation. In fact, also in the case of entry **III**, as highlighted by the high ΔH value, the three interaction modes, namely H-bonding, cation-dipole and $^{+}$N-CH$\cdots\pi$, are involved in the complexation event. In the case of guests **4-7** only two interactions are possible, the cation–dipole one and the H-bonding. The lack of one interaction is reflected in the lower value enthalpic contribute that causes the loss of one order of magnitude in the K_a value.

2.2.3 Complexation and Competitive NMR Experiments

Both proton and phosphorous NMR experiments were performed in deuterated methanol at -20°C. The amino acids used in NMR experiments were the same set used in ITC measurements. In the NMR experiments 1 eq of the selected guest was dissolved in deuterated methanol and added to a NMR tube containing 1 eq of **2** (host) dissolved in deuterated methanol. Both ^{1}H and ^{31}P spectra were then recorded. Through the ^{1}H NMR the shift of the guest protons were monitored, while through the ^{31}P NMR the shift of the host P signal was monitored. Both the shifts are diagnostic of the complexation event. As example, in Figure 2.4 we reported the proton NMR spectra of cavitand **2** (Figure 2.4a), N-Me-Ala·HCl guest (Figure 2.4b) and of the **2**·*N*-Me-Ala·HCl complex (Figure 2.4c).

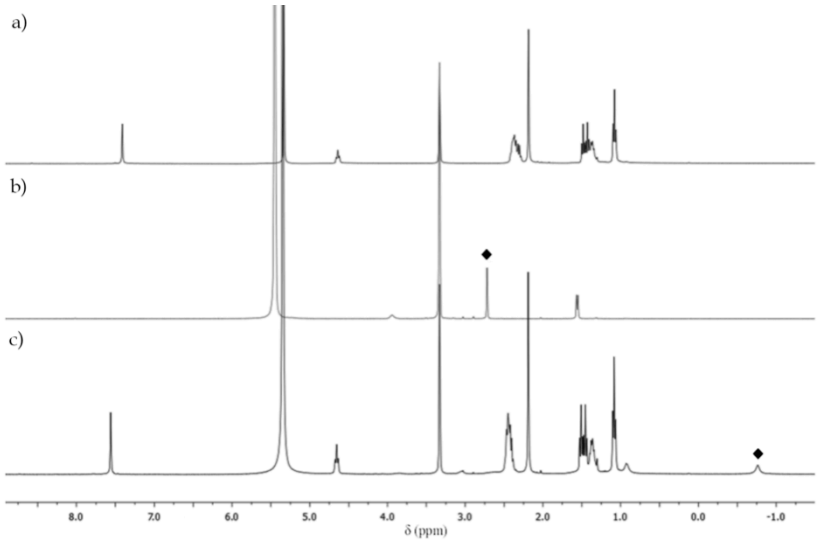

Figure 2.4 *^{1}H NMR spectra of free host* **2** *(a), free N-Me-Ala·HCl guest (b), 1:1* **2**·*N-Me-Ala·HCl complex (c); Signal related to N-methyl protons of the guest is labeled (◆).*

Diagnostic upfield shifts of guest signals were observed, as expected for included species that experience the shielding effect of the cavity. In particular the $^{+}$N-CH3 resonance moved more than 3 ppm upfield. After the addition of *N*-Me-Ala·HCl, the ^{31}P resonance of the four P=O groups moved downfield of 2.7 ppm (from 25 to 27.7 ppm, Figure 2.5). The downfield shift of P=O signals is a clear indication of the participation of phosphonates in the guest complexation.

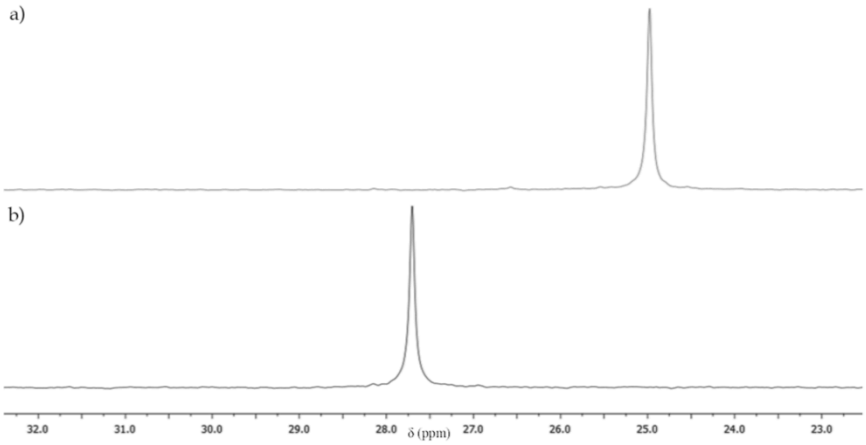

Figure 2.5 *^{31}P NMR spectra of free host* **2** *(a) and 1:1* **2**·*N-Me-Ala·HCl complex (b).*

The same procedure was used to determine the complexation of the other six amino acids into the host cavity. The upfield shift experienced by the *N*-Me-Leu·HCl and Pro·HCl protons upon complexation was evident as in the case of the *N*-Me-Ala·HCl, while the proton shift of the other four amino acids upon complexation were not so significant.

The analysis of the ^{31}P spectra revealed to be more interesting (Figure 2.6). The seven amino acids seem to be divided into two main classes: the complexation of *N*-Me-Ala·HCl, Pro·HCl and *N*-Me-Leu·HCl evidenced the biggest downfield shift, while **2**·Thr·HCl, **2**·Tyr·HCl, **2**·Cys·HCl and **2**·Ala·HCl, showed a downfield shift of phosphorous signal in the range of 0.5-0.9 ppm. This trend perfectly matches the ΔH values, obtained through ITC measurements, reported in Table 2.1. The higher ΔH value was calculated for *N*-Me-Ala·HCl, followed by Pro·HCl and *N*-Me-Leu·HCl complexation. For the second class of amino acids the enthalpic contribute is not so strong, while the entropic one is predominant. These results highlighted $N^{+}\cdots O{=}P$ cation–dipole contribution to complexation process enthalpy, which benefits from the deeper inclusion of the guest.

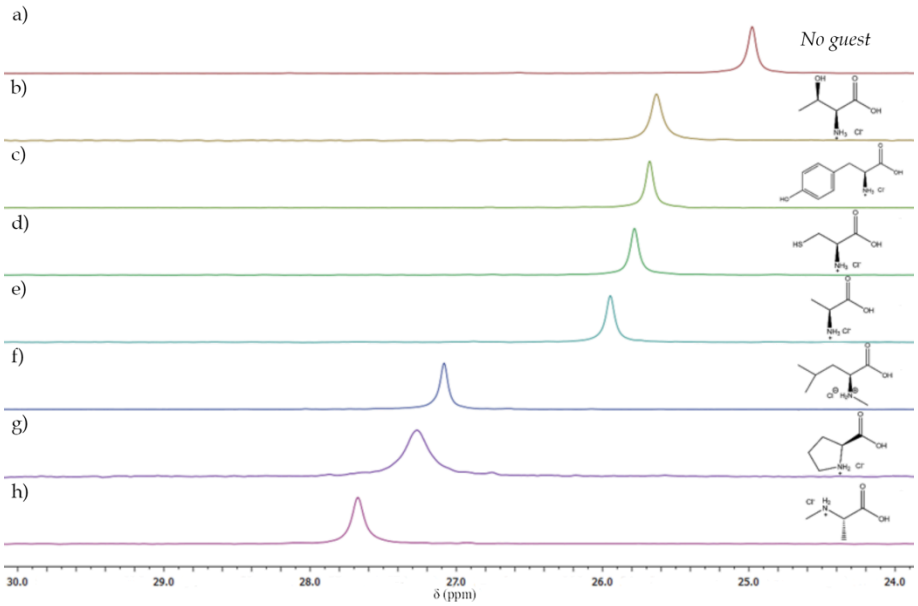

Figure 2.6 *^{31}P NMR spectra of free host* **2** *(a),* **2***·Thr·HCl complex (b),* **2***·Tyr·HCl complex (c),* **2***·Cys·HCl complex (d),* **2***·Ala·HCl complex (e),* **2***·N-Me-Leu·HCl complex (f),* **2***·Pro·HCl complex (g),* **2***·N-Me-Ala·HCl complex (h); for all the complexes a 1:1 stoichiometry was respected.*

To complete the NMR studies, three competitive experiments were performed in order to assess the stability of the complex in presence of a competitive guest. Considering ITC data, we decided to study the competition between four amino acids, namely *N*-Me-Ala·HCl, Ala·HCl, Cys·HCl and Pro·HCl. All the experiments were performed adding 1 eq of chlorinated salt dissolved in deuterated methanol to a solution of deuterated methanol containing 1 eq of **2**. Once the complex was formed and characterized by ^{1}H NMR (see Appendix B) and ^{31}P NMR, 1 eq of a competitive amino acid, dissolved in deuterated methanol, was added to the same NMR tube, and both ^{1}H and ^{31}P spectra recorded. To confirm the results, the same procedure was repeated reversing the two amino acids.

The competitive experiment between *N*-Me-Ala·HCl and Pro·HCl was performed in order to compare two different guests that, although having similar ΔH values, exhibit different K_a values. In particular, K_a of *N*-Me-Ala·HCl complex was found to be one order of magnitude higher than the K_a of **2**·Pro·HCl complex. The addition of one equivalent of *N*-Me-Ala·HCl to the **2**·Pro·HCl complex causes proline decomplexation and the subsequent complexation of *N*-Me-Ala, as demonstrated by the appearance of the *N*-methyl

peak at -0.77 and the free proline peaks. In Figure 2.7a, the ^{31}P NMR spectra are reported. The addition of 1 eq of *N*-Me-Ala·HCl to the **2**·Pro·HCl complex causes the shift of the phosphorous peak at lower field.

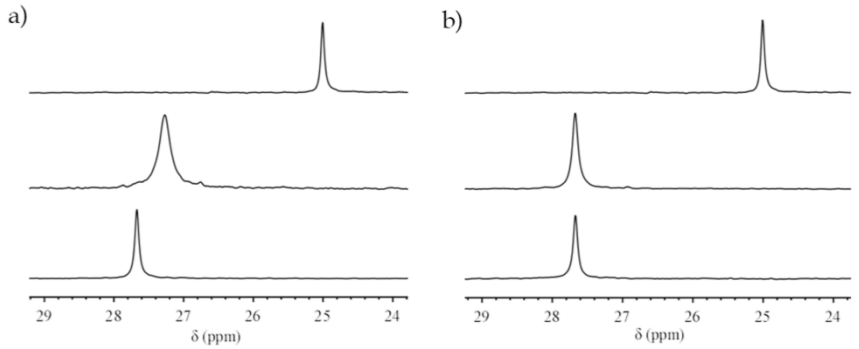

Figure 2.7 *^{31}P NMR spectra: a) free host* **2** *(top),* **2***·Pro·HCl complex (middle), addition of 1 eq of N-Me-Ala·HCl to the formed complex (down); b) free host* **2** *(top),* **2***·N-Me-Ala·HCl complex (middle), addition of 1 eq of Pro·HCl to the formed complex (down).*

The opposite experiment was then performed: to the **2**·*N*-Me-Ala·HCl complex one equivalent of Pro·HCl was added and NMR spectra recorded. No shift of the *N*-Me-Ala·HCl peaks was recorded, in particular the *N*-methyl peak was still present at -0.77 ppm, evidence of the stability of complex. In addition, as reported in figure 2.7b, the phosphorous peak did not shift upon addition of proline.

The second competitive experiment was performed between *N*-Me-Ala·HCl and Ala·HCl. This experiment was chosen to clearly point out the importance of having one more interaction mode in the inclusion process. In fact, alanine has the same molecular structure of *N*-Me-Ala, except for the presence of the CH_3 group on the NH_2 group. The acidic $+N–CH_3$ group is able to interact with the π basic cavity through CH–π interactions, joining the other two interaction modes, namely cation-dipole and H-bonding. As previously, one equivalent of *N*-Me-Ala·HCl was added to the **2**·Ala·HCl complex causing the decomplexation of the alanine and the subsequent complexation of *N*-Me-Ala. This was observed in the ^{1}H NMR by the appearance of the *N*-methyl peak at -0.77 ppm and of the free L-Alanine peaks. After the addition of *N*-Me-L-Alanine also the phosphorous peak of the **2**·Ala·HCl complex experienced a downfield shift (Figure 2.8a). The addition of one equivalent of *N*-Me-Ala·HCl to **2**·*N*-Me-Ala·HCl complex did not cause the decomplexation of *N*-Me-alanine, as demonstrated by the unchanged NMR spectra (Figure 2.8b).

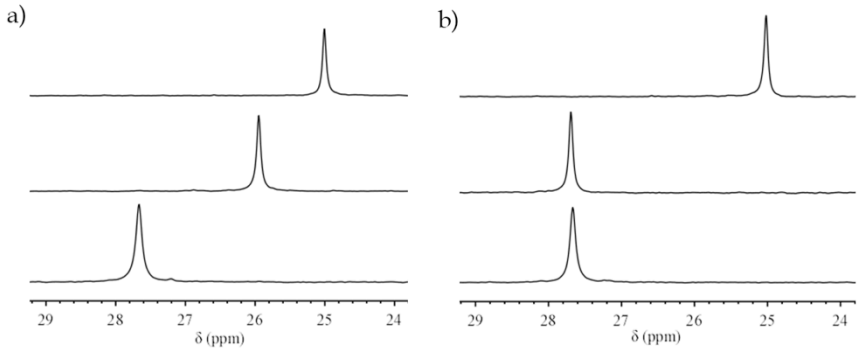

Figure 2.8 *^{31}P NMR spectra: a) free host* ***2*** *(top),* ***2****·Ala·HCl complex (middle), addition of 1 eq of N-Me-Ala·HCl to the formed complex (down); b) free host* ***2*** *(top),* ***2****·N-Me-Ala·HCl complex (middle), addition of 1 eq of Ala·HCl to the formed complex (down).*

The last competitive experiment was performed between cysteine, the amino acid that present the lower K_a value, and *N*-methyl alanine. While the addition of one equivalent of *N*-Me-Ala·HCl to **2**·Cys·HCl complex causes the cysteine decomplexation (Figure 2.9a), the addition of 1 equivalent of cysteine to **2**·*N*-Me-Ala·HCl had no effect on the complex (Figure 2.9b), as expected.

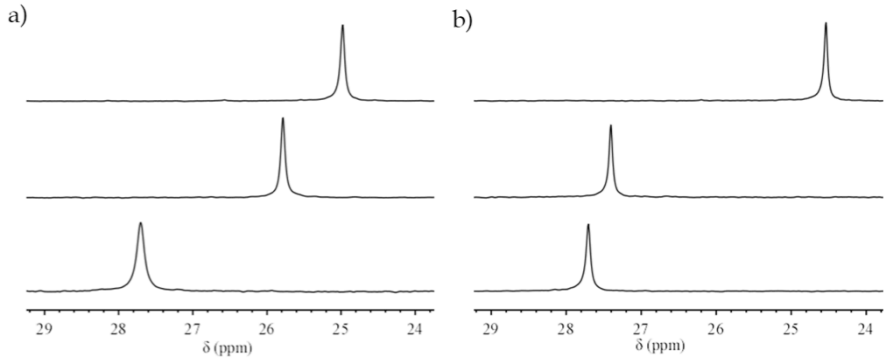

Figure 2.9 *^{31}P NMR spectra: a) free host* ***2*** *(top),* ***2****·Cys·HCl complex (middle), addition of 1 eq of N-Me-Ala·HCl to the formed complex (down); b) free host* ***2*** *(top),* ***2****·N-Me-Ala·HCl complex (middle), addition of 1 eq of Cys·HCl to the formed complex (down).*

The NMR competitive experiments performed demonstrate that **2** shows a clean preference towards *N*-Me-Ala·HCl with respect to the other amino acids tested, thanks to the presence of an additional interaction between the host and the guest: the CH–π interaction of the acidic $^{+}N–CH_3$ group with the π basic cavity, lacking in the complexes with alanine and cysteine. Moreover the

preference of *N*-Me-Ala·HCl with respect to proline is depending on the deeper inclusion of *N*-methyl alanine into the cavity and on its higher ΔH value.

2.2.4 Amino Acids Complexation in Water

Molecular recognition events are highly solvent dependent. Therefore, for a better understanding of a complexation event in solution, also solvent effects have to be addressed. Water is an essential biological fluid, which promotes apolar aggregation and complexation processes necessary to sustain all functions of life. Therefore, complexation studies in aqueous media are of special interest since they can directly model molecular recognition in biologic systems.[14] To perform host-guest complexation studies in water, we synthesized the new water-soluble tetraphosphonate cavitand **3**. This new receptor, bearing four pyridinium feet that provide water solubility, was obtained in four steps from tetrahydroxyl footed resorcinarene,[15] with 48% overall yield (Scheme 2.2).

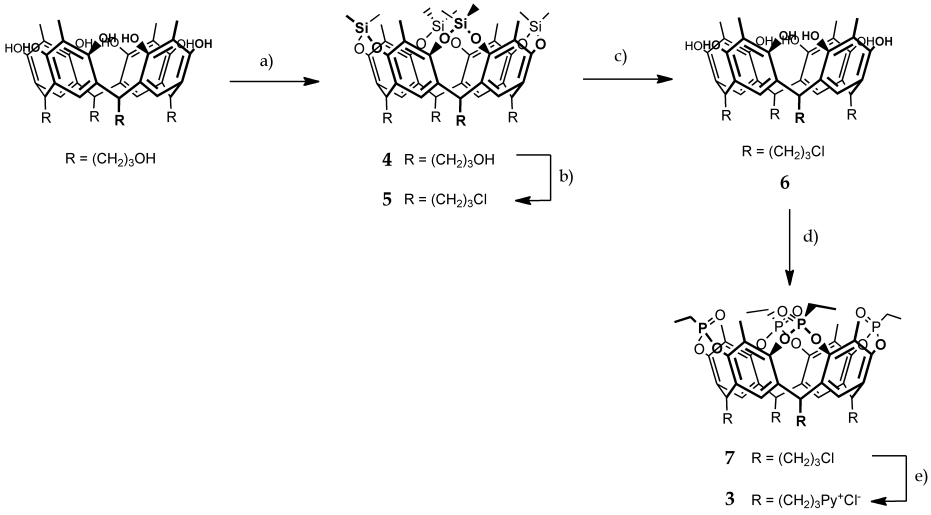

Scheme 2.2 *Synthesis of water-soluble tetraphosphonate cavitand* **3***: a)* $(CH_3)_2SiCl_2$*, Pyridine, 100°C, 3h, 85%; b) thionyl chloride, DMF cat., toluene, 55°C, 12 h, quant.; c) HF aq., DMF, 50°C, 12 h, quant.; d) (1)* $EtPCl_2$*, Py, 70°C, 3 h; (2)* H_2O_2 *35%, r.t, 30 min, 57% (over two steps); e) pyridine, 110°C, 72 h, quant.*

To selectively chlorinate the hydroxyl groups at the lower rim, phenolic groups were initially protected through bridging reaction with dichlorodimethylsilane, affording cavitand **4**. Chlorinated cavitand **5** was obtained reacting **4** with thionyl chloride in presence of a catalytic amount of DMF. The subsequent

deprotection of siloxanes with hydrofluoric acid afforded resorcinarene **6**. Bridging reaction with dichloroethylphosphine in pyridine gave P(III) intermediate, which was oxidized *in situ* with hydrogen peroxide to afford cavitand **7**, bearing four inward phosphonate bridges at the upper rim. In the last step, the nucleophilic substitution of the four chlorides with pyridine[16] afforded water-soluble cavitand **3**, which was characterized by NMR spectroscopy and ESI-MS spectrometry.

The ability of these water-soluble cavitand to complex amino acids in water was tested both through NMR (see Appendix B) and ITC studies. In particular, we focus our attention on two well-studied guest,[12] namely sarcosine (**Sarc**) and sarcosine methyl ester (**SarcME**) in their hydrochloride form.

For a better understanding of the binding event in water, we performed ITC measurements to calculate the thermodynamic characteristics for **3**·**SarcME**. ITC experiment in H_2O showed good fit to the theoretical binding isotherm for a 1:1 complex. The returned association constant K_a, ΔH and ΔS are summarized in Table 2.2. Non-covalent isotopic effect was also investigated by ITC experiments. Only NH_2 protons from **SarcME** are expected to exchange for deuterium atoms when dissolved in D_2O, maintaining the rest of the system unperturbed, as reported in Table 2.2.

In order to evaluate how the ionic strength influences the binding affinity, we decided to titrate the cavitand **3** (host) with **SarcME** in phosphate buffer solution (PBS) (0.1 M; pH = 7). ^{1}H NMR spectrum of free cavitand in deuterated-PBS solution shows a broadening of the signals compared to the spectrum of the same cavitand in pure D_2O. This observation can be attributed to a self-aggregation of the cavitand in this medium. Addition of incremental amounts of guest produces a shift of the signals assigned to host in a similar manner than in plane D_2O as well as a sharpening of proton signals of the receptor. These observations suggest first that the formed complex must be identical in both media and second that **3** disaggregates during the complex formation.

We also evaluate the complexation process of **3** with zwitterionic sarcosine in water by ^{1}H and ^{31}P NMR. The ^{1}H NMR spectra acquired during titration experiments of the cavitand with **Sarc** show a behavior similar to that obtained for sarcosine methyl ester hydrochloride. The protons assigned to the receptor do not show a significant change, while both protons signals of the guest experience an up field shift. The larger up field shift observed for CH_3 ($\Delta\delta < -2$ ppm) compared with the observed for CH_2 ($\Delta\delta \leq -1$ ppm) strongly suggest us, that in the same manner as in the previous case, the methylammonium group is

located in the deep aromatic cavity of the receptor, while the carboxylate is outwardly directed with respect to the cavity.
The complexation of **Sarc** with the water-soluble cavitand **3** was also observed by ^{31}P NMR. The phosphorous spectra acquired during the titration shows a shift of more than $\Delta\delta$ = 1.5 ppm for the signal belonging to bridging phosphonate group of the cavitand. This observation proves the participation of the P=O groups in the stabilization of the **3**·**Sarc** complex.
We decided to quantify the binding affinity of **3**·**Sarc** complex by ITC experiments. The values of binding constant, ΔH and ΔS for **3**·**SarME and 3**·**Sar** complexes are summarized in Table 2.2.

Guest (Solvent)	$K_a \pm \sigma_{Ka}$ (M^{-1})	$\Delta H \pm \sigma_{\Delta H}$ (KJ·mol^{-1})	$\Delta G \pm \sigma_{\Delta G}$ (KJ·mol^{-1})	$T\Delta S \pm \sigma_{T\Delta S}$ (KJ·mol^{-1})
Sarc (H_2O)	1.02 ± 0.01·10^3	-27.3 (± 0.3)	-17.17 (± 0.04)	-10.2 (± 0.3)
SarcME (H_2O)	3.43 ± 0.03·10^3	-33.0 (± 0.1)	-20.18 (± 0.04)	-12.8 (± 0.1)
SarcME (D_2O)	3.75 ± 0.06·10^3	-35.7 (± 0.25)	-20.39 (± 0.04)	-15.3 (± 0.25)
SarcME (PBS)	1.89 ± 0.07·10^3	-35.0 (± 0.2)	-18.71 (± 0.08)	-16.3 (± 0.2)

Table 2.2 *ITC data for complexation of* ***Sarc*** *and* ***SarcME*** *with water-soluble cavitand* ***3****.*

The K_a in water is two orders of magnitude lower than the K_a measured in methanol. Also in this case, the complexation event in water is only enthalpy driven (large negative ΔH), whilst the entropy contribute is unfavorable (negative $T\Delta S$). The negative ΔS contribute is the signature of these complex formation in water. Oppositely to the methanol case, the favorable desolvation entropies seem to be partially masked by a large entropy loss due to monomer association that leads to the formation of a tight complex in water. Upon aggregation, the biding partners lose rotational and translational entropy and this loss is bigger for binding event in water with respect to methanol.
This entropy loss is due to the formation of a highly ordered structure between the solvent molecules and the water molecules released into the bulk after the desolvation step. The formation of this hydrogen-bonded network can also be reflected in the higher ΔH contributes observed for binding events in water with respect to methanol.

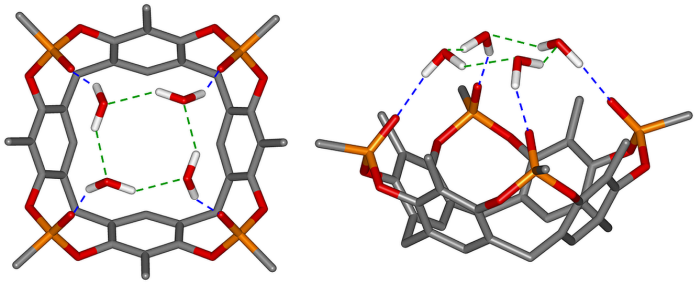

Figure 2.10 *Top and side view of the crystal structure of* ***1*** *and four molecules of water. The dashed lines depicted in blue indicate hydrogen bonding between the cavitands and water, while water-water interactions are depicted in green.*[17]

Interestingly, in previous studies we have shown that cavitand **1** forms a stable complex with four water molecules in which water molecules act as hydrogen bond donors to P=O groups (Figure 2.10, blue dotted line) and acceptors towards adjacent water molecules (green dotted lines).[17] In this case no high energy water molecules are present inside the host cavity, which resulted empty.[18]

2.2.5 Complexation in Methanol vs. Water: the Nε-Methyl-L-Lysine Case

Tetraphosphonate cavitand complexation of *N*ε-methyl-L-lysine, a relevant modified amino acid widely present in biologic systems, is remarkable for the presence of two different binding sites. In fact, crystallization of cavitand **1** from trifluoroethanol in the presence of *N*-Me-Lys afforded a 2:1 host·guest complex structure, which was determined by single crystal X-ray diffraction (Figure 2.11a). Opposite to the alcohol case, growing crystals of **3**·*N*-Me-Lys complex in water, we obtained a 1:1 stoichiometry. The *N*ε-methyl-lysine was found to interact with the cavity of the host through the usual synergistic three interactions discussed above (Figure 2.11b). Hydrogen bond interactions are still present in water thanks to the strong hydrophobic interaction between the electron-rich cavity of the host and the methyl group of the guest, which brings the ammonic hydrogens and the P=O groups closer and releases the water molecules bonded to the phosphonates groups.

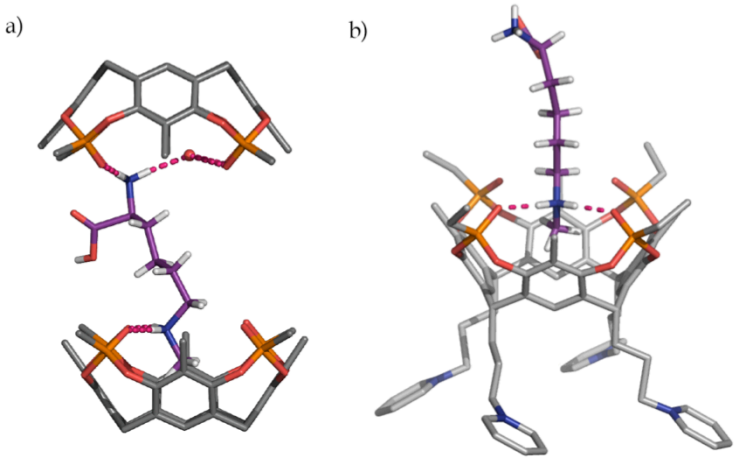

Figure 2.11 *Side view of X Ray molecular structures of complex* **1**.*N-Me-Lys (a) and* **3**.*N-Me-Lys (b) complexes. The dashed lines depicted in magenta indicate hydrogen bonding interactions.*

We studied the complexation process of *N*ε-Methyl-L-Lysine di-hydrochloride with **2** in methanol. ^{1}H and ^{31}P NMR spectra acquired during the titration of cavitand **2** with incremental amounts of guest showed a monotonic shift of proton signals assigned to the receptor. In particular, the shift of the N_{ε}-methyl at negative ppm was observed. After addition of more than one equivalent, no more changes were observed for the cavitand ^{1}H and ^{31}P signals.

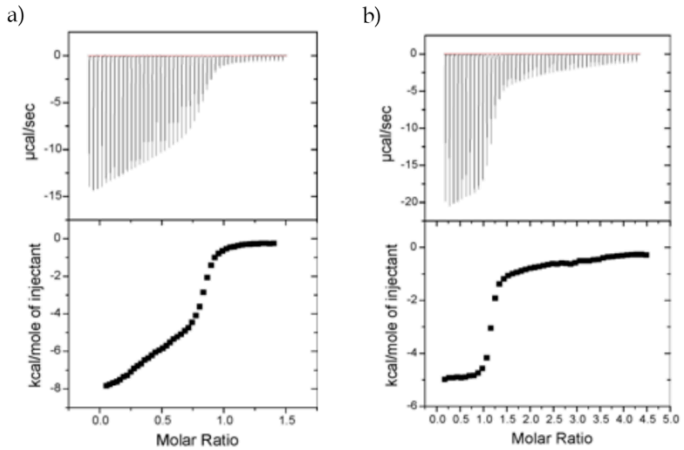

Figure 2.12 *ITC experiments: a) host was placed in the cell and the guest in the syringe (***2** *= 1.04 mM, N-Me-Lys = 6.74 mM); b) the guest was placed in the cell and the host in the syringe (***2** *= 14.72 mM, N-Me-Lys = 0.71 mM); Top trace: Raw data for the ITC titration in methanol; Bottom trace: Binding isotherm of calorimetric titration data.*

An accurate estimation of the two binding constant was performed by ITC experiments. As shown is Figure 2.12, more than one binding event were observed. We were not able to fit the data with a 1:1 model, so we applied a model that consider the formation of 1:1 and 2:1 complexes using HypDH software. To confirm these hypothesis we performed two sets of titrations: in the first small quantities of a guest solution were added to a host solution placed in the cell (Figure 2.12a, entry **III** in Table 2.3); for the second, the guest was placed in the cell and titrated with the host (Figure 2.12b, entry **V** in Table 2.3).

	$K_{1:1} \pm \sigma_{Ka}$ (M-1)	$\Delta H_{1:1} \pm \sigma_{\Delta H}$ (KJ•mol-1)	$K_{1:2} \pm \sigma_{Ka}$ (M-1)	$\Delta H_{1:2} \pm \sigma_{\Delta H}$ (KJ•mol-1)
I	$1.12 \cdot 10^6$	-24.28	$1.38 \cdot 10^3$	-13.86
II	$1.10 \cdot 10^6$	-24.49	$1.41 \cdot 10^3$	-12.77
III	$0.98 \cdot 10^6$	-24.58	$1.55 \cdot 10^3$	-12.48
IV	$0.78 \cdot 10^6$	-21.14	$0.74 \cdot 10^3$	-16.54
V	$0.76 \cdot 10^6$	-20.93	$0.68 \cdot 10^3$	-16.33
Av.	$0.95 (\pm 0.15) \cdot 10^6$	-23.07 (± 1.7)	$1.15 (\pm 0.37) \cdot 10^3$	-14.24 (± 1.8)

Table 2.3 *Association constant values (K_a, M^{-1}), and corresponding enthalpic component measured in methanol solution at 298 K.*

In Table 2.3, entries **I-III** are related to the first type of titration, while values in entries **IV** and **V** were obtained titrating the guest with the host. Final averaged values highlight the presence of two different binding events. In particular the association constants of the first binding reveled to be three orders of magnitude higher than the second event.

Ongoing ITC experiments in water and PBS and with **3** will complete this study. According to the sarcosine case, we expect a significant drop of the association constants, which can explain the 1:1 complexation observed in the solid state.

2.3 Conclusions

The molecular recognition properties of tetraphosphonate cavitands toward amino acids have been thoroughly investigated in the solid state *via* X ray diffraction and in solution by complementary ITC analyses and NMR titration experiments. The overall pictures emerging from these studies point out the pivotal role played by the monomethylated ammonium ion. Its presence inside the cavity acts as a "hook" to reinforce both cation-dipole and H-bonding interactions, to the point that it revealed to be necessary to ensure complexation in water. Complexation experiments in methanol showed a remarkable selectivity among amino acids. The ^{13}P chemical shift correlates nicely with the enthalpic contribution to complexation. The thermodynamic profile of complexes formation for several amino acids clearly indicates an inversion of the entropic contribution upon moving from methanol to water. This entropy loss could be due to the formation of a highly ordered structure between solvent molecules and the water molecules released into the bulk after the desolvation step. In water, the entropy loss leads to a drop of two orders of magnitude in K_a. However, this drop is associated to a dramatic increase in selectivity, since in aqueous solutions only *N*-methylated amino acids are recognized.

2.4 Acknowledgments

Special thanks to Dr. Roberta Pinalli from the department of Chemistry, University of Parma, for NMR studies and to Prof. Pablo Ballester and Daniel Hernández from the Institute of Chemical Research of Catalonia (ICIQ), Tarragona (Spain), for ITC and NMR measurements in water. Thanks to Prof. Silvano Geremia and Dr. Giovanna Brancatelli from the department of Chemical and Pharmaceutical Sciences, University of Trieste, for crystals growth and structures determination.

2.5 Experimental Section

Tiiii [C_3H_7, CH_3, Et] (2)
To a solution of resorcinarene[19] (1 g, 1.41 mmol) in 20 mL of dry pyridine, dichloroethylphosphine (0.6 mL, 5.92 mmol) was added. The solution was stirred at 70°C for 3h, than the mixture was cooled to room temperature and H_2O_2 (15 mL) was added. The mixture was stirred for additional 30 min at room temperature, quenched with water and filtered. The obtained white precipitate was collected and dried under vacuum (1.14 g, 1.13 mmol, 80%).
^{1}H NMR ($CDCl_3$, 400 MHz): δ (ppm) = 7.61 (s, 4H, Ar**H**), 4.58 (t, 4H, J=7.5 Hz, C**H**CH_2,), 2.51-2.42 (m, 8H, CHC**H_2**), 2.28 (dq, 8H, J_{H-P}=18.8 Hz, J=7.6 Hz, P(O)C**H_2**CH_3), 2.13 (s, 12H, ArC**H_3**), 1.48 (dt, 12H, J_{H-P}= 21.7 Hz, J=7.6 Hz, P(O)CH_2C**H_3**), 1.42-1.36 (m, 8H, C**H_2**CH_3), 1.05 (t, 12H, J=7.3 Hz, CH_2C**H_3**).
^{31}P NMR ($CDCl_3$, 162 MHz): δ (ppm) = 25.9 (s, P=O).
ESI-MS: *m/z* = 1026.6 $[M+NH^4]^+$, 1031.5 $[M+Na]^+$.

Tetra(dimethylsiloxy)-bridged cavitand (4)
Tetrahydroxy-footed resorcinarene[16] (4.5 g, 5.80 mmol) was dissolved in 70 mL of dry pyridine. The solution was cooled at 0°C and $(CH_3)_2SiCl_2$ (8.55 mL, 70.2 mmol) was added. The mixture was stirred at room temperature for 20 min and heated at 100 °C for 3 h. The reaction was cooled to room temperature and quenched with MeOH (50 mL). The obtained precipitate was filtered, wash with methanol and dried, to give the white product **4** (4.9 g, 4.26 mmol, 85% yield).
^{1}H NMR ($CDCl_3$, 300 MHz): δ (ppm) = 7.47 (s, 4H, Ar**H**), 4.54 (t, 4H, J=7.9 Hz, Ar**CH**), 3.66 (bt, 8H, **CH_2**OH), 2.46-2.43 (m, 8H, **CH_2**CH_2CH_2OH), 1.87 (s, 12H, Ar**CH_3**), 1.50-1.46 (m, 8H, CH_2**CH_2**CH_2OH), 0.46 (s, 12H, Si**$CH_{3,out}$**), -0.73 (s, 12H, Si**$CH_{3,in}$**).
ESI-MS: *m/z* = 1002.5 $[M+H]^+$.

Tetrachloride-footed dimethylsiloxy cavitand (5)
To a solution of **4** (2.48 g, 2.48 mmol) in 40 mL of toluene, thionyl chloride (2.19 mL, 29.9 mmol) was added, followed by a catalytic amount of DMF. The reaction was heated at 55 °C overnight. The solvent was evaporated and the residue was dissolved in chloroform, washed with water and dried over $MgSO_4$. After solvent evaporation, product **5** was obtained as brownish solid (2.6 g, quantitative yield).
^{1}H NMR ($CDCl_3$, 300 MHz): δ (ppm) = 7.20 (s, 4H, Ar**H**), 4.64 (t, 4H, J=8.2 Hz, ArC**H**), 3.65 (t, 8H, J=6.4 Hz, CH_2CH_2C**H_2**Cl), 2.40 (m, 8H, C**H_2**CH_2CH_2Cl), 1.93

(s, 12H, ArC**H**$_3$), 1.90–1.69 (m, 8H, $CH_2C\mathbf{H}_2CH_2Cl$), 0.54 (s, 12H, J=7.9 Hz, 12H, Si**CH**$_{3,out}$), -0.66 (s, 12H, Si**CH**$_{3,in}$).
ESI-MS: *m/z* = 1075.4 $[M+H]^+$, 1094.5 $[M+Na]^+$.

Tetrachloride-footed resorcinarene [C_3H_6Cl, CH_3] (6)
An aqueous 40% HF solution (0.15 mL) was added to **5** (1.72 g, 1.6 mmol) dissolved in 15 mL of DMF. The mixture was heated at 55 °C overnight. The reaction was quenched with water and the precipitate was filtered, washed with water and dried. Resorcinarene **6** was obtained as a light orange solid (1.33 g, quantitative yield).
^{1}H NMR (DMSO-d_6, 400 MHz): δ (ppm) = 8.71 (s, 8H, ArO**H**), 7.26 (s, 4H, Ar**H**), 4.25 (t, 4H, J=7.9 Hz, ArC**H**), 3.66 (t, 8H, J=6.7 Hz, $CH_2CH_2C\mathbf{H}_2Cl$), 2.36 (m, 8H, $C\mathbf{H}_2CH_2CH_2Cl$), 1.96 (s, 12H, ArC**H**$_3$), 1.74–1.54 (m, 8H, $CH_2C\mathbf{H}_2CH_2Cl$).
ESI-MS: *m/z* = 847.4 $[M-H]^-$.

Tiiii [C_3H_6Cl, CH_3, Et] (7)
To a solution of resorcinarene **6** (1.0 g, 1.18 mmol) in 50 mL of pyridine, dichloroethylphosphine (0.512 mL, 4.94 mmol) was added. The solution was heated at 70 °C for 3 h. The mixture was cooled at 0°C, and 15 mL of aqueous 35% H_2O_2 were added. The reaction was stirred at room temperature for 30 min then quenched with 100 mL of water. The precipitate was filtered, washed with water and dried. The crude was dissolved in $CHCl_3$ and precipitated with hexane, then recrystallized from CH_2Cl_2/MeOH. Cavitand **7** was obtained as white solid (0.77 g, 0.67 mmol, 57% yield).
^{1}H NMR ($CDCl_3$, 400 MHz): δ (ppm) = 7.05 (s, 4H, Ar**H**), 4.66 (t, 4H, J=7.4 Hz, ArC**H**), 3.69 (t, 8H, J=6.2 Hz, $CH_2CH_2C\mathbf{H}_2Cl$), 2.48-2.43 (m, 8H, $C\mathbf{H}_2CH_2CH_2Cl$), 2.30–2.09 (m, 20H, ArC**H**$_3$ + $P(O)C\mathbf{H}_2CH_3$), 1.89-1.84 (m, 8H, $CH_2C\mathbf{H}_2CH_2Cl$), 1.46 (dt, 12H, J_{P-H}=21.0 Hz, J= 7.7 Hz, $P(O)CH_2C\mathbf{H}_3$).
^{31}P NMR ($CDCl_3$, 162 MHz): δ (ppm) = 21.5 (s, P=O).
ESI-MS: *m/z* = 1169.9 $[M+Na]^+$, 1185.9 $[M+K]^+$.

Tiiii [$C_3H_6Py^+Cl^-$, CH_3, Et] (3)
A solution of cavitand **7** (0.05 g, 0.044 mmol) in 10 mL pyridine was heated at 110°C for 72 h. The mixture was cooled at room temperature and the solvent was evaporated under vacuum. The residue was triturated with CH_2Cl_2, filtered, washed with CH_2Cl_2 (3×20 mL) and dried under vacuum to afford cavitand **3** as a white solid (0.06 g, quantitative yield).
^{1}H NMR (D_2O, 400 MHz): δ (ppm) = 8.76 (d, 8H, J_o=5.8 Hz, Py**H**$_o$), 8.44 (t, 4H, J_o=7.7 Hz, Py**H**$_p$), 7.95 (t, 8H, J_o=6.8 Hz, Py**H**$_m$), 7.53 (s, 4H, Ar**H**), 4.64 (t, 8H,

$CH_2CH_2C\mathbf{H_2}Py$), 4.46 (t, 4H, Ar**CH**), 2.66 (m, 8H, $C\mathbf{H_2}CH_2CH_2Py$), 2.29 (dt, 8H, J_{P-H}=26.0 Hz, J=7.3 Hz, $P(O)C\mathbf{H_2}CH_3$), 2.13 (m, 8H, $CH_2C\mathbf{H_2}CH_2P$), 1.97 (s, 12H, $ArC\mathbf{H_3}$), 1.32 (dt, 12H, J_{P-H}=22.4 Hz, J= 7.6 Hz, $P(O)CH_2C\mathbf{H_3}$).
^{31}P NMR ($CDCl_3$, 162 MHz): δ (ppm) = 28.0 (s, P=O).
ESI-MS: *m/z* = 452.1 $[M-3Cl]^{3+}$, 695.2 $[M-2Cl]^{2+}$.
ESI-FT-Orbitrap: calculated for $C_{72}H_{84}N_4O_{12}P_4$ $[M-4Cl]^{4+}$ *m/z* = 330.1254, found *m/z* = 330.1256.

Crystal structures geometric parameters

Amino acid	NH ··O (Å)	OH ··O (Å)	Naa ··OOp (Å)	(CH_3/CH_2/SH)aa ··OOp (Å)
Ala (I)	2.81(1); 2.81(1)		0.717(9)	
Ala (II)	2.79(1); 2.89(1)		0.789(9)	
Ala·HCl (I)	2.708(6); 2.760(6)	2.549(6)	0.692(6)	-1.158(7)
Ala·HCl (II)	2.704(6); 2.814(6)	2.386(9)	0.759(9)	-1.287(7)
Cys (I)	2.712(5); 2.827(5)		1.028(1)	-1.470(3)[a]
Cys (II)	2.794(5); 2.715(5)		0.965(1)	-1.426(2)
4-Hyp (I)	2.724(6); 2.784(6)		0.574(4)	-0.198(5); 0.903(6)
4-Hyp (II)	2.730(6); 2.894(7)		0.839(5)	0.112(6); 1.235(6)
Ile·HCl	2.770(6); 2.810(5)		0.545(4)	
Leu·HCl (I)	2.756(5); 2.904(4)		0.664(4)	
Leu·HCl (II)	2.752(4); 2.850(5)		0.631(4)	
***N*-Me-Ile·HCl (I)**	2.78(1); 2.79(1)	2.530(9)	0.15(1)	-1.13(1)
***N*-Me-Ile·HCl (II)**	2.74(1); 2.83(1)		0.21(1)	-0.99(1)
***N*-Me-Ala (I)**	2.698(6); 2.779(6)		0.048(4)	-1.171(5)
***N*-Me-Ala (II)**	2.820(7); 2.839(7)		0.182(5)	-0.995(6)
***N*-Me-Ala (III)**	2.94(1); 2.763(9)		0.158(8)	-0.98(1)

***N*-Me-Ala (IV)**	2.785(7); 2.834(7)		0.089(5)	-1.075(6)
Pro (I)	2.697(7); 2.791(7)		0.250(6)	-0.718(8)[b]; -1.035(7)[c]
Pro (II)	2.732(7); 2.840(7)		0.497(6)	-0.479(8) [b]; -0.680(7)
Ser (I)	2.71(2); 2.85(2)		0.70(1)	
Ser (II)	2.76(2); 2.80(2)		0.77(1)	
Ser (III)	2.60(3)		0.84(2)	
Ser (IV)	2.70(2); 2.89(2)		0.73(1)	
Thr	2.737(4); 2.866(4)	2.654(5)	1.049(4)	-1.163(4)
Tyr·HCl (I)	2.770(6); 2.851(7); 2.945(7)	2.586(6)	0.288(5)	
Tyr·HCl (II)	2.834(6); 2.838(7); 2.908(7)	2.585(6)	0.319(6)	
Val (I)	2.793(5); 2.903(5)		0.727(4)	
Val (II)	2.757(6)		1.226(6)	

Table S2.1 *Geometric parameters describing the host–guest interaction for the amino acids–cavitand complexes a) value referred to the sulfur atom on the cysteine side chain; b) value referred to the C_γ of the five-membered proline ring; c) value referred to the C_D of the five-membered proline ring.*

2.6 References

[1] A. Späth, B. König, *Beilstein J. Org. Chem.* **2010,** *6,* No. 32.

[2] a) A. Metzger, K. Gloe, H. Stephan, F. P. Schmidtchen, *J. Org. Chem.* **1996,** *61,* 2051-2055; b) X. X. Zhang, J. S. Bradshaw, R. M. Izatt, *Chem. Rev.* **1997,** *97,* 3313-3361; c) D. P. Weimann, H. D. F. Winkler, J. A. Falenski, B. Koksch, C. A. Schalley, *Nat. Chem.* **2009**, *1*, 573-577; d) Späth, A. and König, B. *Tetrahedron* **2010**, *66*, 1859–1873; e) Y. Chen, M. T. Rodgers, *J. Am. Chem. Soc.* **2012**, *134*, 5863-5875.

[3] L. Mutihac, J. H. Lee, J. S. Kim, J. Vicens, *Chem. Soc. Rev.* **2011**, *40*, 2777–2796.

[4] a) P. Rajgariah, A. R. Urbach, *J. Inclusion Phenom. Macrocyclic Chem.* **2008,** *62,* 251–254; b) T. Minami, N. A. Esipenko, B. Zhang, L. Isaacs, P. Anzenbacher, Jr. *Chem. Commun.* **2014**, 61-63; c) G. Ghale, W. M. Nau, *Acc. Chem. Res.* **2014**, *47*, 2150-2159.

[5] a) M. Wehner, T. Schrader, P. Finocchiaro, S. Failla, G. Consiglio, *Org. Lett.* **2000,** *2,* 605–608; b) M. Fokkens, T. Schrader, F.-G. Klärner, *J. Am. Chem. Soc.* **2005,** *127,* 14415–14421.

[6] a) V. Villari, P. Mineo, N. Micali, N. Angelini, D. Vitalini, E. Scamporrino, *Nanotechnology* **2007**, *18*, 375503; b) V. Villari, P. Mineo, E. Scamporrino, N. Micali, *Chem. Phys.* **2012**, *402*, 118–123.

[7] a) N. Douteau-Guevel, A. W. Coleman, J.-P. Morel, N. Morel-Desrosiers, *J. Chem. Soc., Perkin Trans. 2* **1999**, 629–634; b) M. Selkti, A. W. Coleman, I. Nicolis, N. Douteau-Guevel, F. Villain, A. Tomas, C. de Rango, *Chem. Commun.* **2000**, 161–162; c) O. Danylyuk, K. Suwinska, *Chem. Commun.* **2009**, 5799–5813; d) M. Torvinen, R. Neitola, F. Sansone, L. Baldini, R. Ungaro, A. Casnati, P. Vainiotalo, E. Kalenius, *Org. Biomol. Chem.* **2010**, *8*, 906–915; e) K. D. Daze, F. Hof, *Acc. Chem. Res.* **2013**, *46*, 937–945.

[8] a) C. S. Beshara, C. E. Jones, K. D. Daze, B. J. Lilgert, F. Hof, *ChemBioChem* **2010**, *11*, 63–66; b) S. A. Minaker, K. D. Daze, M. C. F. Ma, F. Hof, *J. Am. Chem. Soc.* **2012**, *134*, 11674-11680.

[9] A. R. Urbach, V. Ramalingam, *Isr. J. Chem.* **2011**, *51*, 664 – 678.

[10] M. Dionisio, G. Oliviero, D. Menozzi, S. Federici, R. M. Yebeutchou, F. P. Schmidtchen, E. Dalcanale, P. Bergese, *J. Am. Chem. Soc.* **2012**, *134*, 2392-2398.

[11] E. Biavardi, C. Tudisco, F. Maffei, A. Motta, C. Massera, G. G. Condorelli, E. Dalcanale, *PNAS* **2012**, *109*, 2263-2268.

[12] a) M. Senćanski, L. Došen-Mićović, V. Šukalović, S. Kostić-Rajačić, *Struct. Chem.* **2015**, *article in press*, doi 10.1007/s11224-015-0574-z; b) K. N.-M. Daeffler, H. A. Lester, D. A. Dougherty, *J. Am. Chem. Soc.* **2012**, *134*, 14890-14896; c) L. M. Salonen, M. Ellermann, F. Diederich, *Angew. Chem. Int. Ed.* **2011**, *50*, 4808-4842; d) H. S. Biswal, S. Wategaonkar, *J. Phys. Chem. A* **2009**, *113*, 12774-12782; e) A. L. Ringer, A. Senenko, C. D. Sherrill, *Protein Science* **2007**, *16*, 2216-2223; f) R. K. Castellano, F. Diederich, E. A. Meyer, *Angew. Chem. Int Ed.* **2003**, *42*, 1210-1250.

[13] M. Egli, S. Sarkhel, *Acc. Chem. Res.* **2007**, *40*, 197-205.

[14] D. B. Smithrud, E. M. Sanford, I. Chao, S. B. Ferguson, D. R. Carcanague, J. D. Evanseck, K. N. Houk, F. Diederich, *Pure & Appl. Chem.* **1990**, *62*, 2227-2236.

[15] a) A. R. Mezo, J. C. Sherman, *J. Org. Chem.* **1998**, *63*, 6824-6829; b) L. Pirondini, D. Bonifazi, E. Menozzi, E. Wegelius, K. Rissanen, C. Massera and E. Dalcanale, *Eur. J. Org. Chem.* **2001**, 2311-2320.

[16] K. D. Zhang, D. Ajami, J. Rebek Jr., *J. Am. Chem. Soc.* **2013**, *135*, 18064-18066.

[17] C. Massera, M. Melegari, F. Uguzzoli, E. Dalcanale, *Chem. Comm.* **2010**, *46*, 88-90.

[18] F. Biedermann, W. M. Nau, H.-J. Schneider, *Angew. Chem. Int. Ed.* **2014**, *53*, 11158–11171.

[19] R. M. Yebeutchou, F. Tancini, N. Demitri, S. Geremia, R. Mendichi, E. Dalcanale, *Angew. Chem. Int. Ed.* **2008**, *47*, 4504-4508.

CHAPTER 3

DYNAMIC EMULSIONS WITH TETRAPHOSPHONATE CAVITAND-BASED SURFACTANTS*

* This work has been carried out in the group of Prof. Timothy M. Swager at Massachusetts Institute of Technology (MIT), Cambridge, MA, USA.

3.1 Introduction

The nucleosome is the fundamental unit of chromatin and it is composed of an octamer of four core proteins, called histones, wrapped by 147 base pairs of DNA. Histones are predominantly globular except for their *N*-terminal tails, which are unstructured. The numerous post-translational modifications present mainly on these tails are usually associated to the "histone code".[1] This code is written and erased by enzymatic processes, such as phosphorylation of serine and threonine, acetylation or ubiquitination of lysine and methylation of lysine and arginine.[2] Post-translational modifications can be recognized by effector proteins or protein complexes that convert them into specific functional chromatin states and regulate downstream responses.[3] For its enormous complexity, the decoding of the histone "language" and its correlation with human diseases is still a challenge in epigenetics. Histones can be modified at many sites with a large variety of functionalities, to produce millions of possible modification sets possible for a single histone tail. There are over 60 different residues on histones where modifications have been detected either by mass spectrometry or by specific antibodies. In particular the latter are the dominant tools for the identification of post-translational modifications even if they present some shortcomings. As reported by Lieb and co-workers in 2011, antibody-based assays suffer from high batch-to-batch variability.[4] They reported that at least 25% of most commercially available histone-modification antibodies have substantial problems of specificity or utility and they needed to be tested independently when purchased. Other known limitations of these systems are the poor selectivity between similar analytes and the misidentification of analytes caused by the presence of a post-translational modification on a nearby residue (epitope masking).[5]

In this field the development of assays based on synthetic receptors is particularly attractive, as batch-to-batch and lab-to-lab reproducibility might be improved using chemicals that can be purified to homogeneity. In particular chemical sensor arrays with broadly specific receptors have been widely studied. Moreover the applicability of these arrays, which are able to produce a patter of signals unique to each analyte, is not hampered by the presence of modifications on nearby residues. A successful application of this approach is the calixarene-based sensor array developed by Hof and co-workers.[6] They reported two sensors based on an indicator displacement scheme in which a fluorescent dye is bound to a suitable host molecule that quenches its fluorescence. Exploiting the well-known concept of the "aromatic cage mimic", the addition of amino acid residues able to compete for the host's binding site

causes the release of some or all of the dye causing a fluorescent turn-on response (Figure 3.1a).

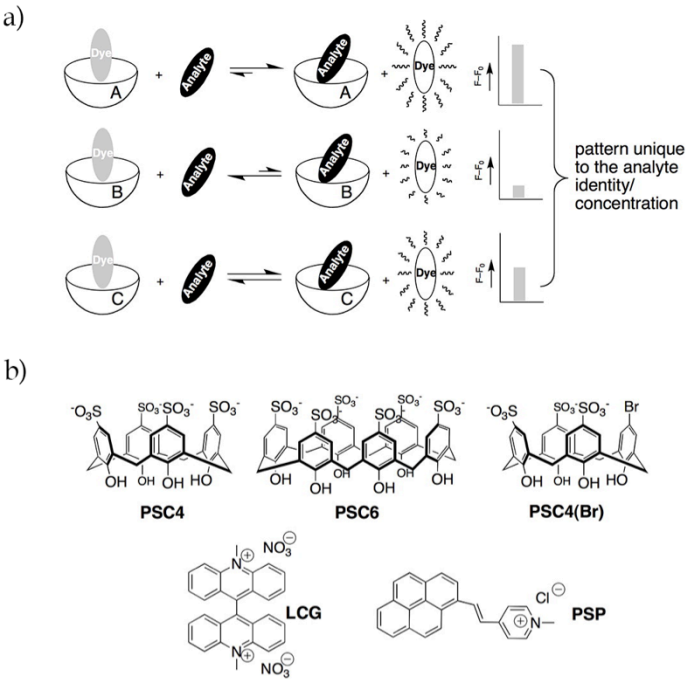

Figure 3.1 *a) Illustration of the principle of using patterns of data produced by multiple systems to identify and quantify analytes; b) Hosts and fluorescent dyes used in the construction of sensor arrays.*[6]

The first array was based on **PSC6·PSP** complex and used the variation of pH and/or organic co-solvent conditions to generate different fluorescent responses for different analytes, while the second system afforded varied analyte-specific fingerprints *via* interactions between different calixarene hosts (**PSC6**, **PSC4**, and **PSC4(Br)**) and **LCG** in water. Performing linear discriminant analysis (LDA) of the fluorescence data, they reported a good discrimination between variously modified peptides and also lysine residues with different methylation states. Even if this approach is limited to *in vitro* analysis and requires higher analyte concentration compered to antibodies, it is cheaper than biological assays and represents a promising application of host-guest recognition to epigenetic research.

Inspired by these studies we focused our attention on lysine methylation, which is one of the most biologically relevant modifications, since its function depends on the precise site and the degree of functionalization of the residue.

Considering tetraphosphonate cavitands ability to complex amino acids with a particular predisposition for *N*-methylated species, we decided to apply histone post-translational methylation detection to a completely new sensing platform, namely dynamic emulsions. Recently, Swager and co-workers reported a simple one-step preparation of three-phase complex emulsions.[7] In their fabrication, the temperature-sensitive miscibility of hydrocarbon and fluorocarbon liquid was used to obtain phase separation inside water-dispersed droplets. Interestingly, the preparation of these multiphasic systems did not require complex and expensive microfluidic devices, but droplets with highly uniform morphology and composition were obtained simply shaking warm emulsions. As reported in Figure 3.2, they demonstrated the possibility to tune droplet morphology between encapsulated and Janus configurations by varying the interfacial tension with a proper combination of hydrocarbon (sodium dodecyl sulfate, SDS) and fluorocarbon surfactants (Zonyl FS-300).

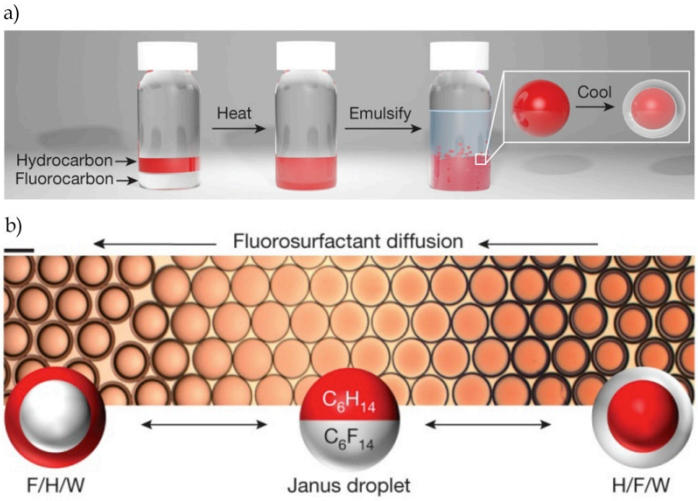

Figure 3.2 *a) Complex emulsion fabrication; b Hexane–perfluorohexane droplets reconfiguration with the variation in the concentration of Zonyl as it diffuses from the right through 0.1% SDS, scale bar: 100 μm.*[7]

These complex emulsions reveled to be extremely dynamic systems: small variations of interfacial tension, favoring hydrocarbon or fluorocarbon phase stabilization, induced dramatic changes in the droplet's morphology. This behavior can be rationalized considering the configurational stability diagram (Figure 3.3) for hexane-perfluorohexane-water system, obtained by plotting the difference between the interfacial tension between the fluorocarbon phase and

water (γ_F) and the one between the hydrocarbon phase and water (γ_H) as a function of the fraction of SDS.

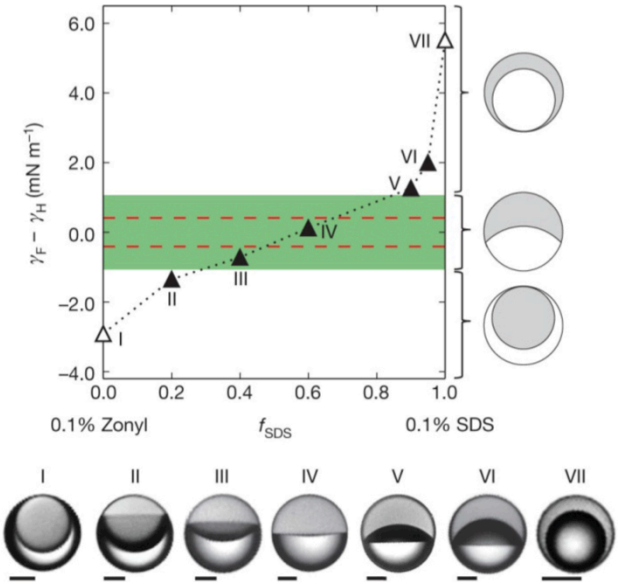

Figure 3.3 *Configurational stability diagram for hexane-perfluorohexane-water system (top) and optical micrographs of hexane–perfluorohexane droplets in solutions of 0.1% Zonyl and 0.1% SDS in varying ratios (down).*[7]

In the right region, the slope of the graph underlines how the small stabilization of the hydrocarbon phase induced by the increase of the SDS fraction caused the switching from a Janus-type droplet (V) to a situation close to the complete encapsulation of the fluorocarbon phase (VII). They were able to obtain significant morphology changes not only playing with the relative amount of Zonyl and SDS, but also by the use of stimuli-responsive surfactants. Droplet configuration was tuned exploiting surfactants that undergo changes in their effectiveness when triggered by stimuli such pH, light or when modified by a chemical reaction.

For their potential biological compatibility and their dynamicity, these water-dispersed systems were envisaged as sensing platforms for analytes containing *N*-methylated ammonium species. The principle behind the detection of these water-soluble species was related to the introduction of specific surfactants, based on supramolecular receptors, capable to modify their effectiveness in the stabilization of one phase upon complexation.

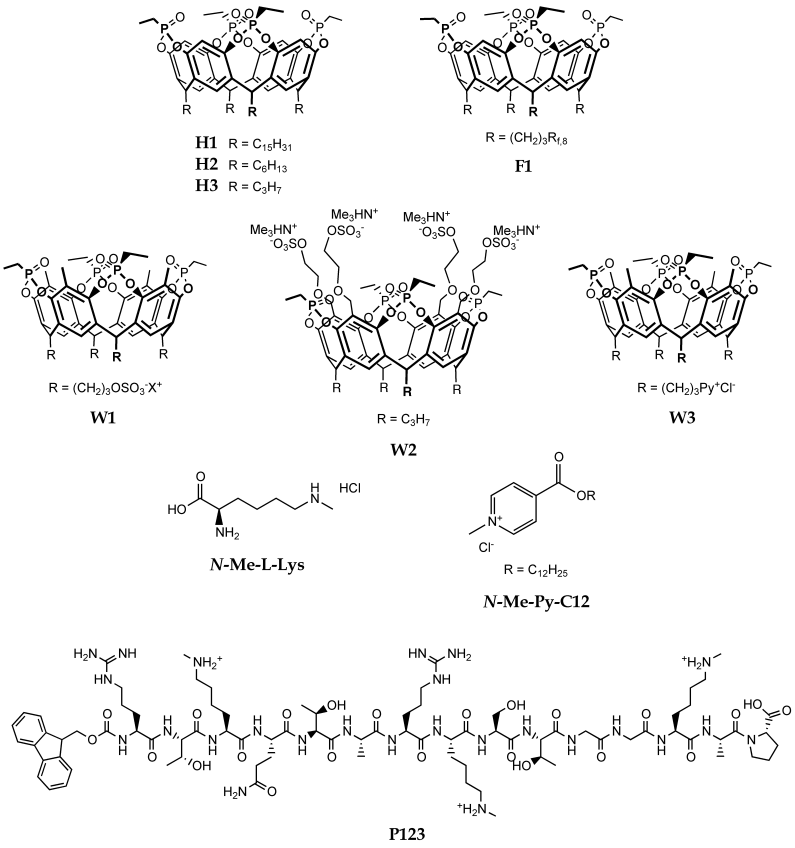

Figure 3.4 *Cavitands and N-methylated species involved in this study.*

We initially synthesized four amphiphilic tetraphosphonate cavitand-based surfactants, three bearing aliphatic tails (**H1-H3)** and the other with fluorinated chains at the lower rim (**F1**), to be introduced inside the droplets. We expected the hydrophilicity of the recognition unit to be increased by the complexation of charged guests (especially for analytes possessing a considerable polar part) leading to an enhancing of surfactant effectiveness. To prove this assumption we studied morphology changes upon addition of N_ε-methyl-L-lysine (**N-Me-L-Lys**), which is a well-characterized guest for Tiiii (see Chapter 2), and peptide **P123** as a model of the unstructured tails of a H3 histone bearing three methylated residues. Subsequently we synthesized two water-soluble cavitands (**W1-W2)** to move the recognition event from the interface to the bulk and avoid analyte diffusion effects. Finally we increased the complexity of the system by studying sensors based on *N*-methylpyridinium surfactant (***N*-Me-Py-C12)** displacement.

3.2 Results and Discussion

3.2.1 Synthesis of Tetraphosphonate Cavitands with Aliphatic or Fluorous Tails

To test tetraphosphonate cavitands ability to behave as functional surfactants when dispersed in the hydrocarbon phase of three-phases emulsions, we synthesized three compounds bearing different aliphatic chains. We designed a Tiiii with four C_{15} tails (**H1**) to maintain a good solubility in common organic solvents. To verify the influence of chain length, we synthesized a tetraphosphonate cavitand with four hexyl tails (**H2**) and a cavitand bearing short propyl groups at the lower rim (**H3**). The first step of **H1** synthesis required the preparation of aldehyde **1**, while for **H2** and **H3** commercially available precursors were used. 1-Hexadecanal (**1**) was obtained from the selective oxidation of cetyl alcohol with pyridinium chlorochromate (PCC), as reported in Scheme 3.1.

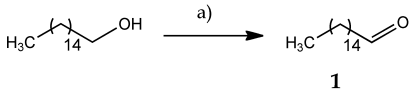

1

Scheme 3.1 *Synthesis of aldehyde 1: a) PCC, AcONa, CH_2Cl_2, r.t., 4 h, 98%.*

Condensation of aliphatic aldehydes in acidic conditions afforded resorcinarenes **2-4** bearing different chains at the lower rim (Scheme 3.2). Bridging reaction with dichloroethylphosphine in pyridine gave P(III) intermediate, which was oxidized *in situ* with hydrogen peroxide to afford cavitands **H1-H3** with the four phosphonate groups directed towards the cavity.

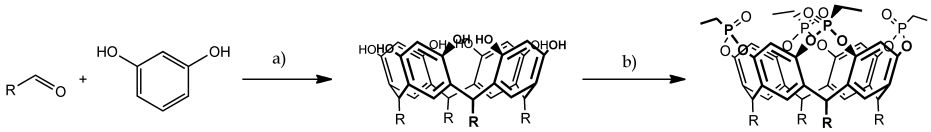

2 R = $C_{15}H_{31}$
3 R = C_6H_{13}
4 R = C_3H_7

H1 R = $C_{15}H_{31}$
H2 R = C_6H_{13}
H3 R = C_3H_7

Scheme 3.2 *Synthesis of tetraphosphonate cavitands with aliphatic tails: a) for **2**: HCl 37%, EtOH, 80 °C, 4 h, 71%; for **3,4**: HCl 37%, MeOH, 50 °C, 5 d; **3** 55%, **4** 57%; b) (1) $EtPCl_2$, Py, 80°C, 3 h; (2) H_2O_2 35%, r.t, 1 h, 37% (over two steps).*

The three compounds were characterized by mass spectrometry, ^{1}H NMR and ^{31}P NMR. The presence of a single peak in phosphorous spectra confirmed the isolation of the designed isomers.

The fluorocarbon-footed tetraphosphonate cavitand **F1** was prepared from resorcinarene **8**, bearing four perfluorooctyl ($R_{f,8}$) moieties. Following similar procedures reported in literature,[8] the synthesis of resorcinarene **8** required the acidic condensation of resorcinol and a fluorinated aldehyde. Aldehyde **7** was obtained in three steps with 59% overall yield (Scheme 3.3). AIBN-initiated radical reaction between heptadecafluoro-1-iodooctane and 3-buten-1-ol afforded iodo-alcohol **5**, as racemic mixture.[9] Treatment with tributyltin hydride and AIBN as radical initiator gave the deiodinated alcohol **6**, which was selectively oxidized to aldehyde **7.** Dess-Martin periodinane was chosen as oxidizer as perfluorinated alcohol revealed to be sensitive to the basic conditions of common procedures (PCC and Swern oxidation).[10]

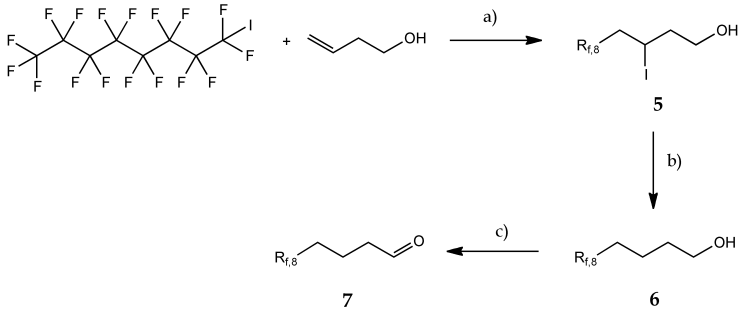

Scheme 3.3 *Synthesis of fluorous aldehyde* ***7****: a) AIBN, 76 °C, 5 h, 76%; b)* Bu_3SnH*, AIBN, Toluene, 70 °C, 4 h, 86%; c) Dess-Martin periodinane,* CH_2Cl_2*, r.t., 2 h, 91%.*

The presence of three methylene groups preserved aldehyde reactivity from electron withdrawing effect of fluorides. Compound **7** was reacted with an equimolar amount of resorcinol in acidic conditions, affording resorcinarene **8** (Scheme 3.4).

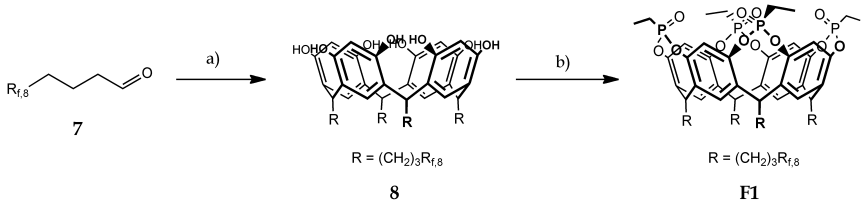

Scheme 3.4 *Synthesis of fluorinated tetraphosphonate cavitand* ***F1****: a) resorcinol, HCl 37%, EtOH, 80 °C, 4 h, 23%; b)* $EtPCl_2$*, Py/ α,α,α-trifluorotoluene, 80°C, 3 h; (2)* H_2O_2 *35%, r.t, 1 h, 23% (over two steps).*

Reaction with dichloroethylphosphine and the subsequent *in situ* oxidization with hydrogen peroxide afforded phosphonate-bridged cavitand **F1**, with all P=O groups pointing inward the cavity, which was characterized by NMR spectroscopy and MALDI-TOF spectrometry.

3.2.2 Emulsions with Inner Surfactants

Morphology of complex emulsions is exclusively controlled by interfacial tensions.[7] If we consider droplets containing two immiscible liquids H and F, dispersed in a third immiscible liquid phase W, three interfacial tensions are present and they are relative to H-W interface (γ_H), F-W interface (γ_F) and F-H interface (γ_{FH}). Possible internal configurations are reported in Figure 3.5 and correspond to liquid H completely encapsulated in F (a), liquids H and F forming a Janus droplet (b) and liquid F completely encapsulated in H (c).

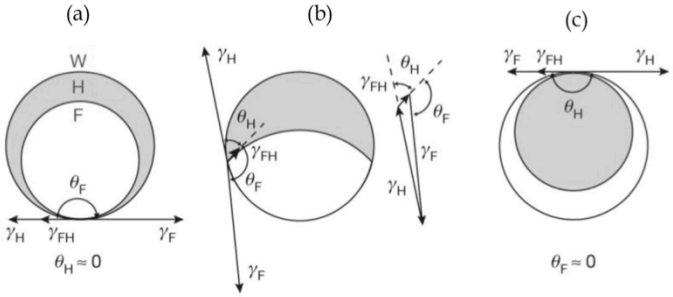

Figure 3.5 *Sketch of possible droplet configurations for complex emulsions: a) $\gamma_F > \gamma_H + \gamma_{FH}$, phase F is encapsulated within phase H; b) Janus droplet generated by intermediate values of γ_F and γ_H, interfacial tensions can be reconfigured into a Neumann triangle solvable for σ_H and σ_F; c) $\gamma_H > \gamma_F + \gamma_{FH}$, phase H is encapsulated within phase F.*[7]

The three interfacial tensions must be at equilibrium for the droplet configuration to be stable and the two contact angles σ_H and σ_F, the former between H-W and F-H interfaces while the latter between F-W and F-H, can be expressed by the following equations:

$$\cos(\theta_H) = \frac{\gamma_F^2 - \gamma_H^2 - \gamma_{FH}^2}{2\gamma_{FH}\gamma_H} \quad (1)$$

$$\cos(\theta_F) = \frac{\gamma_H^2 - \gamma_F^2 - \gamma_{FH}^2}{2\gamma_{FH}\gamma_F} \quad (2)$$

For cases (a) and (c) in figure 3.5, that are limiting of configuration (b) as $\sigma_H \rightarrow 0$ and $\sigma_F \rightarrow 0$ respectively, limiting contact angle can be translate into interfacial tension conditions as follow:

$$\theta_H = 0 \quad \Rightarrow \quad \gamma_F = \gamma_H + \gamma_{FH} \tag{3}$$

$$\theta_F = 0 \quad \Rightarrow \quad \gamma_H = \gamma_F + \gamma_{FH} \tag{4}$$

Recast as difference between γ_H and γ_F and considering real situations, droplets assume configuration (a) when relation (5) is fulfilled, while (6) is associated to the situation (c):

$$\gamma_F - \gamma_H \geq \gamma_{FH} \tag{5}$$

$$\gamma_H - \gamma_F \geq \gamma_{FH} \tag{6}$$

When the difference between γ_H and γ_F is in the order of γ_{FH} the droplets adopt a Janus configuration (b). The driving force of system dynamicity is that for H and F below the critical temperature (T_c) the value of γ_{FH} is significantly low and small changes in γ_H and γ_F balance can dramatically change droplet morphology.

The choice of the hydrocarbon/fluorocarbon phases for the preparation of complex emulsion is pivotal and two important factors must be considered:

- The two solvents must be immiscible at 0°C<T<r.t, in order to observe segregation of the two phases when the mixture is cooled.
- The T_c must be below the boiling temperature of the external phase (usually water), to avoid separation of the two phases before the emulsification step.

Solvent mixtures used in this study, with an indication of operating temperatures, are reported in Table 3.1:

Liquid H	Liquid F	Two phases at (°C)	One phase at (°C)
oDCB	HFE-7200	r.t.	>> r.t.
Hexane	Perfluorohexanes	0°	r.t.
Heptane	FC 770	r.t.	> r.t.

Table 3.1 *Solvent mixtures used in this study with indicative operating temperatures.*

As a consequence of cavitand **H1-H3** solubility in chlorinated solvents, we initially decided to solubilize our receptors in pure *o*-dichlorobenzene (oDCB). Emulsification with perfluorobutyl ethyl ether (HFE-7200) in water containing different ratios of Zonyl and SDS failed to evidence homogeneity and control over droplet morphology. The solubility of the three cavitands revealed to be insufficient in hexanes, so a mixture of hexanes/oDCB 99:1 was used as H phase, in combination with pure perfluorohexanes. Unlike **H1** and **H2** good stability in these complex emulsions, emulsification of **H3** solutions, even at concentration close to 10^{-5} M, caused the formation of extremely heterogeneous mixtures inferable to the precipitation of the cavitand. **F1** revealed to be completely soluble only in oDCB/HFE-7200 mixtures but its promiscuous solubility in chlorinated and perfluorinated solvents hampered its applicability. From the first observations, cavitand **H1** afforded a higher stabilization of two- and three-phases emulsion and its behavior in biphasic H-W systems was further analyzed. Preliminary interfacial tension measurements were made using the pendant-drop method (ramé-hart Model 500 Advanced Goniometer). Surface tensions measurements were performed by fitting droplet shape every 1 s until the interfacial tension approached the equilibrium or the droplet became unstable. Instrumental setting allowed the study of only pure liquids so the behavior of **H1** in oDCB and Hexanes was studied separately (Figure 3.6).

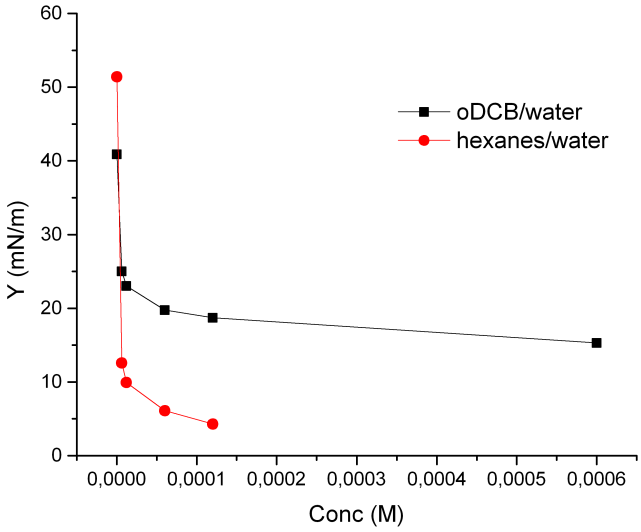

Figure 3.6 *Interfacial tension as function of **H1** concentration in oDCB (black) and hexanes (red) droplets in distilled water. Concentration values for hexanes solutions are not precise as related to the dilution of a saturated solution of **H1**.*

The oDCB–water interfacial tension was measured to be 41 mN m^{-1}, while hexane–water interfacial tension was found to be 51 mN m^{-1}. Unexpectedly, cavitand **H1** revealed a pronounced capability for hydrocarbon droplets stabilization in water, even in the absence of guests. Interestingly, the cavitand was found to stabilized oil-in-water (o/w) dispersion when solubilized in the inner phase (anti-Bancroft behavior), without any external surfactants. This observation can be rationalized considering the geometry and packing properties of the molecule: the large optimal surface area of the hydrophilic head has a prominent role compared to hydrocarbon chains volume.[11]
To prove that guest complexation can effectively alter the interfacial tension between H-W phases, we evaluated droplet shape variation in water solutions of **N-Me-L-Lys** and **P123**. Considering that measurements in hexanes-water systems were strongly affected by the poor solubility of **H1** and the high instability of hanging droplets, we decided to limit our study to oDCB solutions (Figure 3.7).

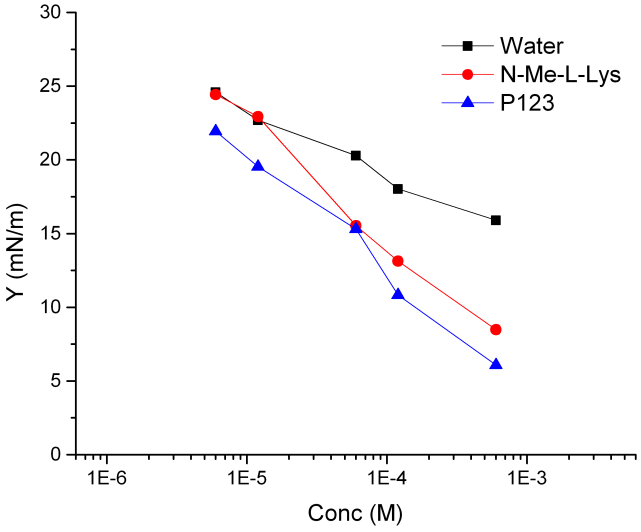

Figure 3.7 *Interfacial tension as function of **H1** concentration in oDCB with water (black), **N-Me-L-Lys** $6{\cdot}10^{-4}$ M (red) and **P123** $2{\cdot}10^{-4}$ M (blue) as external phase. Measured tensions for pure oDCB are 41 mN m^{-1} (water), 40 mN m^{-1} (**N-Me-L-Lys**) and 35.5 mN m^{-1} (**P123**).*

Interestingly **P123** was found to slightly stabilize H-phase even in the absence of cavitands (From 41 to 35.5 mN m^{-1}). For concentration of **H1** higher than $1{\cdot}10^{-5}$ M we observed a significant increase of **H1** effectiveness in the presence of guests, but discrimination between the two analytes reveled to be difficult.

Starting from these promising results we prepared stable complex emulsions stabilized by **H1**. To obtain Janus type droplets we emulsified a 1:1 mixture of **H1** $2{\cdot}10^{-5}$ M in hexanes/oDCB 99:1 and perfluorohexanes in water containing 0.1% of Zonyl (Figure 3.8). Lower concentrations of cavitand afforded H-phase encapsulation, while a higher content of **H1** provided droplets with F/H/W morphology also if more concentrated Zonyl solutions (up to 1%) were used.

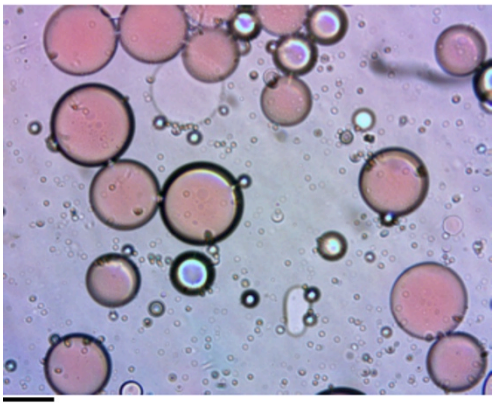

Figure 3.8 *Janus-type droplets obtained mixing 500 µL of Zonyl 0.1% in water with 100 µL of a 1:1 mixture of* ***H1*** *0.012 mM in oDCB 1% in hexanes and perfluorohexane, scale bar: 100 µm.*

However, addition of both analytes failed to evidence any morphology changes even after 12 hours (Table 3.2). We modified our emulsions replacing hexanes/perfluorohexanes with heptane/FC 770, allowing us to work at room temperature, and water with phosphate buffered saline (PBS). For all tested systems droplets maintained their Janus conformation.

	H phase	F phase	W phase	Ratio	Addition	
I	**H1** $1.2{\cdot}10^{-5}$ M in hex/oDCB	Perfluoro-hexanes	Zonyl 0.1%	1:1:10	1 eq **P123**	✗
II	**H1** $1.2{\cdot}10^{-5}$ M in hex/oDCB	Perfluoro-hexanes	Zonyl 0.1%	1:1:10	10 eq **NMeLys**	✗
III	**H1** $1.2{\cdot}10^{-5}$ M in hex/oDCB	Perfluoro-hexanes	Zonyl 0.1%	1:1:10	water	✗

Table 3.2 *Analytes additions to Janus-type emulsion stabilized by* ***H1****. No visible changes are indicated with (✗).*

3.2.3 Systems Based on Water-soluble Cavitands

In reconfigurable complex emulsions reported by Swager and co-workers the modification of surfactant effectiveness happens in the bulk. The subsequent interfacial tension variation is a consequence of surfactant shell reorganization *via* interface-bulk equilibria. In designed sensing platforms reported in the previous paragraph, the analyte must diffuse from the bulk to the interface and the recognition events have to occur at the interface in order to modify droplet morphology. To avoid analyte diffusion effects and replicate the configuration of dynamic systems present in literature, we decided to synthesize water-soluble cavitands as surfactants. This expedient allowed us to move the recognition events from droplet interfaces to the exterior water phase, where analytes were added.

In analogy with water-soluble tetraphosphonate cavitand bearing four pyridinium cations (**W3**, for the synthesis see Chapter 2) used for amino acids complexation studies, we decided to introduce four sulfates groups at the lower rim of our receptor. The four negative charges were necessary for the cavitand to be used as additive in SDS/Zonyl systems. Tiiii cavitand with four sulfates (**W1**) was synthesized in five steps from tetrahydroxyl footed resorcinarene,[12] with 55% overall yield (Scheme 3.5).

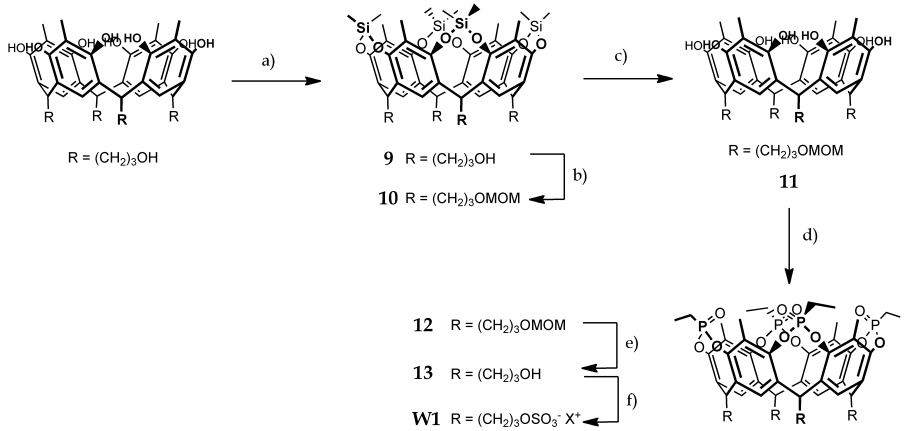

Scheme 3.5 *Synthesis of sulfate-footed tetraphosphonate cavitand* ***W1****: a) $(CH_3)_2SiCl_2$, Pyridine, 100°C, 3h, 85%; b) chloromethyl methyl ether, DIPEA, DMF, 40°C, 24 h, 97%; c) HF aq., DMF, 50°C, 12 h, 96%; d) (1) $EtPCl_2$, Py, 70°C, 3 h; (2) H_2O_2 35%, r.t, 30 min, 60% (over two steps); e) HCl 37%, $CHCl_3$/MeOH, 40°C, 12 h, 96%; f) $NMe_3{\cdot}SO_3$ complex, DMF, 50°C, 6 h, quant.*

The key step was the stereospecific introduction of four inward phosphonate bridges at the upper rim of the resorcinarene. To react phenolic groups with dichloroethylphosphine without affecting the lower rim, an orthogonal protection of aryl and aliphatic hydroxyl groups was required. The upper rim was initially protected through bridging reaction with dichlorodimethylsilane, affording cavitand **9**. The four aliphatic hydroxyl groups were protected as methoxymethyl (MOM) ethers (step b), then the selective deprotection of siloxanes with hydrofluoric acid afforded MOM-protected resorcinarene **11**. Bridging reaction with dichloroethylphosphine in pyridine gave P(III) intermediate, which was oxidized *in situ* with hydrogen peroxide to afford cavitand **12**. Finally, deprotection of hydroxyl groups at the lower rim under acidic conditions (step e), followed by reaction with sulfur trioxide pyridine complex, afforded water-soluble cavitand **W1**.

The cavitand was characterized by NMR spectroscopy and ESI-MS spectrometry and its ability to behave as surfactant was tested in biphasic and triphasic systems. In both cases compound **W1** failed to stabilize the H-phase and was used as additive in SDS/Zonyl based emulsions. However, any attempts to modify droplet morphology upon addition of ***N*-Me-L-Lys** and **P123** failed to evidence significant changes (See Experimental Section, Table S3.1). The origin of this behavior may be ascribed to the presence of polar groups in both sides of the molecule. In fact, in an optimal design of the cavitand-based surfactant, charged groups should be placed at the upper rim.[13] This setting allows resorcinarene scaffold and tails to act as the hydrophilic part of an amphiphilic molecule and to mimic SDS behavior in emulsions.

Following these considerations, we synthesized cavitand **W2**, bearing four sulfates groups at the upper rim, in four steps from resorcinarene **4** with 12% overall yield (Scheme 3.6). Mannich reaction with alcohols represents a straightforward strategy for the functionalization of resorcinarene apical positions.[14] Iminodiacetic acid-catalyzed reaction of **4** with 2-allyloxyethanol and formaldehyde afforded resorcinarene **14** with four allyl-protected hydroxyl groups in apical position. Protection of aliphatic alcohol allowed bridging of resorcinarene phenols with dichloroethylphosphine and the subsequent *in situ* oxidization with hydrogen peroxide afforded tetraphosphonate cavitand **15**. Pd-catalyzed deprotection, using 1,3-dimethylbarbituric acid as scavenger, gave tetrahydroxyl cavitand **16**. In the last step, reaction of **16** with sulfur trioxide pyridine complex, afforded cavitand **W2**.

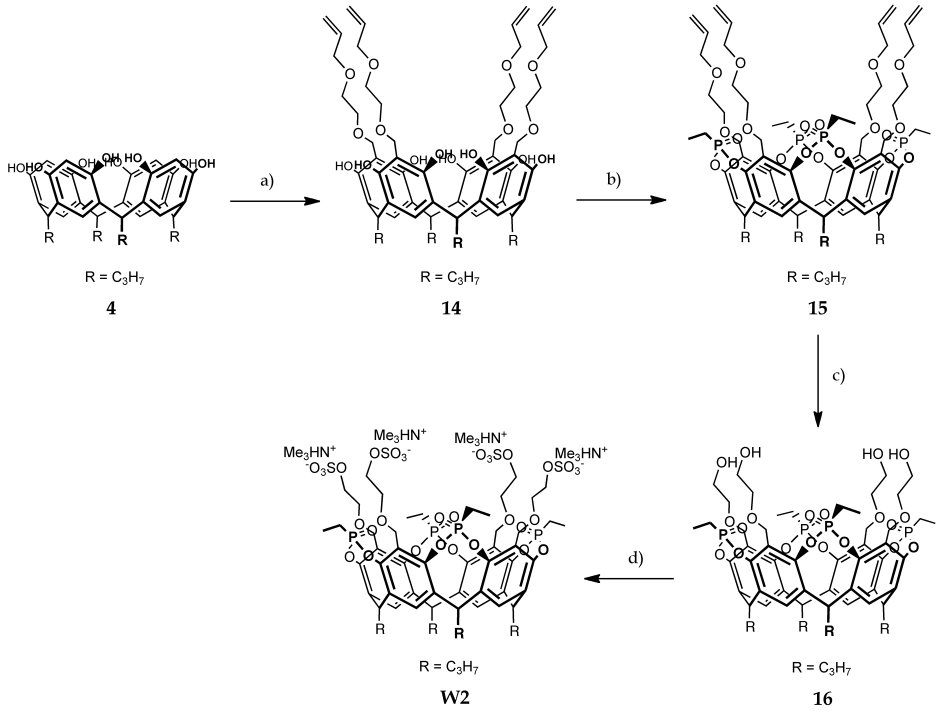

Scheme 3.6 *Synthesis of tetrasulfate-functionalized tetraphosphonate cavitand* ***W2****: a) 2-allyloxyethanol, CH_2O aq. 37%, iminodiacetic acid, acetonitrile, 84°C, 12 h, 33%; b) (1) $EtPCl_2$, Py, 80°C, 3 h; (2) H_2O_2 35%, r.t, 1 h, 89% (over two steps); c) $Pd(PPh_3)_4$, 1,3-dimethylbarbituric acid, CH_2Cl_2/MeOH, r.t., 12 h, 56%; d) $NMe_3{\cdot}SO_3$ complex, DMF, 50°C, 12 h, 74%.*

The cavitand was characterized by ESI-MS spectrometry, ^{1}H NMR and ^{31}P NMR spectroscopy. Water solubility revealed to be low, but in diluted water solutions ($6{\cdot}10^{-5}$ M) **W2** was found to stabilize oil-in-water emulsions. In combination with Zonyl (from 0.01% to 1%) complex emulsion with the H-phase encapsulated in the F-phase were obtained. For sensing experiments, Janus droplets were prepared mixing cavitand **W2** with SDS and Zonyl (See Experimental Section, Table S3.2). Also in this case, addition of ***N*-Me-L-Lys** and **P123** did not afford any variation of emulsion morphology.

3.2.4 Sensing Systems Based on Surfactant Displacement

Guest displacement is a powerful tool in supramolecular host-guest sensing. Complexation of molecules able to form stronger interactions with the receptor is thermodynamically favored. By affecting guest complexation equilibria, the initial guest can be removed from the cavity and a new host-guest system, with

a higher association constant, is formed. We effectively applied this concept to biological remarkable analytes detection with tetraphosphonate cavitands.[15] Tiiii complexes with *N*-methylpyridinium salts shows an association constant one order of magnitude lower than *N*-methylammonium ones, both in non-polar and protic solvents.[16] When *N*-methylammonium salts are added to a solution containing the weaker complex, the pyridinium cation is released from the cavity. Interestingly, *N*-alkyl pyridinium salts are widely used as cationic surfactants. Encapsulation of less common *N*-methylpyridinium molecules bearing long aliphatic chains in 4 or 3 position may shields the positive charge lowering surfactant effectiveness. Considering this assumption we synthesized the guest ***N*-Me-Py-C12**, bearing a *N*-methylated pyridinium moiety and an aliphatic chain. We tested two different displacement systems. In *System 1* the surfactant was complexed by hydrocarbon-soluble cavitands **H1** and encapsulated inside the droplets. We expected analytes complexation to release ***N*-Me-Py-C12**, increasing H-phase stabilization. *System 2* was based on the formation of a supramolecular surfactant, constituted by **W3**·***N*-Me-Py-C12**, with a different effectiveness compared to the free pyridinium salt. We expect the displacement of ***N*-Me-Py-C12** from the cavity, induced by the addition of an *N*-methylated ammonium salt, to alter H-phase interfacial tension.
We synthesized *N*-methylpyridinium-based surfactant ***N*-Me-Py-C12** in two steps, with 77% overall yield (Scheme 3.7).

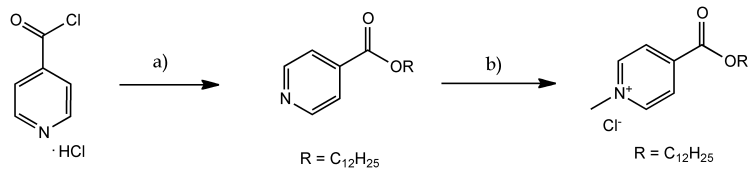

Scheme 3.7 *Synthesis of N-methylpyridinium-based surfactant **N-Me-Py-C12**: a) 1-dodecanol, TEA, CH_2Cl_2, r.t., 12 h, 85%; b) (1) CH_3I, acetonitrile, 84 °C, 12 h; (2) MeOH, Amberlite IRA-400, 91% (over two steps).*

Isonicotinoyl chloride was reacted with 1-dodecanol affording ester-functionalized pyridine **17**.[17] Methylation of **17** with iodomethane, followed by anion exchange, provided surfactant ***N*-Me-Py-C12**, which was characterized by ^{1}H NMR spectroscopy.

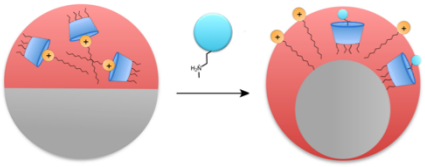

Figure 3.9 *Sketch of System 1, addition of an analyte causes droplet morphology change.*

In *System 1*, depicted in Figure 3.9, ***N*-Me-Py-C12** was complexed with an equimolar amount of **H1**. The surfactant was dispersed in oDCB and the solution became clear after addition of the receptor, proving that the complexation occurred. The solution was diluted with hexanes to reach 99:1 ratio of hexanes/oDCB. Emulsions were prepared mixing the complex containing solution plus perfluorohexanes (1:1) with 0.1% aqueous solution of Zonyl. Unfortunately these emulsions showed the lack of dynamicity typical of **H1** containing systems; no morphology variations were observed upon addition of ***N*-Me-L-Lys** and **P123** (even if ten equivalent were added).
Finally, we tested a system based on supramolecular surfactant cleavage (*System 2*). The controllable self-assembly and disassembly of these non-covalent amphiphilic molecules has been used to effectively tune vesicles and emulsions morphology.[18] A similar approach has been successfully applied to the detection of cholic acids by Fang and co-workers.[19]

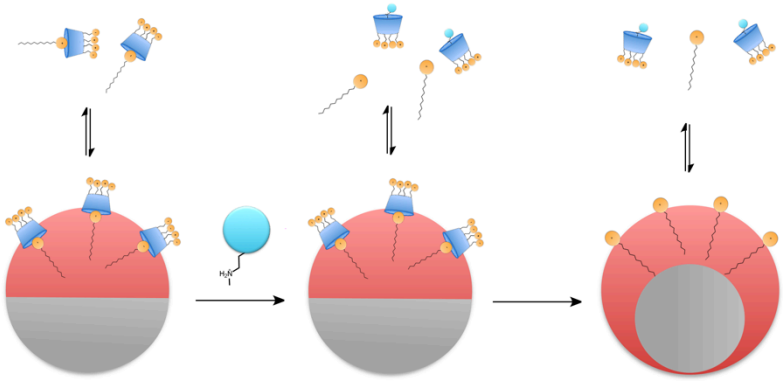

Figure 3.10 *Sketch of System 2, addition of an analyte causes supramolecular surfactant cleavage and the subsequent droplet morphology change.*

We initially prepare **W3·*N*-Me-Py-C12** mixing an equimolar amount of the components in water (Figure 3.10). Janus droplets were obtained emulsifying heptane/FC 770 with the solution and a proper amount of Zonyl. Also in this

case, addition of one equivalent of ***N*-Me-L-Lys** failed to cause any droplet morphology variation (See Experimental Section, Table S3.3).

3.3 Conclusions

Tetraphosphonate cavitand-based surfactants have been successfully introduced in complex emulsions. Cavitand **H1** was found to effectively stabilize oil-in-water dispersion when solubilized in the H-phase. Negatively charged cavitand **W2** showed to behave as surfactant in diluted water solutions but its complexation abilities toward *N*-methylated ammonium salts need to be further characterized. We pushed forward the design of our platform introducing the displacement of a *N*-methylpyridinium-based surfactant. All attempts to modify Janus-type droplet morphology of emulsion containing these surfactants were unsuccessful. The lack of dynamicity in tested systems might be explained considering that absorption/desorption of big molecules from an interface requires high energies and rigidifies the interface. Although this approach to methylation sensing in biological systems looks promising on paper, a deeper investigation of complexation role in the modification of interfacial tensions equilibria need be done before moving to applications.

3.4 Acknowledgments

Special thanks to Prof. Timothy M. Swager and all his group, in particular Dr. Lauren Zarzar and "Colloids" subgroup members, from Department of Chemistry, Massachusetts Institute of Technology, Cambridge (USA).

3.5 Experimental Section

1-Hexadecanal (1)
Pyridinium chlorochromate (2.66 g, 12.4 mmol) was suspended in 50 mL of CH_2Cl_2 and sodium acetate (1.02 g, 12.4 mmol) was added. To the vigorously stirred mixture, a solution of 1-hexadecanol (2.00 g, 8.25 mmol) in 25 mL of CH_2Cl_2 was added dropwise at 0 °C. The reaction was kept at room temperature for 4 h. The brown precipitate was filtered through a pad of silica gel and washed with Et_2O (150 mL). The solvent was removed under reduced pressure affording pure compound **1** (1.95 g, 8.1 mmol, 98%) as a white solid.
^{1}H NMR (Acetone-d_6, 400 MHz): δ (ppm) = 9.74 (t, 1H, J=1.7 Hz, $CH_2C\mathbf{H}O$), 2.44 (td, 2H, J=7.3 Hz, J=1.7 Hz, $C\mathbf{H_2}CHO$), 1.61 (m, 2H, $C\mathbf{H_2}CH_2CHO$), 1.31 (m, 24H, -$C\mathbf{H_2}$-), 0.89 (t, 3H, J=6.7 Hz, $C\mathbf{H_3}$).

Resorcinarene [$C_{15}H_{31}$, H] (2)
Resorcinol (0.89 g, 8.1 mmol) was dissolved in 5 mL of EtOH and a 37% solution of HCl (1mL, 12 mmol) was slowly added at 0 °C. At the same temperature a solution of aldehyde **1** (1.95 g, 8.1 mmol) in 20 mL of EtOH was added dropwise. The mixture was allowed to warm over 90 min and then heated at 80 °C for 4 h. After cooling, the white precipitate was filtered and washed with cold EtOH. Recrystallization from EtOH afforded resorcinarene **2** as a white solid (1.91 g, 1.4 mmol, 71%).
^{1}H NMR (Acetone-d_6, 400 MHz): δ (ppm) = 8.47 (s, 8H, O**H**), 7.55 (s, 4H, Ar$\mathbf{H_{up}}$), 6.25 (s, 4H, Ar$\mathbf{H_{down}}$), 4.32 (t, 4H, J=7.9 Hz, C**H**CH_2), 2.30 (m, 8H, CHC$\mathbf{H_2}$), 1.50-1.23 (m, 104H, -$C\mathbf{H_2}$-), 0.90 (t, 12H, J=7.0 Hz, $CH_2C\mathbf{H_3}$).
MALDI-TOF: calculated for $C_{88}H_{144}O_8Na$ $[M+Na]^+$ *m/z* = 1352.076, found *m/z* = 1352.141.

Tiiii [$C_{15}H_{31}$, H, Et] (H1)
To a solution of resorcinarene **2** (0.5 g, 0.38 mmol) in 25 mL of pyridine, dichloroethylphosphine (0.172 mL, 1.65 mmol) was added. The mixture was heated at 80 °C for 3 h. After cooling at 0 °C, 3 mL of aqueous 35% H_2O_2 were added and the mixture was allowed to warm at room temperature over 1 h. The reaction was quenched with 200 mL of water and the precipitate was filtered, washed with water and dried. Recrystallization from acetonitrile afforded the pure cavitand **H1** (0.256 g, 0.14 mmol, 37%) as a white solid.
^{1}H NMR ($CDCl_3$, 400 MHz): δ (ppm) = 8.66 (s, 4H, Ar$\mathbf{H_{up}}$), 6.56 (s, 4H, Ar$\mathbf{H_{down}}$), 4.48 (t, 4H, J=7.9 Hz, C**H**CH_2), 2.90 (m, 8H, CHC$\mathbf{H_2}$), 2.18 (m, 8H,

P(O)C**H₂**CH₃), 1.55-1.11 (m, 116H, P(O)CH₂C**H₃** + -C**H₂**-), 0.90 (t, 12H, J=7.0 Hz, CH₂C**H₃**).
³¹P NMR ($CDCl_3$, 162 MHz): δ (ppm) = 23.7 (s, P=O).
MALDI-TOF: calculated for $C_{96}H_{157}O_{12}P_4$ $[M+H]^+$ *m/z* = 1627.065, found *m/z* = 1627.377; calculated for $C_{96}H_{160}NO_{12}P_4$ $[M+NH_4]^+$ *m/z* = 1644.092, found *m/z* = 1644.188; calculated for $C_{96}H_{156}O_{12}P_4Na$ $[M+Na]^+$ *m/z* = 1649.047, found *m/z* = 1649.190; calculated for $C_{96}H_{156}O_{12}P_4K$ $[M+K]^+$ *m/z* = 1665.021, found *m/z* = 1665.084.

Resorcinarene [C_6H_{13}, H] (3)
To a solution of resorcinol (15 g, 0.14 mol) in 85 mL of MeOH a 37% solution of HCl (20 mL, 0.24 mol) was slowly added at 0 °C. At the same temperature heptaldehyde (19 mL, 0.14 mol) was added dropwise over 45 min. The mixture was vigorously stirred at 50 °C for 5 days. Water was added and the orange precipitate was filtered, washed with water, dried under vacuum and recrystallized twice from MeOH. Resorcinarene **3** was obtained as a pale yellow powder (16 g, 0.02 mol, 57%).
¹H NMR (Acetone-d_6, 300 MHz): δ (ppm) = 8.46 (s, 8H, O**H**), 7.57 (s, 4H, Ar**H$_{up}$**), 6.25 (s, 4H, Ar**H$_{down}$**), 4.32 (t, 4H, J=7.8 Hz, C**H**CH₂), 2.30 (q, 8H, J=7.8 Hz, CHC**H₂**) 1.37-1.30 (m, 32H, -C**H₂**-), 0.90 (t, 12H, J=6.6 Hz, CH₂C**H₃**).
ESI-MS: *m/z* = 825 $[M+H]^+$, 847 $[M+Na]^+$.

Tiiii [C_6H_{13}, H, Et] (H2)
To a solution of resorcinarene **3** (0.3 g, 0.36 mmol) in 5 mL of pyridine, dichloroethylphosphine (0.166 mL, 1.60 mmol) was added. The solution was stirred at 80 °C for 3 h. The mixture was cooled at 0°C and 2 mL of 35% aqueous H_2O_2 were added. The reaction was stirred at room temperature for 1 h and then quenched with 100 mL of water. CH_2Cl_2 (100 mL) was added and the organics were extracted and washed twice with water. The solvent was removed under reduce pressure affording cavitand **H2** as a white solid (0.302 g, 0.27 mmol, 74%).
¹H NMR ($CDCl_3$, 400 MHz): δ (ppm) = 7.17 (s, 4H, Ar**H$_{up}$**), 6.87 (s, 4H, Ar**H$_{down}$**), 4.59 (t, 4H, J=7.9 Hz, C**H**CH₂), 2.26 (m, 8H, CHC**H₂**), 2.13 (m, 8H, P(O)C**H₂**CH₃), 1.55-1.10 (m, 44H, P(O)CH₂C**H₃** + -C**H₂**-), 0.93 (t, 12H, J=7.0 Hz, CH₂C**H₃**).
³¹P NMR ($CDCl_3$, 162 MHz): δ (ppm) = 24.5 (s, P=O).
ESI-MS: *m/z* = 1143.7 $[M+Na]^+$.

Resorcinarene [C_3H_7, H] (4)

Resorcinol (15.0 g, 0.14 mol) was dissolved in 50 mL of MeOH and a 37% solution of HCl (20 mL, 0.24 mol) was slowly added at 0 °C. At the same temperature a solution of butyraldehyde (12.3 mL, 0.14 mol) in 30 mL of MeOH was added dropwise. The mixture was allowed to warm over 30 min and heated at 50 °C for 5 days. After cooling, water (500 mL) was added and the precipitate was filtered, washed with water and dried. The crude was recrystallized twice from MeOH affording resorcinarene **15** as a yellowish solid (12.3 g, 0.02 mol, 55%).

^{1}H NMR (Acetone-d_6, 400 MHz): δ (ppm) = 8.45 (s, 8H, O**H**), 7.60 (s, 4H, Ar$\mathbf{H_{up}}$), 6.25 (s, 4H, Ar$\mathbf{H_{down}}$), 4.35 (t, 4H, J=7.9 Hz, C**H**CH_2), 2.30 (q, 8H, J=7.5 Hz, CHC$\mathbf{H_2}CH_2$), 1.33 (sext, 8H, J=7.5 Hz, $CH_2C\mathbf{H_2}CH_3$), 0.90 (t, 12H, J=7.3 Hz, $CH_2C\mathbf{H_3}$).

ESI-MS: *m/z* = 655.7 $[M-H]^-$.

Tiiii [C_3H_7, H, Et] (H3)

To a solution of resorcinarene **4** (0.5 g, 0.76 mmol) in 8 mL of pyridine, dichloroethylphosphine (0.348 mL, 3.35 mmol) was added. The solution was stirred at 80 °C for 3 h. The mixture was cooled at 0°C and 2 mL of 35% aqueous H_2O_2 were added. The reaction was stirred at room temperature for 1 h. Water (150 mL) was added and the precipitate was filtered, washed with water and dried. Cavitand **H3** was obtained as a white solid (0.565 g, 0.59 mmol, 78%).

^{1}H NMR ($CDCl_3$, 400 MHz): δ (ppm) = 7.16 (s, 4H, Ar$\mathbf{H_{up}}$), 6.87 (s, 4H, Ar$\mathbf{H_{down}}$), 4.64 (t, 4H, J=7.9 Hz, C**H**CH_2), 2.26 (q, 8H, J=7.8 Hz, CHC$\mathbf{H_2}$), 2.12 (m, 8H, P(O)C$\mathbf{H_2}CH_3$), 1.47-1.30 (m, 20H, P(O)$CH_2C\mathbf{H_3}$ + -C$\mathbf{H_2}$-), 0.93 (t, 12H, J=7.4 Hz, $CH_2C\mathbf{H_3}$).

^{31}P NMR ($CDCl_3$, 162 MHz): δ (ppm) = 22.7 (s, P=O).

ESI-FT-ICR-MS: calculated for $C_{48}H_{60}O_{12}P_4Na$ $[M+Na]^+$ *m/z* = 975.293, found *m/z* = 975.291.

1H,1H,2H,2H,3H,4H,4H-heptadecafluoro-3-iododododecan-1-ol (5)

In a round-bottom flask, heptadecafluoro-1-iodooctane (2.42 mL, 9.1 mmol) was mixed with 3-buten-1-ol (0.945 mL, 10.1 mmol). The solution was degassed (3 × freeze-pump-thaw) and AIBN (0.075 g, 0.46 mmol) was added. The mixture was heated at 76 °C for 2 h. A second portion of AIBN (0.075 g, 0.46 mmol) was added and the heating was maintained for 3 h. The solid mass was solubilized in hot hexane (80 mL) and passed through filter paper. Pure alcohol **5** was collected as a white solid upon cooling the filtrate (4.297 g, 6.95 mmol, 76%).

^{1}H NMR ($CDCl_3$, 400 MHz): δ (ppm) = 4.56 (m, 1H, C**H**I), 3.87 (m, 2H, C**H_2**OH), 2.95 (m, 2H, C**H_2**CH_2OH), 2.06 (m, 2H, CF_2C**H_2**CHI).
^{19}F NMR ($CDCl_3$, 376 MHz): δ (ppm) = -80.7 (t, 3F, J_{F-F}=10 Hz, C**F_3**), -111.5 (dt, J_{F-F} = 270 Hz, J_{F-F} = 15 Hz, 1F, C**F_2**CH_2), -114.2 (dt, J_{F-F} = 270 Hz, J_{F-F} = 15 Hz, 1F, C**F_2**CH_2), -121.5 (m, 2F), -121.9 (m, 4F), -122.7 (m, 2F), -123.6 (m, 2F), -126.1 (m, 2F).

1H,1H,2H,2H,3H,3H,4H,4H-heptadecafluorododecan-1-ol (6)
To a suspension of compound **5** (3.0 g, 4.9 mmol) in 15 mL of toluene, tributyltin hydride (2.6 mL, 9.7 mmol) was added. After degassing, AIBN was added (0.08 g, 0.5 mmol) and the mixture was heated at 70 °C for 4 h. The solvent was removed under reduced pressure and flash column chromatography (Hex/EtOAc 8:2) afforded the pure alcohol **6** as a white solid (2.08 g, 4.2 mmol, 86%).
^{1}H NMR ($CDCl_3$, 400 MHz): δ (ppm) = 3.72 (m, 2H, C**H_2**OH), 2.14 (m, 2H, CF_2C**H_2**), 1.81-1.61 (m, 4H –C**H_2**-).
^{19}F NMR ($CDCl_3$, 376 MHz): δ (ppm) = -80.7 (t, 3F, J_{F-F}=10 Hz, C**F_3**), -114.4 (t, 2F, J_{F-F}=13 Hz, C**F_2**CH_2), -121.7 (m, 2F), -121.9 (m, 4F), -122.7 (m, 2F), -123.5 (m, 2F), -126.1 (m, 2F).

1H,1H,2H,2H,3H,3H-heptadecafluorododecanal (7)
To a suspension of Dess-Martin periodinane (1.93 g, 4.5 mmol) in 15 mL of CH_2Cl_2, a solution of alcohol **6** (2.04 g, 4.1 mmol) in 25 mL of CH_2Cl_2 was slowly added over 15 min. The reaction was stirred at room temperature for 2 h then 50 mL of Et_2O were added. The mixture was poured into a solution of $Na_2S_2O_3$ (5.03 g, 31.8 mmol) in 100 mL of saturated aqueous $KHCO_3$. The organic phase was extracted, washed twice with saturated aqueous $KHCO_3$ and dried over $MgSO_4$. The solvent was removed under reduced pressure affording pure aldehyde **7** (1.84 g, 3.75 mmol, 91%) as a clear oil.
^{1}H NMR ($CDCl_3$, 400 MHz): δ (ppm) = 9.82 (s, 1H, C**H**O), 2.62 (m, 2H, C**H_2**CHO), 2.15 (m, 2H, CF_2C**H_2**), 1.98 (m, 2H, -C**H_2**-).
^{19}F NMR ($CDCl_3$, 376 MHz): δ (ppm) = -80.8 (t, 3F, J_{F-F}=10 Hz, C**F_3**), -114.6 (t, 2F, J_{F-F}=14 Hz, C**F_2**CH_2), -121.8 (m, 2F), -122.0 (m, 4F), -122.8 (m, 2F), -123.6 (m, 2F), -126.2 (m, 2F).

Resorcinarene [$C_3H_6R_{f8}$, H] (8)
To a solution of resorcinol (0.112 g, 1 mmol) in 2 mL of EtOH, a 37% solution of HCl (0.3 mL, 4 mmol) was slowly added at 0 °C. At the same temperature a solution of aldehyde **7** (0.500 g, 1 mmol) in 3 mL of EtOH was added dropwise.

The mixture was allowed to warm over 90 min and then heated at 80 °C for 4 h. After cooling, the solvent was removed and the crude was purified by flash column chromatography (Hex/EtOAc 1:3). Resorcinarene **8** was obtained as a white solid (0.136 g, 0.06 mmol, 23%).

^{1}H NMR (CD_3OD, 400 MHz): δ (ppm) = 7.19 (s, 4H, Ar**H$_{up}$**), 6.27 (s, 4H, Ar**H$_{down}$**), 4.37 (t, 4H, J=7.8 Hz, C**H**CH_2), 2.31-2.16 (m, 16H, CHC**H$_2$** + C**H$_2$**CF_2), 1.61 (m, 8H, -C**H$_2$**-).

^{19}F NMR (CD_3OD, 376 MHz): δ (ppm) = -82.6 (t, 3F, J_{F-F}=10 Hz, C**F$_3$**), -115.6 (t, 2F, J_{F-F}=15 Hz, C**F$_2$**CH_2), -122.8 (m, 2F), -123.1 (m, 4F), -123.9 (m, 2F), -124.8 (m, 2F), -127.5 (m, 2F).

ESI-FT-Orbitrap-MS: calculated for $C_{72}H_{43}F_{68}O_8$ $[M-H]^-$ *m/z* = 2327.187, found *m/z* = 2327.181.

Tiiii [C$_3$H$_6$R$_{f8}$, H, Et] (F1)

Resorcinarene **8** (0.060 g, 0.025 mmol) was suspended in 5 mL of a 2:1 mixture of pyridine/α,α,α-trifluorotoluene and dichloroethylphosphine (0.012 mL, 0.11 mmol) was added. The mixture was heated at 80 °C for 3 h. After cooling, 0.5 mL of aqueous 35% H_2O_2 were added at 0 °C and the mixture was stirred for 1 h. The reaction was quenched with 20 mL of water and extracted with a 1:1 mixture of $CHCl_3$/HFE-7100. The organics were washed with water and the solvent was removed under reduced pressure. Cavitand **F1** (0.015 g, 0.006 mmol, 23%) was obtained as a white solid.

^{1}H NMR ($CDCl_3$, 400 MHz): δ (ppm) = 8.88 (s, 4H, Ar**H$_{up}$**), 6.59 (s, 4H, Ar**H$_{down}$**), 4.50 (t, 4H, J=8.0 Hz, C**H**CH_2), 3.11 (m, 8H, CHC**H$_2$**), 2.36 (m, 8H, C**H$_2$**CF_2), 2.21 (m, 8H, P(O)C**H$_2$**CH_3), 1.62 (m, 8H, $CHCH_2$C**H$_2$**), 1.43 (m, 12H, P(O)CH_2C**H$_3$**).

^{19}F NMR (CD_3OD, 376 MHz): δ (ppm) = -80.9 (t, 3F, J_{F-F}=10 Hz, C**F$_3$**), -115.0 (m, 2F, C**F$_2$**CH_2), -122.0 (m, 2F), -122.2 (m, 4F), -123.0 (m, 2F), -123.3 (m, 2F), -126.3 (m, 2F).

^{31}P NMR ($CDCl_3$, 162 MHz): δ (ppm) = 28.9 (s, P=O),

MALDI-TOF: calculated for $C_{80}H_{57}F_{68}O_{12}P_4$ $[M+H]^+$ *m/z* = 2625.171, found *m/z* = 2625.125; calculated for $C_{80}H_{56}F_{68}O_{12}P_4Na$ $[M+Na]^+$ *m/z* = 2647.153, found *m/z* = 2647.135; calculated for $C_{80}H_{56}F_{68}O_{12}P_4K$ $[M+K]^+$ *m/z* = 2663.127, found *m/z* = 2663.124.

Tetra(dimethylsiloxy)-bridged cavitand (9)

Tetrahydroxy-footed resorcinarene (4.5 g, 5.80 mmol) was dissolved in 70 mL of dry pyridine. The solution was cooled at 0°C and $(CH_3)_2SiCl_2$ (8.55 mL, 70.2 mmol) was added. The mixture was stirred at room temperature for 20 min and

heated at 100 °C for 3 h. The reaction was cooled down to room temperature and quenched with MeOH (50 mL). The obtained precipitate was filtered, wash with methanol and dried, to give the white product **9** (4.9 g, 85% yield).
^{1}H NMR ($CDCl_3$, 300 MHz): δ (ppm) = 7.47 (s, 4H, Ar**H**), 4.54 (t, 4H, J=7.9 Hz, Ar**CH**), 3.66 (bt, 8H, **CH_2**OH), 2.46-2.43 (m, 8H, **CH_2**CH_2CH_2OH), 1.87 (s, 12H, Ar**CH_3**), 1.50-1.46 (m, 8H, CH_2**CH_2**CH_2OH), 0.46 (s, 12H, Si**CH_{3out}**), -0.73 (s, 12H, Si**CH_{3in}**).
ESI-MS: *m/z* = 1002.5 $[M+H]^+$.

Tetra(dimethylsiloxy)-bridged MOM protected cavitand (10)
To a solution of cavitand **9** (2.2 g, 2.20 mmol) in 25 mL of dry DMF, N,N-diisopropylethylamine (5.77 mL, 32.97 mmol) and chloromethyl methyl ether (1.67 mL, 22.0 mmol) were added. The mixture was stirred at 40 °C for one day. The reaction was cooled down to room temperature and the solvent was evaporated under reduced pressure. The obtained precipitate was wash with water and dried, to give a beige product (2.5 g, 97% yield).
^{1}H NMR ($CDCl_3$, 300 MHz): δ (ppm) = 7.17 (s, 4H, Ar**H**), 4.63 (s, 8H, O**CH_2**O), 4.62 (t, 4H, J=8.2 Hz, Ar**CH**), 3.58 (t, 8H, J=6.3 Hz, CH_2CH_2**CH_2**O), 3.38 (s, 12H, O**CH_3**), 2.29 (q, J= 7.1 Hz, 8H, **CH_2**CH_2CH_2O), 1.90 (s, 12H, Ar**CH_3**), 1.58 (quint, 8H, J=7.1 Hz, CH_2**CH_2**CH_2O), 0.51 (s, 12H, Si**CH_{3out}**), -0.69 (s, 12H, Si**CH_{3in}**).
ESI-MS: *m/z* = 1177.5 $[M+H]^+$.

Resorcinarene [C_3H_6OMOM, CH_3] (11)
To a solution of cavitand **10** (1.24 g, 1.05 mmol) in 15 mL of DMF, an aqueous 40% HF solution (1.2 mL, 11.54 mmol) was added. The suspension was stirred overnight at 50 °C. The product was precipitated by adding water to the reaction mixture. The white solid was filtered, washed with water and dried (0.95 g, 96% yield).
^{1}H NMR (DMSO-d_6, 300 MHz): δ (ppm) = 8.68 (s, 8H, Ar**OH**), 7.29 (s, 4H, Ar**H**), 4.53 (s, 8H, O**CH_2**O), 4.22 (t, 4H, J=7.7 Hz, Ar**CH**), 3.48 (t, 8H, J=6.4 Hz, CH_2CH_2**CH_2**O), 3.33 (s, 12H, O**CH_3**), 2.28 (m, 8H, **CH_2**CH_2CH_2O), 1.94 (s, 12H, Ar**CH_3**), 1.43 (m, 8H, CH_2**CH_2**CH_2O).
ESI-MS: *m/z* = 953.5 $[M+H]^+$.

Tiiii [C_3H_6OMOM, CH_3, Et] (12)
To a solution of resorcinarene **11** (0.77 g, 8.08 mmol) in 30 mL of dry pyridine, dichloroethylphosphine (0.344 mL, 3.31 mmol) was added under argon atmosphere. The solution was stirred at 70 °C for 3 h. The mixture was cooled at 0°C and 10 mL of 35% aqueous H_2O_2 were added. The reaction was stirred at

room temperature for 30 min and then quenched with 100 mL of water. The precipitate was filtered, washed with water and dried. The solid was dissolved in CH_2Cl_2 and precipitated with hexane. After filtration, cavitand **12** was obtained as white solid (0.68 g, 60% yield)

^{1}H NMR ($CDCl_3$, 400 MHz): δ (ppm) = 7.30 (s, 4H, Ar**H**), 4.88-4.80 (m, 12H, O**CH_2**O + Ar**CH**), 3.89 (t, 8H, J = 6.2 Hz, $CHCH_2CH_2$**CH_2**O), 3.61 (s, 12H, O**CH_3**), 2.46-2.42 (m, 8H, **CH_2**CH_2CH_2O), 2.29 (s, 12H, Ar**CH_3**), 2.29-2.225 (m, 8H, P(O)**CH_2**CH_3), 1.90-1.85 (quint, 8H, J=7.3 Hz, CH_2**CH_2**CH_2O), 1.66 (dt, 12H, J=7.7 Hz, J_{P-H}=21.0 Hz, P(0)CH_2**CH_3**).

^{31}P NMR ($CDCl_3$, 162 MHz): δ (ppm) = 23.1 (s, P=O).

ESI-MS: *m/z* = 1271.3 $[M+Na]^+$.

Tiiii [C_3H_6OH, CH_3, Et] (13)

Cavitand **12** (0.48 g, 0.3.8 mmol) was dissolved in 10 mL of MeOH and 5 mL of $CHCl_3$. A 37% solution of HCl (0.307 mL, 3.87 mmol) was added and the solution was stirred overnight at 40 °C. After evaporation of the solvent, the crude was dissolved in CH_2Cl_2 and precipitated with hexane. The solid was filtered and dried to give cavitand **13** as off white solid (0.4 g, 96% yield).

^{1}H NMR (DMSO-d_6, 400 MHz): δ (ppm) = 7.59 (s, 4H, Ar**H**), 4.47 (t, 4H, J=7.6 Hz, Ar**CH**), 3.49 (m, 8H, $CHCH_2CH_2$**CH_2**OH), 3.17 (d, 4H, CH_2**OH**), 2.43-2.40 (m, 8H, **CH_2**CH_2CH_2OH), 2.28–2.22 (dd, 8H, J=7.7 Hz, J_{P-H}=18.7 Hz, P(O)**CH_2**CH_3), 2.04 (s, 12H, Ar**CH_3**), 1.43-1.39 (m, 8H, CH_2**CH_2**CH_2OH), 1.33 (dt, 12H, J = 7.6 Hz, J_{P-H} = 21.0 Hz, P(O)CH_2**CH_3**).

^{31}P NMR (DMSO-d_6, 162 MHz): δ (ppm) = 23.5 (s, P=O).

ESI-MS: *m/z* = 1105.4 $[M+CH_3OH+H]^+$.

Tiiii [$C_3H_6OSO_3^-X^+$, CH_3, Et] (W1)

$NMe_3{\cdot}SO_3$ complex (0.234 g, 1.68 mmol) was added to a solution cavitand **13** (150 mg, 0.14 mmol) in dry DMF (10 mL). The mixture was stirred under nitrogen atmosphere at 50°C for 6 h. The solvent was removed under vacuum, the crude was dissolved in methanol and the solution left at 0°C for 1 h. The precipitate was filter and cavitand **W1** was recovered as white solid. Quantitative yield.

^{1}H NMR (D_2O, 400 MHz): δ (ppm) = 7.57 (s, 4H, Ar**H**), 4.64 (t, 4H, J=7.2 Hz, Ar**CH**), 4.10 (bm, 8H, $CHCH_2CH_2$**CH_2**OSO_3^-), 2.51 (m, 8H, **CH_2**$CH_2CH_2OSO_3^-$), 2.46 (dd, 8H, J=7.7, J_{P-H}=18.7 Hz, P(O)**CH_2**CH_3), 2.05 (s, 12H, Ar**CH_3**), 1.67 (m, 8H, CH_2**CH_2**$CH_2OSO_3^-$), 1.40 (dt, 12H, J=7.6 Hz, J_{P-H}=21.0 Hz, P(O)CH_2**CH_3**).

^{31}P NMR (D_2O, 162 MHz): δ (ppm) = 29.7 (s, P=O).

ESI-MS: *m/z* = 482.7 $[M-3HNMe_3]^{3-}$, 725.0 $[M-4HNMe_3+Na+K]^{2-}$.

Resorcinarene [C_3H_7, $CH_2OCH_2CH_2OAllyl$] (14)

To a suspension of resorcinarene **4** (0.5 g, 0.76 mmol) in 8 mL of acetonitrile, 2-allyloxyethanol (3.26 mL, 30.45 mmol) was added, followed by a 37% aqueous solution of formaldehyde (0.286 mL, 3.81 mmol). After the addition of iminodiacetic acid (0.051g, 0.38 mmol), the mixture was refluxed for 16 h. After cooling, chloroform (100 mL) was added and the organics were separated and washed with water (3 × 100 mL). The solvent was removed under reduced pressure and flash column chromatography (gradient from Hex/EtOAc 7:3 to Hex/EtOAc 1:1) afforded pure resorcinarene **14** as a white solid (0.283 g, 0.25 mmol, 33%).

^{1}H NMR ($CDCl_3$, 400 MHz): δ (ppm) = 8.60 (s, 8H, O**H**), 7.19 (s, 4H, Ar$\mathbf{H_{down}}$), 5.95 (m, 4H, $OCH_2C\mathbf{H}=CH_2$), 5.28 (m, 8H, $CH_2CH=C\mathbf{H_2}$), 4.84 (s, 8H, $ArC\mathbf{H_2}O$), 4.35 (t, 4H, J=7.9 Hz, $C\mathbf{H}CH_2$), 4.05 (dt, 8H, J=5.7 Hz, J=1.4 Hz, $OC\mathbf{H_2}CH=CH_2$), 3.71 (m, 8H, $ArCH_2OC\mathbf{H_2}CH_2O$), 3.62 (m, 8H, $ArCH_2OCH_2C\mathbf{H_2}O$), 2.30 (q, 8H, J=7.4 Hz, $CHC\mathbf{H_2}CH_2$), 1.32 (sext, 8H, J=7.4 Hz, $CH_2C\mathbf{H_2}CH_3$), 0.99 (t, 12H, J=7.4 Hz, $CH_2C\mathbf{H_3}$).

ESI-FT-ICR-MS: calculated for $C_{64}H_{92}NO_{16}$ $[M+NH_4]^+$ *m/z* = 1130.642, found *m/z* = 1130.642; calculated for $C_{64}H_{88}O_{16}Na$ $[M+Na]^+$ *m/z* = 1135.597, found *m/z* = 1135.603.

Tiiii [C_3H_7, $CH_2OCH_2CH_2OAllyl$, Et] (15)

To a solution of resorcinarene **14** (0.170 g, 0.15 mmol) in 8 mL of pyridine, dichloroethylphosphine (0.07 mL, 0.67 mmol) was added. The mixture was heated at 80 °C for 3 h. After cooling, 2 mL of aqueous 35% H_2O_2 were added at 0 °C and the mixture was stirred for 1 h. The reaction was quenched with water (100 mL) and the precipitate was filtered, washed with water and dried. Cavitand **15** was obtained as a white solid (0.191 g, 0.14 mmol, 89%).

^{1}H NMR ($CDCl_3$, 400 MHz): δ (ppm) = 7.13 (s, 4H, Ar$\mathbf{H_{down}}$), 5.91 (m, 4H, $OCH_2C\mathbf{H}=CH_2$), 5.27 (m, 8H, $CH_2CH=C\mathbf{H_2}$), 4.73-4.62 (m, 12H, $C\mathbf{H}CH_2$ + $ArC\mathbf{H_2}O$), 4.02 (d, 8H, J=5.7 Hz, $OC\mathbf{H_2}CH=CH_2$), 3.68 (m, 8H, $ArCH_2OC\mathbf{H_2}CH_2O$), 3.62 (m, 8H, $ArCH_2OCH_2C\mathbf{H_2}O$), 2.23 (m, 16H, J=7.4 Hz, $P(O)C\mathbf{H_2}CH_3$ + $CHC\mathbf{H_2}CH_2$), 1.53-1.32 (m, 20H, $P(O)CH_2C\mathbf{H_3}$ + $CH_2C\mathbf{H_2}CH_3$), 1.03 (t, 12H, J=7.4 Hz, $CH_2C\mathbf{H_3}$).

^{31}P NMR ($CDCl_3$, 162 MHz): δ (ppm) = 22.3 (s, P=O).

ESI-FT-ICR-MS: calculated for $C_{72}H_{104}NO_{20}P_4$ $[M+NH_4]^+$ *m/z* = 1426.610, found *m/z* = 1426.609; calculated for $C_{72}H_{100}O_{20}P_4Na$ $[M+Na]^+$ *m/z* = 1431.566, found *m/z* = 1431.571.

Tiiii [C_3H_7, $CH_2OCH_2CH_2OH$, Et] (16)

Cavitand **15** (0.378 g, 0.27 mmol) was dissolved in 20 mL of a degassed mixture of CH_2Cl_2/MeOH (1:3), followed by the addition of $Pd(PPh_3)_4$ (0.031 g, 0.027 mmol). 1,3-dimethylbarbituric acid (0.335 g, 2.15 mmol) was added and the reaction mixture was stirred at room temperature for 18 h. The solvent was removed under reduced pressure and the crude was recrystallized from toluene twice affording pure cavitand **16** as yellowish solid (0.188 g, 0.15 mmol, 56%).

^{1}H NMR (CD_3OD, 400 MHz): δ (ppm) = 7.55 (s, 4H, Ar**H$_{down}$**), 4.74 (t, 4H, J=7.9 Hz, C**H**CH_2), 4.59 (s, 8H, ArC**H$_2$**O), 3.66 (m, 8H, $ArCH_2OC$**H$_2$**CH_2OH), 3.55 (m, 8H, $ArCH_2OCH_2C$**H$_2$**OH), 2.47-2.29 (m, 16H, J=7.4 Hz, P(O)**CH_2**CH_3 + CHC**H$_2$**CH_2), 1.55-1.34 (m, 20H, $P(O)CH_2$**CH_3** + CH_2C**H$_2$**CH_3), 1.08 (t, 12H, J=7.4 Hz, CH_2C**H$_3$**).

^{31}P NMR (CD_3OD, 162 MHz): δ (ppm) = 25.8 (s, P=O).

ESI-FT-ICR-MS: *m/z* = 1266.55 $[M+NH_4]^+$.

Tiiii [C_3H_7, $CH_2OCH_2CH_2OSO_3^-Me_3NH^+$, Et] (W2)

To a solution of cavitand **16** (0.070 g, 0.056 mmol) in 8 mL of DMF, $NMe_3{\cdot}SO_3$ complex (0.062 g, 0.448 mmol) was added and the mixture was heated at 50 °C overnight. After cooling, the reaction was quenched with 5 mL of water and the solvent was evaporated under reduced pressure. The crude was dissolved in MeOH and precipitated from a 10:1 mixture of Hex/CH_2Cl_2, affording cavitand **W2** as a yellow solid (0.075 g, 0.042 mmol, 74%).

^{1}H NMR (CD_3OD, 400 MHz): δ (ppm) = 7.62 (s, 4H, Ar**H$_{down}$**), 4.77 (t, 4H, J=7.9 Hz, C**H**CH_2), 4.57 (s, 8H, ArC**H$_2$**O), 4.13 (m, 8H, CH_2C**H$_2$**OSO_3^-), 3.73 (m, 8H, $ArCH_2OC$**H$_2$**CH_2), 2.75 (s, 36H, (C**H$_3$**)$_3NH^+$), 2.55-2.40 (m, 16H, J=7.4 Hz, P(O)**CH_2**CH_3 + CHC**H$_2$**CH_2), 1.58-1.33 (m, 20H, $P(O)CH_2$**CH_3** + CH_2C**H$_2$**CH_3), 1.08 (t, 12H, J=7.2 Hz, CH_2C**H$_3$**).

^{31}P NMR (CD_3OD, 162 MHz): δ (ppm) = 27.9 (s, P=O).

ESI-MS: *m/z* = 391.1 $[M\text{-}4{\cdot}Me_3NH]^{4-}$.

Dodecyl isonicotinate (17)

To a solution of isonicotinoyl chloride (2.0 g, 10.7 mmol) in 50 mL of CH_2Cl_2, TEA (3.27 mL, 23.5 mmol) was slowly added at 0 °C. At the same temperature a solution of 1-dodecanol (2.63 mL, 11.6 mmol) in 15 mL of CH_2Cl_2 was added drop by drop over 30 min. The mixture was stirred at room temperature overnight, then filtered. The solvent was removed under reduced pressure and flash column chromatography (basic aluminum oxide, Hex/EtOAc 9:1) afforded pure ester **17** as colorless waxy oil (2.64 g, 9.1 mmol, 85%).

^{1}H NMR ($CDCl_3$, 400 MHz): δ (ppm) = 8.80 (XX' of a AA'XX' system, 2H, Ar**H**$_{2,6}$), 7.78 (AA' of a AA'XX' system, 2H, Ar**H**$_{3,5}$), 3.76 (t, 2H, J=6.7 Hz, OC**H**$_2$CH$_2$), 1.80 (quint, 2H, J=6.7 Hz, OCH$_2$C**H**$_2$), 1.51-1.22 (m, 18H, - C**H**$_2$-), 0.90 (t, 3H, J=6.7 Hz, C**H**$_3$).

4-((dodecyloxy)carbonyl)-1-methylpyridinium chloride (*N*-Me-Py-C12)
In a schlenk tube, iodomethane (0.73 mL, 11.8 mmol) was added to a solution of **17** (1.14 g, 3.9 mmol) in 25 mL of acetonitrile. The mixture was refluxed for 48 h. After cooling, the solvent was removed under reduced pressure and the crude was recrystallized from a hot mixture of acetone/EtOAc 1:3. The resulting yellow solid was solubilized in MeOH and passed through Amberlite IRA-400. Chloride salt ***N*-Me-Py-C12** was obtained as a white solid (1.22 g, 3.55 mmol, 91%).
^{1}H NMR (DMSO-d_6, 400 MHz): δ (ppm) = 9.17 (XX' of a AA'XX' system, 2H, Ar**H**$_{2,6}$), 8.49 (AA' of a AA'XX' system, 2H, Ar**H**$_{3,5}$), 4.44 (s, 3H, NC**H**$_3$), 4.39 (t, 2H, J=6.5 Hz, OC**H**$_2$CH$_2$), 1.75 (quint, 2H, J=7.6 Hz, OCH$_2$C**H**$_2$), 1.46-1.18 (m, 18H, -C**H**$_2$-), 0.86 (t, 3H, J=7.0 Hz, CH$_2$C**H**$_3$).
ESI-MS: *m/z* = 306.5 $[M\text{-}Cl]^+$.

Emulsions preparation and sensing attempts:

	H phase	F phase	W phase	Ratio	Addition	
I	Hept.	FC 770	1 mL SDS 0.1% + 0.5 mL Zonyl 0.1%	1:1:20	50 µL **W1** $1.2{\cdot}10^{-4}$ M + 15 µL **P123** $1.0{\cdot}10^{-4}$ M	✗
II	Hept.	FC 770	1 mL SDS 0.1% + 0.5 mL Zonyl 0.1%	1:1:20	50 µL **W1** $1.2{\cdot}10^{-4}$ M + 15 µL **NMeLys** $3.0{\cdot}10^{-3}$ M	✗
III	Hept.	FC 770	1 mL SDS 0.1% + 0.5 mL Zonyl 0.1%	1:1:20	50 µL **W1** $1.2{\cdot}10^{-4}$ M + 15 µL water	✗

Table S3.1 *Analytes additions to Janus-type emulsion containing **W1**. No visible changes are indicated with (✗). The same systems gave no results with PBS instead of water.*

	H phase	F phase	W phase	Ratio	Addition	
I	Hept.	FC 770	1 mL SDS 0.1% + 0.5 mL Zonyl 0.1% + 0.1 mL **W2** $6.0 \cdot 10^{-4}$ M	1:1:20	30 µL **P123** $1.0 \cdot 10^{-3}$ M	✗
II	Hept.	FC 770	1 mL SDS 0.1% + 0.5 mL Zonyl 0.1% + 0.1 mL **W2** $6.0 \cdot 10^{-4}$ M	1:1:20	15 µL **NMeLys** $3.0 \cdot 10^{-3}$ M	✗
III	Hept.	FC 770	1 mL SDS 0.1% + 0.5 mL Zonyl 0.1% + 0.1 mL **W2** $6.0 \cdot 10^{-4}$ M	1:1:20	30 µL water	✗

Table S3.2 *Analytes additions to Janus-type emulsion containing* ***W2****. No visible changes are indicated with (✗). The same systems gave no results with PBS instead of water.*

	H phase	F phase	W phase	Ratio	Addition	
I	Hept.	FC 770	(0.5 mL ***N*-Me-Py-C12** 0.1% + 1 eq **W3**) + 0.5 mL Zonyl 0.1%	1:1:20	50 µL **NMeLys** $3.0 \cdot 10^{-2}$ M	✗
II	Hept.	FC 770	(0.5 mL ***N*-Me-Py-C12** 0.1% + 1 eq **W3**) + 0.5 mL Zonyl 0.1%	1:1:20	50 µL water	✗

Table S3.3 *Analytes additions to Janus-type emulsion stabilized by supramolecular surfactant* ***W3*·*N*-Me-Py-C12****. No visible changes are indicated with (✗). The same systems gave no results with PBS instead of water.*

3.6 References

[1] a) B. D. Strahl, C. D. Allis, *Nature* **2000**, *403*, 41-45; b) T. Jenuwein, C. D. Allis, *Science* **2001**, *293*, 1074-1080.

[2] T. Kouzarides, *Cell* **2007**, *128*, 693-705.

[3] A. Izzo, R. Schneider, *Briefings Funct. Genom.* **2010**, *9*, 429-443.

[4] T. A. Egelhofer, A. Minoda, S. Klugman, K. Lee, P. Kolasinska-Zwierz, A. A. Alekseyenko, M. S. Cheung, D. S. Day, S. Gadel, A. A. Gorchakov, T. T. Gu, P. V. Kharchenko, S. Kuan, I. Latorre, D. Linder-Basso, Y. Luu, Q. Ngo, M. Perry, A. Rechtsteiner, N. C. Riddle, Y. B. Schwartz, G. A. Shanower, A. Vielle, V. Ahringer, S. C. R. Elgin, M. I. Kuroda, V. Pirrotta, B. Ren, S. Strome, P. J. Park, G. H. Karpen, R. D. Hawkins, J. D. Lieb, *Nature Struct. Mol. Biol* **2011**, *18*, 91-94.

[5] N. L. Young, P. A. DiMaggio, B. A. Garcia, *Cell. Mol. Life Sci.* **2010**, *67*, 3983-4000.

[6] S. A. Minaker, K. D. Daze, M. C. F. Ma, F. Hof, *J. Am. Chem. Soc.* **2012**, *134*, 11674-11680.

[7] L. D. Zarzar, V. Sresht, E. M. Sletten, J. A. Kalow, D. Blankschtein, T. M. Swager, *Nature* **2015**, *518*, 520-524.

[8] a) S. Shimizu, T. Kiuchi, N. Pan, *Angew. Chem. Int. Ed.* **2007**, *46*, 6442-6445; b) Q. Chu, K. O'Neal, M. Osipov, J. N. Ngwendson, S. J. Geib, S. G. Weber, D. P. Curran, *New. J. Chem.* **2010**, *34*, 2732-2734.

[9] L. J. Alvey, R. Meier, T. Soós, P. Bernatis, J. A. Gladysz, *Eur. J. Inorg. Chem.* **2000**, 1975-1983.

[10] L. Lévêque, M. Le Blanc, R. Pastor, *Tetrahedron Lett.* **1998**, *39*, 8857-8860.

[11] J. N. Israelachvili, *Intermolecular and Surface Forces (3rd Edition)* **2010**, Elsevier Science and technology, Saint Louis, MO, USA.

[12] L. Pirondini, D. Bonifazi, E. Menozzi, E. Wegelius, K. Rissanen, C. Massera, E. Dalcanale, *Eur. J. Org. Chem.* **2001**, 2311-2320.

[13] L. Trembleau, J. Rebek Jr., *Chem. Commun.* **2004**, 58–59.

[14] a) S. Nummelin, D. Falabu, A. Shivanyuk, K. Rissanen, *Org. Lett.* **2004**, *6*, 2869-2872; b) M. Urbaniak, J. Mattay, W. Iwanek, *Synth. Commun.* **2011**, *41*, 670–676.

[15] a) E. Biavardi, G. Battistini, M. Montalti, R. M. Yebeutchou, L. Prodi, E. Dalcanale, *Chem. Commun*. **2008**, 1638–1640; b) E. Biavardi, M. Favazza, A. Motta, I. L. Fragalà, C. Massera, L. Prodi, M. Montalti, M. Melegari, G. G. Condorelli, E. Dalcanale, *J. Am. Chem. Soc.* **2009**, *131*, 7447–7455.

[16] D. Menozzi, E. Biavardi, C. Massera, F.-P. Schmidtchen, A. Cornia, E. Dalcanale, *Supramol. Chem.* **2010**, *22*, 768–775.

[17] R. Hulst, I. Muizebelt, P. Oosting, C. van der Pol, A. Wagenaar, J. Šmisterová, E. Bulten, C. Driessen, D. Hoekstra, J. B. F. N. Engberts, *Eur. J. Org. Chem*. **2004**, 835-849.

[18] a) G.Yu, K. Jie, F. Huang, *Chem. Rev.* **2015**, *115*, 7240-7303; b) Q. He, Y.-F. Ao, Z.-T. Huang, D-X Wang, *Angew. Chem. Int. Ed.* **2015**, *54*, 11785-11790.

[19] J. Deng, X. Lu, C. Constant, A. Dogariuc, J. Fang, *Chem. Commun.* **2015**, *51*, 8912-8915.

CHAPTER 4

$TbPc_2$ OLIGOMERIZATION *VIA* OLEFIN METATHESIS REACTION

4.1 Introduction

In recent years single-molecule magnets (SMMs), functional molecules that show slow magnetization relaxation of purely molecular origin, have been widely studied as they couple classical magnetic properties with quantum effects. At liquid-helium temperatures these coordination compounds retain magnetization for long periods of time in the absence of external magnetic fields.[1] Single-molecule magnet behavior was observed for the first time by Gatteschi and co-workers in dodecanuclear mixed-valent III/IV manganese oxide cluster $Mn_{12}O_{12}(O_2CCH_3)_{16}(H_2O)_4$.[2] Since magnetic properties of this polymetallic cage were reported, a great variety of SMMs has been developed and studied.[3] The particular interest in these compounds arises not only from their intrinsic properties but also from the possibility to access outstanding technological applications. If we consider SMMs as analogues of classical bulk ferromagnets, their molecular nature allows information to be stored with extremely high densities and to be processed at unprecedented speeds.[4] Quantum effects, which appear in magnetism when the nanometre scale is attained, may be exploited in molecular spintronic devices.[5] Unfortunately SMMs-based technology application is limited by two aspects: first, as the unique properties of SMMs are accessible only at liquid-helium temperatures, the operating temperatures need to be increased significantly; second, depositing and addressing individual molecules of SMMs on surfaces preserving their magnetic properties is still challenging. In this chapter we focus our attention on the first aspect, while a novel approach to SMMs surface functionalization will be described in Chapter 8.

Before discussing the possibility to improve SMMs operating temperature we must define what are the properties involved and how we can compare the performances of different molecular magnets.[6] Magnetic blocking temperature (T_B), which is the highest temperature at which a molecular magnet displays hysteresis in plots of magnetization (M) versus magnetic field (H), is often used to evaluate SMM behavior. This property however strongly depends on the sweep rate of the magnetic field and on the technique used for the measurement. By far the most used parameter in SMM studies is the effective energy barrier to the reversal of magnetization (U_{eff}), also called anisotropy barrier, which is the energy required to convert a SMM back into a simple paramagnet. In 3d-SMMs the barrier U_{eff} scales with the square of the total spin of the molecule (S) and linearly with the axial zero-field splitting parameter (D):

$$U_{eff} = |D|S^2 \quad (1)$$

Therefore, in order to improve SMMs magnetic properties, larger *S* values and appreciable negative *D* values must be achieved. Following this principle, a great number of SMMs based on various transition metal clusters have been reported.[7] The first attempts to maximize the anisotropy barrier were focused on increasing *S* by designing systems with ferromagnetic exchange coupling. Following this approach, an anisotropy barrier of U_{eff} = 86.4 K (~12-13 K higher than that of the Mn_{12}) for the dodecametallic phenolate-bridged cage $[Mn_6O_2(sao)_6(O_2CPh)_2(EtOH)_4]$ ({Mn_6}; $saoH_2$ = 2-hydroxybenzaldehye oxime) was reported. The deliberate structural distortion of the metal complex resulted in a molecule possessing an *S* = 12 ground state with *D* = -0.43 cm^{-1}.[8] These values, which are the highest reported for 3d-SMMs, emphasize the importance of obtaining synthetic control over SMMs. However, although it is possible to synthesize polymetallic complexes with very large *S* values, factors beyond the control of the synthetic chemists can result in an overall lack of anisotropy, compromising the SMM properties.[9] Theoretical studies reveled that anisotropy strongly influences U_{eff} and suggested that the energy barrier may even be *S*-independent.[10] As a consequence, anisotropy plays a crucial role in the design of new SMMs with higher operating temperature.

In 2003 Ishikawa and co-workers moved the attention to a new class of SMMs, composed by lanthanide organometallic compounds.[11] In particular they reported that lanthanide phthalocyanine double-deckers ($LnPc_2$), sandwich-type complexes made by a lanthanide(III) ion complexed by two phthalocyanines, behave as magnets at a single-molecule level. For their square-antiprismatic lanthanide coordination geometry (Figure 4.1), that usually shows D_{4d}-symmetry, $LnPc_2$ complexes have significantly large axial magnetic anisotropy.

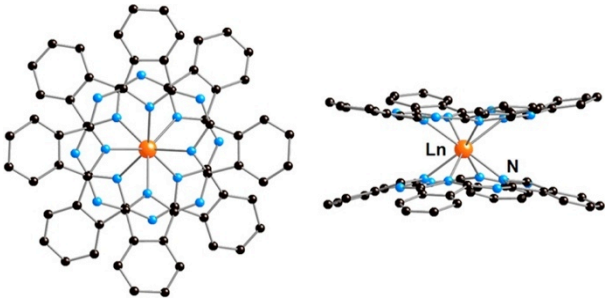

Figure 4.1 *Structure of the complex anion $[LnPc_2]^-$. Color scheme: Ln, orange; N, blue.*

In fact, in lanthanide-based SMMs the anisotropy is given by the ligand field (LF) in which the lanthanide ion is placed.[12] This mechanism is essentially different form the one of 3*d* metal cluster-based SMMs, where the easy axis type magnetic anisotropy is caused by the magnetic interactions among high-spin 3*d* metal ions in a molecule. In $LnPc_2$ the energy terms, determined by strong coupling between the spin (*S)* and orbital angular (*L)* momenta of the lanthanide ions that give rise to a total angular momentum (*J)*, are further split by crystal-field effects. The great advantages of these SMMs are their structural simplicity compared to 3d metal clusters and the possibility to fine tune the anisotropic barrier selecting the metal ion or altering the ligand field. It has been proved that 4f electron density of terbium(III) in its ground state has a distinct oblate shape, which means that it extends into the *xy* plane and it is strongly stabilized by axially symmetric complex, simply considering an electrostatic model. In contrast to this, the lowest excited state has a prolate electron density making it extremely unfavorable for the sandwich-type geometry. The large separation between the two states matches the requisite for strong single-molecule magnet behavior and explains $TbPc_2$ superior magnetic properties between $LnPc_2$.[13]

Set terbium(III) as central ion, efforts to increase the anisotropy barrier turned to the perturbation of the ligand field. Phthalocyanines (Pcs) are extremely versatile compounds and offer functionalization sites in α and β positions. Introduction of functional groups on peripheral portions of one or both ligands is a straightforward strategy to reach higher U_{eff}. Torres and co-workers obtained a record anisotropy barrier for peripherally functionalized $TbPc_2$ with OC_6H_4-*p*-^{t}Bu substituents.[14] In our group we recently investigated the magnetic properties of $TbPc_2$ bearing iodine moieties in β position.[15] Considering their amorphous form those double deckers revealed anisotropy barriers (915 K for the homoleptic and 864 K for the heteroleptic complex) slightly higher than amorphous pristine $TbPc_2$ (856 K), but lower than its crystalline form (965 K).[16]

In our attempts to understand the relationship between structure and properties we also studied the effect of coordination geometry distortion on SMM behavior. Zefirov and co-workers reported in 2012 the synthesis of a particular class of clamshell type double deckers, obtained from two phthalocyanines connected by a semiflexible spacer.[17] They found that the constrained ligand influenced the relative arrangement of phthalocyanine moieties causing a deviation of the skew angle form the theoretical 45° value to 35° (obtained by DFT calculations). We performed magnetic measurements on a similar clamshell-type structure but we evidenced that this type of distortion has a negative effect on the anisotropy barrier (U_{eff} = 789 K). However those

results emphasize how a synthetic control over magnetic properties of SMMs is still a challenge.
In this chapter we explore a novel approach based on the organization of $TbPc_2$ in ordinate rod-like 1D structures. As indicated by Wernsdorfer's pioneering work on supramolecular dimers, new interesting magnetic properties may arise from the interconnection of SMMs centers.[18] To date different SMM-based 1D, 2D and 3D structures have been designed by association of 3d-SMMs, often exploiting the coordination with polytopic ligands.[19] However the behavior of lanthanide-based SMMs in similar organized structures is still unexplored. We focused our attention on the synthesis of $TbPc_2$-based covalent linear oligomers *via* metathesis reaction of properly functionalized double-deckers (Figure 4.2). Carbon-carbon bonds formed between the SMMs ensured structure stability. To simplify magnetic measurements, the dimer was separated from the mixture of oligomers and its behavior was compared to unconnected pristine $TbPc_2$. Our aim was to verify if the presence of inter-SMM interactions over a controlled SMM spatial organization could have a positive effect on the anisotropy barrier of the molecular magnets.

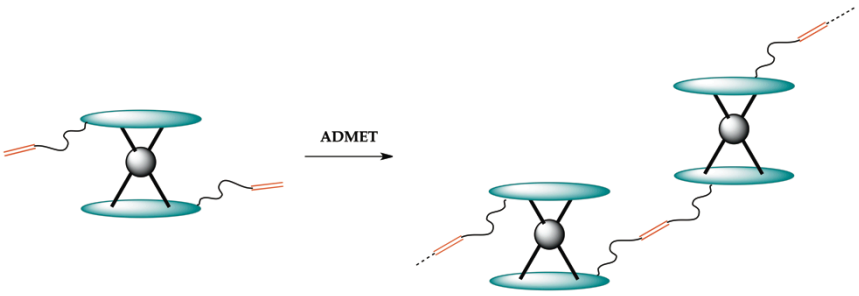

Figure 4.2 *Schematization of $TbPc_2$ oligomerization via acyclic diene metathesis reaction.*

4.2 Results and Discussion

The organization of $TbPc_2$ in a 1D ordered structure required an ad-hoc design of the double-deckers involved. In particular we decided to synthesize covalently linked SMM-based oligomers. As reported in Figure 4.3, linear chains were formed connecting two phthalocyanine ligands of subsequent terbium(III) ions with an aliphatic spacer. Ideally a similar structure could be obtained reacting a Tb(III) salt with covalently linked metal-free

phthalocyanines, but only the connection of $TbPc_2$ after complex formation ensures a superior control over the final material composition (uncomplexed ligands and half-sandwich complexes are avoided). Even if harsh conditions required for $TbPc_2$ synthesis preclude the use of many common functional groups, terminal double bonds can survive complex formation[20] and they are eligible for different polymerization reactions. For this reason we decided to synthesized a bis-alkene functionalized $TbPc_2$ monomer to form linear 1D structures *via* acyclic diene metathesis (ADMET) reaction.

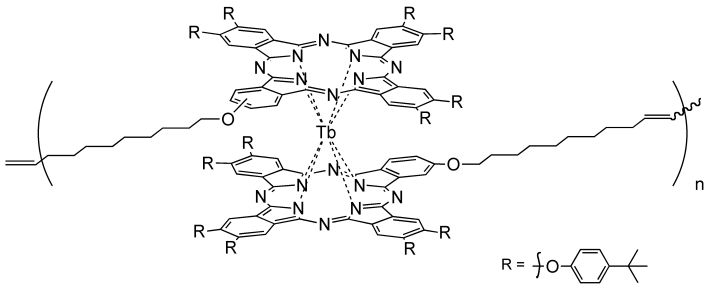

Figure 4.3 *Structure of $TbPc_2$-based oligomers designed.*

4.2.1 Synthesis of Bis-alkenyl $TbPc_2$ Monomer

The formation of linear 1D structures required the presence of two reactive functional groups. Following a straightforward synthetic approach we decided to synthesize a homoleptic terbium double decker from a mono-alkene functionalized phthalocyanine. Initially we focused our attention on the preparation of the asymmetric phthalocyanine bearing a ω-functionalized alkyl chain. Ethers were designed as linkers for their stability in the harsh conditions of double decker formation. Synthesis and purification of asymmetric phthalocyanine is not trivial and requires a careful design of the molecule. In fact, the cyclization reaction of different phthalonitriles leads to the formation of a statistical mixture of differently substituted Pcs. For this reason the presence of polar groups able to guide the purification of the asymmetric Pcs is pivotal. Following similar approaches present in the literature,[21] we developed a straightforward protocol for the synthesis of the A_3B type phthalocyanine **3** (Scheme 4.1). The presence of the *p*-methoxybenzyl protected alcohol allows not only the discrimination between differently substituted Pcs, but also the successive introduction of the alkenyl functionality. In phthalonitrile **1**, obtained from the commercially available 4-hydroxy-phthalonitrile, the

hydroxyl group was protected with a *p*-methoxybenzyl group (PMB) as it revealed to be unstable in the conditions of phthalocyanine formation.

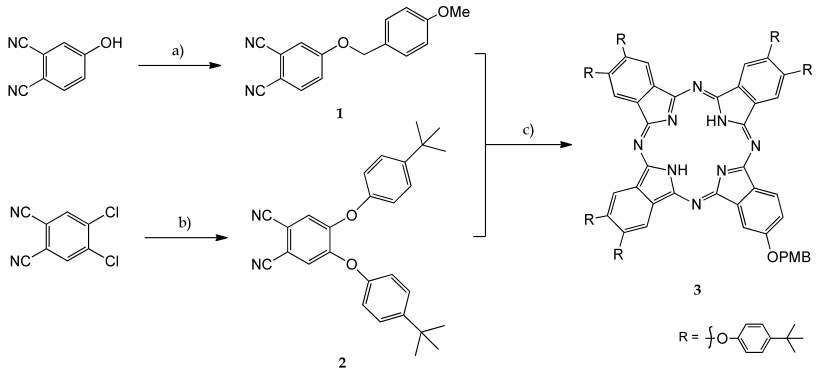

Scheme 4.1 *Synthesis of A_3B type phthalocyanine **3**: a) 4-methoxybenzil chloride, NaH, DMF, 65°C, 4 h, 86%; b) 4-tert-butylphenol, K_2CO_3, DMSO, 90 °C, 2 h, 81%; c) Lithium, 1-pentanol, reflux, 3 h, 17%.*

Phthalonitrile **2** was synthesized following a reported procedure,[22] starting from 4,5-dichlorophthalonitrile *via* nucleophilic aromatic substitution with 4-*tert*-butylphenol. We chose to introduce bulky groups on phthalocyanine peripherals positions to increase Pc solubility and to reduce at the same time their tendency to aggregate. Linstead cyclization[23] of the two phthalonitriles in presence of lithium pentanolate afforded the *p*-methoxybenzyl protected phthalocyanine **3**. Considering the lower reactivity of **1**, the two functionalized phthalonitriles were reacted in non-stoichiometric ratio (**1/2** of 1:2 instead of 1:3). After repeated purifications by column chromatography, the pure A_3B type Pc **3** was obtained in 17% of yield (product characterized by MALDI-TOF and ^{1}H NMR).

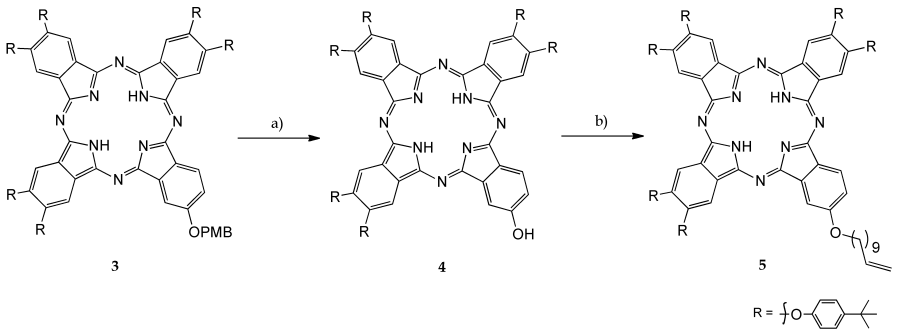

Scheme 4.2 *Synthesis of alkenyl phthalocyanine **5**: a) TFA, $CDCl_3$, r.t., 2 h, 88%; b) 11-bromo-1-undecene, K_2CO_3, KI, DMF, 120°C, 3 h, 57%.*

As reported in Scheme 4.2, deprotection of the hydroxyl group with trifluoroacetic acid (TFA) under mild conditions afforded phthalocyanine **4** in 88% yield. The mono-alkene functionalized phthalocyanine **5** was obtained by Williamson reaction of compound **4** with 11-bromo-1-undecene. Column chromatography afforded phthalocyanine **5** in 57% of yield. The product was characterized by MALDI-TOF (Figure 4.4) and ^{1}H NMR.

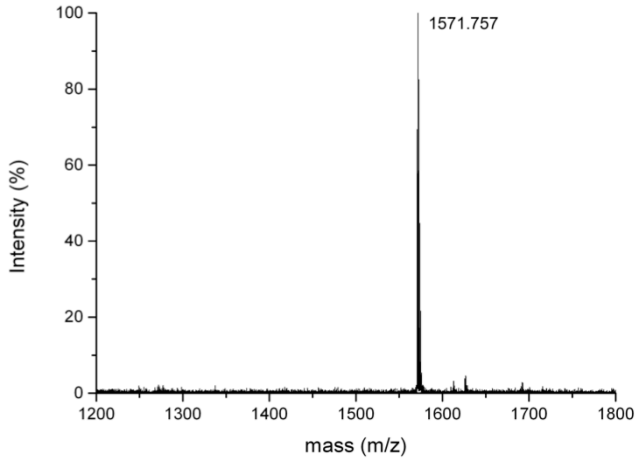

Figure 4.4 *High-resolution MALDI-TOF spectrum of phthalocyanine **5**.*

$TbPc_2$ formation was performed reacting the phthalocyanine ligand **5** with terbium(III) acetylacetonate hydrate in 1-hexadecanol at 180 °C in presence of lithium methoxide (Scheme 4.3).

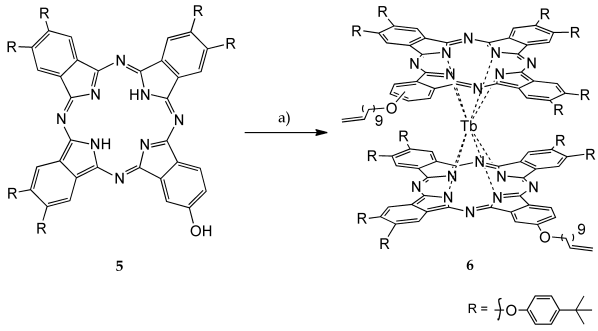

Scheme 4.3 *Synthesis of bis-alkenyl $TbPc_2$ **6**: a) $[Tb(acac)_3]\cdot nH_2O$, MeOLi, 1-hexadecanol, 180°C, 1 h, 49%.*

Lithium methoxide was preferred to 1,8-diazabicyclo[5.4.0]undec-7-ene (DBU), commonly used for the activation of phthalocyanine ligands in metal complexation, as it allowed higher yields of the double decker **6**. In fact, after the first complexation event, DBU has the tendency to coordinate the terbium forming what is called a half-sandwich complex[24] and to hinder the complexation of the second phthalocyanine hampering double-decker formation. Column chromatography, followed by preparative thin layer chromatography (TLC), afforded pure $TbPc_2$ **6** in 49% yield. The presence of the molecular peak in MALDI-TOF spectrum (Figure 4.5) confirmed the formation of the complex. Characterization *via* NMR spectroscopy was prevented by $TbPc_2$ magnetic dipolar term, determined by the anisotropy of the magnetic susceptibility of the lanthanide ion.

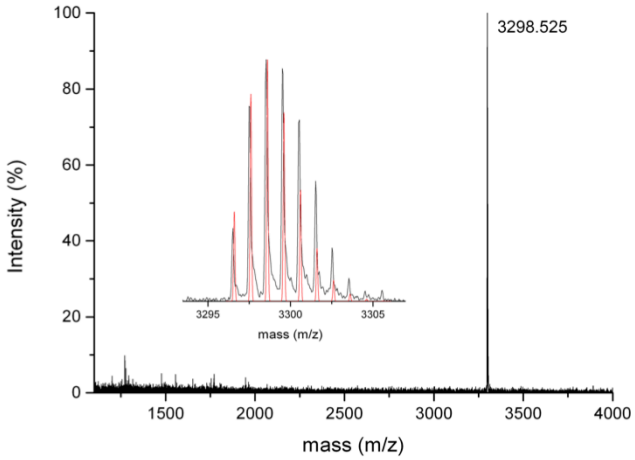

Figure 4.5 *High-resolution MALDI-TOF spectrum of bis-alkenyl $TbPc_2$ **6**, with experimental (black line) versus theoretical (red line) isotopic distribution in the insert.*

4.2.2 $TbPc_2$ Metathesis Oligomerization

Starting from Wagener's pioneering work in the early 1990s,[25] applications of cyclic diene metathesis (ADMET) polymerization increased rapidly.[26] Although ADMET shows some similarity with the more common ring-opening metathesis polymerization (ROMP), these two reactions are mechanistically different. In each ADMET propagation step, the catalytic species is released from the polymer chain, making ADMET a steplike condensation polymerization.[27] In contrast, ROMP is a chain-growth polymerization, which means that the coordination of a single chain is maintained until a specific

cleavage event occurs. Therefore, ADMET reaction is less active and affords polymers with lower molecular weight but it can be applied to a broader range of polymers and architectures.

Figure 4.6 *Scheme of a generic ADMET polymerization.*

Since metathesis is an equilibrium reaction, in ROMP the products are favored by the release of ring tension. In ADMET instead, the equilibrium must be moved in the direction of polymer formation removing the byproduct (Figure 4.6). The use of terminal olefins leads to the formation of ethylene that, as a gas, can be easily removed from the reaction. ADMET polymerization has been successfully applied to metallated phthalocyanines by Kobayashi and co-workers.[28]

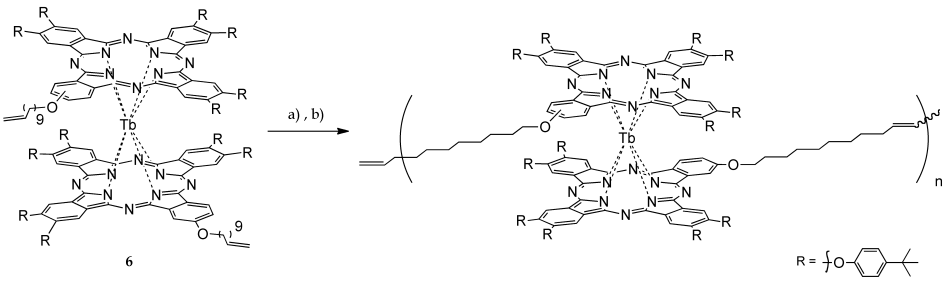

Scheme 4.4 *ADMET oligomerization of $TbPc_2$* ***6****: a)* ***[6]*** *= 2.4 mM, Grubbs Catalyst (2nd generation), CH_2Cl_2, r.t., 24 h; b)* ***[6]*** *= 24.2 mM, Grubbs Catalyst (2nd generation), DCE, r. t., 72 h.*

ADMET polymerization reaction with second generation Grubbs catalyst was performed twice, varying the concentration of monomer **6** (Scheme 4.4). In both cases the reaction was kept at room temperature and nitrogen was bubbled trough the mixture to remove ethylene. The first attempt was performed with an initial monomer concentration of 2.4 mM. After 24 hours the reaction was quenched and the crude mixture was analysed by MALDI-TOF spectrometry. A "low molecular weight" fraction was found to be the major component. Interestingly the *m/z* of the most intense signal was lower than monomer molecular weight (Figure 4.7). The peak was attributed to the product of the intramolecular reaction between the two chains, **6′**.

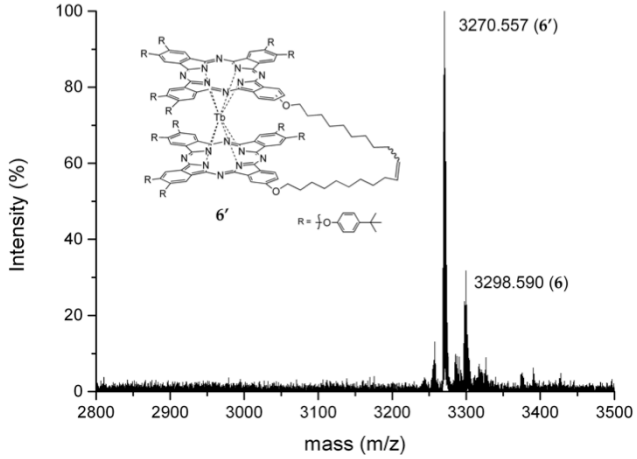

Figure 4.7 *High-resolution MALDI-TOF spectrum (zoom) of the crude obtained with reaction conditions a (Scheme 4.4), structure of the intramolecular reaction product* ***6′*** *in the insert.*

To favor the formation of intermolecular oligomers the concentration of the monomer was increased of an order of magnitude ([**6**] = 24 mM). Reaction time was also incremented to 72 hours and 1,2-dichloroethane (DCE) was preferred as solvent to reduce solvent evaporation. From MALDI-TOF analysis of the crude we observed the presence of signals in the high molecular weight region of the spectrum (Figure 4.8), which demonstrated the effective formation of oligomers (up to pentamer).

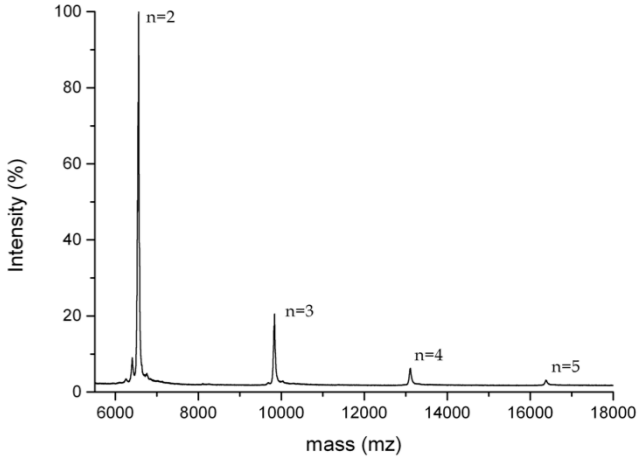

Figure 4.8 *MALDI-TOF spectrum of the crude obtained from reaction conditions b (Scheme 4.4).*

To simplify the study of the magnetic properties of covalently connected $TbPc_2$ isolating one contribution we decided to purify the dimeric structure **7**, as it was the main oligomeric product of the reaction. Preparative TLC afforded $TbPc_2$ dimer **7** with 23% of yield. MALDI-TOF characterization of the isolated solid revealed the presence of monomeric and trimeric impurities (Figure 4.9). Magnetic properties of **7** were studied without further purification.

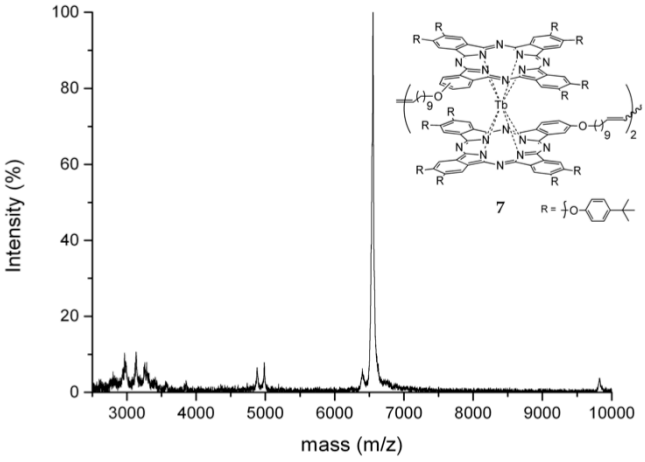

Figure 4.9 *MALDI-TOF spectrum of purified $TbPc_2$ dimer* **7**.

4.2.3 Magnetic Characterization of $TbPc_2$ Dimer

Preliminary magnetic characterization of $TbPc_2$ dimer **7** was performed with standard dc magnetic techniques in order to verify its SMM behavior (Figure 4.10). Magnetization was measured varying the applied field between 30 and -30 kOE (scan rate 200 Oe s^{-1}), at three different temperatures (2, 3 and 5 K). We observed an opening of the hysteresis with the typical butterfly shape, due to the enhancement of the quantum tunneling relaxation (QTM) at zero applied field. Comparing these results with the monomeric unsubstituted $TbPc_2$,[16] we noticed that the dimer **7** showed a less pronounced hysteresis for each temperature measured. However the magnetization saturation value appeared to be comparable with the reference compound.

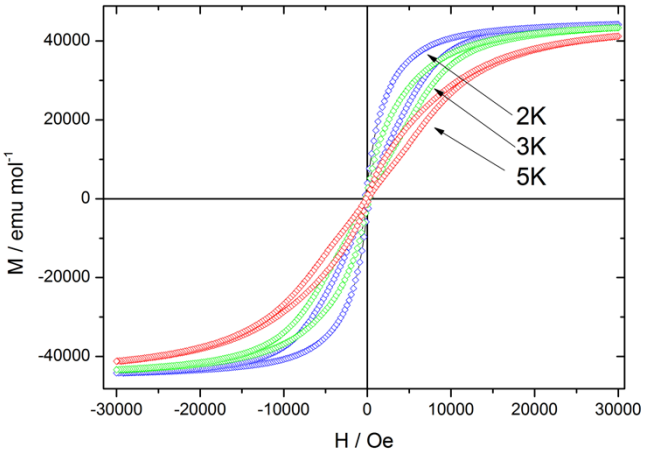

Figure 4.10 *Temperature dependence of the hysteresis loop recorded on TbPc$_2$ dimer* **7**, *field sweeping rate of 200 Oe s^{-1}.*

We performed also AC measurements on compound **7**: the out-of-phase susceptibility (χ'') was measured at temperatures between 2 and 60 K, varying the frequency from 0.1 Hz to 10 kHz. The $\chi''(\nu)$ isotherms provide the most reliable means of determining the energy barrier to magnetization reversal (U_{eff}) and the relaxation time (τ_0). Each $\chi''(\nu)$ curve allowed us to establish an average relaxation time (τ) at a given temperature. The relationship between τ and T is reported in the following equation:

$$\tau(T) = \tau_0 exp\,(U_{eff}/k_B T) \qquad (2)$$

The Arrhenius-type relationship was used to determine the anisotropy barrier from the slope of versus T^{-1}. This operation is possible only if two conditions are met: the graph must be linear and ln τ temperature dependent. For this reason the fitting was possible only for initial points and consequently for a limited range of temperates. Thus calculated values of τ_0 and U_{eff}, measured at zero field or with a magnetic field of 5 kOe, must be consider as an indication of the behavior of **7**. As reported in Table 4.1, comparing our results with values relative to amorphous pristine TbPc$_2$, we did not observe a significant increase of the anisotropy barrier through the covalent connection of two TbPc$_2$ SMMs.

	τ_0 (s)	U_{eff} (K)
	H = 0 Oe	
$TbPc_2$ [1]	$(1.50 \pm 0.1)^{*}10^{-12}$	856 ± 20
7	$3.77^{*}10^{-11}$	698 ± 61
	H = 5 kOe	
$TbPc_2$ [1]	$(1.50 \pm 0.1)^{*}10^{-12}$	856 ± 20
7	$1.88^{*}10^{-12}$	861 ± 54

Table 4.1 *Magnetic parameters extracted from ac susceptibility data under static applied field.*

4.3 Conclusions

ADMET reaction was successfully applied to the oligomerization of a $TbPc_2$ monomer (**6**) bearing two terminal double bonds. Selectivity between intramolecular and intermolecular reaction was found to be concentration depended. However the limited solubility of $TbPc_2$ precluded any further improvement of oligomerization yield. Other attempts can be spent on the optimization of different parameters (e.g. temperature). We isolated the $TbPc_2$ covalent dimer **7** in good purity and we investigated its magnetic behavior. The anisotropy barrier U_{eff} of the two connected SMMs was found to be comparable to the monomeric pristine $TbPc_2$. A possible explanation is that the long and flexible spacer used to connect the two metal cores prevents the interconnection between the two magnetic centers. Further attempts may be directed to the use of shorter or conjugated spacers. It might be also interesting to investigate the organization of SMM-based 1D structures on surfaces with scanning probe microscopy (SPM).

4.4 Acknowledgments

Thanks to Dr. Gianluca Paredi from the interdepartmental Centre SITEIA.PARMA, University of Parma, for mass spectrometry measurements. Thanks to Prof. Roberta Sessoli and Dr. Matteo Mannini from the department of Chemistry "Ugo Schiff", University of Firenze, for magnetic measurements.

4.5 Experimental Section

4-((4-Methoxybenzyl)oxy)phthalonitrile (1)
To a solution of 4-hydroxyphthalonitrile (0.50 g, 3.47 mmol) in DMF, NaH (0.21 g, 8.67 mmol) was added followed by 4-methoxybenzyl chloride (0.56 mL, 4.16 mmol). The mixture was heated at 65 °C for 4 h. After cooling at room temperature, the solvent was removed under reduced pressure. The crude was dissolved in EtOAc and washed three times with water. The organic phase was dried over $MgSO_4$ and the solvent was evaporated under reduced pressure. Flash column chromatography (Hex/CH_2Cl_2 8:2) afforded compound **1** as a white solid (0.80 g, 2.98 mmol, 86%).
^{1}H NMR ($CDCl_3$, 300 MHz): δ (ppm) = 7.72 (d, 1H, J=8.8 Hz, Ar**H**), 7.36-7.33 (m, 3H, Ar**H** and ArOCH_2Ar**H$_o$**), 7.26 (dd, 1H, J_o=8.8 Hz, J_m=2.6 Hz, Ar**H**), 6.97 (d, 2H, J=8.7 Hz, ArOCH_2Ar**H$_m$**), 5.10 (s, 2H, ArOC**H$_2$**Ar), 3.84 (s, 3H, ArOC**H$_3$**).
ESI-MS: *m/z* = 287.2 $[M+Na]^+$, 302.9 $[M+K]^+$.

4,5-Bis((4-*tert*-butylphenyl)oxy)phthalonitrile (2)
To a stirred solution of 4,5-dichlorophthalonitrile (1.0 g, 5.07 mmol) and 4-*tert*-butylphenol (1.68 g, 11.2 mmol) in 20 mL of DMSO at 90 °C, K_2CO_3 (6 x 1.03 g, 44.8 mmol total) was added in portions over 30 min. The reaction is quenched by addition of HCl 1 N and the yellow precipitate was filtered, washed with water and dried. Recrystallization from MeOH afforded pure compound **2** as a white solid (1.74 g, 4.11 mmol, 81%).
^{1}H NMR ($CDCl_3$, 400 MHz): δ (ppm) = 7.49 (d, 4H, J=8.8 Hz, ^{t}Bu-Ar**H$_m$**), 7.15 (s, 2H, Ar**H**), 7.04 (d, 4H, J=8.8 Hz, ^{t}Bu-Ar**H$_o$**), 1.39 (s, 18H, ArCC**H$_3$**).
ESI-MS: *m/z* = 447.3 $[M+Na]^+$, 463.2 $[M+K]^+$.

Pc(OPMB) (3)
Lithium (0.031 g, 4.55 mmol) was suspended in 1-pentanol and the mixture was heated at 110 °C until complete dissolution of the metal. To the resulting solution, phthalonitriles **1** (0.100 g, 0.38 mmol) and **2** (0.321 g, 0.76 mmol) were added and the mixture was heated at 140 °C for 3 h. Solvent was evaporated and the green residue was purified by flash column chromatography (gradient from Hex/CH_2Cl_2 1:1 to Hex/CH_2Cl_2 3:7), affording A_3B type phthalocyanine **3** as a green solid (0.066 g, 0.043 mmol, 17%).
^{1}H NMR ($CDCl_3$, 400 MHz): δ (ppm) = 8.52-7.06 (m, 37H, Ar**H**), 4.05 (s, 3H, ArOC**H$_3$**), 1.37 (s, 54H, ArCC**H$_3$**).
MALDI-TOF: calculated for $C_{100}H_{98}N_8O_8$ $[M]^+$ *m/z* = 1538.751, found *m/z* = 1538.792.

Pc(OH) (4)

To a solution of phthalocyanine **3** (0.066 g, 0.043 mmol) in 5 mL of $CHCl_3$, 1 mL of TFA was added and the reaction mixture was stirred at room temperature for 2 h. The solvent was removed and the crude was purified by flash column chromatography (gradient from Hex/CH_2Cl_2 2:8 to CH_2Cl_2 100%) to afford compound **4** as a green solid (0.053 g, 0.037 mmol, 87%).

UV-Vis: λ_{max} ($CHCl_3$) = 703, 670, 648, 612, 345 nm.

MALDI-TOF: calculated for $C_{92}H_{90}N_8O_7$ $[M]^+$ *m/z* = 1418.693, found *m/z* = 1418.676.

Pc(OC$_9$H$_{18}$CH=CH$_2$) (5)

Phthalocyanine **4** (0.131 g, 0.09 mmol) was suspended in 10 mL of DMF and K_2CO_3 (0.025 g, 0.18 mmol) was added, followed by a catalytic amount of KI. After the addition of 11-bromo-1-undecene (0.03 mL, 0.14 mmol), the mixture was heated at 120 °C for 3 h. The reaction was cooled and the solvent was removed under reduced pressure. Flash column chromatography (Hex/CH_2Cl_2 4:6) afforded pure phthalocyanine **5** (0.082 g, 0.05 mmol, 57%) as a green solid.

^{1}H NMR ($CDCl_3$, 400 MHz): δ (ppm) = 8.78-8.10 (m, 8H, Ar**H**), 7.57-7.26 (m, 25H, ^{t}Bu-Ar**H** + Ar**H**), 5.88 (m, 1H, CH_2C**H**=CH_2), 5.04 (m, 2H, CH_2CH=C**H$_2$**), 4.37 (m, 2H, OC**H$_2$**CH_2), 2.12 (m, 4H, C**H$_2$**CH=CH_2 + OCH_2C**H$_2$**), 1.72-1.28 (m, 66H, ArCC**H$_3$** + -C**H$_2$**-), -3.41 (bs, 2H, N**H**).

UV-Vis: λ_{max} ($CHCl_3$) = 703, 670, 641, 602, 396, 346 nm.

MALDI-TOF: calculated for $C_{103}H_{110}N_8O_7$ $[M]^+$ *m/z* = 1571.853, found *m/z* = 1571.757.

Tb[Pc(OC$_9$H$_{18}$CH=CH$_2$)]$_2$ (6)

Phthalocyanine **5** (0.083 g, 0.052 mmol) was dispersed in 0.3 g of n-hexadecanol. $[Tb(acac)_3]\cdot nH_2O$ (0.012 g, 0.026 mmol) and lithium methoxide (0.006 g, 0.156 mmol) were added and the mixture was heated at 180 °C for 1 h. After cooling, hexane was added and the mixture was filtrated. The solvent was removed under reduced pressure and the crude was purified by flash column chromatography (gradient from Hex/CH_2Cl_2 1:1 to Hex/CH_2Cl_2 3:7). Further purification by preparative TLC (Hex/CH_2Cl_2 1:1) afforded product **6** as a green solid (0.041 g, 0.012 mmol, 49%).

UV-Vis: λ_{max} ($CHCl_3$) = 915, 681, 614, 490, 364, 330 nm.

MALDI-TOF: calculated for $C_{206}H_{216}N_{16}O_{14}Tb$ $[M]^+$ *m/z* = 3298.600, found *m/z* = 3298.525.

Metathesis oligomerization of $Tb[Pc(OC_9H_{18}CH=CH_2)]_2$

Method a: $TbPc_2$ **6** (0.011 g, 0.003 mmol) was dissolved in 1.5 mL of freshly distilled and degassed CH_2Cl_2. Second generation Grubbs catalyst (0.14 mg, 5 mol %) was added and the mixture was stirred at room temperature overnight. The reaction was quenched with MeOH (100 mL) and the green precipitate was filtered and dried.

Method b: $TbPc_2$ **6** (0.080 g, 0.024 mmol) was dissolved in 1 mL of freshly distilled and degassed DCE. Second generation Grubbs catalyst (0.001 g, 5 mol %) was added and the mixture was stirred at room temperature for 4 days.

The reaction was quenched with MeOH (100 mL) and the green precipitate was filtered and dried. $TbPc_2$ dimer **7**, isolated by preparative TLC (Hex/CH_2Cl_2 1:1), was obtained as a green solid (0.018 g, 0.003 mmol, 23%).

UV-Vis: λ_{max} ($CHCl_3$) = 916, 681, 616, 493, 363, 330 nm.

MALDI-TOF: linear scan mode, calculated for $C_{410}H_{428}N_{32}O_{28}Tb_2$ $[M]^+$ *m/z* = 6569.2, found *m/z* = 6569.4.

4.6 References

[1] D. Gatteschi, R. Sessoli, J. Villain, *Molecular Nanomagnets* **2006**, Oxford University Press, Oxford.

[2] a) A. Caneschi, D. Gatteschi, R. Sessoli, A. L. Barra, L. C. Brunel, M. Guillot, *J. Am. Chem. Soc.* **1991**, *113*, 5873-5874; b) R. Sessoli, L. Hui, A. R. Schake, S. Wang, J. B. Vincent, K. Folting, D. Gatteschi, G. Christou, *J. Am. Chem. Soc.* **1993**, *115*, 1804-1816; c) R. Sessoli, D. Gatteschi, A. Caneschi, M. A. Novak, *Nature* **1993**, *365*, 141-143.

[3] R. A. Layfield, *Organometallics* **2014**, *33*, 1084-1099.

[4] a) M. N. Leuenberger, D. Loss, *Nature* **2001**, *410*, 789-793; b) A. Ardavan, O. Rival, J. J. L. Morton, S. J. Blundell, A. M. Tyryshkin, G. A. Timco, R. E. P. Winpenny, *Phys. Rev. Lett.* **2007**, *98*, 057201(4).

[5] M. Mannini, F. Pineider, C. Danieli, F. Totti, L. Sorace, P. Sainctavit, M. A. Arrio, E. Otero, L. Joly, J. C. Cezar, A. Cornia, R. Sessoli, *Nature* **2010**, *468*, 417-421.

[6] D. N. Woodruff, R. E. P. Winpenny, R. A. Layfield, *Chem. Rev.* **2013**, *113*, 5110-5148.

[7] a) W. Wernsdorfer, T. Ohm, C. Sangregorio, R. Sessoli, D. Mailly, C. Paulsen, *Phys. Rev. Lett.* **1999**, *82*, 3903-3906; b) A. J. Tasiopoulos, A. Vinslava, W. Wernsdorfer, K. A. Abboud, G. Christou, *Angew. Chem. Int. Ed.* **2004**, *43*, 2117–2121; c) S. Wang, J. L. Zuo, S. Gao, Y. Song, H. C. Zhou, Y. Z. Zhang, X. Z. You, *J. Am. Chem. Soc.* **2004**, *126*, 8900-8901; d) E. Pardo, R. Ruiz-Garcia, F. Lloret, J. Faus, M. Julve, Y. Journaux, F. Delgado, C. Ruiz-Pérez, *Adv. Mater.* **2004**, *16*, 1507-1600; e) Y. Song, P. Zhang, X. M. Ren, X. F. Shen, Y. Z. Li, X. Zeng You, *J. Am. Chem. Soc.* **2005**, *127*, 3708-3709; f) T. Kajiwara, M. Nakano, Y. Kaneko, S. Takaishi, T. Ito, M. Yamashita, A. Igashira-Kamiyama, H. Nojiri, Y. Ono, N. Kojima, *J. Am. Chem. Soc.* **2005**, *127*, 10150-10151.

[8] C. J. Milios, A. Vinslava, W. Wernsdorfer, S. Moggach, S. Parsons, S. P. Perlepes, G. Christou, E. K. Brechin, *J. Am. Chem. Soc.* **2007**, *129*, 2754-2755.

[9] A. M. Ako, I. J. Hewitt, V. Mereacre, R. Clérac, W. Wernsdorfer, C. E. Anson, A. K. Powell, *Angew. Chem., Int. Ed.* **2006**, *45*, 4926-4929.

[10] F. Neese, D. A. Pantazis, *Faraday Discuss.* **2011**, *148*, 229-238.

[11] N. Ishikawa, M. Sugita, T. Ishikawa, S. Koshihara, Y. Kaizu, *J. Am. Chem. Soc.* **2003**, *125*, 8694-8695.

[12] N. Ishikawa, *Functional Phthalocyanine Molecular Materials Structure and Bonding* **2010**, Springer Berlin Heidelberg, *135*, 211-228.

[13] J. D. Rinehart, J. R. Long, *Chem. Sci.* **2011**, *2*, 2078-2085.

[14] C. R. Ganivet, B. Ballesteros, G. de la Torre, J. M. Clemente-Juan, E. Coronado, T. Torres, *Chem. Eur. J.* **2013**, *19*, 1457-1465.

[15] F. Bertani, N. Cristiani, M. Mannini, R. Pinalli, R. Sessoli, E. Dalcanale, *Eur. J. Org. Chem.* **2015**, 7036-7042.

[16] L. Malavolti, M. Mannini, P. Car, G. Campo, F. Pineider, R. Sessoli, *J. Mater. Chem. C* **2013**, *1*, 2935–2942.

[17] V. E. Pushkarev, A. Y. Tolbin, F. E. Zhurkin, N. E. Borisova, S. A. Trashin, L. G. Tomilova, N. S. Zefirov, *Chem. Eur. J.* **2012**, *18*, 9046-9055.

[18] W. Wernsdorfer, N. Aliaga-Alcalde, D. N. Hendrickson, G. Christou, *Nature* **2002**, *416*, 406-409.

[19] a) M. Ferbinteanu, H. Miyasaka, W. Wernsdorfer, K. Nakata, K.-i Sugiura, M. Yamashita, C. Coulon, R. Clérac, *J. Am. Chem. Soc.* **2005**, *127*, 3090-3099; b) L. Lecren, W. Wernsdorfer, Y. G. Li, A. Vindigni, H. Miyasaka, R. Clérac, *J. Am. Chem. Soc.* **2007**, *129*, 5045-5051; c) O. Roubeau, R. Clérac, Eur. *J. Inorg. Chem.* **2008**, *28*, 4325-4342; d) H. Miyasaka, K. Takayama, A. Saitoh, S. Furukawa, M. Yamashita, R. Clérac, *Chem. Eur. J.* **2010**, *16*, 3656-3662; e) I.-R. Jeon, R. Clérac, *Dalton Trans.* **2012**, *41*, 9569-9586; f) H.-L. Tsai, C.-I Yang, W. Wernsdorfer, S.-H. Huang, S.-Y. Jhan, M.-H. Liu, G.-H. Lee, *Inorg. Chem.* **2012**, *51*, 13171-13180. g)

R. Ababei, C. Pichon, O. Roubeau, Y.-G.Li, N. Bréfuel, L. Buisson, P. Guionneau, C. Mathonière, R. Clérac, *J. Am. Chem. Soc.* **2013**, *135*, 14840-14853.

[20] M. Mannini, F. Bertani, C. Tudisco, L. Malavolti, L. Poggini, K. Misztal, D. Menozzi, A. Motta, E. Otero, P. Ohresser, P. Sainctavit, G. G. Condorelli, E. Dalcanale, R. Sessoli, *Nature Commun.* **2014**, *5*, article number: 4582.

[21] a) A. Y. Tolbin, V. E. Pushkarev, L. G. Tomilova, N. S. Zefirov, *Mendeleev Commun.* **2009**, *19*, 78-80; b) N. W. Polaske, H.-C. Lin, A. Tang, M. Mayukh, L. E. Oquendo, J. T. Green, E. L. Ratcli, N. R. Armstrong, S. S. Saaverda, D. V. McGrath, *Langmuir* **2011**, *27*, 14900-14909.

[22] S. E. Maree, T. Nyokong, *J. Porphyrins Phthalocyanines* **2001**, *5*, 782–792.

[23] P. A. Barrett, D. A. Frye, R. P. Linstead, *J. Chem. Soc.* **1938**, 1157-1163.

[24] V. E. Pushkarev, A. Y. Tolbin, N. E. Borisova, S. A. Trashin, L. G. Tomilova, *Eur. J. Inorg. Chem.* **2010**, 5254–5262.

[25] a) M. Lindermark-Hamberg, K. B. Wagener, *Macromolecule* **1987**, *20*, 2949-2951; b) K. B. Wagener, J. G. Nel, J. Konzelman, J. M. Bonicella, *Macromolecules* **1990**, *23*, 5155-5157.

[26] H. Mutlu, L. Montero de Espinosa, M. A. R. Meier, *Chem. Soc. Rev.* **2011**, *40*, 1404–1445.

[27] K. B. Wagener, J. M. Boncella, J. G. Nel, *Macromolecules* **1991**, *24*, 2649–2657.

[28] M. Kimura, K. Wada, K. Ohta, K. Hanabusa, H. Shirai, N. Kobayashi, *Macromolecules* **2001**, *34*, 4706-4711.

CHAPTER 5

SELF-ASSEMBLY OF $TbPc_2$ SINGLE-MOLECULE MAGNETS ON SURFACES

5.1 Introduction

The recent interest on single-molecule magnets (SMMs) lies in the development of a new generation of sensors, transistors and high-density data storage devices based on spin states.[1] Magnetic properties of purely molecular origin, coupled with quantum effects, make SMMs preponderant in spintronics,[2] although real-life applications are far to be possible. However, the low operating temperature, discussed in the previous chapter, is not the only factor hampering SMMs effectiveness. Before such devices become a reality, the development of new strategies that allow the organization of SMMs on surfaces preserving their properties need to be addressed.[3]

Sub-monolayer deposition of $LnPc_2$ on different substrates *via* sublimation under Ultra-High Vacuum (UHV) has been largely investigated.[4] Despite their high thermal and chemical stability, $LnPc_2$ magnetic behavior was found to be altered, or even suppressed, by the deposition process. These results suggest that magnetization dynamics are strongly affected by the environment especially when crystalline packing is lost. $TbPc_2$ magnetic behavior in different phases has been extensively studied by Sessoli and co-workers.[5] Pristine $TbPc_2$ was evaporated in UHV at 400 °C on Kapton and an opening of the typical butterfly-shaped hysteresis (Figure 5.1a) was observed at lower temperature compared to microcrystals of the same compound (10 K instead of 15 K).

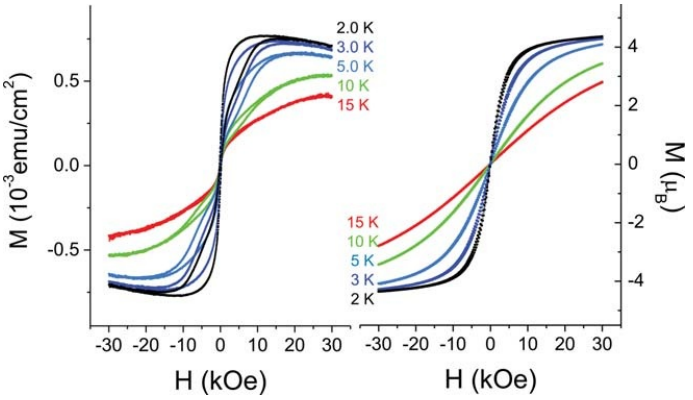

Figure 5.1 *$TbPc_2$ magnetic hysteresis curves in (a) sublimated film on Kapton, (b) heated powder in the crucible before film deposition.*[5]

To understand the origin of this difference, a fraction of the heated sample was extracted from the crucible before the evaporation of the film and magnetically characterized. Interestingly no measurable hysteresis was reported for this powder over the whole investigated temperature range (Figure 5.1b).

Degradation of the complex can be excluded considering magnetic properties reappearance after the sublimation. The origin of this phenomenon remains unclear, although it should be considered that the harsh thermal treatment might cause small distortions of the two phthalocyaninato ligands from the exactly staggered situation (45°), corresponding to D_{4d} symmetry. Such deformations, though not so drastic as chemical decomposition, can be very efficient in promoting a tunnelling mechanism of relaxation.
Other aspects must be evaluated transferring $TbPc_2$ from bulk materials to monolayers: surface effects as well as interaction with the substrate can completely change the characteristic SMM behavior observed in crystals, either increasing its magnetic anisotropy or completely removing it. Perturbations arising upon molecule–surface interactions can induce numerous changes, such as chemical modifications (e.g. redox processes), that completely alter the magnetic properties. As reported in our recent communication,[6] $TbPc_2$ covalently grafted on silicon surface showed an enhancement of the magnetic bistability compared to monolayer deposits evaporated on noble and ferromagnetic metals. Photoelectron spectroscopy investigations on the robust monolayer, obtained by hydrosilylation of a ω-alkenes functionalized double decker (Figure 5.2a), suggested a non-innocent role played by the surface.

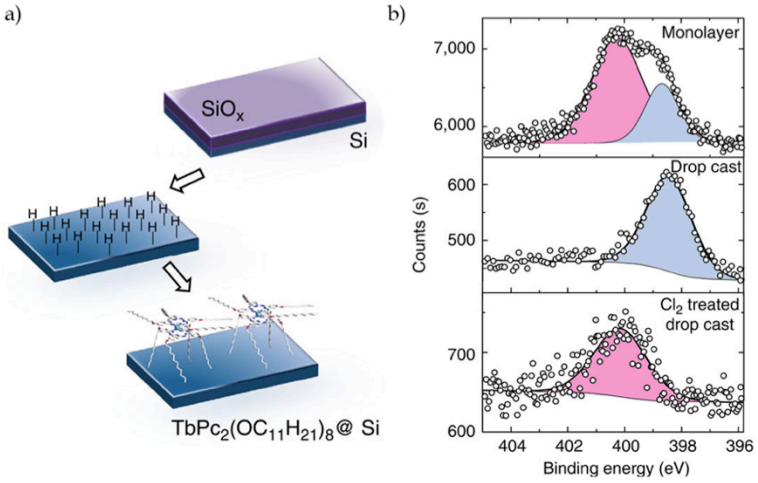

Figure 5.2 *a) Sketch of the $TbPc_2(OC_{11}H_{21})_8$ grafting procedure; b) High-resolution N 1s XPS spectra of the $TbPc_2(OC_{11}H_{21})_8$@Si monolayer (top), the drop cast deposited $TbPc_2(OC_{11}H_{21})_8$ (center), and the drop cast sample treated with chlorine gas (bottom).*[6]

In fact, the analysis of N*1s* signal in the XPS spectrum (Figure 5.2b) revealed an energy shift inferable either from stabilization effects of a cationic species

formed during grafting reaction by the silicon surface or from an electron depletion of the molecular system induced by the interaction with the surface. This covalent approach, beyond the great stability of the grafted monolayer, highly suffers for the lack of control over the deposited $TbPc_2$ and for the limited choice of the substrate.

To overcome these limitations, we developed a novel protocol based on the reversible self-assembly of properly functionalized $TbPc_2$. As shown in Figure 5.3, the complexation between a $TbPc_2$ derivatized with a 2-ureido-4[1H]-pyrimidinone (UPy) and an anchored 2,7-diamido-1,8-naphthyridine (NaPy) unit, allows the functionalization of a surface. The anchoring is guaranteed by the strong association constant of the multiple hydrogen bond complex.

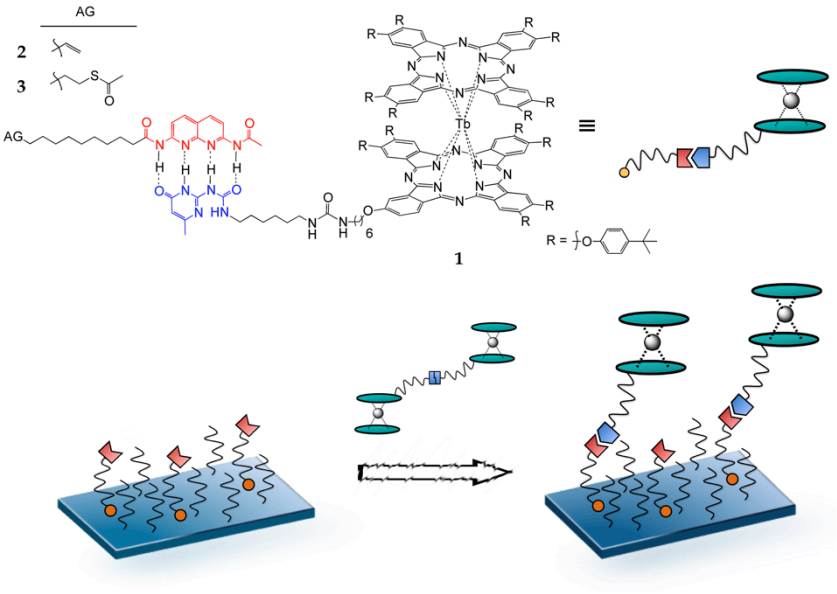

Figure 5.3 *UPy-functionalized $TbPc_2$ **1** and NaPy counterparts **2**,**3** with alkenyl/S-acetyl anchoring groups (AG) (top); sketch of the self-assembly on a functionalized surface (down).*

Compared to $TbPc_2$ non-covalent anchoring through π-π interactions[7] or S-Au bonds[8] reported in the literature, this approach guarantees a long-term stability related to the hydrogen bond architecture, coupled with a reversibility driven by external stimuli (e.g. temperature and solvent). Considering that the development of a general protocol for the functionalization of different surfaces is highly attractive, the ad-hoc derivatization of the NaPy counterpart can give the access to the introduction of $TbPc_2$ on ideally all types of surfaces. To support this assumption we performed the self-assembly of UPy-functionalized

$TbPc_2$ **1** on two technologically relevant platforms, namely silicon and gold surfaces. For this purpose, a proper design of two NaPy anchors was required.

5.2 Results and Discussion

5.2.1 Synthesis of UPy-functionalized $TbPc_2$

The degree of functionalization of $TbPc_2$ molecules can be tuned following different synthetic pathways (Table 5.1). These sandwich complexes are divided in two main classes according to the structure of the ligands: homoleptic double deckers ($TbPc_2$), constituted by two identical phthalocyanines, and heteroleptic complexes (TbPcPc'), characterized by different ligands.

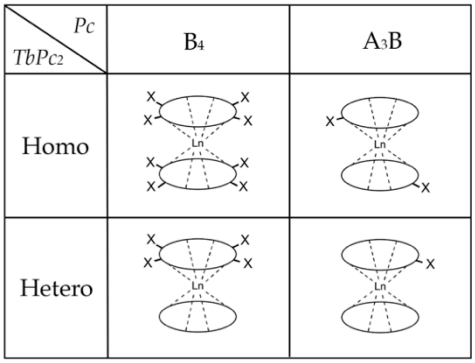

Table 5.1 *Common degrees of functionalization of $TbPc_2$ as function of complex type and phthalocyanine structure starting from monofunctionalized phthalonitriles.*

Octofunctionalized homoleptic $TbPc_2$ are usually prepared by the classical De Cian cyclotetramerization of a monosubstituted phthalonitrile in presence of terbium(III) salts.[9] As described in the previous chapter, the ligand exchange between an A_3B phthalocyanine and a Tb(III) salt leads to the formation of homoleptic double deckers with two functional groups. In analogy, heteroleptic $TbPc_2$ can be prepared following two main synthetic routes. The first method involves the treatment of terbium(III) salts with a 1:1 mixture of the two preformed phthalocyanines. The statistical reaction produces a substantial amount of the two homoleptic complexes as side products. The second and most convenient method involves the formation of an intermediate mononuclear terbium(III) Pc half-sandwich complex, starting from a free-base phthalocyanine. The subsequent cyclotetramerization of a phthalonitrile

around the lanthanide ion center affords the final double decker. Following this method, heteroleptic complexes can be obtained in higher yields, as the amount of side products is sensibly reduced. For the preparation of a heteroleptic $TbPc_2$ based on B_4-type Pc the choice of the starting Pc is arbitrary, while in the synthesis of a monofunctionalized $TbPc_2$ the second cyclotetramerization cannot be performed with the functionalized phthalonitrile.

In the design of the UPy-functionalized $TbPc_2$ **1**, it must be consider that 2-ureido-4[1H]-pyrimidinonic units can form homodimers with an association constant one order of magnitude higher then UPy-NaPy heterocomplexation. The presence of more than one UPy moiety on the complex scaffold is detrimental as the formation of a strong intramolecular UPy-UPy complex highly prevents $TbPc_2$ anchoring on surface *via* intermolecular UPy-NaPy interactions. For this reason, the synthesis of a heteroleptic monosubstituted $TbPc_2$ bearing a single UPy moiety revealed to be crucial. Moreover, the 2-ureido-4[1H]-pyrimidinone is not stable under harsh reaction conditions required for phthalocyanine and $TbPc_2$ synthesis hence its introduction after complex formation was mandatory.

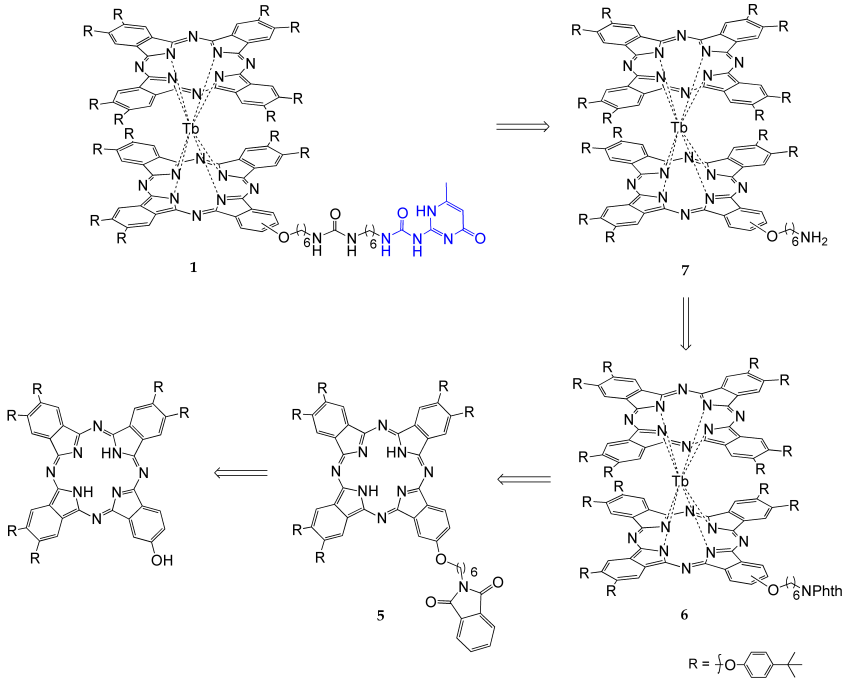

Scheme 5.1 *Retrosynthetic approach to UPy-functionalized $TbPc_2$ **1** synthesis.*

As reported in the retrosynthetic Scheme 5.1, the UPy functionality was introduced in the last step reacting 2(6-isocyanatohexylamino-carbonylamino)-6-methyl-4[1H]pyrimidinone[10] with heteroleptic mono-amino $TbPc_2$ **7**. For its instability in complex formation conditions, the primary amine was protected as phthalimide (Phth). This group also provided a good discrimination between the heteroleptic $TbPc_2$ and the side-products in the purification step, allowing a relatively easy isolation of **6**. The synthesis of heteroleptic mono-functionalized $TbPc_2$ **6** started from A_3B-type phthalocyanine **5,** bearing a protected amino group. Surprisingly, the phthalimide group revealed to be unstable under phthalocyanine formation conditions[11] and the post-functionalization of a hydroxyl phthalocyanine was required. An ether group was chosen for its stability, while the hexyl spacers guaranteed a good accessibility of the amino group in post-derivatization reactions.
The phthalimide-functionalized phthalocyanine **5** was synthesized *via* Williamson reaction between a mono-hydroxyl phthalocyanine (**Pc(OH)**, for the synthesis see Chapter 4) and bromide **4**, obtained from the nucleophilic substitution of 1,6-dibromohexane with potassium phthalimide[12] (Scheme 5.2).

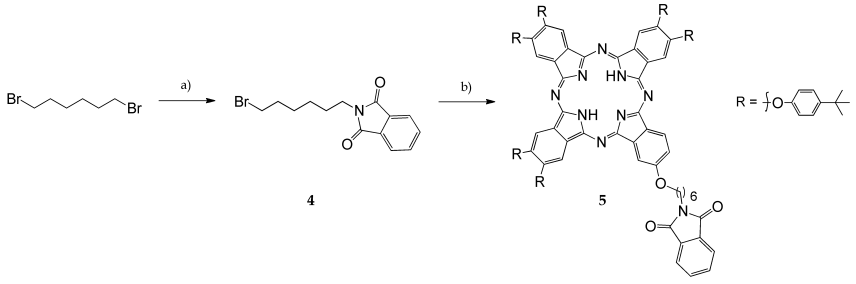

Scheme 5.2 *Synthesis of phthalimide-functionalized Pc* **5***: a) potassium phthalimide, acetone, 60°C, 12 h, 86%; b) Pc(OH), K_2CO_3, KI, DMF, 120°C, 4 h, 82%.*

The identity of compound **4** was confirmed by MALDI-TOF and ^{1}H NMR. The phthalocyanine **4** was then reacted with an equimolar amount on terbium acetylacetonate in the presence of 1,8-diazabicyclo[5.4.0]undec-7-ene (DBU). The reaction, performed in *o*-dichlorobenzene (o-DCB) at 170 °C, afforded half-sandwich complex **6'**, which was used immediately for the next step without purification (Scheme 5.3). The formation of mono-phthalocyaninato intermediate **6'** was monitored by UV-Vis spectroscopy, which showed a decrease of the two Q-bands distinctive of metal-free Pcs and the growth of a new band between them.[13] The cyclotetramerization of 4,5-Bis((4-tert-butylphenyl)oxy)-phthalonitrile in the presence of **6'** as a template, was

performed in a 1:1 mixture of o-DCB and 1-pentanol at 160 °C, in the presence of DBU. The crude was treated with 2,3-dichloro-5,6-dicyano-p-benzoquinone (DDQ) to partially oxidize the aliquot of reduced double decker formed during the reaction. The neutral heteroleptic mono-functionalized $TbPc_2$ **6** was obtained in 26% yield after column chromatography.

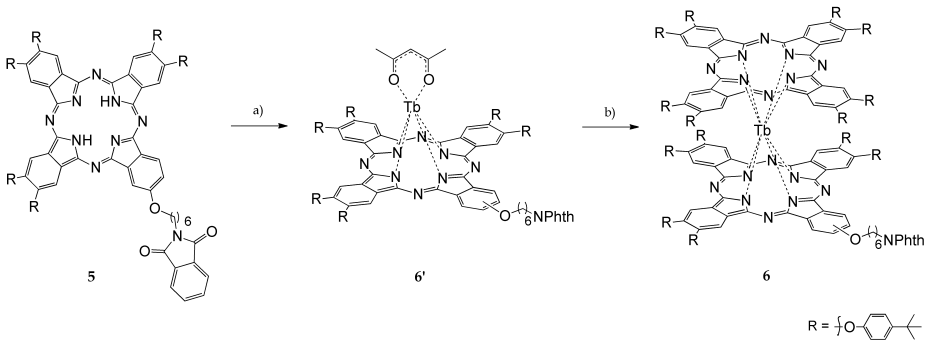

Scheme 5.3 *Synthesis of $TbPc_2$ **6**: a) $[Tb(acac)_3]\cdot nH_2O$, DBU, o-DCB, 170 °C, 1 h; b) 4,5-Bis((4-tert-butylphenyl)oxy)-phthalonitrile, DBU, o-DCB/1-pentanol, 160 °C, 4 h; 26% (over two steps)*

The presence of the molecular peak in MALDI-TOF spectrum confirmed the formation of product **6** (Figure 5.4). Characterization *via* NMR spectroscopy was prevented by the typical perturbation of the signals caused by $TbPc_2$ magnetic dipolar term.

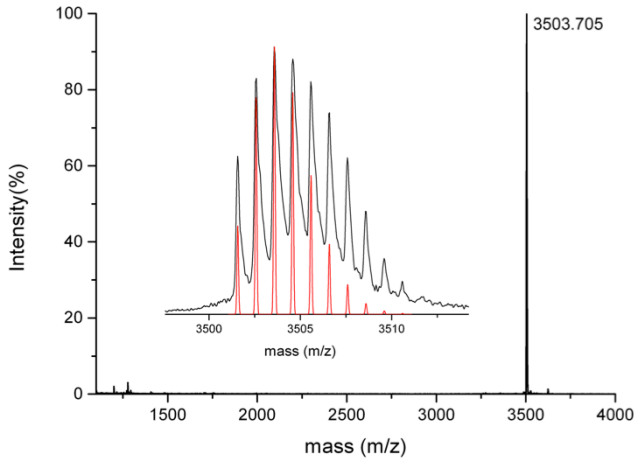

Figure 5.4 *High-resolution MALDI-TOF spectrum of mono-functionalized $TbPc_2$ **6**, with experimental (black line) versus theoretical (red line) isotopic distribution in the insert.*

Heteroleptic $TbPc_2$ **6** was deprotected with hydrazine hydrate affording double decker **7**, bearing a primary amine in 74% yield (Scheme 5.4). As hydrazine is a well-know reducing agent for $TbPc_2$,[13] the product was initially obtained in its anionic form and was reoxidized at the air prior to being purified. Compound **7** was characterized by MALDI-TOF spectrometry and UV-Vis spectroscopy.

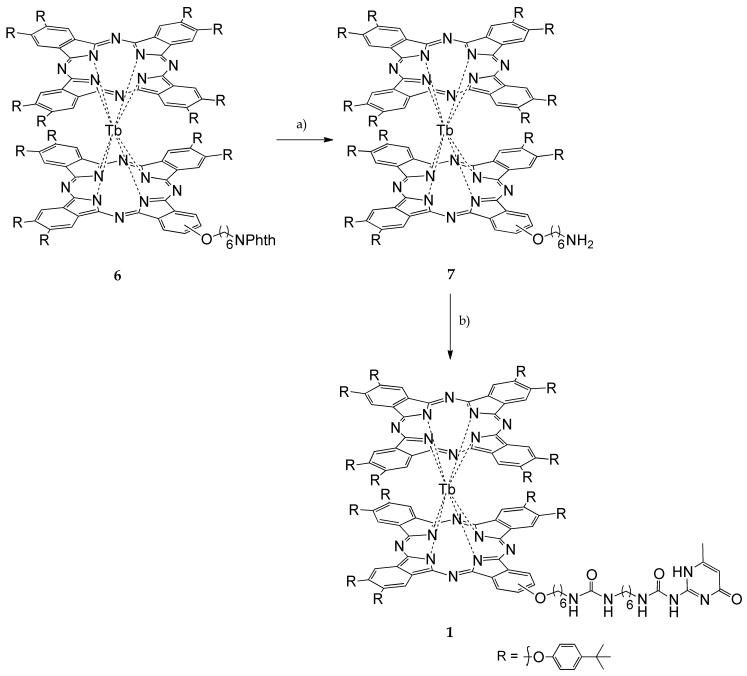

Scheme 5.4 *Synthesis of UPy-functionalized $TbPc_2$ **1**: a) $NH_2NH_2{\cdot}H_2O$, $CHCl_3$/MeOH, r.t., 12 h, 74%; b) 2(6-isocyanatohexylamino-carbonylamino)-6-methyl-4[1H]pyrimidinone, $CHCl_3$, r.t., 12 h, 52%.*

Amino-functionalized $TbPc_2$ **7** was reacted with 2(6-isocyanatohexylamino-carbonylamino)-6-methyl-4[1H]pyrimidinone affording UPy-functionalized $TbPc_2$ **1** in 52% yield. The resulting urea group guarantees the stability of $TbPc_2$ functionalization and its interference in the final hydrogen bond-driven UPy-NaPy complexation can be considered marginal. MALDI-TOF spectrum of compound **1** presented a fragmentation pattern and the molecular peak was not detectable (Figure 5.5).

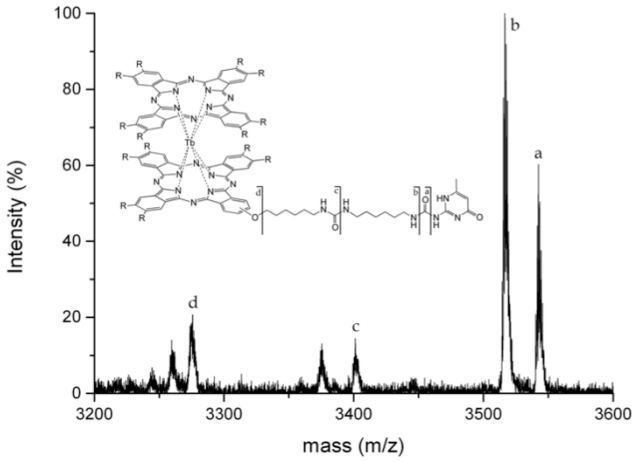

Figure 5.5 *High-resolution MALDI-TOF spectrum of UPy-functionalized $TbPc_2$* ***1****, with fragments attribution the insert.*

To unambiguously prove the identity of the isolated compound **1** an ESI-FT-Orbitrap-MS analysis (negative mode) was performed. The presence of the molecular peak, with an isotopic distribution in agreement with the theoretical one, confirmed the formation of heteroleptic UPy-functionalized $TbPc_2$ **1** (Figure 5.6). Interestingly, the signal of the UPy·UPy homodimer **1**·**1** was found to be overlapped to $[M]^-$.

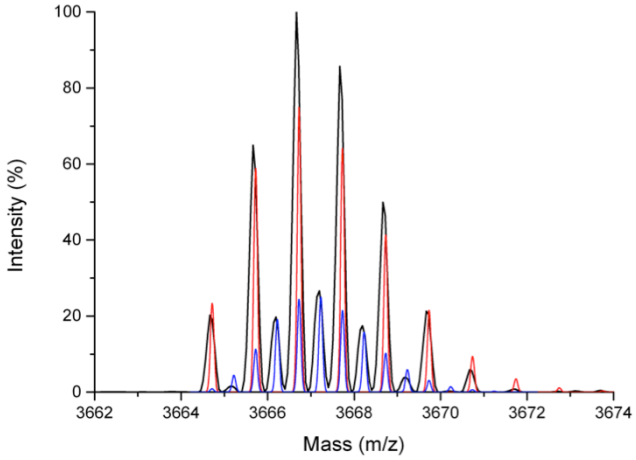

Figure 5.6 *Molecular peak of UPy-functionalized $TbPc_2$* ***1*** *(High-resolution ESI-FT-Orbitrap-MS): experimental isotopic distribution (black line), theoretical $[M]^-$ (red line) and theoretical $[2M]^{2-}$ (blue line) are reported.*

The UV-Vis spectrum, reported in Figure 5.7, showed an intense Q-band at 682 nm, two broad absorption bands, characteristic of a radical Pc ligand, at 490 and 919 nm and a split Soret band around 300 nm. The shoulder of the Q-band at 615 nm has been reported to be due to the weak π-π interactions between the two Pc ligands.[14]

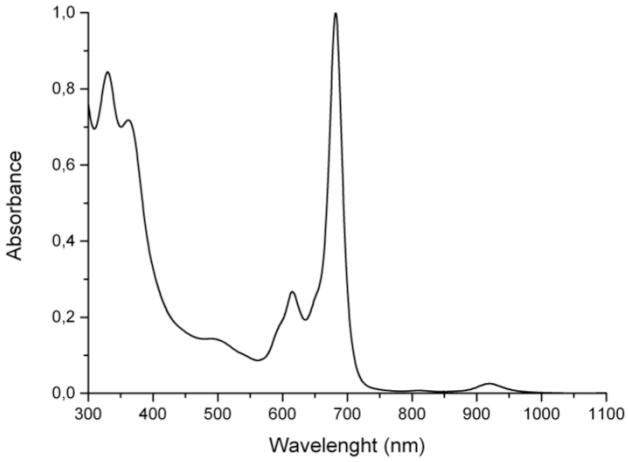

Figure 5.7 *UV-Vis absorption spectrum of UPy-functionalized $TbPc_2$ **1** in $CHCl_3$.*

5.2.2 Silicon Functionalization and $TbPc_2$ Self-Assembly

For the self-assembly of UPy-functionalized $TbPc_2$ **1**, two different NaPy monolayers on silicon surface were prepared. 2-(10-Undecenoylamino)-7-acetylamino-1,8-naphthyridine (**2**), synthesized according to literature procedure,[15] was grafted on freshly etched silicon wafers *via* thermal hydrosilylation of the double bond.[16]

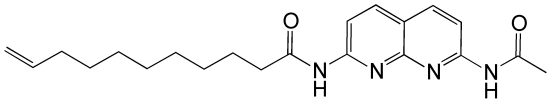

2

Figure 5.8 *Terminal alkene-functionalized NaPy used in this study.*

Treating H-terminated Si(000) with a solution of pure NaPy afforded the first robust covalent monolayer (Si@NaPy100%), while a mixed monolayer

NaPy/dodecene (Si@NaPy20%) was obtained from a 2:8 solution of the two compounds. The atomic compositions of the two grafted samples, obtained by X-ray photoelectron spectroscopy (XPS), are reported in Table 5.2. In both cases the appearance and the shape of N*1s* signal (Figure 5.9) is an indication of NaPy monolayer formation.

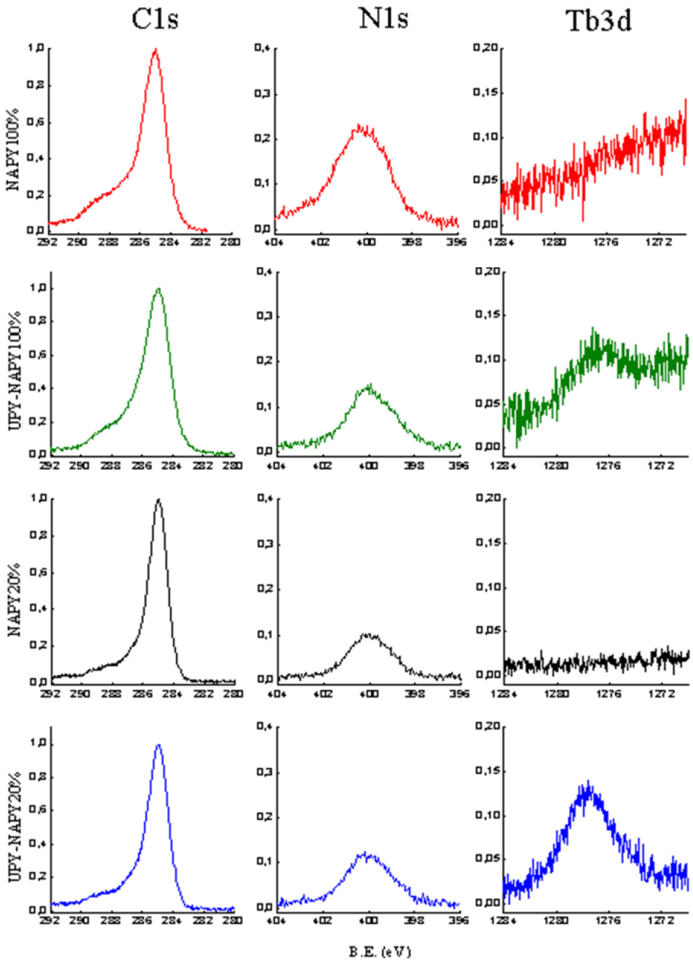

Figure 5.9 *C1s, N1s and Tb3d$_{3/2}$ regions of functionalized substrate before, Si@NaPy100% (red line) and Si@NaPy20% (black line), and after the self-assembly of* ***1***, ***1***·*Si@NaPy100% (green line) and* ***1***·*Si@NaPy20% (blue line).*

In particular, N*1s* band consists of two main components of equal intensity (Figure 5.10): (i) a feature at 400.3 eV assigned to the two amidic nitrogen atoms and (ii) a feature at 399.2 eV due the two N atoms of the naphthyridine ring. A low component at 401.6 eV due to N atoms protonated or forming hydrogen bond is also present. In addition, the shape of C*1s* band is consistent with the molecular formula of the grafted molecule. A main signal at 285.0 eV, related to the aliphatic carbons of the hydrocarbon chain, and a broad shoulder around 287.5 eV, due to carbon atoms bonded to N and O atoms, are present. As expected, this component is lower for Si@NaPy20% compared to Si@NaPy100% due to the presence of dodecyl chains. The C/N ratio of Si@NaPy20% is consistent with the presence of a mixed NaPy/dodecene layer with a NaPy percentage on the surface of about 25%. In the case of Si@NaPy100%, the C/N ration is higher than the value expected for a pure well-packed NAPY monolayer, likely due to the presence of adventitious carbon deposited between the NAPY molecules.

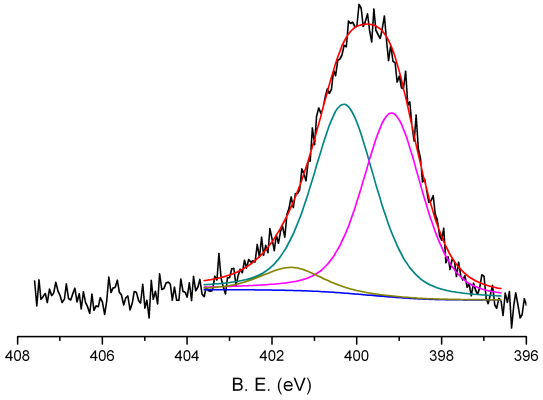

Figure 5.10 *Typical deconvolution of high-resolution N1s band of NaPy 100%. A similar result was obtained for Si@NaPy20%.*

After treatment with UPy-functionalized $TbPc_2$ **1**, the presence of Tb signals is an indication of the success of the complexation process. Atomic compositions of the grafted layers after $TbPc_2$ complexation are reported in Table 5.2. After the self-assembly of **1**, the Tb$3d_{3/2}$ spin-orbit component is the most suited to evaluate Tb concentration and bonding state, since the $3d_{5/2}$ spin-orbit component overlaps with the KVV Auger peak of C while *4d* peak of Tb is hidden by the Si2*s* signal. The Tb$3d_{3/2}$ sensitivity factor was empirically verified from Tb(III)acetate hydrate powder and pristine $TbPc_2$ powders. The concentration has been estimated taking into account the reduced thickness of

the grafted layer (assumed around 2 nm). The N/Tb ratio in samples obtained from Si@NaPy100% is higher than the nominal values (26:1) expected for 100% of complexation, indicating a lower yield (about 50 %) that can be ascribed to the bulkiness of $TbPc_2$ **1** compared to NaPy molecules. For the samples obtained on Si@NaPy20%, the N/Tb ratio revealed to be lower than in the case of Si@NaPy100%, indicating a higher yield of complexation. In this case, the little Tb excess is likely due to some degradation of $TbPc_2$ on the Si surface. The binding energy (BE) position of Tb$3d_{3/2}$ peak at 1277.0 eV is consistent with the presence of a Tb^{3+} species.

	N	C	Tb[a]	C/N	N/Tb
Si@NaPy100%	9.9	90.1	-	9.1	-
1·Si@NaPy100%	7.2	92.5	0.16	12.8	45.3
Si@NaPy20%	5.9	94.1	-	15.9	-
1·Si@NaPy20%	7.4	92.1	0.32	12.4	23.1

Table 5.2 *Atomic concentration estimated by XPS; a) Tb value has been corrected assuming a layer thickness of 2 nm.*

5.2.3 Hierarchical Self-Assembly on Gold

To anchor UPy-functionalized $TbPc_2$ **1** on gold, this surface was decorated with properly derivatized NaPy units. We decided to functionalize the 2,7-diamido-1,8-naphthyridine moiety with an aliphatic spacer bearing a terminal acetyl protected thiol. S-acetyl NaPy **3** was conveniently synthesized in one step from compound **2** (Scheme 5.5). Terminal alkene-functionalized NaPy **2** was reacted with thioacetic acid in the presence of AIBN as radical initiator affording **3** in 61% yield.

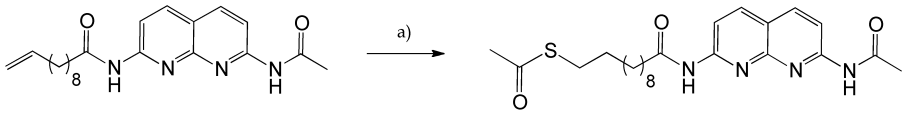

2 **3**

Scheme 5.5 *Synthesis of S-acetyl NaPy* **3***: a) thioacetic acid, AIBN, toluene, 110°C, 12 h, 61%.*

As all the attempts to deprotect the thiol in basic conditions (MeONa) prior to performing the self-assembly were unsuccessful, S-acetyl NaPy **3** was directly used for gold functionalization. Similarly to the Si case, two monolayers were prepared exposing Au(111) surfaces to two solutions containing a different concentration of **3**. Incubation in pure S-acetyl NaPy **3** ($1 \cdot 10^{-3}$ M in $CHCl_3$/MeOH 1:1) afforded the first monolayer Au@NaPy100%, while treatment with a mixture of **3**/1-decanethiol 2:8 gave the mixed monolayer Au@NaPy20%.[17] The subsequent hierarchical self-assembly was performed exposing the two monolayers to a solution of UPy-functionalized $TbPc_2$ **1** in anhydrous CH_2Cl_2 ($1 \cdot 10^{-5}$ M). The decorated surfaces were then washed with pure solvent to remove physisorbed **1** and directly exposed to synchrotron light for magnetic measurements.

5.2.4 Magnetic Characterizations

Magnetic properties of UPy-functionalized $TbPc_2$ **1** were preliminary tested in bulk *via* standard DC magnetometry. Hysteresis measurements, performed at 3K with a quantum design PPMS setup equipped with a Vibrating Sample Magnetometer (VSM) unit, are reported in Figure 5.11a. As clearly observable, the introduction of the Upy functionalization on the double decker scaffold does not alter significantly the SMM behavior of the complex. The ΔM/Msat vs field plot, reported in Figure 5.11b figure, is a valuable reference for estimating the opening of the hysteresis loop of these systems.[6]

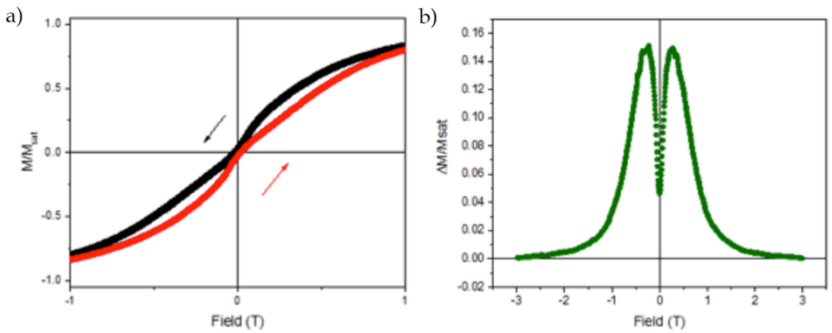

Figure 5.11 *(a) Magnetization curve at 3 K and (b) hysteresis opening (ΔM/Msat vs field plot) of bulk UPy-functionalized $TbPc_2$* **1**.

The same bulk system was drop casted and studied by XMCD at the DEIMOS beamline at the Soleil synchrotron (France).[18]

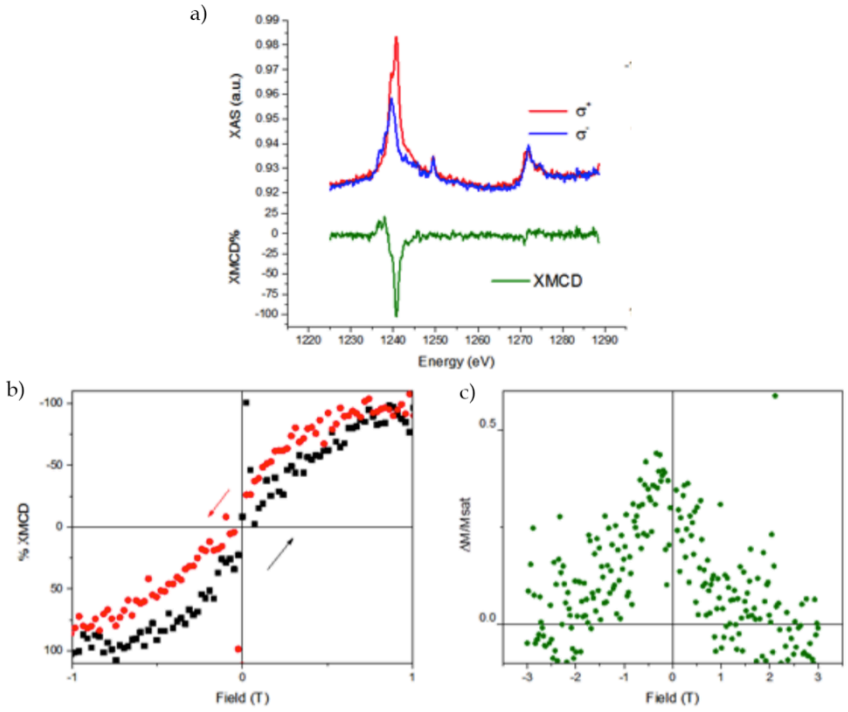

Figure 5.12 *(a) XAS and XMCD measurements, (b) XMCD-detected magnetization curve at 3 K and (c) hysteresis opening of a drop casted layer of UPy-functionalized $TbPc_2$* ***1****.*

XAS spectra (Figure 5.12a) at the $M_{4,5}$ edges of Tb with circularly left and right polarized light have been collected under a 3 Tesla external magnetic field along the x-ray propagation vector adopting a standard averaging approach to minimize the spurious effect.[19] This characterization allowed us to extract the XMCD spectrum defined as the difference between the two XAS spectra. Obtained spectra were found to be in agreement with previously reported bulk $TbPc_2$ investigations.[4b,20] XMCD measurements, normalized with respect to the isotropic spectrum, [4b,21] perfectly match the values expected for an intact $TbPc_2$ complex at 3K. More importantly, the extracted field dependence of the XMCD at the maximum of the dichroism, reported in Figure 5.12b, evidences (within the limit of the noise due to the limited signal to noise ratio of these spectra) that the opening of the magnetization hysteresis is clearly observable also with this technique. The "aperture plot" in Figure 5.12c, highlights that the XMCD-based hysteresis are affected by a larger error close to zero field. Therefore the

chances of evaluate the effect of the coupling with the surface on tunneling relaxation mechanism are limited.

Confirmed the SMM behavior of bulk UPy-functionalized $TbPc_2$ **1**, we investigated the magnetic properties of the self-assembled monolayers on silicon and gold. The four monolayers were characterized using XMCD technique since the amount of magnetic material present on these (sub)monolayer deposits was not sufficient for a meaningful characterization with traditional magnetometry.

We initially focused our attention on the two "full" monolayers, namely **1**·Au@NaPy100% and **1**·Si@NaPy100%, to better understand the results and compare the two surfaces.

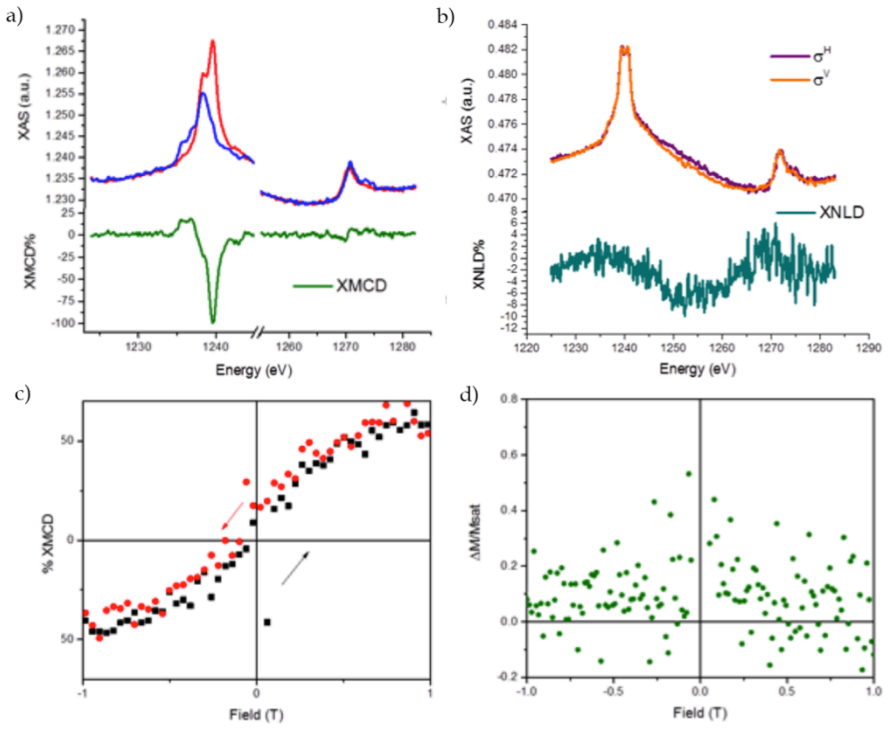

Figure 5.13 *(a) XAS and XMCD measurements, (b) XNLD measurements, (c) XMCD-detected magnetization curve at 3 K and (d) hysteresis opening for* ***1****·Au@NaPy100%.*

XMCD characterization of **1**·Au@NaPy100%, reported in Figure 5.13a, evidenced a fine structure characteristic of Tb(III) ion, while edge jump analysis of the isotropic spectrum revealed an amount of Tb-containing molecules corresponding to about 0.1 monolayer if compared with previous data.[6] The

small amount of molecules present on the surface justifies the difficulties in observing a clear opening in the magnetization curve. The same sample has been investigated using linearly polarized x-ray light (Figure 5.13b). Attempts to extracting an XNLD contribution evidenced that, being the broad oscillation of detected in the difference spectrum not significant, the tiny amount of $TbPc_2$ molecules did not present a preferential orientation with respect to the substrate.[4b]

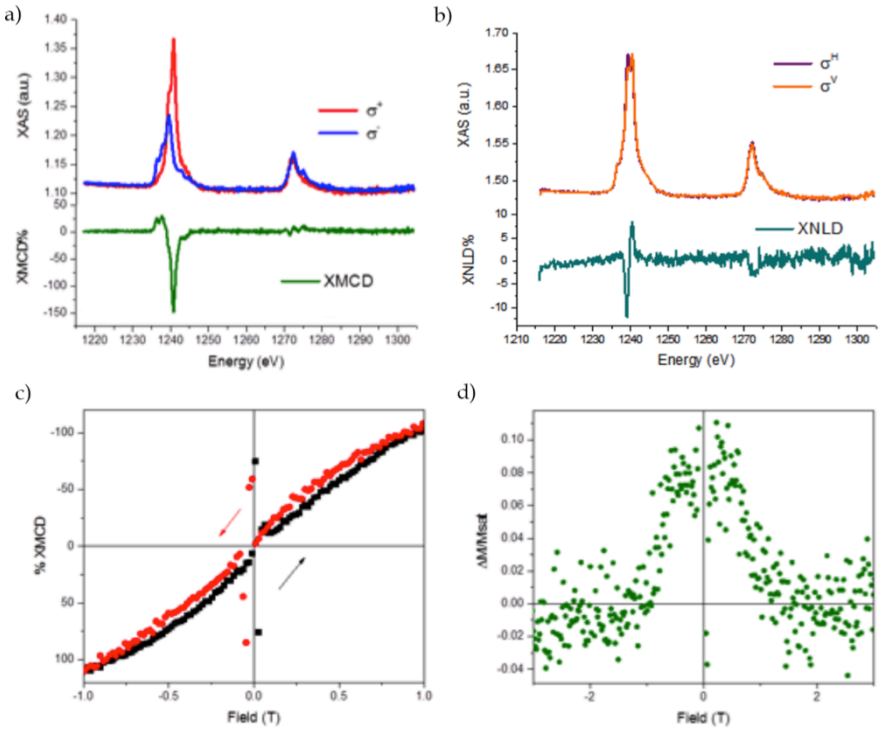

Figure 5.14 *(a) XAS and XMCD measurements, (b) XNLD measurements, (c) XMCD-detected magnetization curve at 3 K and (d) hysteresis opening for* ***1***·*Si@NaPy100%.*

Results obtained on **1**·Si@NaPy100% were found to be more promising (Figure 5.14). A 0.6 ML equivalent thickness was obtained from the edge jump analysis of the data. As a consequence of the higher signal to noise ratio in the XAS/XMCD analysis (Figure 5.14c and Figure 5.14d), an evident opening in the magnetization curves was observed. From a raw estimation of the resulting data we can assert that the adopted deposition strategy is capable to retain $TbPc_2$ magnetic properties on silicon. However, the enhancement observed in the covalent grafting of $TbPc_2$ molecules on the same surface[6] is absent. This can

be ascribed to the milder reaction condition as well as to the increased distance between the complex and the surface. Additionally, the XNLD spectrum indicates a partial orientation of the molecules on silicon, with the two phthalocyaninato ligands parallel to the surface, as observed also for covalently grafted $TbPc_2$ on Si.

The same characterization protocol was then applied to UPy-functionalized $TbPc_2$ **1** assembled on the two mixed monolayers.

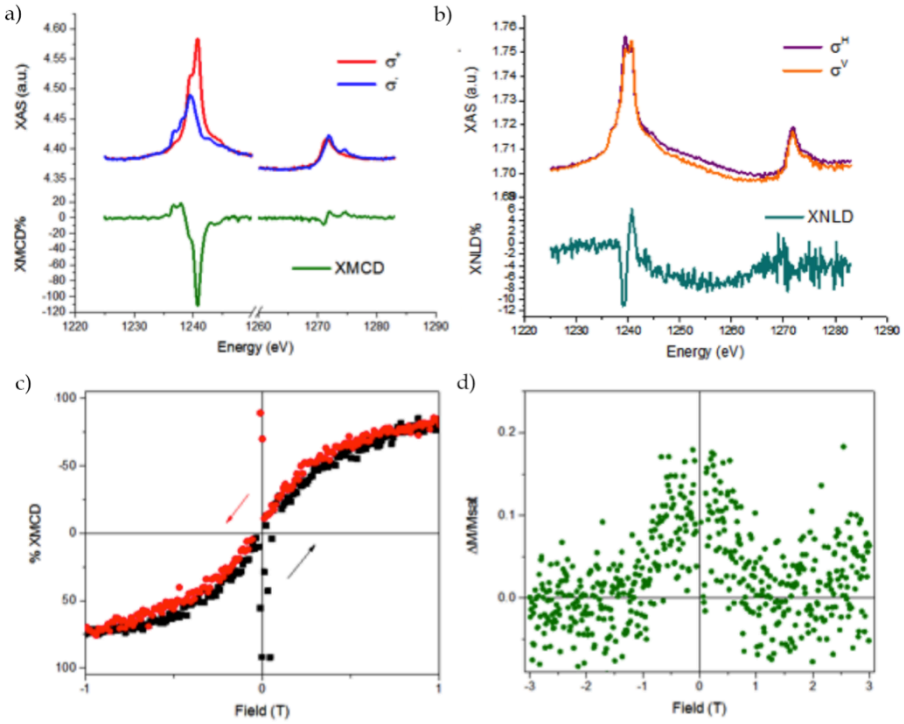

Figure 5.15 *(a) XAS and XMCD measurements, (b) XNLD measurements, (c) XMCD-detected magnetization curve at 3 K and (d) hysteresis opening for* ***1****·Au@NaPy20%.*

In the case of **1**·Au@NaPy20%, XAS/XMCD characterization suggested the presence of an amount of $TbPc_2$ molecules equivalent to 0.7 ML, probably due to a counterintuitive increase of NaPy derivative concentration on the surface allowing the interaction with a larger number of UPy-functionalized $TbPc_2$ **1**. The opening in the magnetization curve in Figure 5.14c is almost visible and, as confirmed by the "aperture plot" (Figure 5.15d), it is in agreement with the one observed on bulk samples indicating that the difficulties in the aperture observation are only due to a low signal to noise ratio. XNLD characterization

(Figure 5.15b) revealed, also in this case, a partial orientation of the $TbPc_2$ molecules with the easy axis perpendicular to the gold substrate. These results allowed us to exclude the presence of relevant amount of physisorbed material.

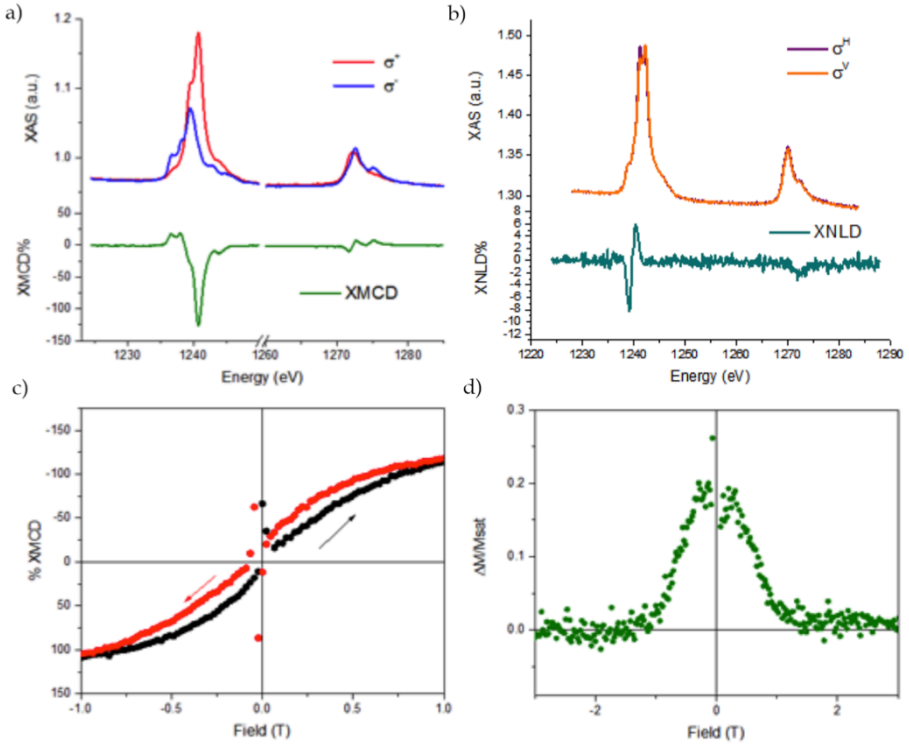

Figure 5.16 *(a) XAS and XMCD measurements, (b) XNLD measurements, (c) XMCD-detected magnetization curve at 3 K and (d) hysteresis opening for* ***1***·*Si@NaPy20%.*

A similar characterization was performed on **1**·Si@NaPy20%. Also in this case a 0.8 ML deposition was observed, as indication of an increased concentration of NaPy derivatives on surface. Interestingly, in this sample the opening of the hysteresis curve (Figure 5.16c) was found to be larger compared to all the other samples and the signal to noise ratio revealed to be very low. Anyway, further analysis need to be performed to correlate the observed increase to an effective enhancement of the magnetization dynamic of $TbPc_2$ assembled with this specific protocol. XNLD characterization (Figure 5.16b) also in this case revealed a partial orientation of the molecules with the Pc rings parallel to the substrate.

5.3 Conclusions

The UPy-NaPy driven self-assembly of $TbPc_2$ on silicon wafers turned out to be successful. The same cannot be said about the hierarchical self-assembly on gold surface, possibly due to the surface mobility/aggregation of thiol-functionalized NaPy molecules. Regarding the monolayer composition, mixed layers revealed to be more efficient compared to "full" monolayers. In fact, the bulkiness of UPy-functionalized $TbPc_2$ **1** prevents the complete complexation of NaPy units. As for covalent grafted $TbPc_2$, a counterintuitive orientation of $TbPc_2$ with the two phthalocyaninato ligands parallel to the surface was observed. The reversibility of this surface decoration remains to be tested.

5.4 Acknowledgments

Special thanks to Martina Torelli and Dr. Federico Bertani from the department of Chemistry, University of Parma. Thanks to Dr. Gianluca Paredi from the interdepartmental Centre SITEIA.PARMA, University of Parma, for mass spectrometry measurements. Thanks to Prof. Roberta Sessoli, Dr. Matteo Mannini, Dr. Lorenzo Poggini and Irene Cimatti from the department of Chemistry "Ugo Schiff", University of Firenze, and Dr. Philippe Ohresser, Prof. Philippe Sainctavit and Dr. Edwige Otero from Synchrotron SOLEIL, Gif-sur-Yvette, France, for magnetic measurements. Thanks to Prof. Guido Condorelli, Dr. Cristina Tudisco and Antonino E. Giuffrida from the department of Chemical Science, University of Catania, for silicon grafting and XPS measurements. Thanks to Dr. Michele Suman and Dr. Francesca Lambertini from Barilla S.p.a. for ESI-FT-Orbitrap-MS analyses.

5.5 Experimental Section

N-(6-Bromohexyl)phthalimide (4)

To a solution of 1,6-dibromohexane (1.24 mL, 8.1 mmol) in 20 mL of acetone, potassium phthalimide (0.500 g, 2.6 mmol) was added in 5 portions over 15 min. The suspension was refluxed overnight, filtered and the solid was washed with acetone. The organics were reduced and purified by flash column chromatography (petrolium ether/EtOAc 9:1). Compound **4** (0.694 g, 2.2 mmol, 86%) was obtained as a white solid.

^{1}H NMR ($CDCl_3$, 400 MHz): δ (ppm) = 7.84 (BB′ of a AA′BB′ system, 2H, J_1=3.1 Hz, J_2=5.5 Hz, Ar**H$_m$**), 7.72 (AA′ of a AA′BB′ system, 2H, J_1=3.1 Hz, J_2=5.5 Hz, Ar**H$_o$**), 3.68 (t, 2H, J=7.2 Hz, NC**H$_2$**CH_2), 3.39 (t, 2H, J=6.8 Hz, CH_2C**H$_2$**Br), 1.85 (m, 2H, NCH_2C**H$_2$**), 1.69 (m, 2H, C**H$_2$**CH_2Br), 1.46 (m, 2H, NCH_2CH_2C**H$_2$**), 1.37 (m, 2H, C**H$_2$**CH_2CH_2Br).

^{13}C NMR ($CDCl_3$, 75 MHz): δ (ppm) = 168.4, 133.9, 132.1, 123.2, 37.8, 33.7, 32.6, 28.4, 27.7, 26.0.

ESI-MS: *m/z* = 332.0 $[M+Na]^+$.

Pc(OC$_6$H$_{12}$NPhth) (5)

Monohydroxyl phthalocyanine (0.210 g, 0.15 mmol) was suspended in 10 mL of dry DMF and K_2CO_3 (0.040 g, 0.30 mmol) was added, followed by a catalytic amount of KI. After the addition of compound **4** (0.069 g, 0.22 mmol), the mixture was heated at 120 °C for 4 h. The reaction was cooled and the solvent was removed under reduced pressure. Flash column chromatography (CH_2Cl_2) afforded pure phthalocyanine **5** (0.203 g, 0.12 mmol, 82%) as a green solid.

^{1}H NMR ($CDCl_3$, 400 MHz): δ (ppm) = 8.9-8.2 (m, 9H, Ar**H**), 7.88 (BB′ of a AA′BB′ system, 2H, J_1=3.1 Hz, J_2=5.4 Hz, Ar**H$_m$**), 7.70 (AA′ of a AA′BB′ system, 2H, J_1=3.1 Hz, J_2=5.4 Hz, Ar**H$_o$**), 7.6-7.2 (m, 24H, ^{t}Bu-Ar**H**), 4.38 (bs, 2H, OC**H$_2$**CH_2), 3.82 (t, 2H, J=7.2 Hz, CH_2C**H$_2$**N), 2.11 (m, 2H, OCH_2C**H$_2$**), 2.0-1.2 (m, 60H, ArCC**H$_3$** + -C**H$_2$**-), -3.31 (bs, 2H, N**H**).

UV-Vis: λ_{max} ($CHCl_3$) = 704, 669, 647, 609, 392, 339 nm.

MALDI-TOF: calculated for $C_{106}H_{105}N_9O_9$ $[M]^+$ *m/z* = 1647.804, found *m/z* = 1647.715.

TbPc′Pc(OC$_6$H$_{12}$NPhth) (6)

To a stirred solution of the phthalocyanine **5** (0.050 g, 0.030 mmol) in 5 mL of o-DCB, $[Tb(acac)_3]\cdot nH_2O$ (0.016 g, 0.036 mmol) was added, followed by DBU (0.006 mL, 0.039 mmol). The solution was heated at 170 °C for 1 h. The resulting dark-blue solution was cooled at room temperature and the solvent was

evaporated under reduced pressure. The residue was washed several times with hexane affording the intermediate [Tb(acac)(Pc)], which was used for the next step without further purification. The blue solid was dissolved in 6 mL of a mixture of o-DCB/1-pentanol (1:1) and 4,5-Bis((4-tert-butylphenyl)oxy)-phthalonitrile (0.056 g, 0.133 mmol) was added, followed by DBU (0.006 mL, 0.039 mmol). The mixture was heated at 160 °C for 4 h, then the reaction was cooled and the solvent was removed under reduced pressure. The residue was redissolved in $CHCl_3$, DDQ (0.014 g, 0.062 mmol) was added and the solution was stirred at room temperature for 1 h. The solvent was removed under reduced pressure and flash column chromatography (gradient from Hex/CH_2Cl_2 1:1 to Hex/CH_2Cl_2 3:7) afforded pure compound **6** (0.027 g, 0.008 mmol, 26%) as a green solid.
UV-Vis: λ_{max} ($CHCl_3$) = 917, 681, 615, 494, 364, 330 nm.
MALDI-TOF: calculated for $C_{218}H_{215}N_{17}O_{17}Tb$ $[M]^+$ *m/z* = 3503.580, found *m/z* = 3503.705.

TbPc'Pc($OC_6H_{12}NH_2$) (7)
The double decker **6** (0.015 g, 0.004 mmol) was dissolved in 6 mL of a 3:1 mixture of $CHCl_3$/MeOH and $NH_2NH_2{\cdot}H_2O$ (80%, 0.2 mL) was added. The green solution immediately turned blue. The mixture was stirred at room temperature overnight. Water was added and the organics were removed under reduced pressure. The precipitate was filtered, washed with water and dried. The blue residue was dissolved in $CHCl_3$ and the solution was left at the air overnight. The green solution was reduced and the crude was purified by flash column chromatography (Hex/CH_2CH_2 1:9 + 1% TEA). Pure compound **7** was obtained as a green solid (0.010 g, 0.003 mmol, 74%).
UV-Vis: λ_{max} ($CHCl_3$) = 917, 681, 615, 491, 364, 330 nm.
MALDI-TOF: calculated for $C_{210}H_{213}N_{17}O_{15}Tb$ $[M]^+$ *m/z* = 3373.574, found *m/z* = 3373.663.

TbPc'Pc($OC_6H_{12}NH(C{=}O)NHC_6H_{12}UPy$) (1)
To a solution of double decker **7** (0.030 g, 0.009 mmol) in 5 mL of freshly distilled $CHCl_3$, 2(6-isocyanatohexylamino-carbonylamino)-6-methyl-4[1H]-pyrimidinone (0.003 g, 0.010 mmol) was added. The mixture was stirred at room temperature overnight. Silica was added, followed by a catalytic amount of dibutyltin dilaurate (DBTL), and the suspension was refluxed for 4 h. After cooling, the silica was filtered, washed with $CHCl_3$ and the filtrate was reduced under vacuum. Two precipitations from MeOH afforded pure compound **1** as a green solid (0.017 g, 0.005 mmol, 52%).

UV-Vis: λ_{max} ($CHCl_3$) = 919, 682, 615, 490, 362, 330 nm.
MALDI-TOF (fragmentation pattern):
calculated for (a) *m/z* = 3541.67, found *m/z* = 3541.49;
calculated for (b) *m/z* = 3514.67, found *m/z* = 3514.47;
calculated for (c) *m/z* = 3399.56, found *m/z* = 3399.90;
calculated for (d) *m/z* = 3273.47, found *m/z* = 3273.75.

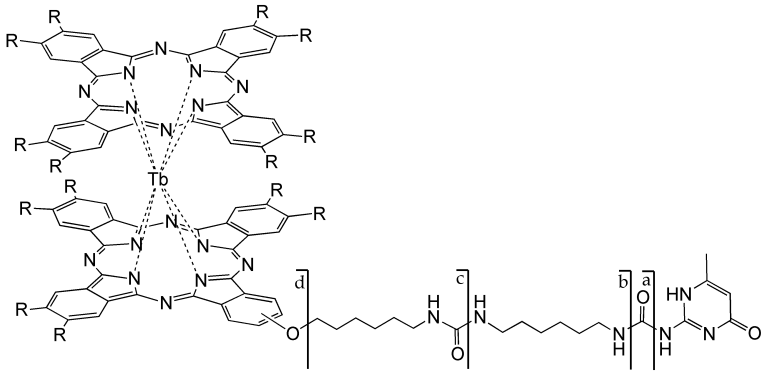

ESI-FT-Orbitrap-MS: calculated for $C_{223}H_{232}N_{22}O_{18}Tb$ $[M]^-$ *m/z* = 3666.724, found *m/z* = 3666.669; calculated for $C_{446}H_{464}N_{44}O_{36}Tb_2$ $[2M]^{2-}$ (dimer) *m/z* = 3667.174, found *m/z* =3667.225.

2-(11-Acetylthioundecanoylamino)-7-acetylamino-1,8-naphthyridine (3)
In a Schlenk tube, thioacetic acid (0.04 mL, 0.5 mmol) was added to a degassed solution of 2-(10-undecenoylamino)-7-acetylamino-1,8-naphthyridine (0.02 g, 0.05 mmol) in 2 mL of toluene. After the addition of a catalytic amount of AIBN, the reaction was stirred overnight at 110°C. The mixture was cooled at room temperature and water was added, followed by EtOAc. The organic phase was washed twice with a saturated aqueous solution of $NaHCO_3$ and once with brine. The solvent was removed under reduced pressure and the crude was purified by preparative TLC ($CHCl_3$/MeOH 98:2) affording compound **3** as a pale yellow solid (0.0135 g, 0.03 mmol, 61%).
^{1}H NMR ($CDCl_3$, 400 MHz): δ (ppm) = 9.04 (bs, 1H, N**H**), 8.82 (bs, 1H, N**H**), 8.47 (m, 2H, Ar$\mathbf{H_{3,6}}$), 8.14 (d, 2H, Ar$\mathbf{H_{4,5}}$), 2.87 (t, 2H, J=7.4 Hz, SC$\mathbf{H_2}$$CH_2$), 2.46 (t, 2H, J=7.4 Hz, CH_2C$\mathbf{H_2}$NH), 2.33 (s, 3H, C$\mathbf{H_3}$C(=O)SCH_2), 2.27 (s, 3H, C$\mathbf{H_3}$C(=O)NH), 1.73 (m, 2H, SCH_2C$\mathbf{H_2}$), 1.57 (m, 2H, C$\mathbf{H_2}$$CH_2$NH), 1.38-1.24 (m, 12H, -C$\mathbf{H_2}$-).
^{13}C NMR ($CDCl_3$, 75 MHz): δ (ppm) = 196.1, 172.6, 169.5, 154.1, 139.1, 118.3, 113.7, 53.4, 37.9, 30.6, 29.7, 29.5-29.1, 28.8, 25.2, 25.0.

ESI-MS: *m/z* = 445.4 $[M+H]^+$, 467.4 $[M+Na]^+$, 483.3 $[M+K]^+$.

Procedure for Si-grafting of NaPy 2

The anchoring of NaPy **2** on a single crystalline, Czochralski grown, p-type boron-doped, (100)-oriented silicon substrate was performed through a well establish thermal hydrosilylation route.[16] Si(100) substrates were first cleaned with "piranha" solution (H_2SO_4(30%)/H_2O_2 70:30, v/v) at room temperature for 12 min, rinsed in double distilled water for 2 min, etched in 2% hydrofluoric acid for 90 s, washed with double distilled water for 20 s and accurately dried with pre-purified N_2. The Si substrate was immediately placed in a three neck flask containing 3,68 mg of **2** ($1.0 \cdot 10^{-3}$ M) or a **2**/1-dodecene mixture 2:8 (($1.0 \cdot 10^{-3}$ M) dissolved in 10 mL of anhydrous mesitylene. The solution was then refluxed at 180 °C for 2 h, under slow N_2 bubbling. After cooling at room temperature, the substrates were removed from the flask, rinsed, and repeatedly sonicated in CH_2Cl_2 to remove any residual unreacted NaPy **2** molecules.

UPy-NaPy complexation on Si

The complexation was carried out dipping functionalized Si substrates into a sealed vial containing a solution of UPy-functionalized $TbPc_2$ **1** ($1.0 \cdot 10^{-3}$ M) in $CHCl_3$ overnight at room temperature. The samples were removed from the reaction environment and rinsed several times in anhydrous $CHCl_3$ in order to remove any residual uncomplexed $TbPc_2$ **1** and dried with N_2.

Hierarchical self-assembly on Au

Step 1) Au(111) samples were incubated at room temperature for 16 h in two solutions: (a) S-acetyl NaPy **3** $1 \cdot 10^{-3}$ M in $CHCl_3$/MeOH 1:1 (Au@NaPy100%); (b) S-acetyl NaPy **3** $0.2 \cdot 10^{-3}$ M **+** 1-decanethiol $0.8 \cdot 10^{-3}$ M in $CHCl_3$/MeOH 1:1 (Au@NaPy20%). The two surfaces were then repeatedly washed with $CHCl_3$ and MeOH and dried under Ar.

Step 2) The two monolayers were incubated at room temperature for 18 h in a $1 \cdot 10^{-5}$ M solution of UPy-functionalized $TbPc_2$ **1** in anhydrous CH_2Cl_2. The gold samples were then washed four times with anhydrous CH_2Cl_2 and dried under Ar.

5.6 References

[1] a) L. Krusin-Elbaum, T. Shibauchi, B. Argyle, L. Gignac, D. Weller, *Nature* **2001**, *410*, 444–446; b) M. N. Leuenberger, D. Loss, *Nature* **2001**, *410*, 789–793.

[2] J. Camarero, E. Coronado, *J. Mater. Chem.* **2009**, *19*, 1678–1684.

[3] N. Domingo, E. Bellido, D. Ruiz-Molina, *Chem. Soc. Rev.* **2012**, *41*, 258–302.

[4] a) K. Katoh, Y. Yoshida, M. Yamashita, H. Miyasaka, B. K. Breedlove, T. Kajiwara, S. Takaishi, N. Ishikawa, H Isshiki, Y. Feng Zhang, T. Komeda, M-Yamagishi, J. Takeya, *J. Am. Chem. Soc.* **2009**, *131*, 9967–9976; b) L. Margheriti, D. Chiappe, M. Mannini, P.-E. Car, P. Sainctavit, M.-A. Arrio, F. B. de Mongeot, J. C. Cezar, F. M. Piras, A. Magnani, E. Otero, A. Caneschi, R. Sessoli, *Adv. Mater.* **2010**, *22*, 5488-5493; c) A. Lodi Rizzini, C. Krull, T. Balashov, J. J. Kavich, A. Mugarza, P. S. Miedema, P. K. Thakur, V. Sessi, S. Klyatskaya, M. Ruben, S. Stepanow, and P. Gambardella, *Phys. Rev. Lett.* **2011**, 107, 177205; d) J. Schwöbel, Y. Fu, J. Brede, A. Dilullo, G. Hoffmann, S. Klyatskaya, M. Ruben, R. Wiesendanger, *Nat. Commun.* **2012**, article number: 953.

[5] L. Malavolti, M. Mannini, P. Car, G. Campo, F. Pineider, R. Sessoli, *J. Mater. Chem. C* **2013**, *1*, 2935-2942.

[6] M. Mannini, F. Bertani, C. Tudisco, L. Malavolti, L. Poggini, K. Misztal, D. Menozzi, A. Motta, E. Otero, P. Ohresser, P. Sainctavit, G. G. Condorelli, E. Dalcanale, R. Sessoli, *Nat. Commun.* **2014**, *5*, article number: 4582.

[7] c) M. Lopes, A. Candini, M. Urdampilleta, A. Reserbat-Plantey, V. Bellini, S. Klyatskaya, L. Marty, M. Ruben, M. Affronte, W. Wernsdorfer, N. Bendiab *ACS Nano* **2010**, *4*, 7531–7537; d) A. Candini, S. Klyatskaya, M. Ruben, W. Wernsdorfer, M. Affronte *Nano Lett.* **2011**, *11*, 2634–2639.

[8] U. Glebe, T. Weidner, J. E. Baio, D. Schach, C. Bruhn, A. Buchholz, W. Plass, S. Walleck, T. Glaser, U. Siemeling, *ChemPlusChem* **2012**, *77*, 889–897.

[9] A. De Cian, M. Moussavi, J. Fischer, R. Weiss, *Inorg. Chem.* **1985**, *24*, 3162-3167.

[10] H. M. Keizer, R. Van Kessel, R. P. Sijbesma, E. W. Meijer, *Polymer* **2003**, *44*, 5505-5511.

[11] S. Albert-Seifried, C. E. Finlayson, F. Laquai, R. H. Friend, T. M. Swager, P. H. J. Kouwer, M. Juríček, H. J. Kitto, S. Valster, R. J. M. Nolte, A. E. Rowan, *Chem. Eur. J.* **2010**, *16*, 10021–10029.

[12] K. Hu, Y.-j. Qi, J. Zhao, H.-f. Jiang, X. Chen, J. Ren, *Eur. J. Med. Chem.* **2013**, *64*, 529-539

[13] C. R. Ganivet, B. Ballesteros, G. de la Torre, J. M. Clemente-Juan, E. Coronado, T. Torres, *Chem. Eur. J.* **2013**, 19, 1457-1465.

[14] A. Iwase, C. Harnoode, Y. Kameda, *J. Alloys Compd.* **1993**, 192, 280–283.

[15] G. B. W. L. Ligthart, H. Ohkawa, R. P. Sijbesma, E. W. Meijer, *J. Org. Chem.* **2006**, *71*, 375-378.

[16] a) J. M. Buriak, *Chem. Rev.* **2002**, *102*, 1217-1308; b) G. G. Condorelli, A. Motta, M. Favazza, I. L. Fragala, M. Busi, E. Menozzi, E. Dalcanale, L. Cristofolini, *Langmuir* **2006**, *22*, 11126–11133; c) A. Gulino, F. Lupo, G. G. Condorelli, M. E. Fragalà, M. E. Amato, G. Scarlata, *J. Mater. Chem.* **2008**, *18*, 5011–5018.

[17] B. Lüssem, L. Müller-Meskamp, S. Karthäuser, R. Waser, M. Homberger, U. Simon, *Langmuir* **2006**, *22*, 3021–3027

[18] P. Ohresser, E. Otero, F. Choueikani, K. Chen, S. Stanescu, F. Deschamps, T. Moreno, F. Polack, B. Lagarde, J.-P. Daguerre, F. Marteau, F. Scheurer, L. Joly, J.-P. Kappler, B. Muller, O. Bunau, Ph. Sainctavit, *Rev. Sci. Instrum.* **2014**, *85*, 013106.

[19] R. Sessoli, M. Mannini, F. Pineider, A. Cornia, Ph. Sainctavit, *Magnetism and Synchrotron Radiation* **2010**, Springer-Verlag, Berlin, Chapter 10.

[20] L. Malavolti, L. Poggini, L. Margheriti, D. Chiappe, P. Graziosi, B. Cortigiani, V. Lanzilotto, F. Buatier de Mongeot, P. Ohresser, E. Otero, F. Choueikani, Ph.

Sainctavit, I. Bergenti, V. A. Dediu, M. Mannini, R. Sessoli, *Chem. Commun.* **2013**, *49*, 11506-11508.

[21] P. Totaro, L. Poggini, A. Favre, M. Mannini, Ph. Sainctavit, A. Cornia, A. Magnani, R. Sessoli, *Langmuir* **2014**, *30*, 8645–8649.

CHAPTER 6

AUXETIC MATERIALS

6.1 Auxetic Behavior

The development of smart materials and structures possessing properties that can be significantly changed by external stimuli has attracted many scientists. In particular, prediction and control of polymers response to tensile forces represent a key issue in Materials Science. Poisson's ratio (v) is defined as the ratio of the lateral contractile strain to the longitudinal tensile strain for an object undergoing uniaxial tension in the longitudinal direction.[1] Despite most common materials, which have Poisson's ratios between 0.2 and 0.4, negative values of ν are not forbidden by thermodynamics. Materials that possess negative ν, referred as auxetics,[2] expand in directions orthogonal to the applied stress and show enhancements in mechanical properties related to the Poisson's ratio. For example, assuming a uniform indentation, the hardness (or indentation resistance) of an isotropic material with a Young's modulus E is proportional to $[(1 - v^2)/E]^{-1}$. Since v should theoretically lie within the range $-1 \leq v < +1/2$, a significant improvement of the hardness, compared to non-auxetic materials, can be obtained for values lower than -1/2. This can be physically explained considering that auxetics contract laterally when compressed by an object, leading to a densification under the impact area (Figure 6.1).[3] Other important mechanical properties, such as shear resistance[4] and fracture toughness,[5] benefit from this behavior.

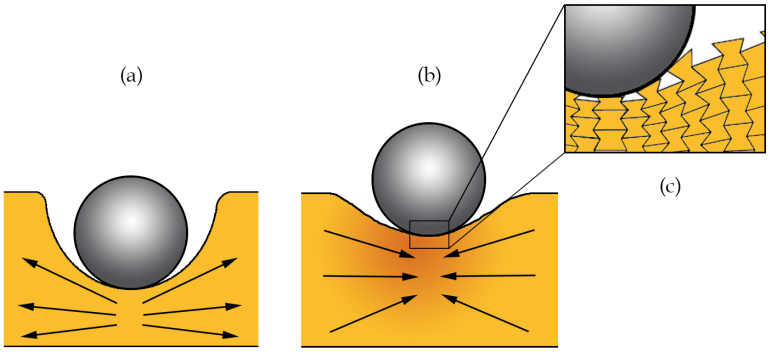

Figure 6.1 *Representation of indentation response for (a) non-auxetic and (b) auxetic materials. A deformation of the re-entrant honeycomb structure is assumed (c).*[6]

Since the theory of elasticity is scale-independent, auxetics can be observed ranging from the macroscopical to the molecular level. Examples of large-scale auxetics are Magnox nuclear reactors[7] and porous constructs based on re-entrant honeycomb structures.[8] The first reported auxetic materials are isotropic polyurethane foams developed by Lakes in 1987.[9] In this case, the

negative Poisson's ratio is related to the microscopic structure. As depicted in Figure 6.2, the convex polyhedral cells, characteristic of conventional foams, are converted through a thermal/mechanical treatment into re-entrant structures.

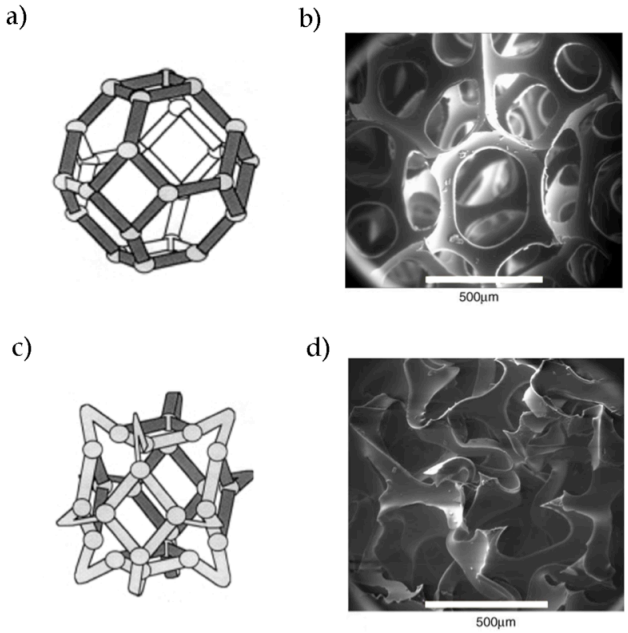

Figure 6.2 *Tetrakaidecahedron cell models and SEM images of a conventional (a,b) and an auxetic (c,d) polyurethane foams.*[10]

Since foams are not stiff enough to benefit from the improved mechanical properties, Evans and coworkers developed an expanded polytetrafluoroethylene (PTFE) with negative Poisson's ratio.[11] Morphology studies revealed that the auxetic behavior of PTFE is due to the microstructure of the polymer, which consists of an array of nodules interconnecting by fibrils creating an analogous of the re-entrant honeycomb structure.[12] Even if most studied auxetics are man-made, materials with negative Poisson's ratio are present also in Nature. Interestingly fibrillar structures are responsible for the auxetic behavior of biomaterials such as cat skin[13] and human tendons.[14]

6.2 Molecular Auxetics

Among naturally occurring auxetic materials, α-cristobalite, a polymorph of crystalline silica, is a well-known example of molecular auxetic.[15] The explanation of its negative Poisson's ratio has been proposed to be the cooperative rotation of the SiO_4 tetrahedral units.[16] More recently a two-dimensional geometry-based model has been used to describe how the cross-section of this silicate is deformed upon loading.[17] Nowadays the design and control of auxetic materials at the molecular level is still an open issue. Inspired by macroscopic re-entrant honeycomb structures, auxetic behavior has been predicted for a great variety of molecular networks constituted by cross-linked rigid aromatic alkynes.[2] In 1993 Baughman and Galvão proposed a different design based on "twisted-chain" polyacetylenes.[18] Starting from a "egg rack" structure, constituted by a square grid made of alternate facing "four-legged claws", Evans and co-workers predicted an auxetic behavior for the calix[4]arene-based 3D polymeric network reported in Figure 6.3.[19]

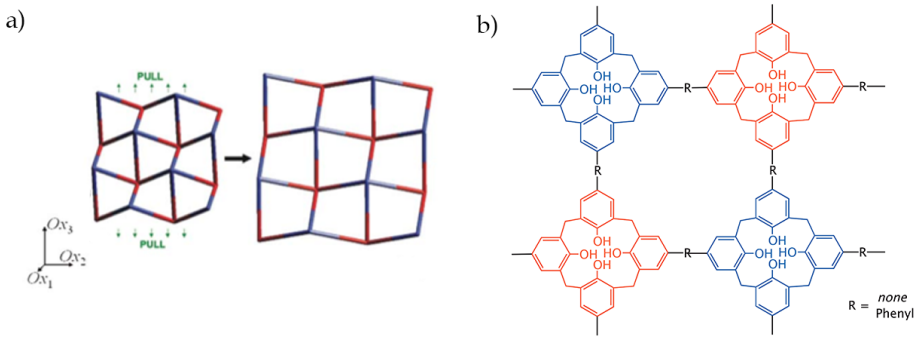

Figure 6.3 *a) "egg-rack" structure; b) calix[4]arene network designed by Evans et co-workers.*[19]

The authors assumed calix[4]arenes to behave as junctions able to propagate the elongation in the transversal direction. The force-induced widening of the calix[4]arene scaffold with respect to the equilibrium conformation was expected to promote the lateral expansion of the material. Although systems with two calix[4]arenes directly connected by a para-para linkage are present in literature,[20] the synthesis of such highly cross-linked structures revealed to be infeasible. However, rigidity of proposed networks can only lead to materials with high melting temperature and poor tractability limiting their applicability. Starting from these considerations, Griffin and co-workers moved the attention to linear polymers.[21a] In order to exhibit auxetic behavior under tensile strain,

interchain distance of these materials should increase in a direction perpendicular to the applied force. Contrariwise, common polymers develop a more ordered and compact structure when stretched. To overcome this problem, a control of the auxetic nature of the material at a molecular level is strictly required. In particular, Griffin and *al.* proposed the introduction of bulky rigid laterally attached rods into the polymer backbone. As depicted in Figure 6.4, force-induced rotation of terphenyl units is expected to increase steric repulsion between neighboring chains. To obtain a unidirectional molecular response capable to induce a macroscopic variation transversal to the elongation, main-chain liquid crystal elastomers (MC-LCE), able to align their chains leading to highly ordered domains,[22] were used. By placing mesogenic units among the polymer backbone, laterally attached rods are also initially oriented parallel to the chain axis as required by an optimal design of the material. Even if a small increase of the interchain distance has been observed by X-ray scattering, the reported system failed to evidence an auxetic behavior.

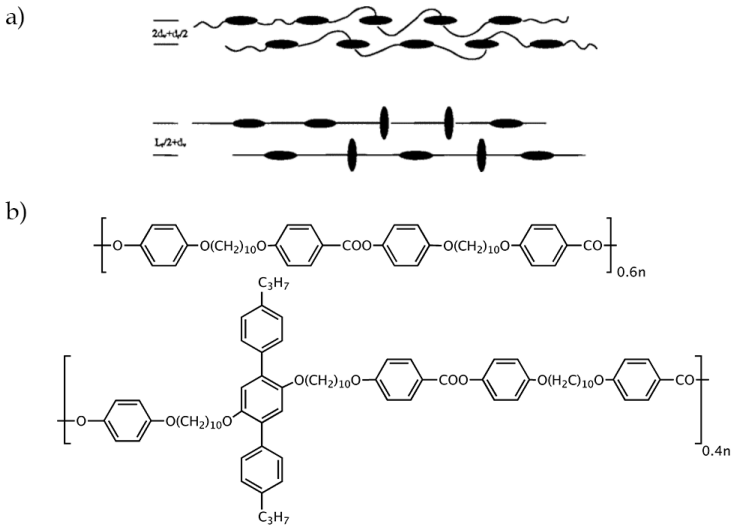

Figure 6.4 *a) Representation of interchain distance increase with the rotation of laterally attached units (depicted as black rods like mesogens); b) chemical structure of tested polymer.*[21a]

Inspired by these polymeric systems, we propose a novel approach for the design of a molecular auxetic based on conformationally switchable monomeric units. In our idea, the introduction of molecules able to reversibly increase their size switching from an initial contracted conformation to an expanded one applying a tensile force can impart auxetic behavior to MC-LCE.

6.3 Tetraquinoxaline Cavitands

Resorcin[4]arene cavitands bridged by four quinoxaline moieties, introduced by Cram and co-workers,[23] are among most attracting molecular receptors. These compounds, usually referred as tetraquinoxaline cavitands (QxCav), are conveniently prepared by the fourfold bridging of corresponding resorcinarene scaffolds with 2,3-dichloroquinoxalines compounds (Figure 6.5).

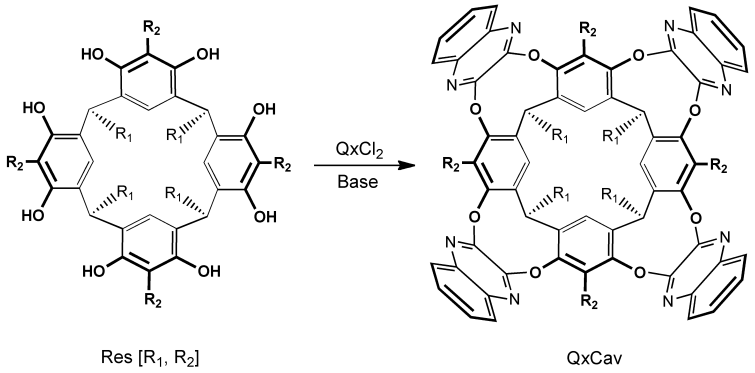

Figure 6.5 *Tetraquinoxaline cavitand synthesis.*

For the presence of electron rich quinoxaline walls, the resulting cavitands possess a hydrophobic and electron rich cavity that is suitable for the complexation of aromatics. The selective recognition properties of tetraquinoxaline cavitands towards aromatic hydrocarbons have been applied to fabricate low-cost systems with sub-ppb detection limits of toxic Volatile Organic Compounds (VOCs) in air.[24] Complex formation is driven by multiple π-π and CH-π interactions between the aromatic guest and the deep, hydrophobic cavity.[25]

Complexation abilities are not the only appealing properties of tetraquinoxaline cavitands. As shown in Figure 6.6, these systems are able to reversibly switch between a closed *vase* conformation (C_{4v} symmetry) and an open extended *kite* conformation (C_{2v} symmetry). According to Cram and co-workers,[23] this interconversion is temperature-dependent and *vase* conformation is prevalent in solution at room temperature and above, while at temperatures approaching –60 °C the cavitand is present only as *kite*. The origin of this behavior should be traced to solvation effects: at low temperature the *kite* conformer exposes to the solvent a larger surface, while the solvation entropic term becomes unfavorable at higher temperatures promoting the *vase* form. Interestingly, *vase* ⥋ *kite* interconversion was found to be sensitive to other external stimuli leading to

tetraquinoxaline cavitands definition as molecular switches.[26] pH decrease upon addition of trifluoroacetic acid (TFA) to a solution of QxCav induced *vase* → *kite* switching as consequence of Coulomb repulsion between protonated quinoxaline nitrogen atoms.[27] The increase of Zn^{2+} ion concentration, instead, stabilized *kite* conformation through the formation of coordination complexes between Zn^{2+} and quinoxaline bases.[28] Electrochemical switching was initially reported by Diederich on a tetrathiafulvalene-functionalized Qx-Cav,[29] and subsequently on quinone-based cavitands able to form intramolecular hydrogen bonds.[30]

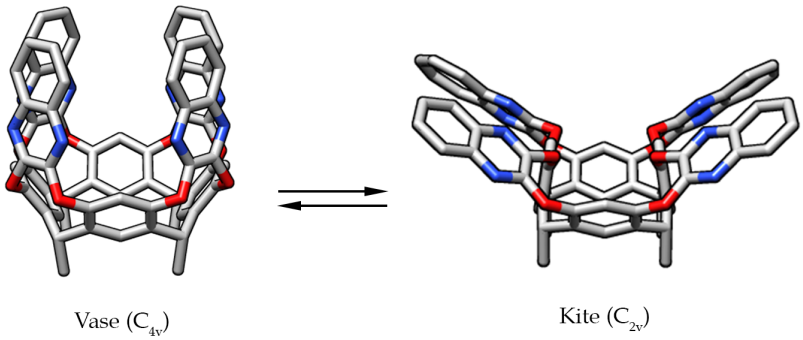

Figure 6.6 *Cavitand switching between vase and kite conformations.*[31]

Mechanochemically induced conformation interconvertion of tetraquinoxaline cavitands is still unexplored. We assume that the application of a tensile force to two opposite quinoxaline walls can induce the complete opening of the cavitand structure. Introducing QxCavs in the backbone of a MC-LCE, this size variation, that it is estimated to correspond to an increase of cavitand size of about 1.4 nm, may lead to an increase of the inter-chain distance.

In Chapter 7, we study *via* NMR tetraquinoxaline cavitand behavior first in simple dimers then in polymers to verify the retention of the *vase* conformation and cavitand capability to switch to the *kite* form applying conventional external stimuli (temperature and pH).

In Chapter 8, we investigate tetraquinoxaline cavitands ability to interconvert from *vase* to *kite* applying a mechanical stress to two opposite quinoxaline walls. For this purpose we introduced QxCav in two polymeric matrixes, namely polybutylmethacrylate (PBMA) and polydimethylsiloxane (PDMS). *Vase* → *kite* switching was followed by UV-Vis spectroscopy.

6.4 References

[1] A. Alderson, *Chem. Ind. (Londo*n) **1999**, *10*, 384-391.

[2] K. E. Evans, M. A. Nkansah, *Nature* **1991**, *353*, 124.

[3] K. E. Evans, A. Alderson, *Adv. Mater.* **2000**, *12*, 617-628.

[4] J. B. Choi, R. S. Lakes, *J. Mater. Sci.* **1992**, *27*, 4678-84.

[5] J. B. Choi, R. S. Lakes, *International Journal of Fracture* **1996**, *80*, 73-83.

[6] J. N. Grima, D. Attard, R. Gatt, R. N. Cassar, *Adv. Eng. Mater.* **2009**, *11*, 533–535.

[7] K. Muto, R. W. Bailey, K. J. Mitchell, *Proc. Inst. Mech. Eng.* **1963**, *177*, 155.

[8] D. J. Fozdar, P. Soman, J. W. Lee, L. H. Han, S. Chen, *Adv. Funct. Mater.* **2011**, *21*, 2712–2720.

[9] R. Lakes, *Science* **1987**, *235*, 1038-1040.

[10] J. N. Grima, R. Gatt, N. Ravirala, A. Alderson, K. E. Evans, *Materials Science and Engineering A* **2006**, *423*, 214–218.

[11] B. D. Caddock, K. E. Evans, *J. Phys. D: Appl. Phys.* **1989**, *22*, 1877-1882.

[12] K. E. Evans, B. D. Caddock, *J. Phys. D: Appl. Phys.* **1989**, *22*, 1883-1887.

[13] D.R. Veronda, R. A. Westmann, *J. Biomechanics* **1970**, *3*, 111-124.

[14] R. Gatt, M. V. Wood, A. Gatt, F. Zarb, C. Formosa, K. M. Azzopardi, A. Casha, T.P. Agius, P. Schembri-Wismayer, L. Attard, N. Chockalingam, J. N. Grima, *Acta Biomaterialia* **2015**, *24*, 201–208.

[15] Y. Yeganeh-Haeri, D. J. Weidner, J. B. Parise, *Science* **1992**, *257*, 650.

[16] N. R. Keskar, J. R. Chelikowsky, *Nature* **1992**, *358*, 222.

[17] J. N. Grima, R. Gatt, A. Alderson, K. E. Evans, *J. Mater. Chem.* **2005**, *15*, 4003–4005.

[18] R. H. Baughman, D. S. Galvão, *Nature* **1993**, *365*, 735-737.

[19] J. N. Grima, J. J. Williams, K. E. Evans, *Chem. Commun.* **2005**, 4065–4067.

[20] P. Neri, A. Bottino, F. Cunsolo, M. Piatterelli, E. Gavuzzo, *Angew. Chem. Int. Ed.* **1998**, *37*, 166-169.

[21] a) C. He, P. Liu, A. C. Griffin, *Macromolecules* **1998**, *31*, 3145-3147; b) D. Kang, M. P. Mahajan, S. Zhang, R. G. Petschek, C. Rosenblatt, C. He, P. Liu, A. C. Griffin, *Phys. Rev. E* **1999**, *60*, 4980-4982; c) W.H. de Jeu, E.P. Obraztsov, B.I. Ostrovskii, W. Ren, P.J. McMullan, A.C. Griffin, A. Sánchez-Ferrer, H. Finkelmann, *Eur. Phys. J. E* **2007**, *24*, 399–409; d) W. Ren, P. J. McMullan, A. C. Griffin, *Phys. Status Solidi B* **2009**, *246*, 2124–2130.

[22] W. H. de Jeu, *Liquid Crystal Elastomers: Materials and Applications* **2012**, Springer, Berlin.

[23] a) J. R. Moran, S. Karbach, D. J. Cram, *J. Am. Chem. Soc.* **1982**, *104*, 5826-5828; b) J. R. Moran, J. L. Ericson, E. Dalcanale, J. A. Bryant, C. B. Knobler, D. J. Cram, *J. Am. Chem. Soc.* **1991**, *113*, 5707-5714.

[24] a) S. Zampolli, P. Betti, I. Elmi, E. Dalcanale, *Chem. Commun.* **2007**, 2790-2792; b) L. Pirondini, E. Dalcanale, *Chem. Soc. Rev.* **2007**, *36*, 695-706; c) G. G. Condorelli, A. Motta, M. Favazza, E. Gurrieri, P. Betti, E. Dalcanale, *Chem. Commun.* **2010**, *46*, 288-290; d) S. Zampolli, I. Elmi, F. Mancarella, P. Betti, E. Dalcanale, G. C. Cardinali, M. Severi, *Sens. Actuators B* **2009**, *141*, 322-328; e) F. Bianchi, M. Matarozzi, P. Betti, F. Biscegle, M. Careri, A. Mangia, L. Sidisky, S. Ongarato, E. Dalcanale, *Anal. Chem.* **2008**, *80*, 6423-6430; f) F. Bertani, N. Riboni, F. Bianchi, G. Brancatelli, E. S. Sterner, R. Pinalli, S. Geremia, T. M. Swager, E. Dalcanale, *Chem. Eur. J.* **2016**, doi: 10.1002/chem.201504229.

[25] a) P. Soncini, S. Bonsignore, E. Dalcanale, F. Ugozzoli, *J. Org. Chem.* **1992**, *57*, 4608-4612; b) M. Vincenti and E. Dalcanale, *J. Chem. Soc., Perkin Trans. 2* **1995**, 1069-1076; c) F. Bianchi, R. Pinalli, F. Ugozzoli, S. Spera, M. Careri, E. Dalcanale, *New J. Chem.* **2003**, *27*, 502-509.

[26] V. A. Azov, A. Beeby, M. Cacciari, A. G. Cheetham, F. Diederich, M. Frei, J. K. Gimzewski, V. Gramlich, B. Hecht, B. Jaun, T. Latychevskaia, A. Lieb, Y. Lill, F. Marotti, A. Schlegel, R. R. Schlittler, P. J. Skinner, P. Seiler, Y. Yamakoshi, *Adv. Funct. Mater.* **2006**, *16*, 147-156.

[27] P. J. Skinner, A. G. Cheetham, A. Beeby, V. Gramlich, F. Diederich, *Helv. Chim. Acta* **2001**, *84*, 2146-2153.

[28] a) P. Amrhein, A. Shivanyuk, D. W. Johnson, J. Rebek Jr., *J. Am. Chem. Soc.* **2002**, *124*, 10349-10358; b) M. Frei, F. Marotti, F. Diederich, *Chem. Commun.* **2004**, 1362-1363.

[29] M. Frei, F. Diederich, R. Tremont, T. Rodriguez, L. Echegoyen, *Helv. Chim. Acta* **2006**, *89*, 2040-2057.

[30] a) I. Pochorovski, C. Boudon, J.-P. Gisselbrecht, M.-O. Ebert, W. B. Schweizer, F. Diederich, *Angew. Chem. Int. Ed.* **2012**, *51*, 262-266. b) I. Pochorovski, M.-O. Ebert, J.-P. Gisselbrecht, C. Boudon, W. B. Schweizer, F. Diederich, *J. Am. Chem. Soc.* **2012**, *134*, 14702-14705. c) I. Pochorovski, J. Milić, D. Kolarski, C. Gropp, W. B. Schweizer, F. Diederich, *J. Am. Chem. Soc.* **2014**, *136*, 3852-3858.

[31] L. Roncucci, L. Pirondini, G. Paderni, C. Massera, E. Dalcanale, V. A. Azov, F. Diederich, *Chem. Eur. J.* **2006**, *12*, 4775–4784.

CHAPTER 7

VASE-KITE INTERCONVERSION IN DIMERIC AND POLYMERIC QXCAV-BASED STRUCTURES

7.1 Introduction

Tetraquinoxaline cavitands, initially reported by Cram and co-workers,[1] are a remarkable example of molecular switchers.[2] As discussed in the previous chapter, these systems are able to reversibly interconvert between a closed *vase* conformation (C_{4v} symmetry) about 1.18 nm wide, and an open *kite* conformation (C_{2v} symmetry), with an extended surface approximately 1.59 nm × 2.04 nm in size (Figure 7.1).[3] This *vase* ⇆ *kite* equilibrium is affected by changes in temperature,[4] pH,[5] and metal ion concentration.[6]

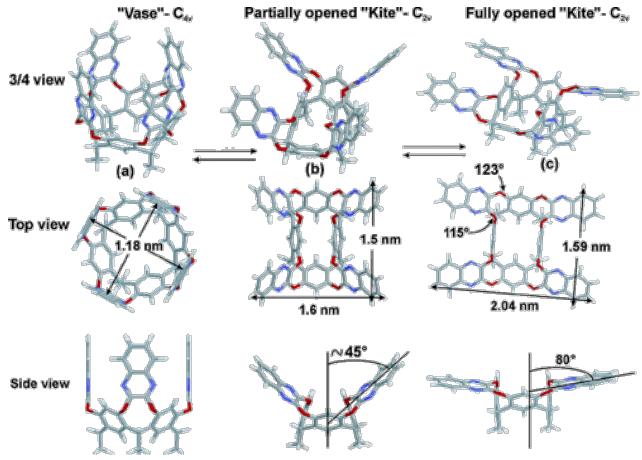

Figure 7.1 *Molecular structures of the quinoxaline-bridged cavitand. (a) "Vase", (b) partially open, and (c) fully open "kite" structures. Molecular dimensions and angles are estimated after structure optimization (Macromodel) taking into consideration the van der Waals radii. The alkyl chains ($C_{11}H_{23}$) are omitted for clarity.*[3]

Considering the molecular diagonal, which goes from 1.18 nm to 2.58 nm, *vase* → *kite* switching causes an increase of cavitand size of about 1.4 nm. This is particularly interesting for the development of monomeric units able to change their dimension into polymeric matrices. *Vase* ⇆ *kite* conformational equilibria of differently substituted cavitands have been studied both in solution, by variable-temperature NMR spectroscopy (VT-NMR)[7] and UV-VIS spectroscopy,[5] and at the interface, using sum-frequency vibrational spectroscopy (SFVS),[8] but their behavior in polymeric matrices is still unknown. To model how *vase* ⇆ *kite* equilibrium in solution is affected moving from monomeric units to polymeric structures, we synthetized and studied a new class of quinoxaline cavitand-based linear homopolymers (Figure 7.2). We choose to functionalize the upper rim with easily accessible amides and esters.

Interactions between connected cavitands were prevented using long alkyl chains as spacers. Tetraquinoxaline cavitands (QxCav) polymerization was achieved following two different synthetic strategies: in the first method we reacted partially bridged quinoxaline cavitands with dichloroquinoxaline-terminated linkers; for the second approach acyclic diene metathesis (ADMET) polymerization was preceded by the introduction of two reactive groups at the upper rim of the cavitand scaffold. Following these strategies, dimers **1a** and **1c** were prepared to gradually increase the complexity of the system and follow *vase* ⇆ *kite* interconversion *via* NMR spectroscopy. External stimuli (temperature and pH variation) allowed us to reversibly perturbate the equilibrium favoring the *kite* form. The same studies were performed on polymeric structures **2b** and **2c.**

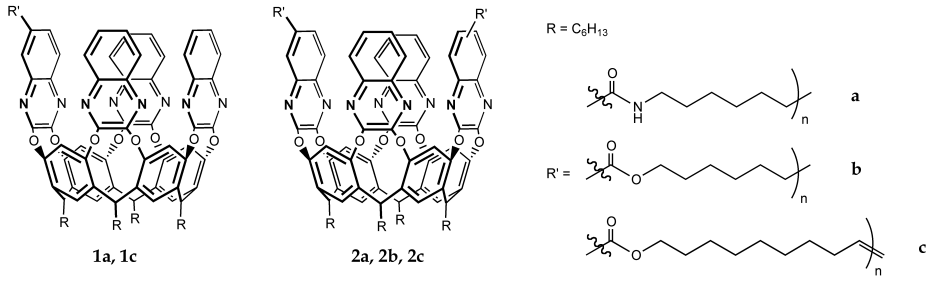

Figure 7.2 *Target dimers (n=2) and polymers (n>2).*

7.2 Results and Discussion

For the synthesis of QxCav-based dimers and polymers two convergent approaches were exploited. Functional groups can be conveniently introduced at the upper rim of tetraquinoxaline cavitands through bridging reactions with prefunctionalized dichloroquinoxalines. It must be considered that modification of quinoxaline units might affect *vase* ⇆ *kite* conformational equilibrium and in some case prevent a fully *vase* structure. To minimize steric hindrance between walls we choose to functionalize quinoxaline units in 6 or 7 position. These quinoxalines were prepared from the easily accessible 2,3-dichloroquinoxaline-6-carbonyl chloride (**4′**).[9] In fact the acyl chloride selectively reacts with nucleophiles under mild conditions (Scheme 7.1). The condensation of commercially available 3,4-diaminobenzoic acid with oxalic acid afforded 2,3-dihydroxy-quinoxaline-6-carboxylic acid (**3**) in quantitative yield. The key intermediate **4′** was synthetized from **3** through reaction with

Vilsmeier reagent.[10] The acyl chloride was not isolated but directly reacted with a diamine or a glycol to give linkers **4a** and **4b** respectively. Nucleophilic acyl substitution with 9-decen-1-ol afforded dichloroquinoxaline **4c,** suitable for the second synthetic strategy.

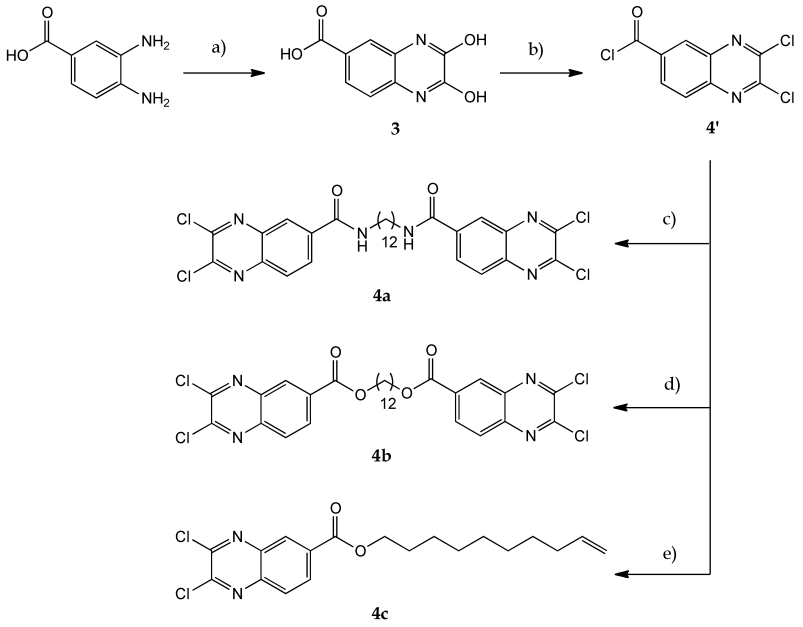

Scheme 7.1 *Synthesis of functionalized dichloroquinoxaline: a) oxalic acid, HCl 4 N, 12 h, reflux, quant.; b) thionyl chloride, DMF cat., 1,2-dichloroethane, reflux, 3h; c) 1,12-diaminododecane, DIPEA, 1,2-dichloroethane, r.t., 2 h, 69%; d) 1,12-dodecandiol, TEA, CH_2Cl_2, r.t., 12 h, 67%; e) 9-decen-1-ol, TEA, CH_2Cl_2, r.t., 12 h, 74%.*

7.2.1 First Strategy: "Bridging" Polymerization

In this first approach dichloroquinoxaline-terminated linkers were used as bridging agents to directly form connected quinoxaline cavitands. To test this novel approach we firstly reacted triquinoxaline cavitand **7** with the linker **4a,** which was preferred to **4b** for the higher stability of amide groups (Scheme 7.2). As reported in literature, **7** was obtained in 2 steps from the corresponding resorcinarene **5**.[11] After the formation of the tetraquinoxaline cavitand **6,** one quinoxaline wall was removed with catechol in basic conditions affording the partially bridged cavitand **7**. This approach revealed to be more efficient than reacting resorcinarenes **5** with a stoichiometric amount of 2,3-dichloro-

quinoxaline.[4] In the last step cavitand **7** was bridged with **4a** in presence of potassium carbonate in DMSO as solvent.

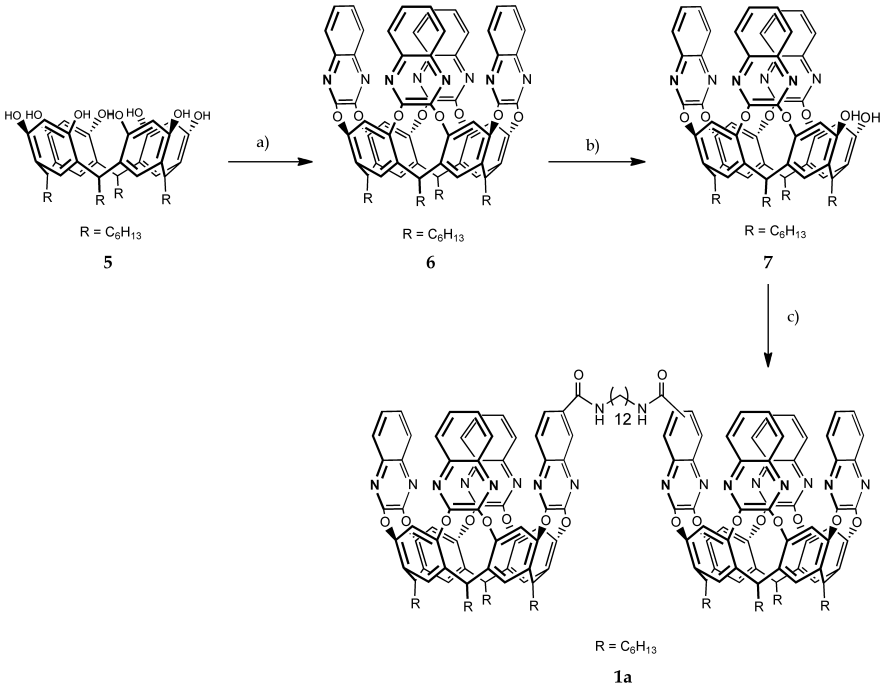

Scheme 7.2 *Synthesis of diamide dimer* ***1a****: a) 2,3-dichloroquinoxaline, K_2CO_3, DMF, 80 °C, 12 h, 59%; b) catechol, CsF, 80 °C, 45 min, 57%; c)* ***4a****, K_2CO_3, DMSO, 70 °C (MW), 90 min, 71%.*

Microwave irradiation allowed us to reach higher yields and sensibly lower reaction times. MALDI-TOF analysis confirmed the formation of the desired product. As a result of the introduction of one functional group on a quinoxaline wall, the cavitand shows planar chirality. Consequently compound **1a**, which possesses two chiral centers, was obtained after column chromatography as a mixture of three inseparable diastereoisomers. The role of NMR spectroscopy in this study is twofold: from ^{1}H-NMR spectrum we were able to obtain not only structural but also conformational information about the cavitand. In particular, the analysis of the chemical shifts of methine protons is diagnostic of the conformation adopted by the cavitand in solution.[4] In ^{1}H NMR spectrum of compound **1a** (Figure 7.3a), the chemical shift of the methine signal was at about 5.6 ppm, proving that *vase* conformation was retained by the two covalently connected cavitands. Most of the signals were found to be splitted in doublets as result of the C-N hindered rotation in amides. We

studied also *vase* → *kite* switching adding TFA (0.5 M) to the NMR sample (Figure 7.3b).

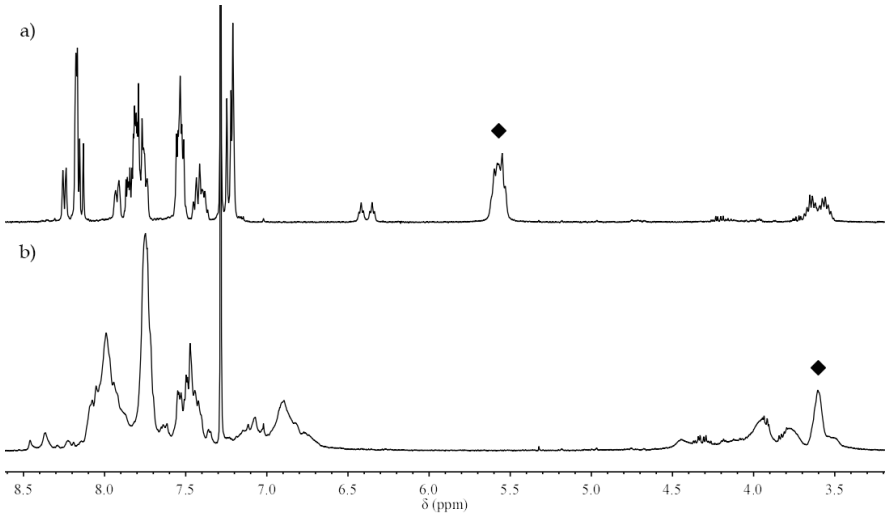

Figure 7.3 *^{1}H NMR spectra of dimer **1a** in $CDCl_3$ (400 MHz) before (a) and after (b) the addition of TFA (0.5 M). Signal related to methine protons is labeled (◆). Only the aromatic region of the spectra is shown.*

As discussed above, protonation of quinoxaline units forces the cavitand scaffold to open causing a downshift of the diagnostic signal. As for the unsubstituted tetraquinoxaline cavitand, we observed a shift of the triplet related to methine protons from 5.6 to 3.6 ppm.

Vase → *kite* interconversion of dimer **1a** was tested also with VT-NMR technique. ^{1}H NMR spectra were recorded at different temperature in the range between 295 K and 213 K (Figure 7.4). The switching to the *kite* form was complete only approaching lower temperature values. Results were in agreement with the protonation experiment, proving that *vase* ⇆ *kite* equilibrium was not affected by the connection of two cavitands.

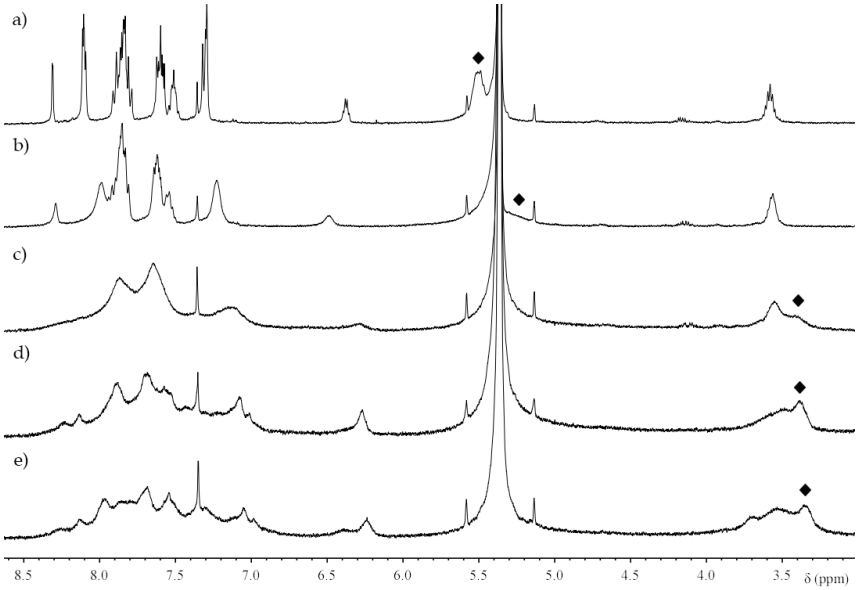

Figure 7.4 *^{1}H NMR spectra of dimer **1a** in CH_2Cl_2 (400 MHz) at 295 K (a), 273 K (b), 253 K (c), 233 K (d) and 213 K (e). Signal related to methine protons is labeled (◆). Only the aromatic region of the spectra is shown.*

To further understand and model the behavior of connected quinoxaline cavitands a homopolymerization reaction was performed. According to the "bridging" polymerization approach, AC-bisquinoxaline cavitand **8**, bearing two opposite quinoxaline walls, was synthesized *via* an excision protocol.[11] Two opposite quinoxaline walls were removed from cavitand **6** with 3.3 equivalents of catechol using cesium fluoride as base (Scheme 7.3). This strategy allowed us to obtain the AC regioisomer in dramatically higher yields compared to one-step synthesis from the resorcinarene. The polymerization was performed reacting **8** with an equimolar amount of **4a** in DMSO under microwave irradiation for two hours.

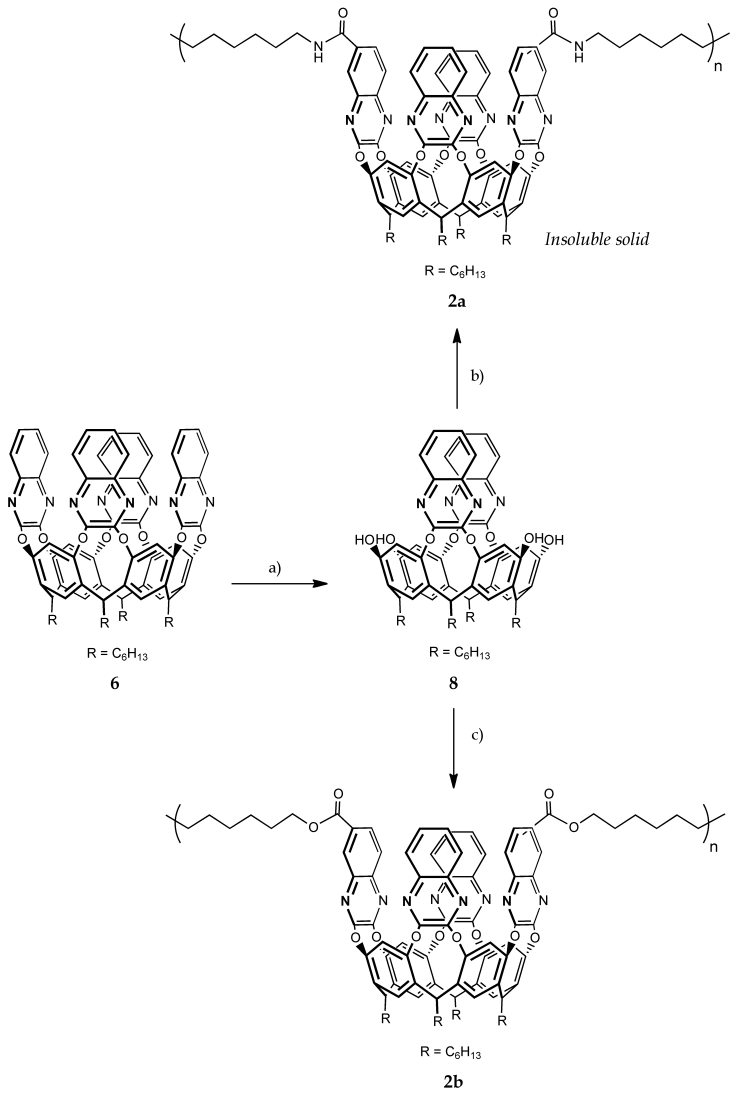

Scheme 7.3 *Synthesis of QxCav-based polymers: a) catechol, CsF, 80°C, 1 h, 54%; b)* ***4a****, K_2CO_3, DMSO, 70 °C (MW), 2 h, insoluble solid; c)* ***4b****, K_2CO_3, DMSO, 70 °C (MW), 2 h, 43%.*

At the end of the reaction a brown solid, insoluble in common laboratory solvents, was collected by filtration. For its intractability we were unable to purify and characterize polyamide **2a**.

To overcome solubility issues we switched to the more soluble polyester **2b**. Following the same procedure, AC-bisquinoxaline cavitand **8** was reacted with linker **4b.** Precipitations from methanol afforded polyester **2b** as a white solid,

soluble in chlorinated solvents. Characterization of **2b** by gel permeation chromatography (GPC) in chloroform was found to be inefficient for the high heterogeneity of the sample (see Figure S7.1). This was reflected also in the complexity of ^{1}H NMR spectrum, as shown in Figure 7.5a. Signals were attributed by comparison with dimer **1a**, but their integration was not in agreement with the stoichiometry of the polymer. However, we observed the shift of the broad signal at 5.6 ppm upon addiction of TFA (0.5 M) as indication of *vase* → *kite* switching retention (Figure 7.5b). Unexpectedly, VT-NMR failed to evidence significant variations of the ^{1}H NMR spectrum. A possible explanation of this result is that the polymerization suppresses the entropy driven *vase* → *kite* interconversion. To prove this assumption, a more homogeneous and reliable polymer should be tested.

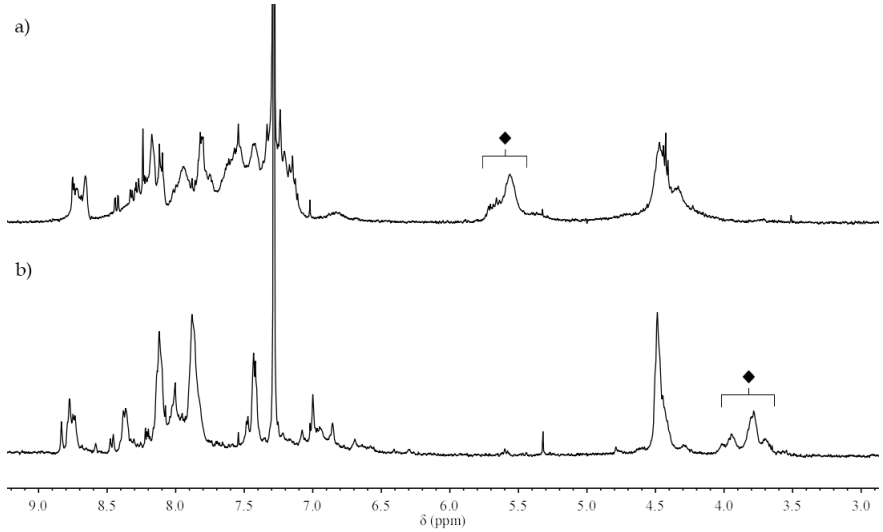

Figure 7.5 *^{1}H NMR spectra of polymer **2b** in $CDCl_3$ (400 MHz) before (a) and after (b) the addition of TFA (0.5 M). Signal related to methine protons is labeled (◆). Only the aromatic region of the spectra is shown.*

7.2.2 Second Strategy: Metathesis Polymerization

The first approach was found to be highly efficient for the synthesis of dimeric structures but failed in the control of the polymerization. This intrinsic limitation can be overcome reacting already formed quinoxaline cavitands. For its compatibility with our system, we designed ADMET as polymerization reaction. Thus we decided to introduce two terminal double bonds on opposite

quinoxaline walls. The reciprocal position was chosen not only to limit intramolecular cyclization but also considering cavitand applicability to the design and study of molecular auxetics (see Chapter 6). Again long alkyl spacers were interposed between the functional groups and the scaffold to preserve their reactivity and impart flexibility to the final polymer.

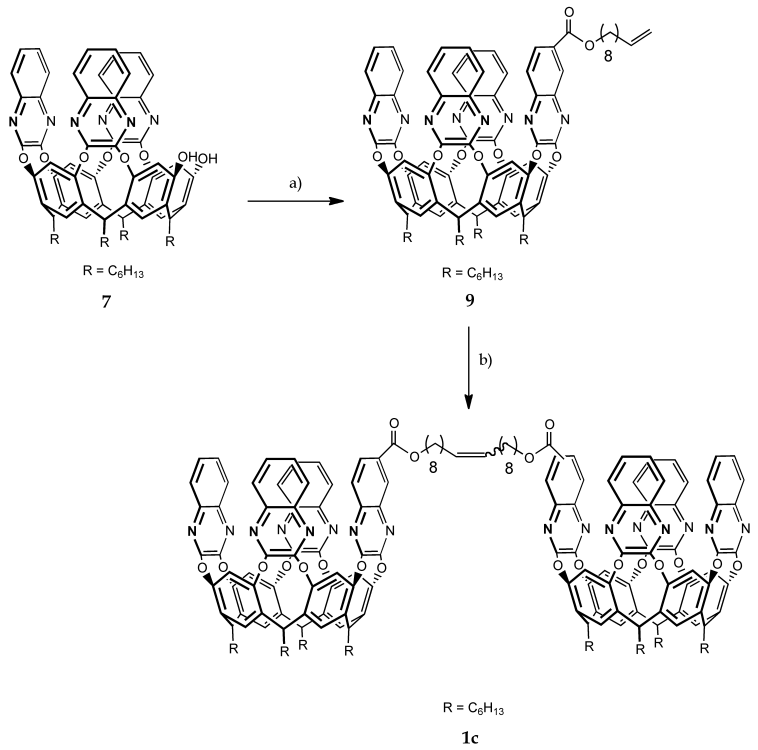

Scheme 7.4 *Synthesis of diester dimer* ***1c****: a)* ***4c****, K_2CO_3, DMSO, 70 °C (MW), 30 min, 65%; b) Grubbs Catalyst (2nd generation), $CHCl_3$, 60 °C, 96 h, 57%.*

As for the first approach, a dimerization reaction was initially performed. For this purpose, we synthesized a monotopic cavitand bearing one terminal double bond. The triquinoxaline cavitand **7** was bridged with dichloroquinoxaline **4c** to afford QxCav **9** in 65% yield (Scheme 7.4). The reaction was performed under microwave irradiation to reduce side products formation and reaction time. In the final step, compound **9** was dimerized through a metathesis reaction promoted by second-generation Grubbs catalyst. After flash chromatography, dimer **1c** was isolated as a mixture of diastereoisomers due to the presence of two stereocenters. *Vase* → *kite* switching of **1c** was studied by NMR spectroscopy. As shown in Figure 7.6, both the

addition of TFA and the decrease of temperature at 213 K caused the downshift of the diagnostic signal.

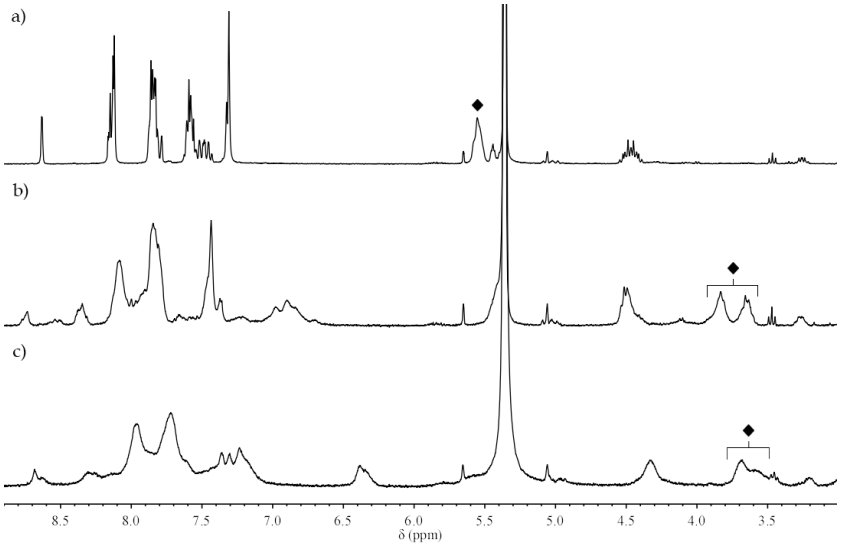

Figure 7.6 *^{1}H NMR spectra of dimer **1c** in CD_2Cl_2 (400 MHz): a) at 295 K; b) after the addition on TFA (0.5 M) c) 213 K. Signal related to methine protons is labeled (◆). Only the aromatic region of the spectra is shown.*

To perform the ADMET polymerization we synthesized the ditopic cavitand **10**. Two terminal double bonds were introduced at the upper rim of the macrocycle bridging AC-bisquinoxaline cavitand **8** with alkene-functionalized quinoxaline **4c**. The reaction, performed in DMSO under microwave irradiation, afforded the compound **10** as a mixture of isomers, as confirmed by the pattern of NMR signals. The formation of **10** was confirmed by MALDI-TOF spectrometry.
Metathesis polymerization was performed adding the second-generation Grubbs catalyst to a concentrated solution of cavitand **10** (0.03 M) in 1,2-dichloroethane. The mixture was heated at 60 °C and the reaction was monitored through the integration of terminal alkenes signals in ^{1}H NMR spectrum. After repeated precipitation from methanol, we isolated a mixture of cyclic and oligomeric products (**2c**), which was characterized by NMR spectroscopy and MALDI-TOF spectrometry. GPC analysis, necessary to determine molecular weight and dispersity of the polymeric fraction, is still ongoing.

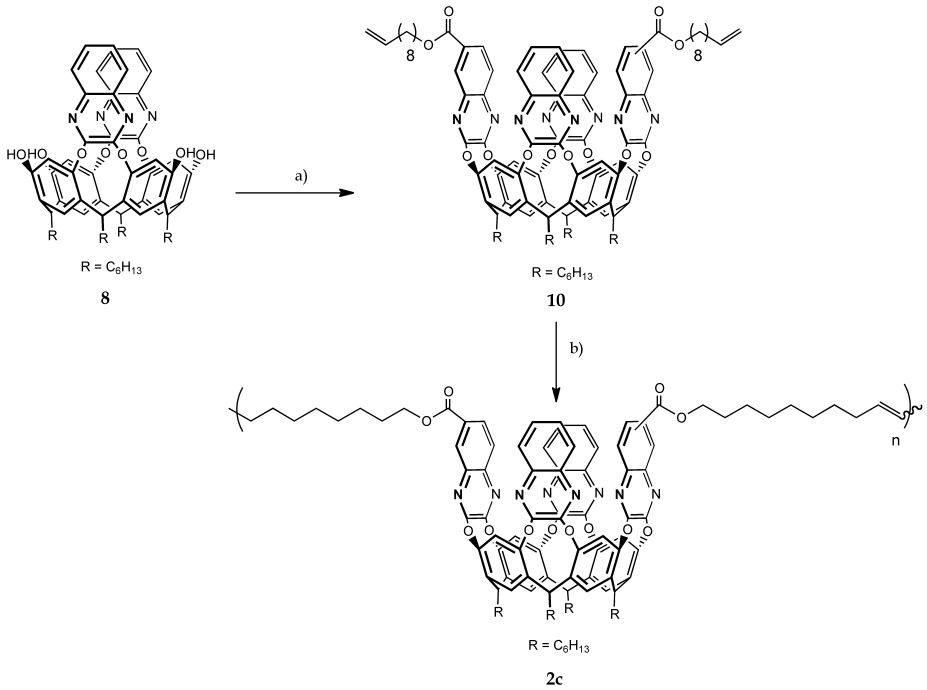

Scheme 7.5 *Synthesis of polyester* **2c***: a)* **4c***, K_2CO_3, DMSO, 70 °C (MW), 1 h, 34%; b) Grubbs Catalyst (2nd generation), 1,2-dichloroethane, 60 °C, 12h, 87% (mixture).*

As indicated by the disappearance of signal relative to cavitand **10** in MALDI-TOF spectrum (Figure 7.7), a quantitative conversion of the monomer was assumed. Interestingly, the intense signal at a lower value of *m/z* was attributed to the product of the intramolecular metathesis reaction between the two alkenes. The extension of the analysis window to higher *m/z* (up to 20 kDa) failed to evidence any oligomerization product. In our experience, this does not demonstrate that the polymerization failed to occur, as MALDI-TOF spectrometry revealed to be inefficient in the analysis of cavitand-based oligomeric and polymeric structures. In ^{1}H NMR spectrum (Figure 7.8a), a broadening of the signals, with respect to the monomer **10**, was observed. The presence of two signals at 5.81 and 4.96 ppm, characteristic of terminal double bonds, was attributed to alkenyl end-groups of cavitand chains. As indication of *vase* → *kite* switching, the shift of the broad methine signal from 5.6 to 3.7 ppm was observed upon addiction of TFA (Figure 7.9b). VT-NMR experiments, reported in Figure 7.8c, evidenced a splitting and a partial downshift of the diagnostic signal that may be ascribed to an incomplete interconversion between the two forms.

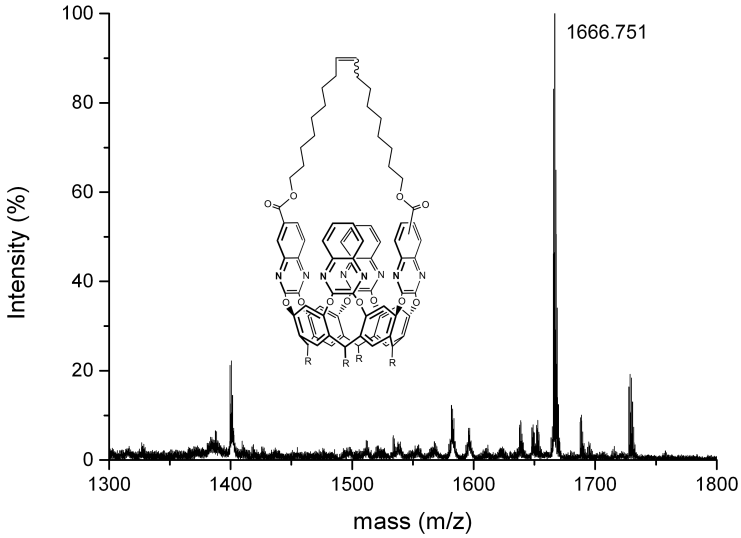

Figure 7.7 *High-resolution MALDI-TOF spectrum (zoom) of* **2c***; structure of the intramolecular product in the insert.*

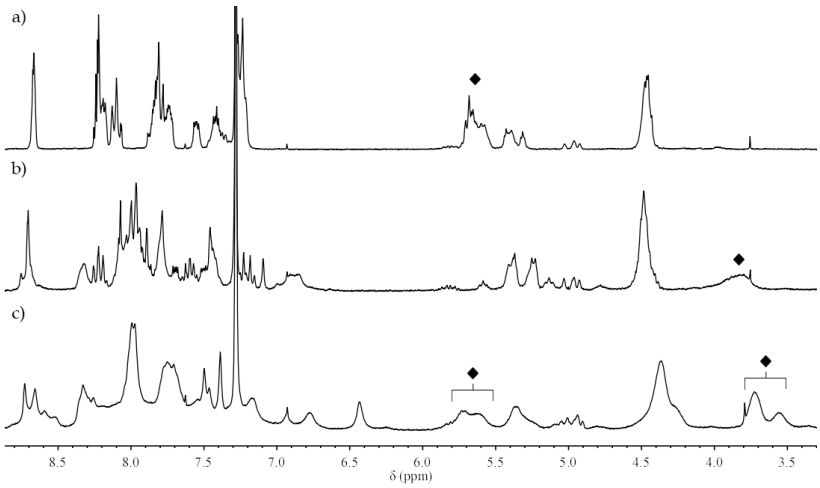

Figure 7.9 *^{1}H NMR spectra of* **2c** *in $CDCl_3$ (300 MHz): a) at 295 K; b) after the addition on TFA (0.5 M) c) 213 K. Signal related to methine protons is labeled (◆). Only the aromatic region of the spectra is shown.*

7.3 Conclusions

Two protocols were successfully applied to the formation of tetraquinoxaline cavitand dimers. The initial *vase* conformation, as well as ability to interconvert to the *kite* form as response to temperature and pH variations, was retained by the covalently linked cavitands. The preparation of polymeric structures revealed to be more complex. The first approach, based on "bridging" reaction with diquinoxaline spacers, failed in the control of the polymerization affording a highly heterogeneous mixture. Anyway, *vase* ⇆ *kite* switching in solution was observed lowering the pH, while temperature decrease failed to evidence significant variation of the ^{1}H NMR spectrum. In our second attempt, ADMET reaction was performed on ditopic cavitand to avoid the presence in the final structure of partially bridged species. The increased homogeneity of the resulting mixture was reflected in the proton NMR spectrum, but the formation of an intramolecular side-product was observed. Also in this case, only addition of TFA in solution afforded a complete *vase* ⇆ *kite* interconversion, while a partial switching was obtained with VT-NMR technique. Ultimately, an unambiguous determination of QxCav behavior was hampered by the intrinsic limitations of the two approaches. However, NMR experiments suggest that introduction of tetraquinoxaline cavitands in polymeric structure may affect the temperature-driven switching. In our opinion this behavior can be related to the entropic nature of the phenomenon.

7.4 Acknowledgments

Thanks to Dr. Alessandro Bedini and Carola Andrea Margheri from the department of Chemistry, University of Parma.

7.5 Experimental Section

2,3-dihydroxyquinoxaline-6-carboxylic acid (3)
To a suspension of oxalic acid (1.3 g, 14.6 mmol) in 15 mL of HCl 4N, 3,4-diaminobenzoic acid (2 g, 13.2 mmol) in 15 mL of HCl 4N was slowly added. The resulting mixture was heated at reflux overnight under stirring. The red-brownish precipitate was filtered, washed with water and dried affording product **3** in quantitative yield (2.7 g, 13.2 mmol).
^{1}H NMR (DMSO-d_6, 300 MHz): δ (ppm) = 12.90 (s, 1H, COO**H**), 12.16 (s, 1H, ArO**H**), 12.04 (s, 1H, ArO**H**), 7.73 (s, 1H, Ar**H**), 7.67 (d, 1H, J_o=9.0 Hz, Ar**H**), 7.18 (d, 1H, J_o=9.0 Hz, Ar**H**).

Bis(2,3-dichloroquinoxaline) diamide linker (4a)
To a suspension of compound **3** (0.100 g, 0.48 mmol) in 5 mL of dry 1,2-dichloroethane, thionyl chloride (0.350 mL, 4.80 mmol) and a catalytic amount of DMF were added. The mixture was refluxed to homogeneity then volatiles were removed under reduced pressure. The resulting pale red solid was dissolved in 5 mL of dry 1,2-dichloroethane, followed by addiction of DIPEA (0.084 mL, 0.48 mmol) and 1,12-diaminododecane (0.048 g, 0.24 mmol). The reaction mixture was stirred at room temperature for 2 h., diluted with CH_2Cl_2 and filtered. The precipitate was washed with HCl 1N and water to give compound **4a** as a white-brownish solid (0.106 g, 0.16 mmol, 69%).
^{1}H NMR (DMSO-d_6, 300 MHz): δ (ppm) = 8.85 (t, 2H, J=5.6 Hz, N**H**), 8.53 (d, 2H, J_m=1.9 Hz, Ar**H**), 8.31 (dd, 2H, J_o=8.8 Hz, J_m=1.9 Hz, Ar**H**), 8.15 (d, 2H, J_o=8.8 Hz, Ar**H**), 3.32 (m, 4H, NHC**H$_2$**), 1.55 (m 4H, NHCH$_2$C**H$_2$**), 1.27 (m, 16H, -C**H$_2$**-).

Bis(2,3-dichloroquinoxaline) diester linker (4b)
Thionyl chloride (0.700 mL, 9.7 mmol) was added to a suspension of compound **3** (0.200 g, 0.97 mmol) in 10 mL of dry 1,2-dichloroethane, followed by a catalytic amount of DMF. The reaction mixture was refluxed until the complete dissolution of the solid and then volatiles were removed under vacuum. The intermediate was suddenly dissolved in 10 mL of dry CH_2Cl_2. TEA (0.135 mL, 0.97 mmol) a 1,12-dodecandiol (0.098 g, 0.47 mmol) were added and the brown solution was stirred overnight at room temperature. Water was added and the organics were washed with a saturated solution of $NaHCO_3$, HCl 1 N and brine. Solvent was evaporated under reduced pressure and recrystallization from DMSO afforded the compound **4b** (0.205 g, 0.31 mmol, 67%) as a white solid.

^{1}H NMR ($CDCl_3$, 300 MHz): δ (ppm) = 8.75 (d, 2H, J_m=1.8 Hz, Ar**H**), 8.43 (dd, 2H, J_o=8.8 Hz, J_m=1.8 Hz, Ar**H**), 8.11 (d, 2H, J_o=8.8 Hz, Ar**H**), 4.42 (t, 4H, J=6.6 Hz, OC**H$_2$**), 1.84 (qui 4H, J=6.6 Hz, OCH_2C**H$_2$**), 1.55-1.27 (m, 16H, -C**H$_2$**-).

Dec-9-en-1-yl 2,3-dichloroquinoxaline-6-carboxylate (4c)
Acid **3** (0.600 g, 2.9 mmol) was suspended in 5 mL of dry 1,2-dichloroethane and thionyl chloride (1,99 mL, 29.1 mmol) was added followed by catalytic DMF. The reaction mixture was refluxed for 2h. Volatiles were removed under reduce pressure and the red-brownish precipitate was redissolved in 8 mL of dry CH_2Cl_2. After the addition of TEA (0.44 mL, 3.2 mmol) and 9-decen-1-ol (0.57 mL, 3.2 mmol) the mixture was stirred at room temperature overnight. The crude was diluted with CH_2Cl_2 and washed with a saturate solution of $NaHCO_3$, HCl 1 N and brine. The solvent was evaporated and flash column chromatography (hexane/EtOAc 95:5) afforded compound **4c** (0.83 g, 2.2 mmol, 74%) as a colorless oil that solidified upon standing.
^{1}H NMR ($CDCl_3$, 400 MHz): δ (ppm) = 8.75 (s, 1H, Ar**H**), 8.43 (d, 1H, J_o=8.8 Hz, Ar**H**), 8.11 (d, 1H, J_o=8.8 Hz, Ar**H**), 5.82 (m, 1H, C**H**=CH_2), 4.99 (m, 2H, CH=C**H$_2$**), 4.43 (t, 2H, J=6.5 Hz, OC**H$_2$**), 2.07 (m, 2H, C**H$_2$**CH=CH_2), 1.84 (m, 2H, OCH_2C**H$_2$**), 1.55-1.29 (m, 10H, -C**H$_2$**-).
^{13}C NMR ($CDCl_3$, 100 MHz): δ (ppm) = 165.2, 147.7, 146.6, 142.5, 139.9, 139.1, 133.0, 131.0, 130.4, 128.4, 114.2, 66.1, 33.8, 29.4, 29.2, 29.0, 28.9, 28.7, 26.1.

Resorcinarene [C_6H_{13}, H] (5)
To a solution of resorcinol (15 g, 0.14 mol) in 85 mL of MeOH a 37% solution of HCl (20 mL, 0.24 mol) was slowly added at 0 °C. At the same temperature heptaldehyde (19 mL, 0.14 mol) was added dropwise over 45 min. The mixture was vigorously stirred at 50 °C for 5 days. Water was added and the orange precipitate was filtered, washed with water, dried under vacuum and recrystallized twice from MeOH. Resorcinarene **5** was obtained as a pale yellow powder (16 g, 0.02 mol, 57%).
^{1}H NMR (Acetone-d_6, 300 MHz): δ (ppm) = 8.46 (s, 8H, O**H**), 7.57 (s, 4H, Ar**H$_{up}$**), 6.25 (s, 4H, Ar**H$_{down}$**), 4.32 (t, 4H, J=7.8 Hz, C**H**CH_2), 2.30 (q, 8H, J=7.8 Hz, CHC**H$_2$**) 1.37-1.30 (m, 32H, -C**H$_2$**-), 0.90 (t, 12H, J=6.6 Hz, CH_2C**H$_3$**).
ESI-MS: *m/z* = 825 $[M+H]^+$, 847 $[M+Na]^+$.

Tetraquinoxaline Cavitand (6)
To a solution of resorcinarene **5** (2 g, 2.42 mmol) in 40 mL of dry DMF, K_2CO_3 (2 g, 14.5 mmol) was added followed by 2,3-dochloroquinoxaline (2.12 g, 10.7 mmol). The pink suspension was stirred at 80°C overnight. The reaction was

quenched with HCl 1 N and the precipitate was filtered, washed with water and dried. Recrystallization from EtOAc afforded cavitand **6** as a white solid (2,33 g, 1.75 mmol, 72%).

^{1}H NMR ($CDCl_3$, 400 MHz): δ (ppm) = 8.17 (s, 4H, Ar**H$_{up}$**), 7.82 (m, 8H, Ar**H**), 7.82 (m, 8H, Ar**H**), 7.49 (m, 8H, Ar**H**), 7.23 (s, 4H, Ar**H$_{down}$**), 5.58 (t, 4H, J=7.8 Hz, C**H**CH_2), 2.28 (q, 8H, J=7.8 Hz, CHC**H$_2$**), 1.55-1.31 (m, 32H, -C**H$_2$**-), 0.95 (t, 12H, J=6.8 Hz, CH_2C**H$_3$**).

MALDI-TOF: calculated for $C_{84}H_{80}N_8O_8$ $[M+H]^+$ *m/z* = 1329.618, found *m/z* = 1329.567.

Triquinoxaline Cavitand (7)

A suspension of cavitand **6** (0.500 g, 0.38 mmol) and CsF (1.154 g, 7.60 mmol) in 100 mL of DMF was heated at 80 °C. Catechol was added (0.045 g, 0.41 mmol) and the mixture was stirred for 45 min. After cooling at room temperature the reaction mixture was poured in 500 mL of ice-cold brine and the precipitate was filtered, washed with water and dried. The crude was purified by flash column chromatography (gradient from 100% CH_2Cl_2 to CH_2Cl_2/EtOAc 95:5) affording compound **7** as pale yellow solid (0.263 g, 0.21 mmol, 57%).

^{1}H NMR ($CDCl_3$, 300 MHz): δ (ppm) = 8.25 (bs, 4H, ArO**H** + Hi), 7.96 (d, 2H, J=8.3 Hz, Hd), 7.85 (m, 2H, He), 7.68 (d, 2H, J=8.3 Hz, Ha), 7.62-7.44 (m, 6H, Hc + Hb + Hf), 7.30 (s, 2H, Hg), 7.15 (s, 2H, Hl), 7.12 (s, 2H, Hk), 5.65-5.43 (m, 3H, Hm + Hn), 4.32 (t, 1H, J=7.7 Hz, Ho), 2.28 (m, 8H, CHC**H$_2$**), 1.57-1.21 (m, 32H, -C**H$_2$**-), 0.93 (m, 12H, CH_2C**H$_3$**).

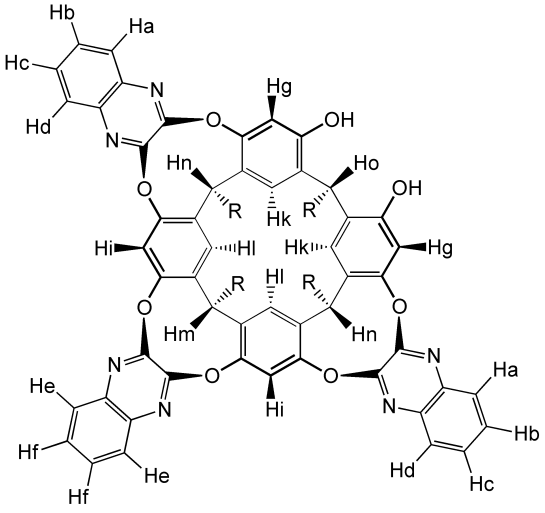

ESI-MS: *m/z* = 1203.6 $[M+H]^+$, 1225.6 $[M+Na]^+$, 1241.5 $[M+K]^+$.

Tetraquinoxaline cavitand-based diamide dimer (1a)

K_2CO_3 (0.018 g, 0.12 mmol) was added under nitrogen to a suspension of triquinoxaline cavitand **7** (0.1 g, 0.08 mmol) in 4 mL of DMSO. After 10 minutes compound **4a** (0.027 g, 0.04 mmol) was added and the mixture was heated at 70°C under microwave irradiation for 90 minutes. After the addition of 100 mL of water the white precipitate was filtered and dried. The crude was purified by flash column chromatography (gradient from CH_2Cl_2/EtOAc 9:1 to CH_2Cl_2/EtOAc 85:15) affording dimer **1a** as a white solid (0.085 g, 0.03 mmol, 71%).

^{1}H NMR ($CDCl_3$, 300 MHz): δ (ppm) = 8.26 (d, 2H, J_m=1.6 Hz, Ha), 8.24 (d, 2H, J_m=1.5 Hz, Ha'), 8.17-8.12 (m, 8H, Hg), 7.92 (m, 2H, Hb), 7.87-7.73 (m, 14H, Hc+Hd), 7.58-7.51 (m, 8H, He), 7.46-7.35 (m, 4H, Hf), 7.24-7.19 (m, 8H, Hi), 6.44 (t, 1H, J=5.6, N**H**), 6.35 (t, 1H, J=5.6, N**H'**), 5.68-5.43 (m, 8H, C**H**CH_2), 3.73-3.48 (m, 4H, NHC**H$_2$**), 2.40-2.15 (m, 16H, CHC**H$_2$**), 1.84-1.05 (m, 84H, -C**H$_2$**-), 0.94 (m, 24H, CH_2C**H$_3$**).

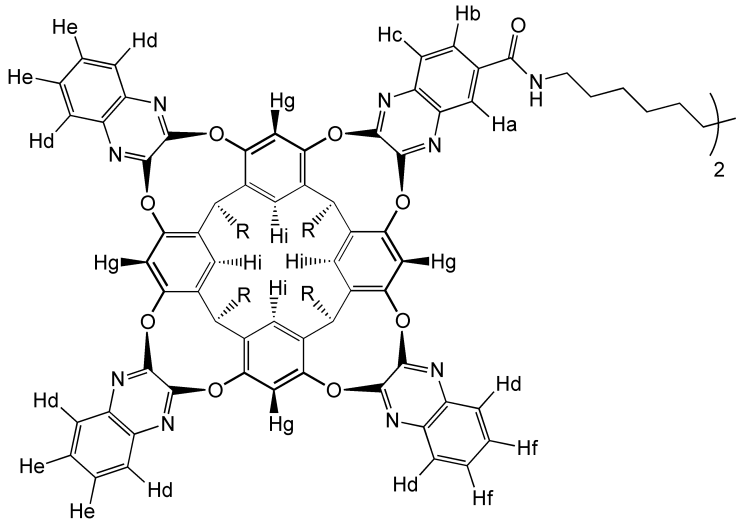

MALDI-TOF: calculated for $C_{182}H_{185}N_{18}O_{18}$ $[M+H]^+$ *m/z* = 2910.411, found *m/z* = 2910.287.

AC-bisquinoxaline cavitand (8)

A suspension of cavitand **6** (0.500 g, 0.38 mmol) and CsF (1.154 g, 7.60 mmol) in DMF was heated to 80°C and catechol (0.133 g, 1.20 mmol) was added. The mixture was stirred for 1 h at 80°C then the reaction was poured into 500 mL of ice-cold brine. The precipitate was filtered, washed with water, and dried. The crude product was purified by flash column chromatography (gradient from

CH_2Cl_2:EtOAc 95:5 to CH_2Cl_2:EtOAc 85:15) affording compound **8** as an off-white solid (0.219 g, 0.20 mmol, 54%).
^{1}H NMR (Acetone-d_6, 300 MHz): δ (ppm) = 9.03 (bs, 4H, ArO**H**), 7.77 (s, 4H, Ar$\mathbf{H_{down}}$), 7.54 (m, 4H, Ar**H**), 7.24 (m, 4H, Ar**H**), 7.16 (s, 4H, Ar$\mathbf{H_{up}}$), 5.52 (t, J=8.0 Hz, 2H, C**H**CH_2 below Qx's), 4.47 (t, J=7.6 Hz, 2H, C**H**CH_2 below OH's), 2.41 (m, 8H, CHC$\mathbf{H_2}$), 1.47-1.26 (m, 32H, -C$\mathbf{H_2}$-), 0.92 (m, 12H, CH_2C$\mathbf{H_3}$).
ESI-MS: *m/z* = 1077.6 $[M+H]^+$, 1099.6 $[M+Na]^+$, 1115.5 $[M+K]^+$.

Tetraquinoxaline cavitand-based polyamide (2a)
In dry conditions compound **4a** (0.099 g, 0.15 mmol) was added to an orange solution of AC-bisquinoxaline cavitand **8** (0.167 g, 0.15 mmol) and K_2CO_3 (0.064, 0.46 mmol) in 5 mL of DMSO. The mixture was heated at 70°C under microwave irradiation for 2 h. A pale brown solid was collected by filtration and washed with water. Purification and characterization of the insoluble crude (0.221 g) was not possible.

Tetraquinoxaline cavitand-based polyester (2b)
AC-bisquinoxaline cavitand **8** (0.100 g, 0.09 mmol) and K_2CO_3 (0.038 g, 0.28 mmol) were suspended in 3 mL of DMSO under nitrogen. After 10 minutes **4b** (0.060 g, 0,09 mmol) was added and the reaction mixture was heated at 70°C under microwave irradiation for 2 h. Water (100 mL) was added to the white suspension and the precipitate was filtered, washed with water and dried. The crude was solubilized in $CHCl_3$, filtered and precipitated twice from MeOH. Polymer **2b** was obtained as a white solid (0.060 g, 43%).

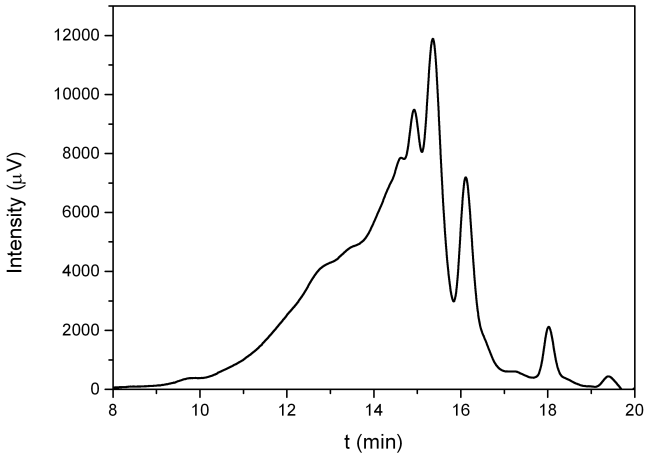

Figure S7.1 *GPC curve of polyester* ***2b****.*

Alkene functionalized tetraquinoxaline cavitand (9)

Triquinoxaline cavitand **7** (0.260 g, 0.22 mmol) and K_2CO_3 (0.039 g, 0.28 mmol) were suspended in 5 mL of DMSO. After the addition of dichloroquinoxaline **4c** (0.091 g, 0.24 mmol) the mixture was heated at 70°C under microwave irradiation for 30 min. The reaction was quenched with water (100 mL) and the precipitate was filtered, washed with water and dried. Flash column chromatography (hexane/EtOAc 9:1) afforded pure cavitand **9** as a white solid (0.215 g, 0.14 mmol, 65%).

^{1}H NMR ($CDCl_3$, 400 MHz): δ (ppm) = 8.65 (s, 1H, Ha), 8.19 (m, 4H, Hg), 8.09 (d, 1H, J=8.7 Hz, Hb), 7.87-7.34 (m, 7H, Hc+Hd), 7.52 (m, 4H, He), 7.42 (t, 1H, J=7.5 Hz, Hf), 7.33 (t, 1H, J=7.5 Hz, Hf), 7.24 (m, 4H, Hi), 5.82 (m, 1H, C**H=**CH_2), 5.60 (m, 4H, C**H**CH_2), 4.98 (m, 2H, CH=C**H$_2$**), 4.48 (m, 2H, OC**H$_2$**CH_2), 2.29 (m, 8H, CHC**H$_2$**), 2.06 (m, 2H, C**H$_2$**CH=CH_2), 1.92 (quint, 2H, J=6.9 Hz, OCH_2C**H$_2$**), 1.60-1.26 (m, 42H, -C**H$_2$**-), 0.95 (t, 12H, J=6.4 Hz, CH_2C**H$_3$**).

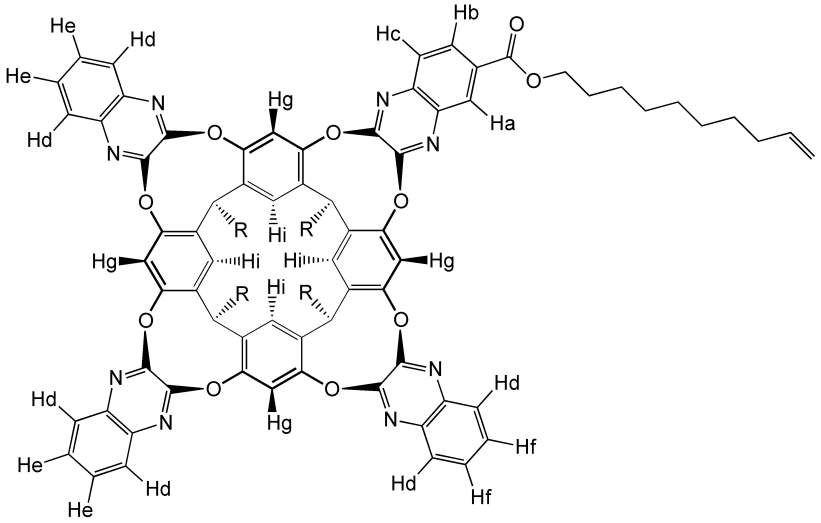

MALDI-TOF: calculated for $C_{95}H_{99}N_8O_{10}$ $[M+H]^+$ *m/z* = 1511.748, found *m/z* = 1511.745.

Tetraquinoxaline cavitand monoalkene dimer (1c)

Cavitand **9** (0.050 g, 0.03 mmol) was dissolved in 5 mL of freshly distilled and degassed $CHCl_3$ and a catalytic amount of 2nd generation Grubbs catalyst was added. The solution was refluxed for 96 h under inert atmosphere. The mixture is diluted with $CHCl_3$, washed three times with water and dried under reduced pressure. The crude was purified by flash column chromatography (gradient

from CH_2Cl_2/EtOAc 99:1 to CH_2Cl_2/EtOAc 95:5) affording compound **1c** as white solid (0.028 g, 0.009 mmol, 57%).

^{1}H NMR ($CDCl_3$, 300 MHz): δ (ppm) = 8.65 (s, 2H, Ha), 8.18 (m, 8H, Hg), 8.08 (d, 2H, J=8.7 Hz, Hb), 7.87-7.74 (m, 14H, Hc + Hd), 7.58-7.47 (m, 8H, He), 7.39 (m, 2H, Hf), 7.34 (m, 2H, Hf), 7.25-7.18 (m, 8H, Hi), 5.68-5.49 (m, 8H, C**H**CH_2), 5.43-5.34 (m, 2H, CH_2C**H**=C**H**CH_2), 4.48 (m, 4H, OC**H$_2$**CH_2), 2.28 (m, 16H, CHC**H$_2$**), 2.09-1.84 (m, 8H, C**H$_2$**CH=CHC**H$_2$** + OCH_2C**H$_2$**), 1.78-1.18 (m, 84H, -C**H$_2$**-), 0.95 (t, 24H, J=6.4 Hz, CH_2C**H$_3$**).

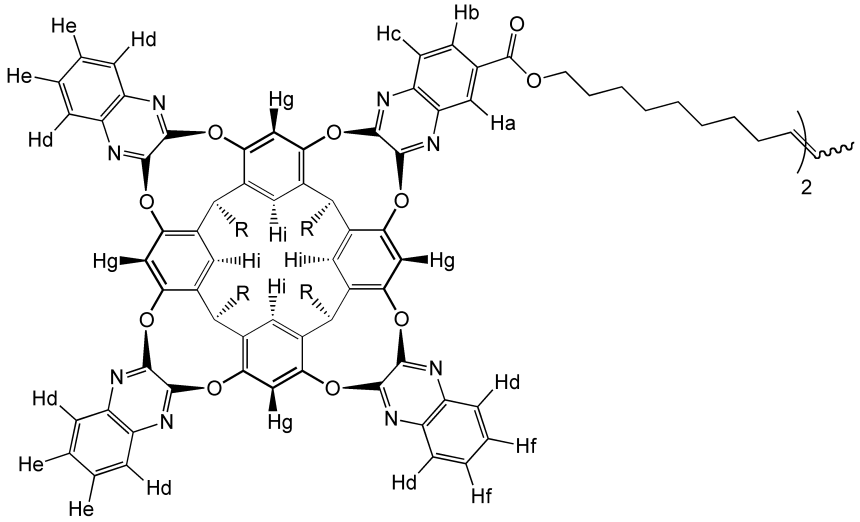

MALDI-TOF: calculated for $C_{188}H_{193}N_{16}O_{20}$ $[M+H]^+$ *m/z* = 2994.458, found *m/z* = 2994.413.

Bis-alkene functionalized tetraquinoxaline cavitand (10)

To a suspension of AC-bisquinoxaline cavitand **8** (0.182 g, 0.17 mmol) and K_2CO_3 (0.069 g, 0.50 mmol) in 5 mL of DMSO dichloroquinoxaline **4c** (0.141 g, 0.37 mmol) was added. The mixture was heated at 70°C under microwave irradiation for 1 h. The reaction was quenched with water (100 mL) and the precipitate was filtered, washed with water and dried. Flash column chromatography (hexane/EtOAc 95:5) afforded pure cavitand **9** as a white solid (0.098 g, 0.06 mmol, 34%).

^{1}H NMR ($CDCl_3$, 400 MHz): δ (ppm) = 8.68 (s, 2H, Ha), 8.20 (m, 4H, Hf), 8.12 (d, 2H, J=8.7 Hz, Hb), 7.88-7.74 (m, 6H, Hc + Hd), 7.56 (m, 1H, He), 7.45 (t, 1H, J=7.8 Hz, He), 7.37 (t, 1H, J=7.8 Hz, He), 7.30-7.20 (m, 5H, Hg + He), 5.82 (m,

2H, C**H=**CH_2), 5.61 (m, 4H, C**H**CH_2), 4.98 (m, 4H, CH=C**H₂**), 4.49 (m, 4H, OC**H₂**CH_2), 2.29 (m, 8H, CHC**H₂**), 2.06 (m, 4H, C**H₂**CH=CH_2), 1.92 (m, 4H, OCH_2C**H₂**), 1.68-1.26 (m, 52H, -C**H₂**-), 0.96 (t, 12H, J=6.4 Hz, CH_2C**H₃**).

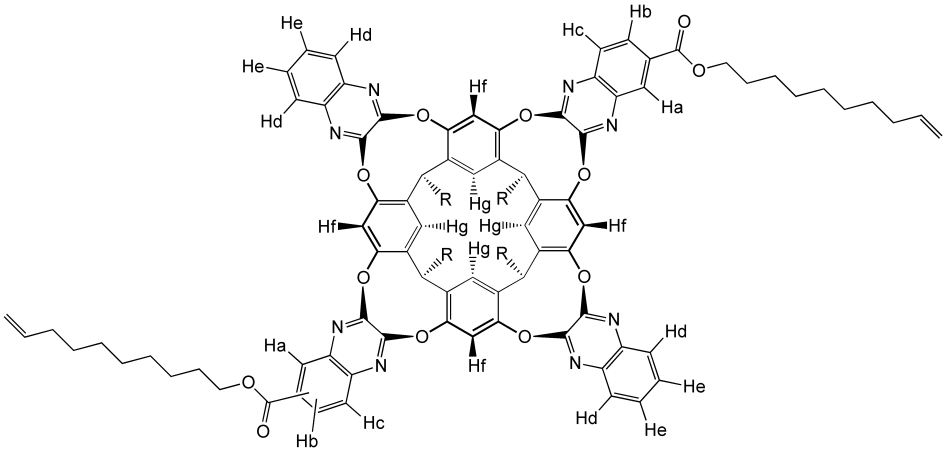

MALDI-TOF: calculated for $C_{106}H_{117}N_8O_{12}$ $[M+H]^+$ *m/z* = 1694.883, found *m/z* = 1694.834; calculated for $C_{106}H_{116}N_8NaO_{12}$ $[M+Na]^+$ *m/z* = 1716.864, found *m/z* = 1716.824.

Tetraquinoxaline cavitand-based alkenyl polyester (2c)

Cavitand **10** (0.100 g, 0.06 mmol) was dissolved in 2 mL of freshly distilled and degassed 1,2-dichloroethane and a catalytic amount of 2nd generation Grubbs catalyst was added. The solution was heated at 60 °C overnight under inert atmosphere. MeOH (20 mL) was added and the precipitate was filtered and dried. A second precipitation from MeOH afforded product mixture **2c** as a white solid (0.085 g, 87% calculated on the total weight).

^{1}H NMR ($CDCl_3$, 300 MHz): δ (ppm) = 8.67 (m, 2H, Ha), 8.22 (m, 4H, Hf), 8.10 (m, 2H, Hb), 7.92-7.66 (m, 6H, Hc + Hd), 7.55 (m, 1H, He), 7.49-7.33 (m, 2H, He), 7.28-7.20 (m, 5H, Hg + He), 5.82 (m, terminal C**H=**CH_2), 5.75-5.52 (m, 4H, C**H**CH_2), 5.46-5.28 (m, CH_2C**H**=C**H**CH_2), 4.96 (m, terminal CH=C**H₂**), 4.46 (m, 4H, OC**H₂**CH_2), 2.29 (m, 8H, CHC**H₂**), 2.12-1.81 (m, 8H, C**H₂**CH=CH_2 + OCH_2C**H₂**), 1.64-1.24 (m, 52H, -C**H₂**-), 0.95 (m, 12H, CH_2C**H₃**).

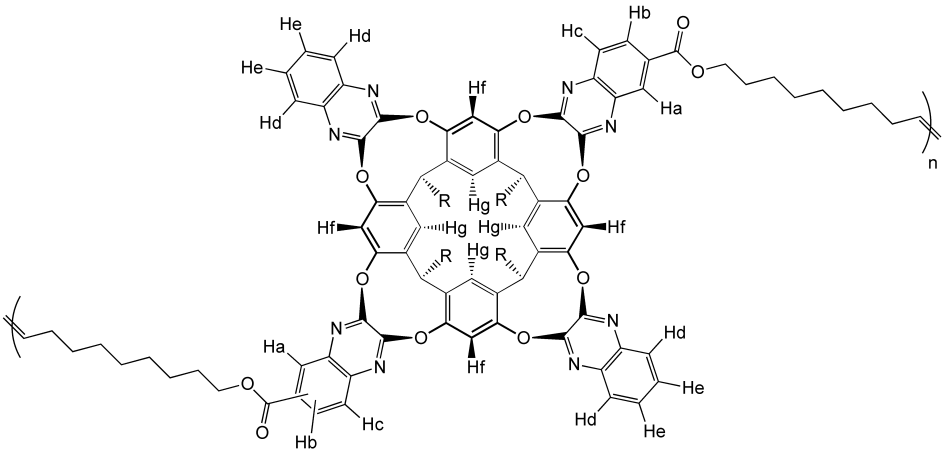

MALDI-TOF: calculated for intramolecular reaction product $C_{104}H_{113}N_8O_{12}$ $[M+H]^+$ *m/z* = 1666.851, found *m/z* = 1666.751.

7.6 References

[1] J. R. Moran, S. Karbach, D. J. Cram, *J. Am. Chem. Soc.* **1982**, *104*, 5826-5828

[2] V. A. Azov, A. Beeby, M. Cacciari, A. G. Cheetham, F. Diederich, M. Frei, J. K. Gimzewski, V. Gramlich, B. Hecht, B. Jaun, T. Latychevskaia, A. Lieb, Y. Lill, F. Marotti, A. Schlegel, R. R. Schlittler, P. J. Skinner, P. Seiler, Y. Yamakoshi, *Adv. Funct. Mater.* **2006**, *16*, 147-156.

[3] F. Lagugné-Labarthet, Y. Q. An, T. Yu, Y. R. Shen, E. Dalcanale, D. K. Shenoy, *Langmuir* **2005**, *21*, 7066-7070.

[4] J. R. Moran, J. L. Ericson, E. Dalcanale, J. A. Bryant, C. B. Knobler, D. J. Cram, *J. Am. Chem. Soc.* **1991**, *113*, 5707-5714.

[5] P. J. Skinner, A. G. Cheetham, A. Beeby, V. Gramlich, F. Diederich, *Helv. Chim. Acta* **2001**, *84*, 2146-2153.

[6] a) P. Amrhein, A. Shivanyuk, D. W. Johnson, J. Rebek Jr., *J. Am. Chem. Soc.* **2002**, 124, 10349-10358; b) M. Frei, F. Marotti, F. Diederich, *Chem. Commun.* **2004**, 1362-1363.

[7] V. A. Azov, B. Jaun, F. Diederich, *Helv. Chim. Acta.* **2004**, *87*, 449-462.

[8] P. Pagliusi, F. Lagugné-Labarthet, D. K. Shenoy, E. Dalcanale, Y. R. Shen, *J. Am. Chem. Soc.* **2006**, *128*, 12610-12611.

[9] K. G. Kleb, *Agew. Chem. Int. Ed.* **1964**, *3*, 408-416.

[10] D. R. Romer, *J. Heterocyclic Chem.* **2009**, *46*, 317-319.

[11] P. P. Castro, G. Zhao, G. A. Masangkay, C. Hernandez, L. M. Gutierrez-Tunstad, *Org. Lett.* **2004**, *6*, 333-336.

Chapter 8

Conformational Mechanochemistry on Tetraquinoxaline Cavitands

8.1 Introduction

Polymer mechanochemistry is a unique and powerful platform to access new reactivity and material properties. The energy required for a reaction to occur is usually provided by heat, light, pressure or electrochemical potential. These external stimuli act either by changing the distribution of the reactants in the ground state or moving them into an excited state with lower activation barrier. A different way to initiate a reaction is the use of force to deform reacting molecules along a specific direction of the reaction coordinate.[1] During the past decade,[2] emerging covalent mechanochemistry made significant progresses in different fields such as mechanoluminescence,[3] mechanochromism[4] and mechanically triggered polymer degradation.[5] Following the same trend new self-healing strategies, including activation of a latent catalyst[6] or reactive species[7] that are able to cross-link the bulk polymer matrix, were developed.

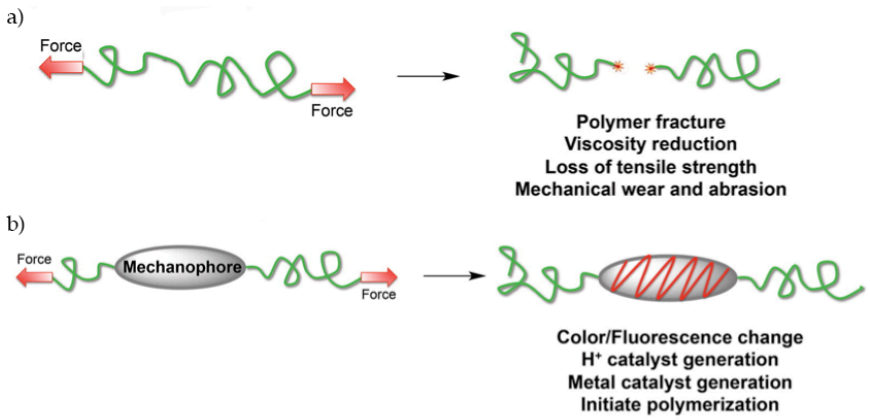

Figure 8.1 *Schematization of force-induced destructive (a) vs. productive (b) chemistry on polymers.*[2]

As schematized in Figure 8.1, all these new properties derive from the introduction of responsive units, called "mechanophores", in polymer backbones. Specifically, in covalent mechanochemistry a mechanophore is defined as a force-sensitive unit that possesses mechanically labile bonds. To exploit its mechanochemical activity, a mechanophore must be placed in the center of polymeric chains or used as cross-linker. Activation of labile bonds can be achieved both in solution and in the bulk. A variety of methods, ranging from ultrasonication[8] to manual elongation, has been developed for supplying and control the force applied to the polymer.[9] The activation of a single mechanophore unit can be evaluated exploiting single molecule force

spectroscopy (SMFS).[10] Although their promising properties, general application of mechanophores is limited by their low activation in bulk. This problem can be approached from a material-level perspective, with the identification of materials and architectures that efficiently transduce forces to a mechanochemical response, or at a molecular level designing more effective mechanophores.[11]

Remarkable examples of mechanochemical systems are spiropyran-based polymers reported by Moore and co-workers.[4a] The light-induced opening of spiropyran rings (colorless) to form merocyanines (colored) was known since 1964,[12] but only the introduction of this functionality in the center of high molecular weight polymers (in the 100 kDa range) allowed a force-induced conversion in polymeric matrixes. As represented in Figure 8.2, thanks to the color change a direct visualization of the mechanochemical reaction in a "dog-bone" specimen was possible.

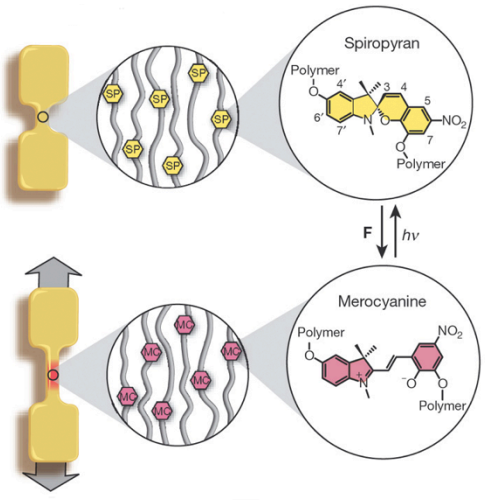

Figure 8.2 *Schematic diagram of application of tensile force to "dog bone" specimens and the conversion between the colorless spiropyran and colored merocyanine forms.*[4a]

While covalent bond cleavage has been widely studied exploiting both pericyclic[13] and strain ring-opening reactions,[14] mechanically induced molecular conformations interconversion is still unexplored. In our group, we applied mechanochemistry tools to the study of *vase* → *kite* switching of tetraquinoxaline cavitands in polymers. We assumed that the application of a tensile force to two opposite quinoxaline walls can induce the complete opening of the cavitand structure. To investigate the role of the substrate we

introduced tetraquinoxaline cavitands in two polymeric matrixes, namely polybutylmethacrylate (PBMA) and polydimethylsiloxane (PDMS), characterized by different mechanical properties. To our knowledge those are the first examples of polymer-embedded quinoxaline cavitands. *Vase* → *kite* switching in polymeric networks was followed by UV-Vis spectroscopy.[15] Initially, protonation-driven interconversion was studied to evaluate cavitand mobility in the substrate.

8.2 Results and Discussion

8.2.1 Alkene functionalized Cavitands Synthesis

For their relatively high stretchability and mechanical strength, polysiloxanes are suitable matrixes for mechanochemical materials. As demonstrated by Craig and coworkers, the introduction of mechanophores into PDMS *via* hydrosilylation reaction requires their functionalization with terminal double bonds.[16] Accordingly we synthesized ditopic cavitands **1a-1c** (Figure 8.3), which were incorporated in the polymeric substrate.

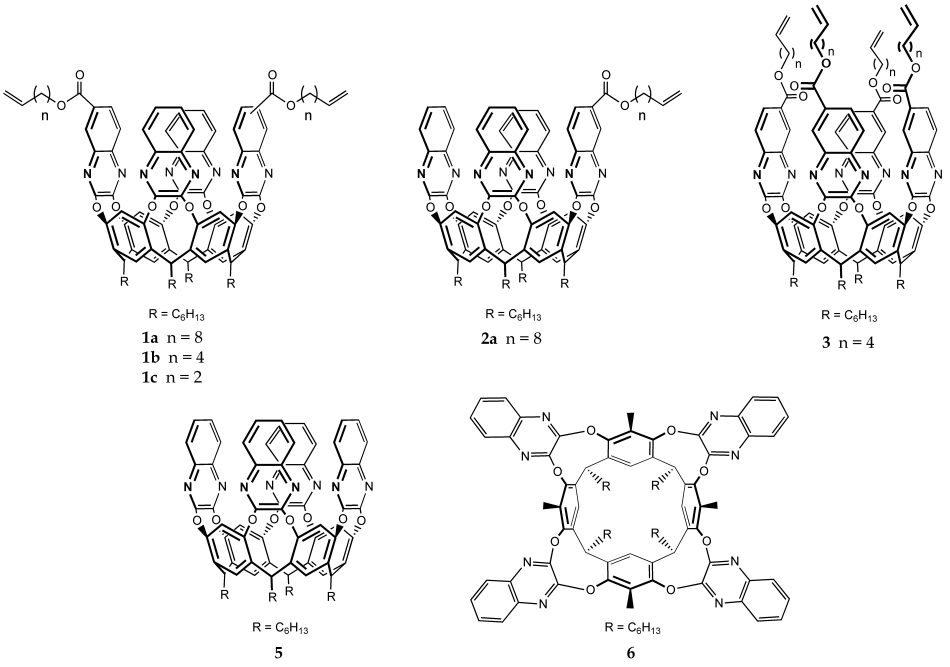

Figure 8.3 *Alkene-functionalized and reference cavitands involved in this study.*

The length of the aliphatic spacers was varied to investigate its influence on the transduction of the macroscopic elongation. Following the protocol developed by Moore and co-workers, samples containing monofunctionalized cavitand **2a** were tested to isolate the effects of the bidirectional strain. Maxima in UV-Vis spectra were compared to two unsubstituted reference compounds: tetraquinoxaline cavitand **5**, that retained his *vase* conformation under stress, and QxCav **6**, bearing four methyl groups in apical position that force the cavitand to assume a *kite* conformation.[17] Finally, tetrafunctionalized QxCav **3b** was used as cross-linker to maximize the applied tension.

A convergent synthesis gave the access to tetraquinoxaline cavitands **1b**, **1c** and **3** (for preparation of compounds **1a**, **2a** and **5** see Chapter 7). As discussed in Chapter 7 functional groups can be introduced on quinoxaline walls reacting resorcinarenes or partially bridged cavitands with functionalized quinoxalines. The 6 or 7 position was preferred to minimize steric hindrance and preserve *vase* ⇆ *kite* equilibrium. Alkene-functionalized dichloroquinoxalines were synthesized from 2,3-dichloroquinoxaline-6-carbonyl chloride (**4'**), following the procedure described in the previous chapter. Nucleophilic acyl substitution with alcohols bearing different aliphatic spacers afforded functionalized 2,3-dichloroquinoxalines **4b-4c** in good yields (Scheme 8.1).

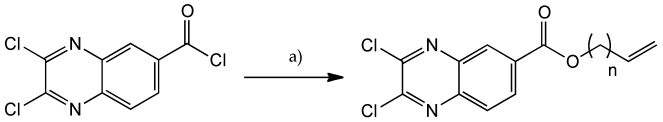

4' **4b** n = 4 **4c** n = 2

Scheme 8.1 *Terminal alkene-functionalized quinoxalines synthesis: a) CH_2=CH(CH_2)$_n$OH, DIPEA, CH_2Cl_2, r.t., 12 h.* ***4b****, n =4, 45%;* ***4c****, n =2, 42%.*

Tetraquinoxaline cavitands with two terminal alkenes on opposite quinoxaline walls were prepared bridging AC-bisquinoxaline cavitand with dichloroquinoxalines **4b-4c**, as reported in Chapter 7 for compound **1a**. Reactions were performed in DMSO under microwave irradiation, with potassium carbonate as base (Scheme 8.2). As a consequence of monosubstituted dichloroquinoxalines prochirality, a mixture of diastereoisomers was obtained after column chromatography.

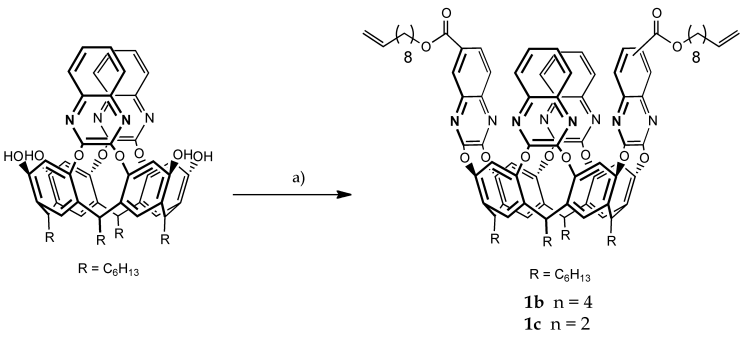

Scheme 8.2 *Bis-ω-alkene functionalized tetraquinoxaline cavitands synthesis: a)* ***4a-4b****, K_2CO_3, 70 °C (MW), 1h.* ***1b****, yield 40%;* ***1c****, yield 40%.*

Tetrafunctionalized cavitand **3** was synthesized from the corresponding resorcinarene (Scheme 8.3). Bridging reaction, performed in conditions analogous to Scheme 8.2, afforded compound **3** in 14% yield. Surprisingly after column chromatography only the two isomers with C_{4v} symmetry were isolated. The high symmetry, reflected in the ^{1}H NMR spectrum, can be explained considering the introduction of the four quinoxalines from the same enantioface. In fact, after the first statistical bridging event, steric hindrance of the aliphatic chains influenced the following insertions.

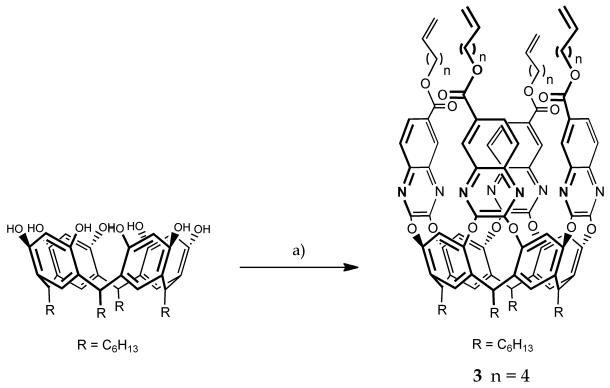

Scheme 8.3 *Tetra-alkene functionalized QxCav synthesis: a)* ***4b****, K_2CO_3, 70 °C (MW), 2h, 14%.*

Finally the *kite* cavitand **6**, also known as velcrand for its capability to form strong π-π dimers, was synthesized according to previously published procedures.[17]

8.2.2 PDMS Functionalization and Stretching Tests

We covalently introduced alkene-functionalized quinoxaline cavitands into PDMS (0.05-0.7% w/w) *via* hydrosilylation, as it is the same reaction used for curing the siloxane network. The effective incorporation of functionalized QxCavs was proved by Soxhlet extraction (for samples preparation and extraction tests see Experimental Section). Unfunctionalized cavitands instead were simply dispersed into the polymer precursors. Initially we measured UV-Vis absorption of cavitands **5** and **6,** both in solution and in PDMS (Figure 8.4).

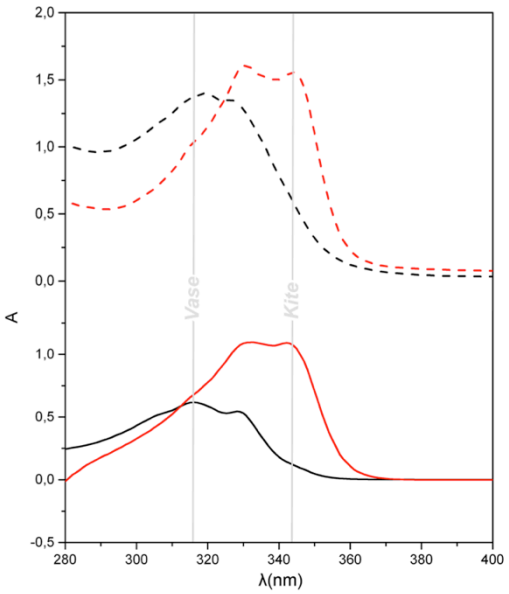

Figure 8.4 *UV-Vis spectra of cavitand* ***5*** *(black) and* ***6*** *(red) in* $CHCl_3$ *(solid line) and in PDMS (dashed line; 0.1% w/w, Table S8.1, entry II and IV respectively).*

Interestingly the optical properties of the two cavitands were retained in the polymeric substrate. The evaluation of maxima in UV-Vis spectra (318 nm for cavitands in *vase* conformation, 348 nm for *kite* ones) provided a powerful alternative to NMR spectroscopy in the study of *vase* → *kite* switching in highly cross-linked insoluble matrixes.[15] Firstly we tested protonation-driven interconversion exposing PDMS-embedded cavitands **1a-1c** (0.1-0.4% w/w, Table S8.2) to TFA vapors.

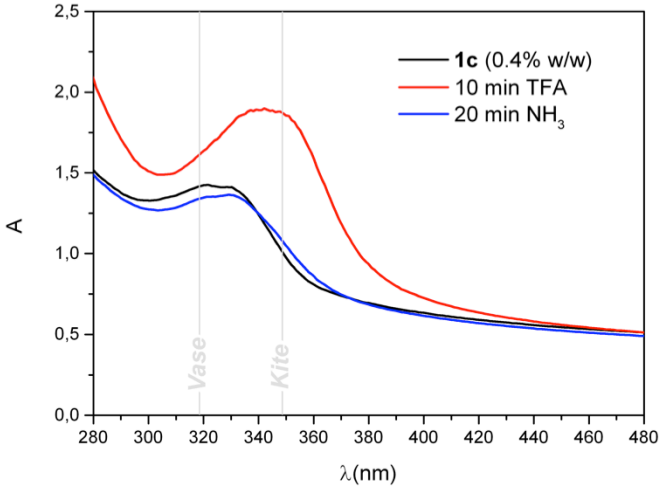

Figure 8.5 *UV-Vis spectra of cavitand* ***1c*** *(0.4% w/w, Table S8.2, entry XIII) in PDMS (black). The specimen was exposed to TFA vapors for 10 min (red) followed by 20 min of exposure to* NH_3 *(blue).*

As indicated by maxima analysis in Figure 8.5, cavitand **1c** underwent *vase* → *kite* switching upon protonation. To investigate the reversibility of *vase* ⇆ *kite* interconversion, TFA-threated samples were exposed to ammonia vapors. The UV-Vis spectrum of the specimens was found to be consistent with the pristine sample. Analogous behaviors were observed for compounds **1a** and **1b** in PDMS. These results suggest that cavitands possess enough free volume to increase their size moving to *kite* conformation. Finally UV-Vis spectra of PDMS-embedded tetraquinoxaline cavitands were measured under tensile stress. Specimens containing mono and difunctionalized cavitands in different concentrations were prepared. In all cases, maxima variation was not observed upon elongation of the polymeric sample. Figure 8.6 is representative of the experiments performed. The λ-independent decrease of the absorption is attributed to the thinning of polymer specimens upon elongation. For the entire set of samples tested we can conclude that the direct observation *via* UV-Vis spectroscopy of *vase* → *kite* interconversion upon elongation was not possible.

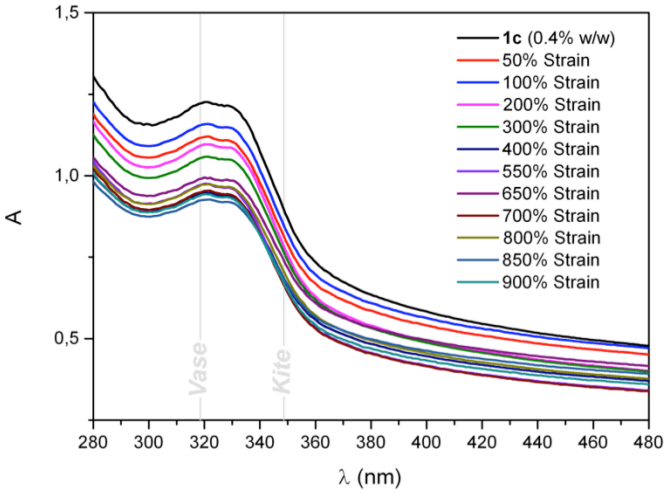

Figure 8.6 *UV-Vis spectra of cavitand* ***1c*** *embedded in PDMS (0.4% w/w, Table S8.2, entry XIII) under tensile strain.*

Cavitand **3** was prepared following the hypothesis that all four quinoxaline walls need to be stressed to induce *vase* → *kite* interconversion. In this case, UV-Vis spectrum in solution showed a slightly shifted maximum (323 nm instead of 318 for compound **5**), while the characteristic shoulder of the protonated *kite* form was not affected by the different functionalization (Figure 8.7). Interestingly, the exposure of the PDMS-embedded cavitand (0.03% w/w, see Table S8.3, entry II) to TFA vapors failed to evidence any remarkable shift. Similar results were obtained varying cavitand **3** concentration in the specimen (Table S8.3). A possible explanation is that that cavitand cross-linking prevents the opening to the *kite* form reducing its mobility. This hypothesis was supported by elongation tests results, as reported in Figure 8.8.

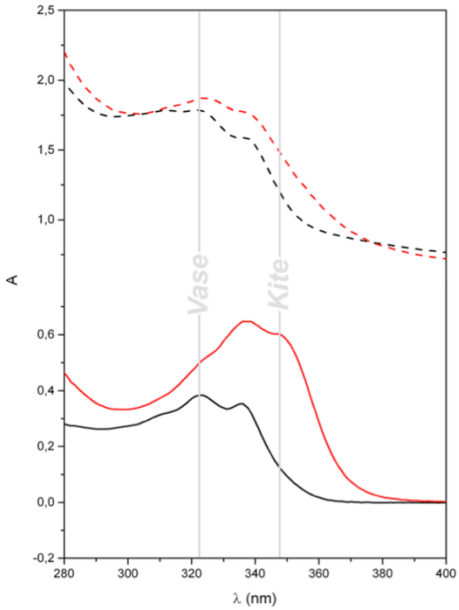

Figure 8.7 *UV-Vis spectra of cavitand* **3** *before (black) and after (red) exposure to TFA in* $CHCl_3$ *(solid line) and in PDMS (dashed line; 0.3% w/w, Table S8.3, entry II).*

UV-Vis measurement during elongation of PDMS specimens containing tetrafunctionalized cavitand **3** as additional cross-linker failed to evidence any significant variation and confirmed the lack of *vase* → *kite* switching.

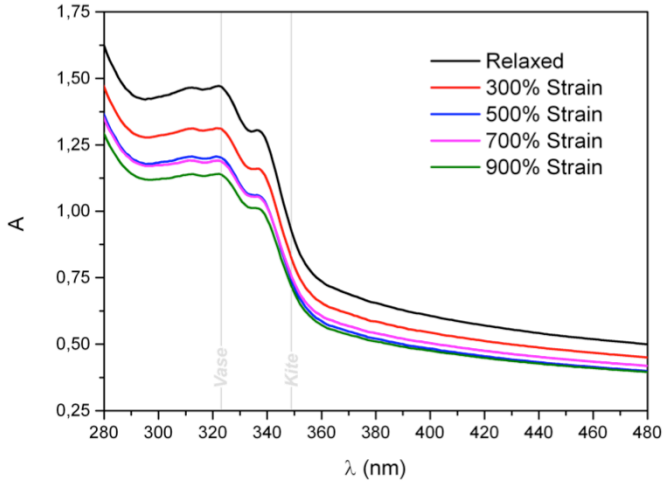

Figure 8.8 *UV-Vis spectra of PDMS specimen containing* **3** *(0.3% w/w, Table S8.3 entry II) under tensile strain.*

Although a similar matrix has been successfully used in mechanochemistry by Craig and coworkers,[16] the *vase* → *kite* interconversion for PDMS-embedded cavitands was not observed. A possible explanation lies in the fact that this elastomeric polymer possesses a high number of cross-linking sites, which can preclude the transmission of the mechanical energy to the cavitand. If for spiropyran-based materials a low degree of conversion (down to 5%) can lead to visible color changes, the detection of tetraquinoxaline cavitands conformation variations by UV-Vis spectroscopy requires a more efficient process.

8.2.3 PBMA-embedded Cavitand Synthesis

To test the influence of the matrix and maximize the addressing of mechanical energy we decided to introduce tetraquinoxaline cavitands as cross-linkers in PBMA. This second approach required the introduction of methacrylic groups at cavitands upper rim. Following the protocol previously described, the ad-hoc functionalized dichloroquinoxaline **4c** was synthesized in 2 steps (Scheme 8.4).

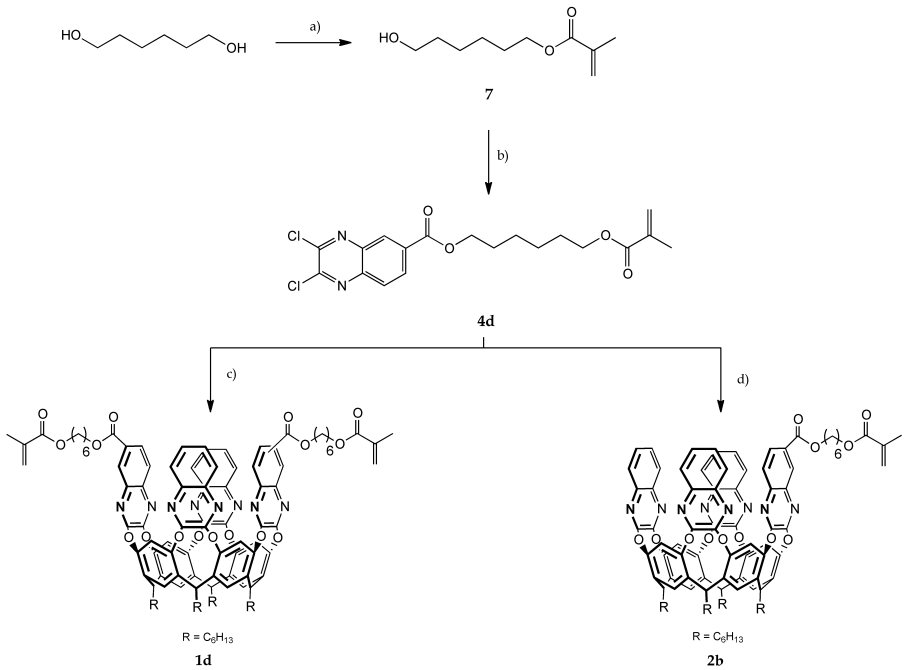

Scheme 8.4 *Synthesis of methacrylate-functionalized cavitands* ***1d*** *and* ***2b****: a) methacryloyl chloride, TEA, CH_2Cl_2, r.t., 12h, 42%; b)* ***4'****, TEA, CH_2Cl_2, r.t., 12h, 57%; c) AC-bisquinoxaline cavitand, K_2CO_3, DMSO, 70 °C (MW), 20 min, 50%; d) triquinoxaline cavitand, K_2CO_3, DMSO, 70 °C (MW), 20 min, 60%.*

The alcohol **7** was prepared reacting an excess of 1,6-hexanediol with methacryloyl chloride. The monoester was isolated with column chromatography with 42% yield. Condensation reaction between compound **7** and intermediate **4'** afforded methacrylate-functionalized dichloroquinoxaline **4d**. Bridging reaction between **4d** and AC-bisquinoxaline or triquinoxaline cavitands under microwave irradiation resulted in the formation of cavitands **1d** and **2b** respectively. Both cavitands were characterized by ^{1}H NMR spectroscopy (Figure 8.9a and Figure 8.11a) and MALDI-TOF spectrometry. The chemical shift of diagnostic methine protons in ^{1}H NMR confirmed their *vase* conformation in solution at room temperature.
To retain polymer solubility we decided to copolymerize 1 mol % of cavitands with butyl methacrylate (BMA). This allowed us to initially study protonation-driven *vase* → *kite* switching in solution with NMR spectroscopy. Radical polymerization of compound **1d** afforded the cross-linked polymer **PBMA-1d** (Scheme 8.5), while reaction of cavitand **2b** under the same conditions gave the side-chain functionalized polymer **PBMA-2b**.

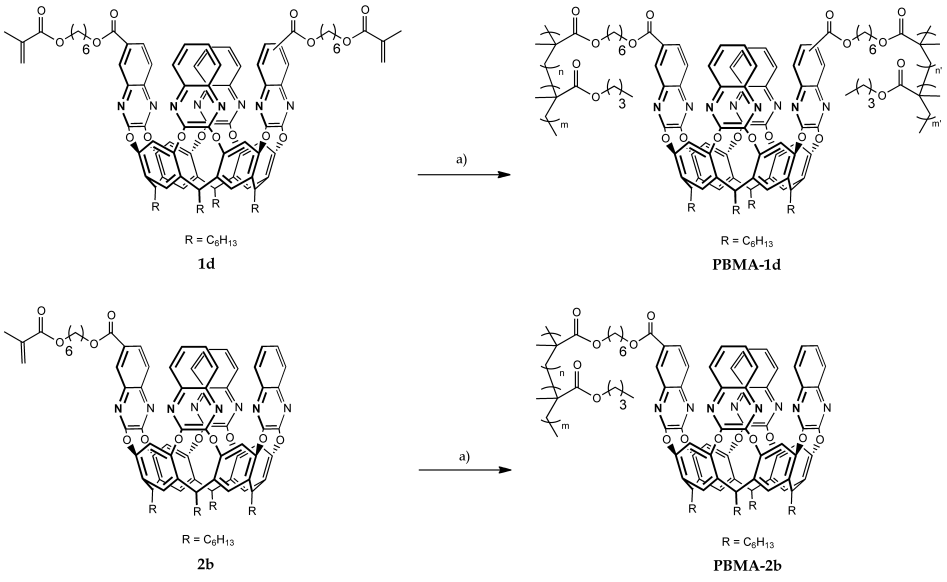

Scheme 8.5 *Synthesis of cavitand-functionalized polymers,* ***PBMA-1d*** *and* ***PBMA-2b****: a) butyl methacrylate, AIBN, toluene, 70°C, 12 h; 48% of yield for* ***PBMA-1d*** *and 84% for* ***PBMA-2b****.*

Thanks to its low cross-linking degree **PBMA-1d** maintained its solubility in chlorinated solvents. The polymer was characterized by ^{1}H NMR (Figure 8.9b) and integration of the signals at 5.7 and 4.3-3.6 ppm confirmed the ratio

between **1d** and BMA units. From chemical shifts analysis *vase* conformation was observed for the polymerized cavitand. The downshift of the methine proton, which probably goes below PBMA signal, upon addiction of TFA revealed that *vase* → *kite* switching was not jeopardized by the polymerization (Figure 8.9c).

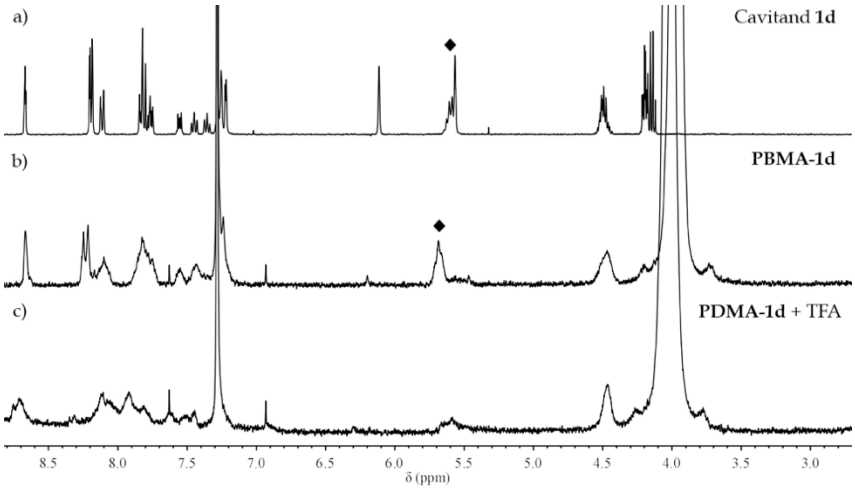

Figure 8.9 *^{1}H NMR spectra ($CHCl_3$, 400 MHz) of cavitand **1d** (a), polymer **PBMA-1d** (b), polymer **PBMA-1d** after addition of TFA (c). Signal related to methine protons is labeled (◆). Only the aromatic region of the spectra is shown.*

We followed protonation-driven *vase* → *kite* switching of **PBMA-1d** with UV-Vis spectroscopy (Figure 8.10). The increase of the shoulder at 348 nm confirms that the polymerized tetraquinoxaline cavitand is able to interconvert to the *kite* form.

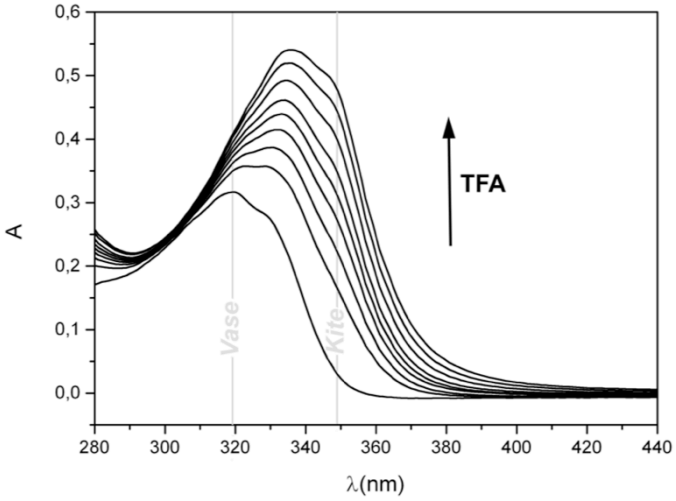

Figure 8.10 *Changes of the UV-Vis spectra of **PBMA-1d** in $CHCl_3$ upon addition of TFA.*

The same techniques were applied to **PBMA-2b** characterization and conformational studies (Figure 8.11b). *Vase* ⇆ *kite* interconversion was observed upon addition of TFA with ^{1}H NMR spectroscopy (Figure 8.11c). Changes in the UV-Vis spectrum confirm that the cavitand behavior was retained after the polymerization (Figure S8.4).

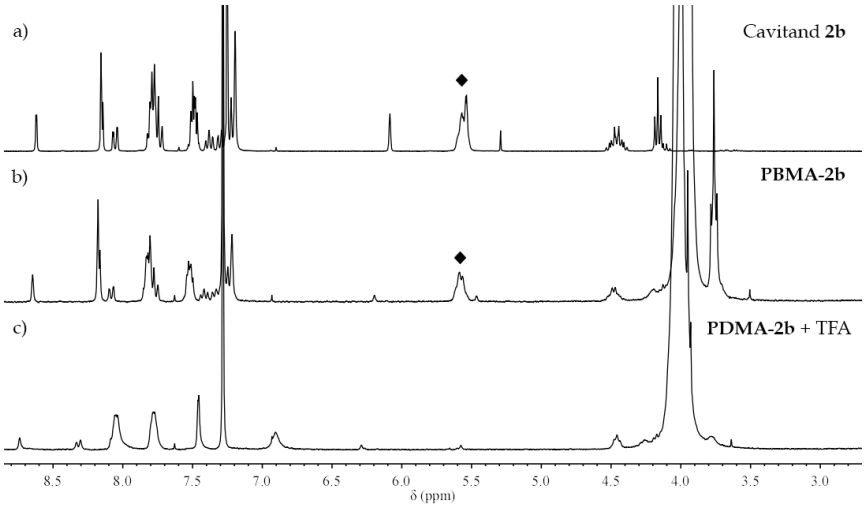

Figure 8.11 *^{1}H NMR spectra ($CHCl_3$, 300 MHz) of cavitand **2b** (a), polymer **PBMA-2b** (b), polymer **PBMA-2b** after addition of TFA (c). Signal related to methine protons is labeled (◆). Only the aromatic region of the spectra is shown.*

The two polymers were characterized by gel permeation chromatography (GPC) to determine their number average molecular weight (Mn), weight average molecular weight (Mw) and the polydispersity index (PDI). GPC analysis results are reported in Table 8.1 (for GPC curves see Figure S8.2 and Figure S8.3).

	Mn (g/mol)	**Mw (g/mol)**	**PDI**
PBMA-1d	17500	29000	1.6
PBMA-2b	14000	25300	1.8

Table 8.1 *GPC analysis results for polymer* ***PBMA-1d*** *and* ***PBMA-2b****.*

The two polymers were completely characterized and their *vase* → *kite* switching was obtained in solution adding TFA. The preparation of optically homogeneous polymeric films is still ongoing and only elongation tests will reveal the effectiveness of PBMA matrix in inducing conformational changes of embedded tetraquinoxaline cavitands.

8.3 Conclusions

Tetraquinoxaline cavitands were successfully introduced in two polymeric matrices, namely polybutylmethacrylate (PBMA) and polydimethylsiloxane (PDMS). A general protocol for their upper rim functionalization with polymerizable groups was developed. PDMS-embedded cavitands were found to undergo *vase* → *kite* interconversion when exposed to TFA vapors, but elongation tests failed to evidence any variation in UV-Vis spectra of the polymeric specimens. Regarding PBMA matrix, to date cavitands switching were obtained only in solution by adding TFA. The preparation of optically homogeneous samples containing tetraquinoxaline cavitands as cross-linkers is still ongoing.

8.4 Acknowledgments

Special thanks to Martina Torelli and Francesca Guagnini from the department of Chemistry, University of Parma. Thanks to Elantas Europe for providing samples of RTV 615.

8.5 Experimental Section

General procedure for alkenyl 2,3-dichloroquinoxaline-6-carboxylates:
2,3-dihydroxyquinoxaline-6-carboxylic acid (0.200 g, 1 mmol) was suspended in 8 mL of dry 1,2-dichloroethane and thionyl chloride (0.66 mL, 10 mmol) was added followed by a catalytic amount of DMF. The reaction mixture was refluxed for 2h. Volatiles were removed under reduce pressure and the red-brownish precipitate was redissolved in 8 mL of dry CH_2Cl_2. After the addition of TEA (0.15 mL, 1.1 mmol) and alken-1-ol (1.1 mmol, 1.1 eq) the mixture was stirred at room temperature overnight. The crude was diluted with CH_2Cl_2 and washed with a saturate solution of $NaHCO_3$, HCl 1 N and brine. The solvent was evaporated and the crude was purified by flash column chromatography.
Hex-5-en-1-yl 2,3-dichloroquinoxaline-6-carboxylate (4b)
Eluent: CH_2Cl_2/Hex 9:1; colorless oil (yield 45%)
^{1}H NMR ($CDCl_3$, 300 MHz): δ (ppm) = 8.75 (s, 1H, Ar**H**), 8.44 (d, 1H, J_o=8.7 Hz, Ar**H**), 8.10 (d, 1H, J_o=8.7 Hz, Ar**H**), 5.82 (m, 1H, C**H**=CH_2), 5.04 (m, 2H, CH=C**H$_2$**), 4.44 (t, 2H, J=7 Hz, OC**H$_2$**), 2.16 (m, 2H, C**H$_2$**CH=CH_2), 1.86 (m, 2H, OCH_2C**H$_2$**), 1.63 (m, 2H, -C**H$_2$**-).
But-3-en-1-yl 2,3-dichloroquinoxaline-6-carboxylate (4c)
Eluent: CH_2Cl_2; colorless oil (yield 42%)
^{1}H NMR ($CDCl_3$, 300 MHz): δ (ppm) = 8.75 (s, 1H, Ar**H**), 8.43 (d, 1H, J_o=8.7 Hz, Ar**H**), 8.10 (d, 1H, J_o=8.7 Hz, Ar**H**), 5.92 (m, 1H, C**H**=CH_2), 5.19 (m, 2H, CH=C**H$_2$**), 4.49 (t, 2H, J=7 Hz, OC**H$_2$**), 2.60 (m, 2H, C**H$_2$**CH=CH_2).

General procedure for bis-ω-alkene functionalized tetraquinoxaline cavitands:
To a suspension of AC-bisquinoxaline cavitand (0.100 g, 0.09 mmol) and K_2CO_3 (0.038 g, 0.28 mmol) in 4 mL of DMSO, a dichloroquinoxaline (0.20 mmol, 2.2 eq) was added. The mixture was heated at 70 °C under microwave irradiation for 1 h. The reaction was quenched with water (100 mL) and the precipitate was filtered, washed with water and dried. Flash column chromatography afforded pure cavitands**.**
Bis-hexene functionalized tetraquinoxaline cavitand (1b)
Eluent: gradient from CH_2Cl_2 to CH_2Cl_2/EtOAc 98:2; white solid (yield 40%)
^{1}H NMR ($CDCl_3$, 300 MHz): δ (ppm) = 8.66 (s, 2H, Ha), 8.18 (m, 4H, Hf), 8.11 (d, 2H, J=8.7 Hz, Hb), 7.83 (m, 6H, Hc + Hd), 7.79 (m, 1H, He), 7.77 (m, 2H, He), 7.30-7.20 (m, 5H, Hg + He), 5.84 (m, 2H, C**H=**CH_2), 5.59 (m, 4H, C**H**CH_2), 5.09

(m, 4H, CH=C**H₂**), 4.51 (m, 4H, OC**H₂**CH₂), 2.30 (m, 8H, CHC**H₂**), 1.96 (m, 4H, C**H₂**CH=CH₂), 1.90 (m, 4H, OCH₂C**H₂**), 1.70-1.28 (m, 36H, -C**H₂**-), 0.96 (m, 12H, CH₂C**H₃**).

MALDI-TOF: calculated for $C_{98}H_{101}N_8O_{12}$ $[M+H]^+$ *m/z*: 1582.757, found *m/z*: 1582.867.

Bis-butene functionalized tetraquinoxaline cavitand (1c)

Eluent: gradient from CH_2Cl_2 to CH_2Cl_2/EtOAc 98:2; white solid (yield 40%)

¹H NMR ($CDCl_3$, 300 MHz): δ (ppm) = 8.65 (s, 2H, Ha), 8.19 (m, 4H, Hf), 8.12 (d, 2H, J=8.7 Hz, Hb), 7.83 (m, 6H, Hc + Hd), 7.78 (m, 1H, He), 7.77 (m, 2H, He), 7.29-7.19 (m, 5H, Hg + He), 5.96 (m, 2H, C**H=**CH₂), 5.58 (m, 4H, C**H**CH₂), 5.25 (m, 4H, CH=C**H₂**), 4.55 (m, 4H, OC**H₂**CH₂), 2.66 (m, 4H, C**H₂**CH=CH₂), 2.30 (m, 8H, CHC**H₂**), 1.44-1.27 (m, 32H, -C**H₂**-), 0.96 (m, 12H, CH₂C**H₃**).

MALDI-TOF: calculated for $C_{94}H_{93}N_8O_{12}$ $[M+H]^+$ *m/z*: 1526.696, found *m/z*: 1526.488; calculated for $C_{94}H_{92}N_8O_{12}Na$ $[M+Na]^+$ *m/z*: 1548.679, found *m/z*: 1548.414.

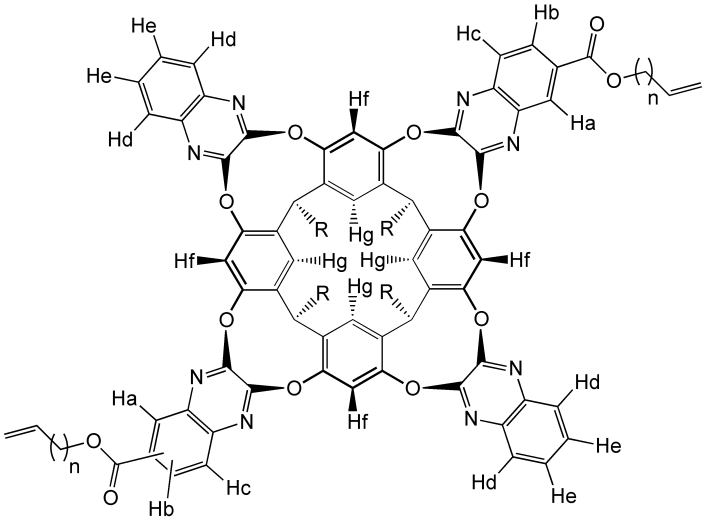

Tetra-ω-hexene functionalized tetraquinoxaline cavitand (3)

K_2CO_3 (0.044 g, 0.26 mmol) was added to a solution of Res[C_6H_{13}, H] (0.051 g, 0.06 mmol) in 2 mL of DMSO, followed by dichloroquinoxaline **4b** (0.085 g, 0.26 mmol). The reaction mixture was heated at 70 °C under microwave irradiation for 2 h. Water (100 mL) was added and the precipitate was filtered, washed with water and dried. The crude was purified by flash column chromatography (CH_2Cl_2/EtOAc 98:2) affording cavitand **3** as a white solid (0.015 g, 0.01 mmol, 14%).

^{1}H NMR ($CDCl_3$, 300 MHz): δ (ppm) = 8.60 (s, 4H, Ar**H**), 8.02 (d, 4H, Ar$\mathbf{H_{up}}$), 8.12 (d, 4H, J=8.7 Hz, Ar**H**), 7.86 (d, 4H, J=8.7 Hz, Ar**H**), 7.26 (s, 4H, Ar$\mathbf{H_{down}}$), 5.85 (m, 4H, C**H=**CH_2), 5.57 (t, 4H, J=8.0 Hz, C**H**CH_2), 5.00 (m, 8H, CH=C$\mathbf{H_2}$), 4.48 (t, 8H, J=6.6 Hz, OC$\mathbf{H_2}CH_2$), 2.37-2.13 (m, 16H, CHC$\mathbf{H_2}$ + $OCH_2C\mathbf{H_2}$), 1.92 (m, 8H, C$\mathbf{H_2}$CH=CH_2), 1.74-1.19 (m, 40H, -C$\mathbf{H_2}$-), 0.93 (m, 12H, $CH_2C\mathbf{H_3}$).
MALDI-TOF: calculated for $C_{112}H_{121}N_8O_{12}$ $[M+H]^+$ *m/z*: 1835.888, found *m/z*: 1535.888; calculated for $C_{112}H_{120}N_8O_{12}Na$ $[M+Na]^+$ *m/z*: 1856.907, found *m/z*: 1856.908.

PDMS samples preparation
RTV 615 was used as polysiloxane substrate. This polymer is a proprietary two-part (Base and Curing Agent, typically mixed in a 10:1 ratio) silicone elastomer comprising vinyl terminated poly(dimethylsiloxane), poly(methylhydro-siloxane-co-dimethylsiloxane) copolymer and platinum catalyst.
In a 15 mL Falcon tube RTV 615 Base (3.0 g) and a THF cavitand solution were homogenized with a vortex. RTV 615 Curing Agent (0.3 g) was added and the tube was extensively shacked with a vortex. The homogenous mixture was degassed under vacuum and poured onto a PTFE plate. After a second degassing the sample was cured in an oven at 60 °C for 16 h. Once cured the film was pealed and cut into strips for testing.

	Cavitand	Conc. (% w/w)
I	**5**	0.05
II	**5**	0.1
III	**5**	0.2
IV	**6**	0.05
V	**6**	0.1
VI	**2a**	0.1

Table S8.1 *Control specimens containing mono functionalized or unfunctionalized cavitands.*

	Cavitand	Conc. (% w/w)
I	**1a**	0.05
II	**1a**	0.1
III	**1a**	0.2
IV	**1a**	0.3
V	**1a**	0.5
VI	**1a**	0.6
VII	**1a**	0.7
VIII	**1b**	0.1
IX	**1b**	0.3
X	**1b**	0.5
XI	**1b**	0.7
XII	**1c**	0.1
XIII	**1c**	0.4
XIV	**1c**	0.5
XV	**1c**	0.7

Table S8.2 *Specimens containing bis-alkene functionalized cavitands.*

	Cavitand	Conc. (% w/w)
I	**3**	0.1
II	**3**	0.3
III	**3**	0.5

Table S8.3 *Specimens containing tetrafunctionalized cavitands.*

Soxhlet extraction tests

To validate the described method we had to prove that cavitand double bonds participated in the hydrosilylation reaction. We performed Soxhlet extraction with $CHCl_3$ on two PDMS samples, one cured in the presence of bis-alkene functionalized cavitand **1a** (Table S8.1, Entry 2) and the other with

unfunctionalized QxCav **5** (Table S8.2, Entry 3). The treated polymer and the organic phase were studied by UV-Vis spectroscopy. As shown in Figure S8.1 for sample containing **1a** the absorption patter of the cavitand is present only in the polymer, while the result is opposite for sample cured in the presence of **5**. This experiment however proved the incorporation of the cavitands in the polysiloxane network but not the effective reaction of all their functionalities.

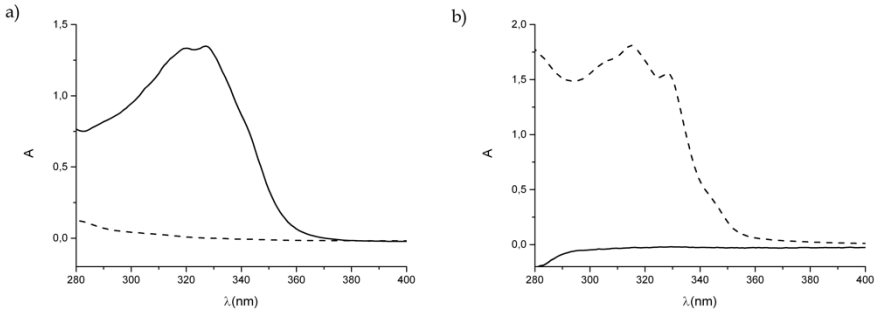

Figure S8.1 *UV-Vis spectra of Soxhlet threated samples (solid line) and extracts (dashed line) from* PDMS containing **1a** (a) and PDMS containing **5** (b).

6-hydroxyhexyl methacrylate (7)

To a solution of 1,6-hexanediol (5.0 g, 42 mmol) in 75 mL of dry CH_2Cl_2, TEA (2.95 mL, 21 mmol) was added. Methacryloyl chloride (1.38 mL, 14 mmol) was slowly added at 0 °C. The solution was warmed at room temperature and stirred overnight. The reaction was quenched with water and the organic phase washed with a saturated solution of $NaHCO_3$, HCl 1 N and brine. The solvent was removed and the crude was purified by flash column chromatography (Hex/EtOAc 7:3) affording monoester **7** (1,11 g, 6 mmol, 42%) as a colorless oil.

^{1}H NMR ($CDCl_3$, 400 MHz): δ (ppm) = 6.10 (s, 1H, $\mathbf{H}_{trans}$HC=C), 5.55 (s, 1H, $\mathbf{H}_{cis}$HC=C), 4.15 (t, 2H, J=6.6 Hz, (C=O)OC$\mathbf{H_2}$CH$_2$), 3.64 (t, 2H, J=6.6 Hz, CH$_2$C$\mathbf{H_2}$OH), 1.94 (s, 3H, C$\mathbf{H_3}$), 1.68 (m, 3H, CH$_2$O$\mathbf{H}$ + (C=O)OCH$_2$C$\mathbf{H_2}$), 1.58 (m, 2H, C$\mathbf{H_2}$CH$_2$OH), 1.41 (m, 4H, -C$\mathbf{H_2}$-).

ESI-MS: *m/z*: 209.3 $[M+Na]^+$.

6-(methacryloyloxy)hexyl 2,3-dichloroquinoxaline-6-carboxylate (4d)

2,3-dihydroxyquinoxaline-6-carboxylic acid (0.300 g, 1.5 mmol) was suspended in 10 mL of dry 1,2-dichloroethane and thionyl chloride (1.0 mL, 14.5 mmol) was added followed by catalytic DMF. The reaction mixture was refluxed for 2h, then volatiles were removed under reduced pressure. The precipitate was recovered in 10 mL of dry CH_2Cl_2. After the addition of TEA (0.22 mL, 1.6

mmol) and alcohol **7** (0.298 g, 1.6 mmol) the mixture was stirred at room temperature overnight. The crude was diluted with CH_2Cl_2 and washed with a saturate solution of $NaHCO_3$, HCl 1 N and brine. The solvent was evaporated and the crude was purified by flash column chromatography (Hex/THF 93:7) affording dichloroquinoxaline **4d** (0.342 g, 0.8 mmol, 57%).

^{1}H NMR ($CDCl_3$, 400 MHz): δ (ppm) = 8.75 (s, 1H, Ar**H**), 8.43 (d, 1H, J_o=8.7 Hz, Ar**H**), 8.13 (d, 1H, J_o=8.7 Hz, Ar**H**), 6.12 (s, 1H, $\mathbf{H_{trans}}$HC=C), 5.57 (s, 1H, $\mathbf{H_{cis}}$HC=C), 4.44 (t, 2H, J=6.5 Hz, Ar(C=O)OC$\mathbf{H_2}CH_2$), 4.19 (t, 2H, J=6.5 Hz, $CH_2C\mathbf{H_2}O$(C=O)), 1.97 (s, 3H, C$\mathbf{H_3}$), 1.87 (m, 2H, Ar(C=O)$OCH_2C\mathbf{H_2}$), 1.75 (m, 2H, C$\mathbf{H_2}CH_2O$(C=O)), 1.53 (m, 4H, -C$\mathbf{H_2}$-).

Bis-methacrylate functionalized tetraquinoxaline cavitand (1d)

To a suspension of AC-bisquinoxaline cavitand (0.215 g, 0.20 mmol) and K_2CO_3 (0.083 g, 0.60 mmol) in 4 mL of DMSO, dichloroquinoxaline **4d** (0.181 g, 0.44 mmol) was added. The mixture was heated at 70 °C under microwave irradiation for 20 min. Water (100 mL) was added and the precipitate was filtered, washed with water and dried. Flash column chromatography (gradient from Hex/EtOAc 85:15 to Hex/EtOAc 8:2) afforded cavitand **1d** (0.182 g, 0.10 mmol, 50%) as a white solid.

^{1}H NMR ($CDCl_3$, 300 MHz): δ (ppm) = 8.67 (s, 2H, Ha), 8.18 (m, 4H, Hf), 8.11 (d, 2H, J=8.7 Hz, Hb), 7.81 (m, 6H, Hc + Hd), 7.56 (m, 1H, He), 7.45 (m, 1H, He), 7.36 (m, 1H, He), 7.23 (m, 5H, Hg + He), 6.12 (s, 2H, $\mathbf{H_{trans}}$HC=C), 5.57 (m, 6H, C**H**CH_2 + $\mathbf{H_{cis}}$HC=C), 4.50 (m, 4H, Ar(C=O)OC$\mathbf{H_2}CH_2$), 4.19 (m, 4H, $CH_2C\mathbf{H_2}$O(C=O)), 2.28 (m, 8H, CHC$\mathbf{H_2}$), 1.95 (m, 10H, C=CC$\mathbf{H_3}$ + Ar(C=O)$OCH_2C\mathbf{H_2}$), 1.76 (m, 4H, C$\mathbf{H_2}CH_2$O(C=O)), 1.65-1.27 (m, 40H, -C$\mathbf{H_2}$-), 0.95 (m, 12H, $CH_2C\mathbf{H_3}$).

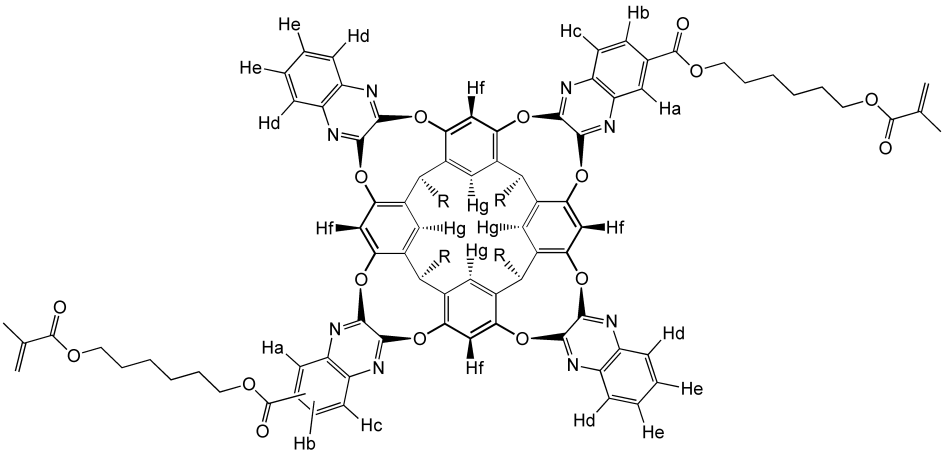

MALDI-TOF: calculated for $C_{106}H_{113}N_8O_{16}$ $[M+H]^+$ *m/z*: 1754.831, found *m/z*: 1754.930.

Methacrylate functionalized tetraquinoxaline cavitand (2b)

To a suspension of triquinoxaline cavitand (0.100 g, 0.08 mmol) in 4 mL of DMSO, K_2CO_3 (0.023 g, 0.17 mmol) and dichloroquinoxaline **4d** (0.041 g, 0.10 mmol) were added. The mixture was heated at 70 °C under microwave irradiation for 20 min then the reaction was quenched with 100 mL of water. The precipitate was filtered, washed with water, dried and purified by flash column chromatography (Hex/EtOAc 85:15). Cavitand **2b** (0.077 g, 0.05 mmol, 60%) was obtained as a white solid.

^{1}H NMR ($CDCl_3$, 300 MHz): δ (ppm) = 8.61 (s, 1H, Ha), 8.16 (m, 4H, Hg), 8.05 (d, 1H, J=8.7 Hz, Hb), 7.78 (m, 7H, Hc + Hd), 7.50 (m, 4H, Hf), 7.36 (t, 1H, J=8.4 Hz, He), 7.29 (t, 1H, J=8.4 Hz, He), 7.21 (m, 4H, Hi), 6.09 (s, 1H, $\mathbf{H}_{trans}$HC=C), 5.54 (m, 5H, C**H**CH_2 + $\mathbf{H}_{cis}$HC=C), 4.45 (m, 2H, Ar(C=O)OC$\mathbf{H_2}CH_2$), 4.16 (m, 2H, $CH_2C\mathbf{H_2}O$(C=O)), 2.25 (m, 8H, CHC$\mathbf{H_2}$), 1.92 (m, 5H, C=CC$\mathbf{H_3}$ + Ar(C=O)O$CH_2C\mathbf{H_2}$), 1.74 (m, 2H, C$\mathbf{H_2}CH_2$O(C=O)), 1.67-1.21 (m, 36H, -C$\mathbf{H_2}$-), 0.92 (m, 12H, $CH_2C\mathbf{H_3}$).

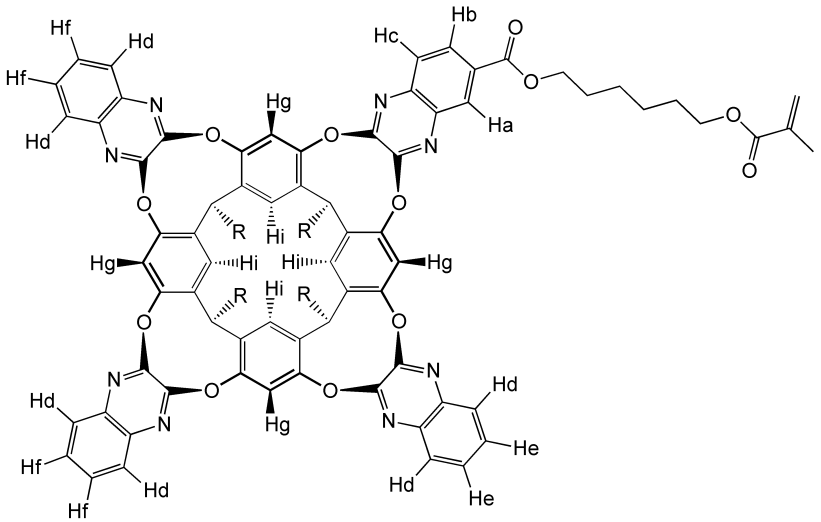

MALDI-TOF: calculated for $C_{95}H_{97}N_8O_{12}$ $[M+H]^+$ *m/z*: 1542.730, found *m/z*: 1542.597.

Copolymerization between n-butyl methacrylate and bis-methacrylate functionalized tetraquinoxaline cavitand (PBMA-1d)

In a schlenk tube cavitand **1d** (0.027 g, 0.015 mmol) and n-butyl methacrylate (0.242 mL, 1,52 mmol) were dissolved in 2 mL of toluene. The solution was degassed and heated at 70 °C, then AIBN (0.005 g) was added. The mixture was maintained at that temperature for 24 h. The copolymer was recovered by precipitation in methanol followed by a trituration in the same solvent (sonication). Polymer **PBMA-1d** was obtained as a white solid (yield 48%).

^{1}H NMR ($CDCl_3$, 400 MHz): δ (ppm) = 8.67 (2H, Ha), 8.25-8.08 (6H, Hf + Hb), 7.82 (6H, Hc + Hd), 7.54 (1H, He), 7.44 (2H, He), 7.25 (5H, Hg + He), 5.57 (m, 4H, C**H**CH_2), 4.47 (4H, Ar(C=O)O**CH_2**CH_2), 4.0 (O**C$H_{2,PBMA}$**CH_2), 2.29 (8H, CHC**H_2**), 2.1-1.7 (-**C$H_{2,PBMA}$**-C(C=O)CH_3), 1.6 (-CH_2-C(C=O)**C$H_{3,PBMA}$** + OCH_2**C$H_{2,PBMA}$**), 1.4 (OCH_2CH_2**C$H_{2,PBMA}$**), 1.0-0.8 (CH_2**C$H_{3,PBMA}$**).

GPC: eluent: chloroform; flux: 1 ml/min; column temperature: 30 °C; standard for the calibration curve: polystyrene.

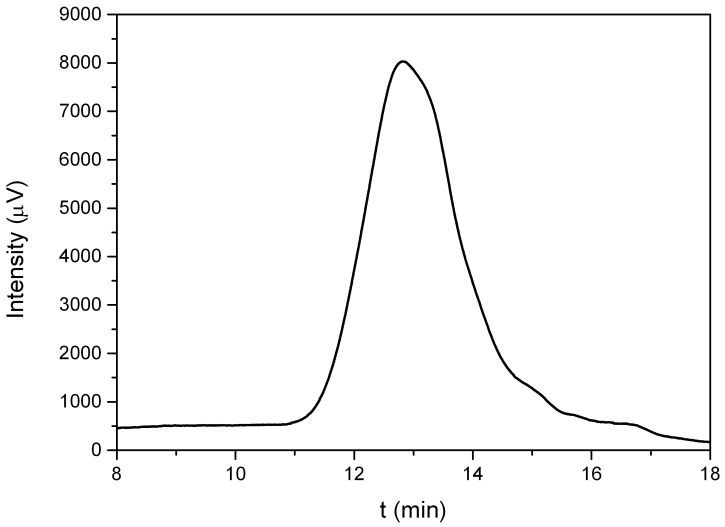

Figure S8.2 *GPC curve of **PBMA-1d**.*

Copolymerization between n-butyl methacrylate and methacrylate functionalized tetraquinoxaline cavitand (PBMA-2b)

In a schlenk tube, n-butyl methacrylate (0.786 mL, 4,9 mmol) was added to a solution of cavitand **2b** (0.077 g, 0.015 mmol) in 5 mL of toluene. The mixture was degassed and heated at 70 °C, then AIBN (0.014 g) was added. The mixture was maintained at 70 °C for 24 h, then cooled at room temperature. The copolymer was recovered by precipitation in MeOH. Trituration in the MeOH (sonication) afforded polymer **PBMA-2b** as a white solid (yield 84%).

^{1}H NMR ($CDCl_3$, 300 MHz): δ (ppm) = 8.65 (1H, Ha), 8.17 (4H, Hg), 8.10 (1H, Hb), 7.82 (7H, Hc + Hd), 7.52 (4H, Hf), 7.42 (1H, He), 7.33 (1H, He), 7.24 (4H, Hi), 5.58 (4H, C**H**CH_2), 4.48 (2H, Ar(C=O)OC**H$_2$**CH_2), 3.9 (OC**H$_{2,PBMA}$**CH_2), 2.27 (8H, CHC**H$_2$**), 2.0-1.7 (-C**H$_{2,PBMA}$**-C(C=O)CH_3), 1.6 (-CH_2-C(C=O)C**H$_{3,PBMA}$** + OCH_2C**H$_{2,PBMA}$**), 1.4 (OCH_2CH_2C**H$_{2,PBMA}$**), 1.1-0.8 (CH_2C**H$_{3,PBMA}$**).

GPC: eluent: chloroform; flux: 1 ml/min; column temperature: 30 °C; standard for the calibration curve: polystyrene.

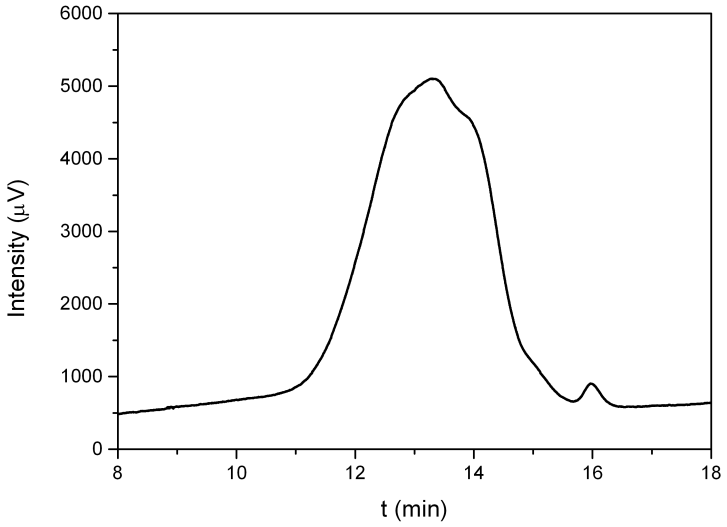

Figure S8.3 *GPC curve of **PBMA-2b**.*

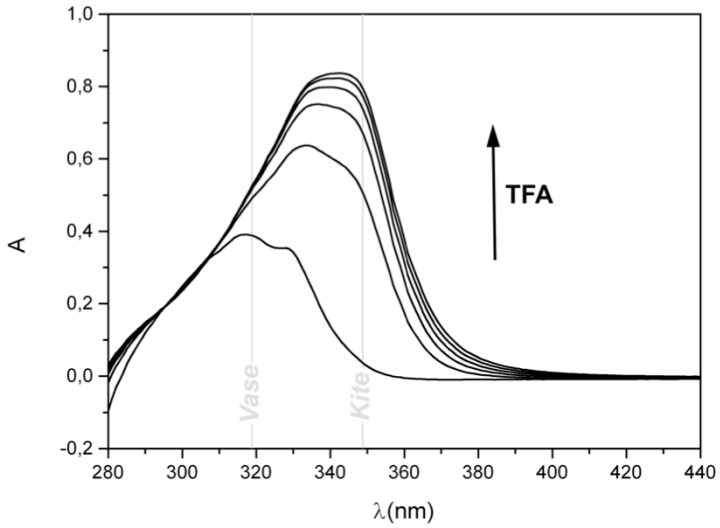

Figure S8.4 *Changes of the UV-Vis spectra of* ***PBMA-2b*** *in* $CHCl_3$ *upon addition of TFA.*

8.6 References

[1] C. R. Hickenboth, J. S. Moore, S. R. White, N. R. Sottos, J. Baudry, S. R. Wilson, *Nature* **2007**, *446*, 423-427.

[2] a) M. K. Beyer, H. Clausen-Schaumann, *Chem. Rev.* **2005**, *105*, 2921-2948; b) M. M. Caruso, D. A. Davis, Q. Shen, S. A. Odom, N. R. Sottos, S. R. White, J. S. Moore, *Chem. Rev.* **2009**, *109*, 5755–5798; c) A. L. Black, J. M. Lenhardt, S. L. Craig, *Mater. Chem.* **2011**, *21*, 1655–1663; d) J. Ribas-Arino, D. Marx, *Chem. Rev.* **2012**, *112*, 5412−5487; e) J. Li, C. Nagamani, J. S. Moore, *Acc. Chem. Res.* **2015**, *48*, 2181-2190.

[3] Y. Chen, A. J. H Spiering, S. Karthikeyan, G. W. M. Peters, E. W. Meijer, R. P. Sijbesma, *Nat. Chem.* **2012**, *4*, 559-562.

[4] a) D. A. Davis, A. Hamilton, J. Yang, L. D. Cremar, D. Van Gough, S. L. Potisek, M. T. Ong, P. V. Braun, T. J. Martínez, S. R. White, J. S. Moore, N. R. Sottos, *Nature* **2009**, *459*, 68-72; b) K. Imato, A. Irie, T. Kosuge, T. Ohishi, M. Nishihara, A. Takahara, H. Otsuka, *Angew. Chem. Int. Ed.* **2015**, *54*, 6168-6172.

[5] C. E. Diesendruck, G. I. Peterson, H. J. Kulik, J. A. Kaitz, B. D. Mar, P. A. May, S. R. White, T. J. Martínez, A. J. Boydston, J. S. Moore, *Nat. Chem.* **2014**, *6*, 623-628.

[6] R. T. M. Jakobs, S. Ma, R. P. Sijbesma, *ACS Macro Lett.* **2013**, *2*, 613-616.

[7] A. L. B. Ramirez, Z. S. Kean, J. A. Orlicki, M. Champhekar, S. M. Elsakr, W. E. Krause, S. L. Craig, *Nat. Chem.* **2013**, *5*, 757-761.

[8] B. Lee, Z. Niu, J. Wang, C. Slebodnick, S. L. Craig, *J. Am. Chem. Soc.* **2015**, *137*, 10826-10832.

[9] K. M. Wiggins, J. N. Brantley, C. W. Bielawski, *Chem. Soc. Rev.* **2013**, *42*, 7130-7147.

[10] a) F. R. Kersey, W. C. Yount, S. L. Craig, *J. Am. Chem. Soc.* **2006**, *128*, 3886-3887; b) J. Wang, T. B. Kouznetsova, Z. S. Kean, L. Fan, B. D. Mar, T. J. Martínez, S. L. Craig, *J. Am. Chem. Soc.* **2014**, *136*, 15162-15165.

[11] C. L. Brown, S. L. Craig, *Chem. Sci.* **2015**, *6*, 2158-2165.

[12] T. Bercovici, E. Fischer, *J. Am. Chem. Soc.* **1964**, *86*, 5687-5688.

[13] a) M. B. Larsen, A. J. Boydston, *J. Am. Chem. Soc.* **2014**, *136*, 1276-1279; b) M. J. Robb, J. S. Moore, *J. Am. Chem. Soc.* **2015**, *137*, 10946-10949; c) Z. S. Kean, G. R. Gossweiler, T. B. Kouznetsova, G. B. Hewage, S. L. Craig, *Chem. Commun.* **2015**, *51*, 9157-9160.

[14] a) S. L. Potisek, D. A. Davis, N. R. Sottos, S. R. White, J. S. Moore, *J. Am. Chem. Soc.* **2007**, *129*, 13808-13809; b) J. M. Lenhardt, A. L. Black, B. A. Beiermann, B. D. Steinberg, F. Rahman, T. Samborski, J. Elsakr, J. S. Moore, N. R. Sottos, S. L. Craig, *J. Mater. Chem.* **2011**, *21*, 8454–8459; c) H. M. Klukovich, T. B. Kouznetsova, Z. S. Kean, J. M. Lenhardt, S. L. Craig, *Nat. Chem.* **2013**, *5*, 110–114.

[15] P. J. Skinner, A. G. Cheetham, A. Beeby, V. Gramlich, F. Diederich, *Helv. Chim. Acta* **2001**, *84*, 2146-2153.

[16] G. R. Gossweiler, G. B. Hewage, G. Soriano, Q. Wang, G. W. Welshofer, X. Zhao, S. L. Craig, *ACS Macro Lett.* **2014**, *3*, 216-219.

[17] D. J. Cram, H. J. Choi, J. A. Bryant, C. B. Knobler, *J. Am. Chem. Soc.* **1992**, *114*, 7748-7765.

MATERIALS AND METHODS

Materials

All commercially obtained reagents were used as received. Unless stated otherwise, reactions were conducted in flame-dried glassware under an atmosphere of argon using anhydrous solvents (either freshly distilled or passed through activated alumina columns).
Silica column chromatography was performed using silica gel 60 (Fluka 230-400 mesh ASTM), or silica gel 60 (MERCK 70-230 mesh).

Methods

• NMR Measurements
^{1}H NMR spectra were obtained using a Bruker AVANCE 300 (300 MHz) or a Bruker AVANCE 400 (400 MHz) spectrometer. All chemical shifts (δ) were reported in ppm relative to the proton resonances resulting from the incomplete deuteration of the NMR solvents. ^{13}C NMR spectra were obtained using a Bruker AVANCE 300 (75 MHz) or a Bruker AVANCE 400 (100 MHz) spectrometer. All chemical shifts (δ) were reported in ppm relative to the carbon resonances of the NMR solvents. ^{31}P NMR spectra were obtained using a Bruker AVANCE 400 (162 MHz) spectrometer. All chemical shifts (δ) were recorded in ppm relative to external 85% H_3PO_4 at 0.00 ppm. ^{19}F NMR spectra were obtained using a Bruker AVANCE 400 (376 MHz) spectrometer. All chemical shifts (δ) were recorded in ppm relative to external CCl_3F at 0.00 ppm.

• MS Measurements
Electrospray ionization ESI-MS experiments were performed on a Waters ZMD spectrometer equipped with an electrospray interface. MALDI was performed on an AB SCIEX MALDI TOF-TOF 4800 Plus (matrix: α–cyano-4-hydroxycinnamic acid). Exact masses were determined also using a LTQ ORBITRAP XL Thermo spectrometer equipped with an electrospray interface.
(Ch. 3): Part of the experiments was performed on a Bruker Daltonics APEXIV 4.7 Tesla Fourier Transform Ion Cyclotron Resonance Mass Spectrometer (FT-ICR-MS) equipped with an electrospray interface.

(Ch. 5): ESI-FT-Orbitrap-MS analyses were performed with a Q Exactive™ Hybrid Quadrupole-Orbitrap Mass Spectrometer.

• **UV-Vis Measurements**

UV-Vis spectra were collected using a Thermo Scientific Evolution 260 Bio spectrophotometer equipped with a Peltier water cooled cell changer device, using matched quartz cells of 1 cm path length.

• **ITC Experiments**

ITC titrations were performed on a MicroCal VP-ITC System. Experimental titration curves were analyzed using MicroCal Origin 5.0 program. The association constant values (K_a) and the enthalpy values (ΔH) were calculated as the average of four titrations for every guest. The titrations were performed at 25 °C. Unless stated otherwise, the host solution was put in the reaction cell and titrated with a ten-folder higher concentrated guest solution. The heat released upon binding was tracked against time. To quantify unspecific heats of dilution, each guest was also titrated into pure solvent (blank titration). In all cases, the signal from blank titrations was subtracted from the binding signal before curve fitting.

• **XPS Measurements**

XPS spectra were run with a PHI 5600 multitechnique ESCA-Auger spectrometer equipped with a monochromatic Al Ka X-ray source. Analyses were carried out with an analyzer pass energy of 23.5 eV and a photoelectron angle of 45° and 10° (relative to the sample surface) with an acceptance angle of ±7°. In all spectra, XPS binding energy scale was calibrated by placing the C*1s* peak due to hydrocarbon moieties and 'adventitious' carbon at 285.0 eV. The elemental composition of the samples was evaluated by estimating the integrated area of each component corrected for the corresponding photo-ionization cross-section. The Tb*3d* sensitivity factor was empirically verified from terbium(III) acetate hydrate and pristine $TbPc_2$ powders.

ADDITIONAL INFORMATION FOR CH. 2

^{1}H NMR Competitive Experiments

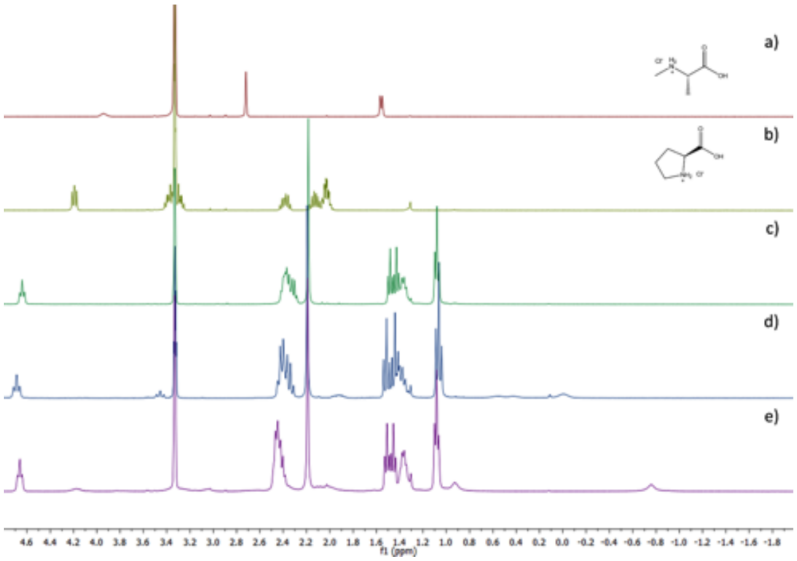

Figure 1 *^{1}H NMR spectra of a) N-Me-Ala·HCl; b) Pro·HCl; c) free host* **2***; d)* **2***·Pro·HCl complex (1:1 stoichiometry); e)* **2***·N-Me-Ala·HCl complex formed after the addition of 1 eq. of N-Me-Ala·HCl to the already formed* **2***·Pro·HCl complex.*

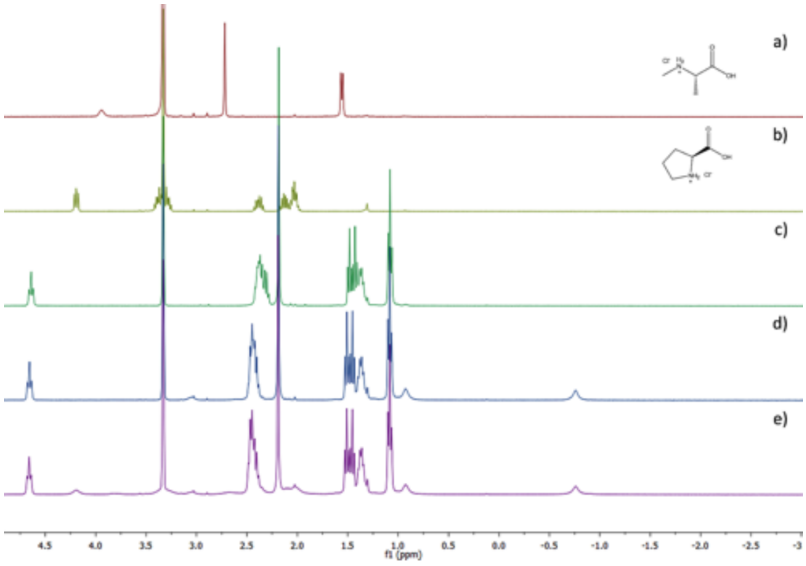

Figure 2 *[1]H NMR spectra of a) N-Me-Ala·HCl; b) Pro·HCl; c) free host* **2***; d)* **2***·N-Me-Ala·HCl complex (1:1 stoichiometry); e)* **2***·N-Me-Ala·HCl complex after the addition of 1 eq Pro·HCl.*

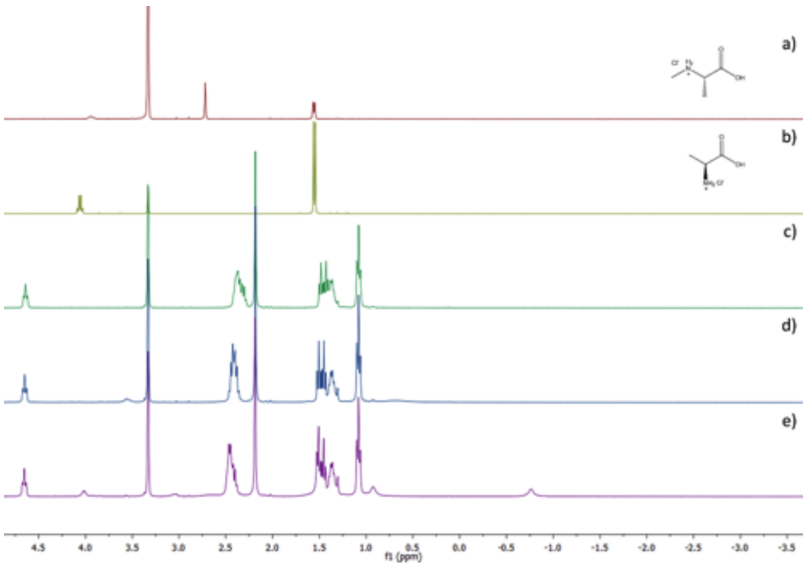

Figure 3 *[1]H NMR spectra of a) N-Me-Ala·HCl; b) Ala·HCl; c) free host* **2***; d)* **2***·Ala·HCl complex (1:1 stoichiometry); e)* **2***·N-Me-Ala·HCl complex formed after the addition of 1 eq. of N-Me-Ala·HCl to the already formed* **2***·Ala·HCl complex.*

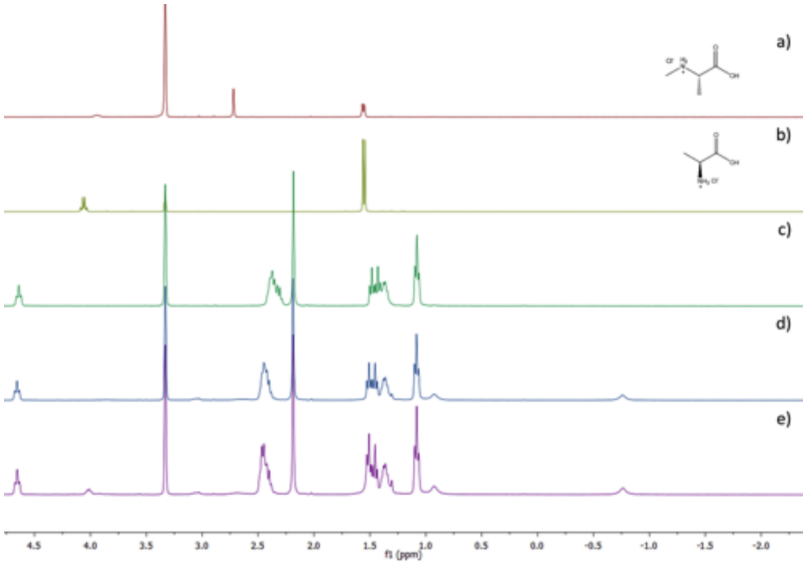

Figure 4 *[1]H NMR spectra of a) N-Me-Ala·HCl; b) Ala·HCl; c) free host* **2***; d)* **2***·N-Me-Ala·HCl complex (1:1 stoichiometry); e)* **2***·N-Me-Ala·HCl complex after the addition of 1 eq Ala·HCl.*

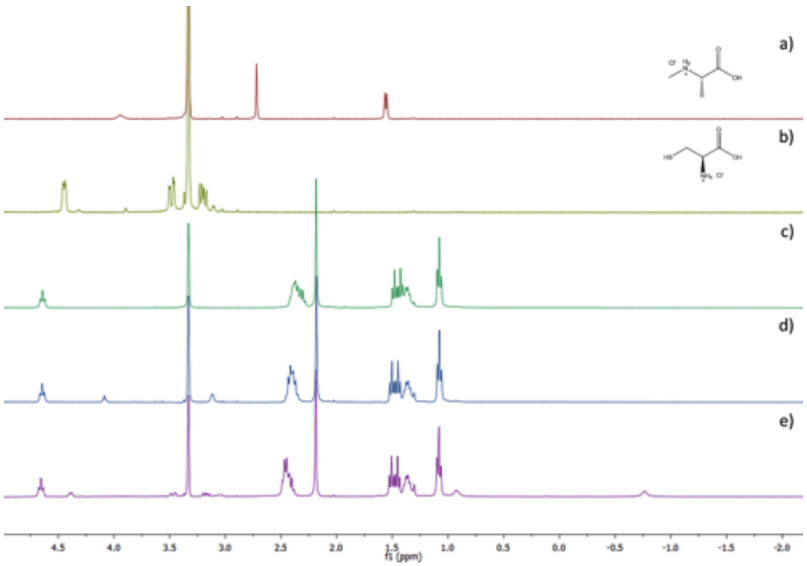

Figure 5 *[1]H NMR spectra of a) N-Me-Ala·HCl; b) Cys·HCl; c) free host* **2***; d)* **2***·Cys·HCl complex (1:1 stoichiometry); e)* **2***·N-Me-Ala·HCl complex formed after the addition of 1 eq. of N-Me-Ala·HCl to the already formed* **2***·Cys·HCl complex.*

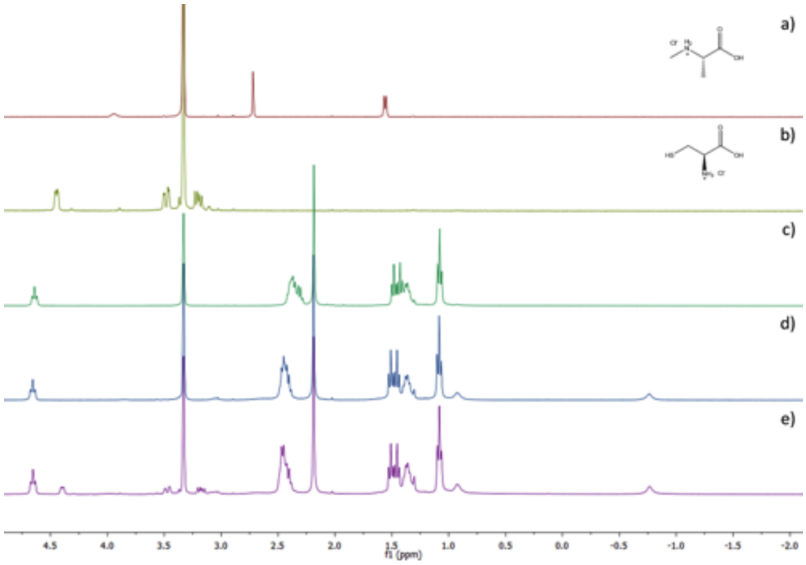

Figure 6 *^{1}H NMR spectra of a) N-Me-Ala·HCl; b) Cys·HCl; c) free host* **2***; d)* **2**·*N-Me-Ala·HCl complex (1:1 stoichiometry); e)* **2**·*N-Me-Ala·HCl complex after the addition of 1 eq Cys·HCl.*

NMR Experiments in Aqueous Solvents

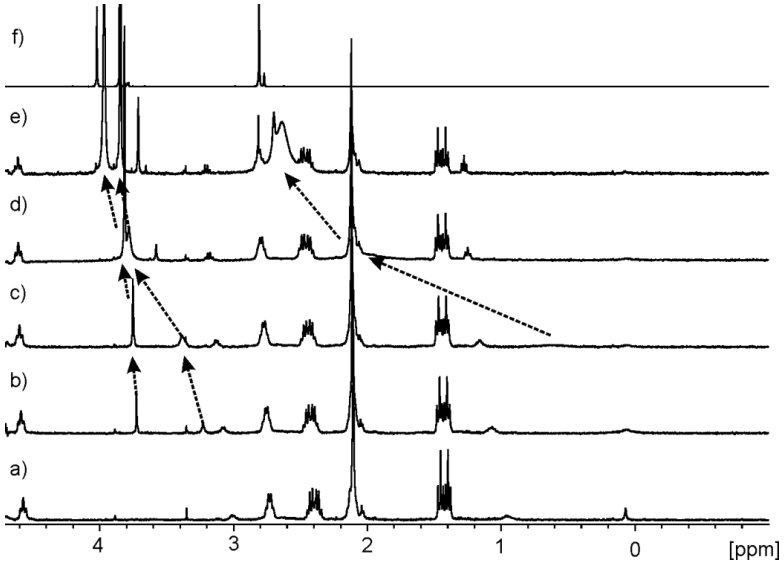

Figure 7 *Selected upfield regions of the ^{1}H NMR (400MHz, D_2O, 298K) spectra acquired during the titration of* **3** *with incremental amounts of* ***SarcME****. a)* **3***; b)* **3** *+ 0.55 eq. of* ***SarcME****; c)* **3** *+ 1.08 eq. of* ***SarcME****; d)* **3** *+ 3.95 eq. of* ***SarcME****; e)* **3** *+ 18.5 eq. of* ***SarcME****; f)* ***SarcME****.*

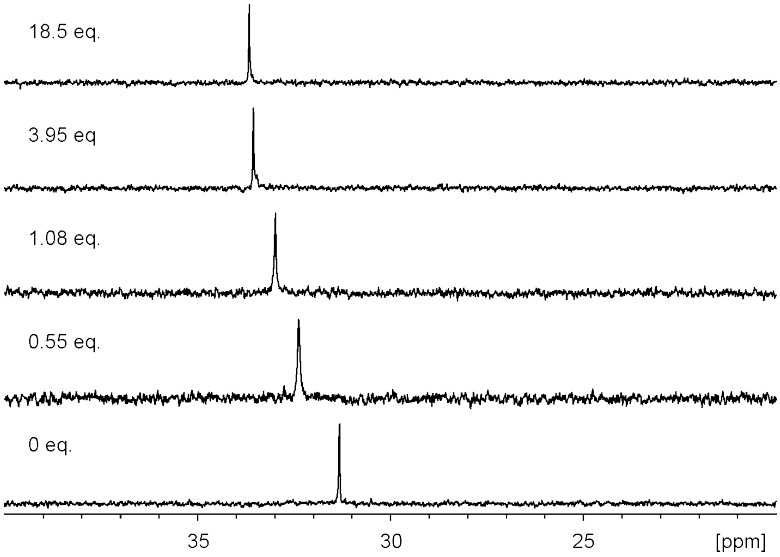

Figure 8 *Selected region of the ^{31}P NMR (162 MHz, D_2O, 298K) spectra acquired during the titration of* ***3*** *with incremental amounts of* ***SarcME****.*

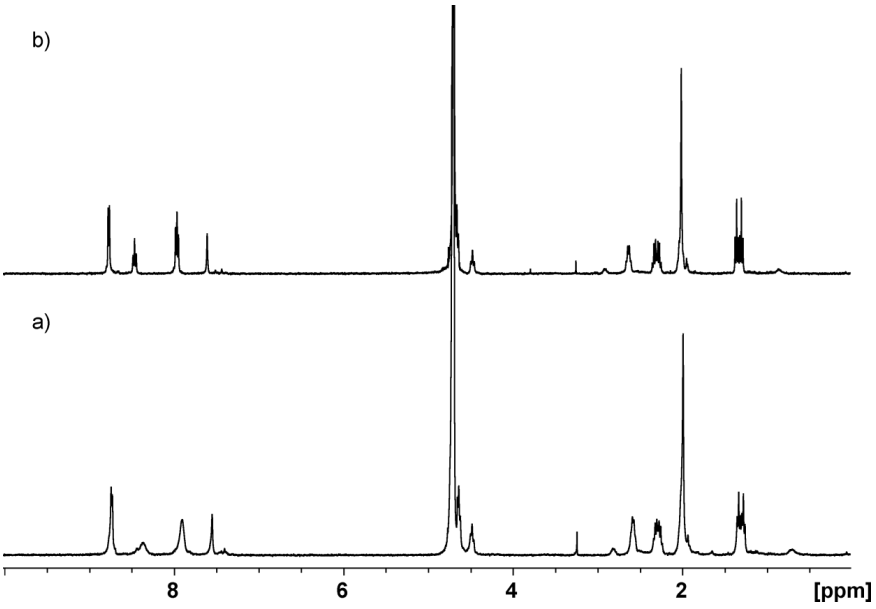

Figure 9 *^1H NMR spectra of cavitand* **3** *a) in deuterated PBS (***3** *= 1.98 mM) b) in D_2O (***3** *= 1.11 mM).*

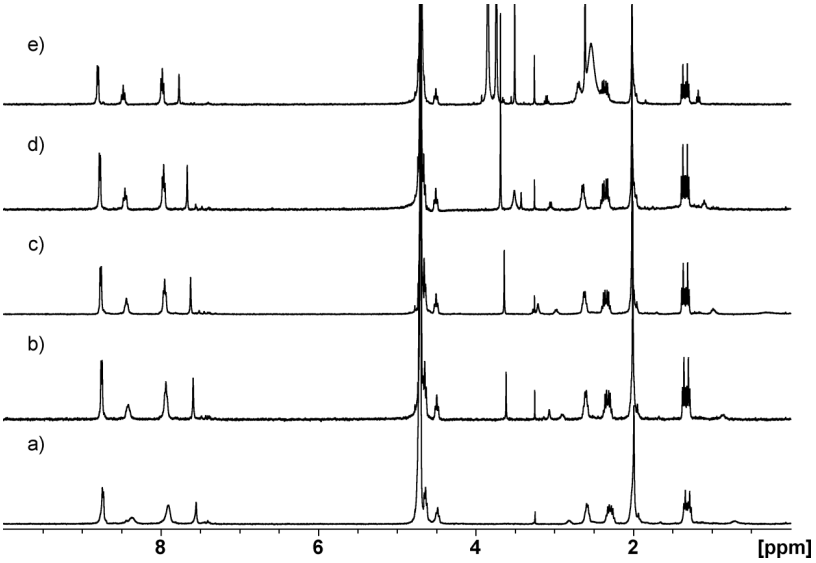

Figure 10 *[1]H NMR (400MHz, deuterated PBS (0.1 M, pH 7, 298K) spectra acquired during the titration of* ***3*** *with incremental amounts of* ***SarcME****. a)* ***3****; b)* ***3*** *+ 0.5 eq. of* ***SarcME****; c)* ***3*** *+ 0.98 eq. of* ***SarcME****; d)* ***3*** *+ 2.38 eq. of* ***SarcME****; e)* ***3*** *+ 21.4 eq. of* ***SarcME****.*

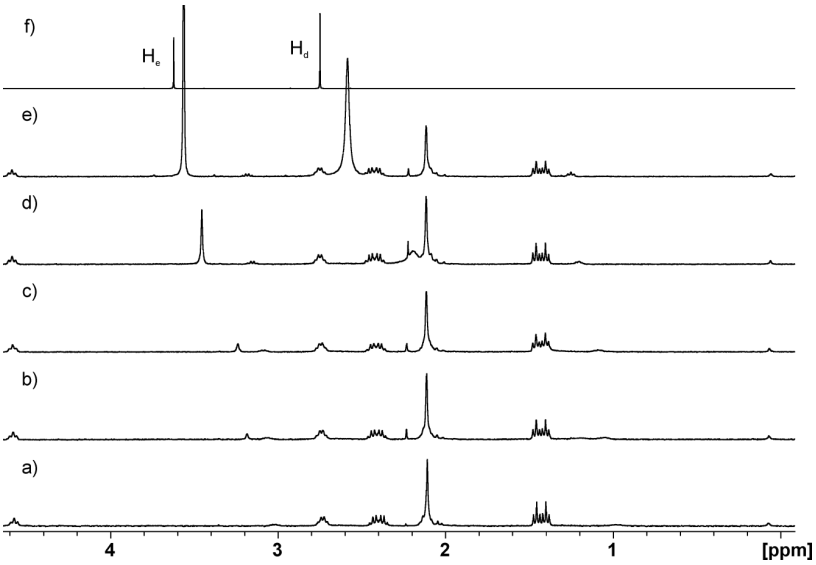

Figure 11 *Selected upfield regions of the [1]H NMR (400 MHz, D_2O, 298K) spectra acquired during the titration of* ***3*** *with incremental amounts of* ***Sarc****. a)* ***3****; b)* ***3*** *+ 0.61 eq. of* ***Sarc****; c)* ***3*** *+ 1.01 eq. of* ***Sarc****; d)* ***3*** *+ 4.67 eq. of* ***Sarc****; e)* ***3*** *+ 20.04 eq. of* ***Sarc****; f)* ***Sarc****.*

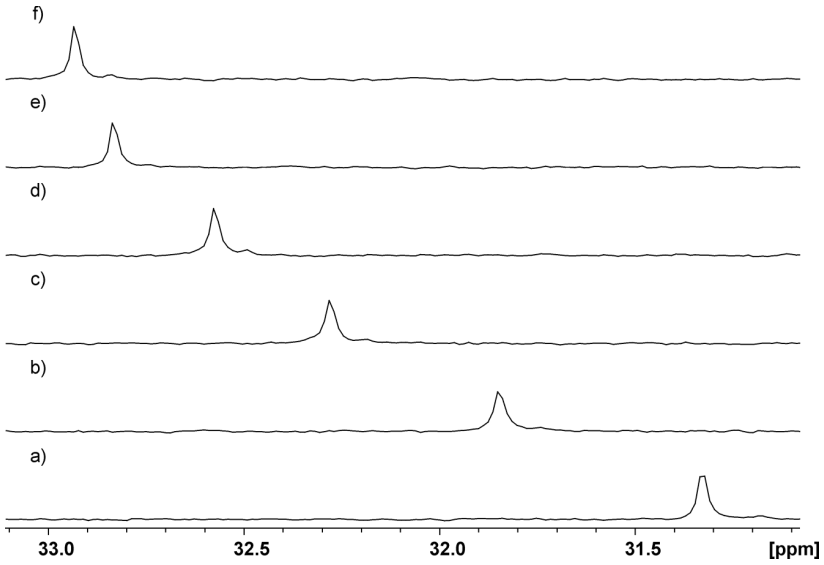

Figure 12 *Selected region of the ^{31}P NMR (162 MHz, D_2O, 298K) spectra acquired during the titration of* ***3*** *with incremental amounts of* ***Sarc****. a)* ***3****; b)* ***3****+ 0.61 eq. of* ***Sarc****; c)* ***3****+ 1.50 eq. of* ***Sarc****; d)* ***3****+ 2.91 eq. of* ***Sarc****; e)* ***3****+ 7.83 eq. of* ***Sarc****; f)* ***3****+ 20.4 eq. of* ***Sarc****.*

Complexation of Nε-Methyl-L-Lysine in Methanol

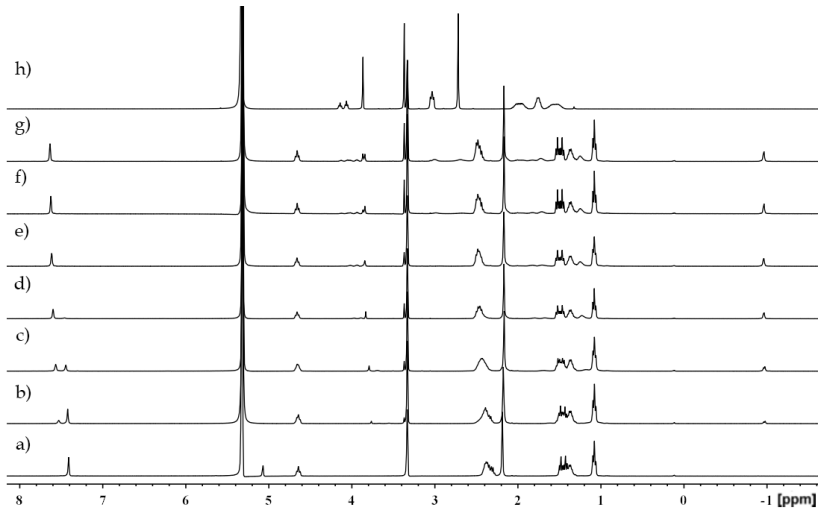

Figure 13 *^1H NMR (400 MHz, CD_3OD, 298K) spectra acquired during the titration of* ***2*** *with incremental amounts of N-Me-Lys. a)* ***2****; b)* ***2*** *+ 0.25 eq. of N-Me-Lys; c)* ***2*** *+ 0.50 eq. of N-Me-Lys; d)* ***2*** *+ 0.75 eq. of N-Me-Lys; e)* ***2*** *+ 1.0 eq. of N-Me-Lys; f)* ***2*** *+ 1.25 eq. of N-Me-Lys; g)* ***2*** *+ 1.5 eq. of N-Me-Lys, h) N-Me-Lys.*

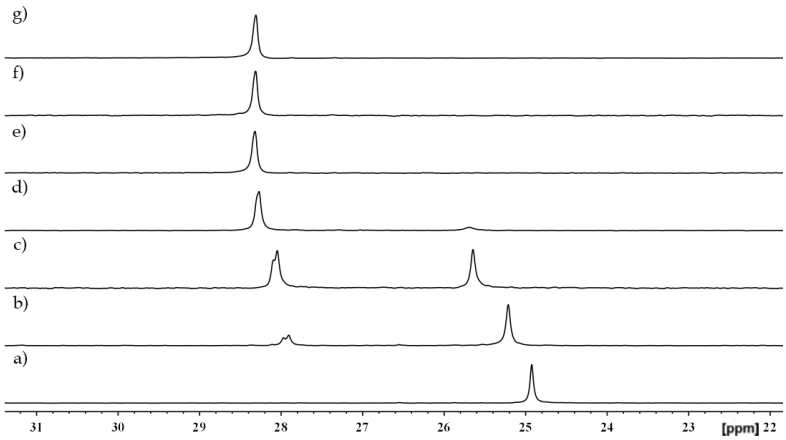

Figure 15 *^{31}P NMR (162 MHz, CD_3OD, 298K) spectra acquired during the titration of* **2** *with incremental amounts of N-Me-Lys. a)* **2***; b)* **2** *+ 0.25 eq. of N-Me-Lys; c)* **2** *+ 0.50 eq. of N-Me-Lys; d)* **2** *+ 0.75 eq. of N-Me-Lys; e)* **2** *+ 1.0 eq. of N-Me-Lys; f)* **2** *+ 1.25 eq. of N-Me-Lys; g)* **2** *+ 1.5 eq. of N-Me-Lys.*

ITC Titrations in Methanol

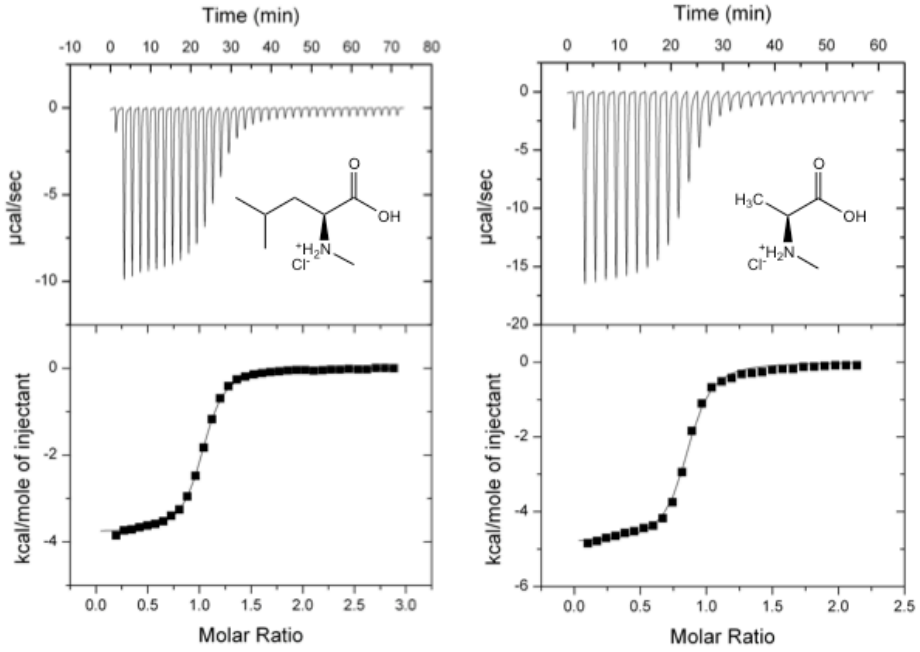

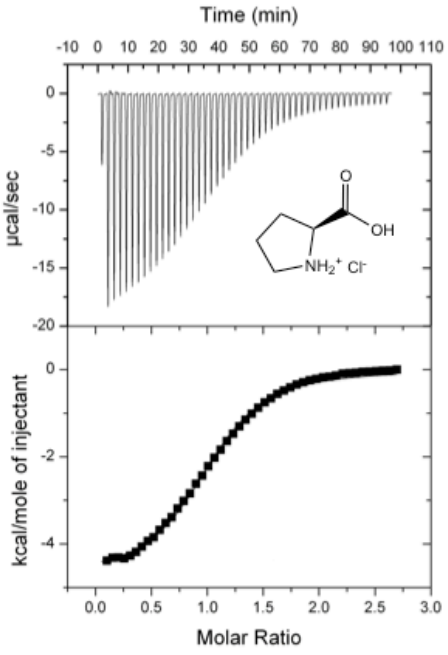
Time (min)
µcal/sec
kcal/mole of injectant
Molar Ratio
O
OH
NH2+ Cl-

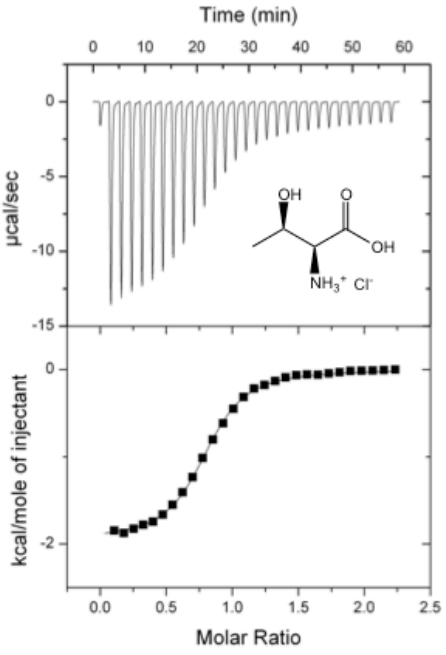
Time (min)
µcal/sec
kcal/mole of injectant
Molar Ratio
OH
O
OH
NH3+ Cl-

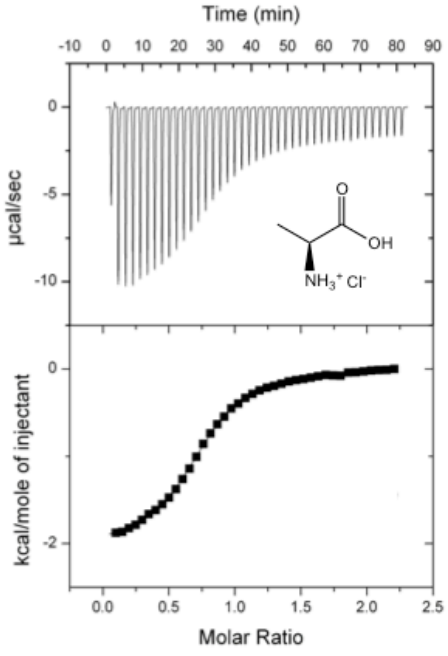
Time (min)
µcal/sec
kcal/mole of injectant
Molar Ratio
O
OH
NH3+ Cl-

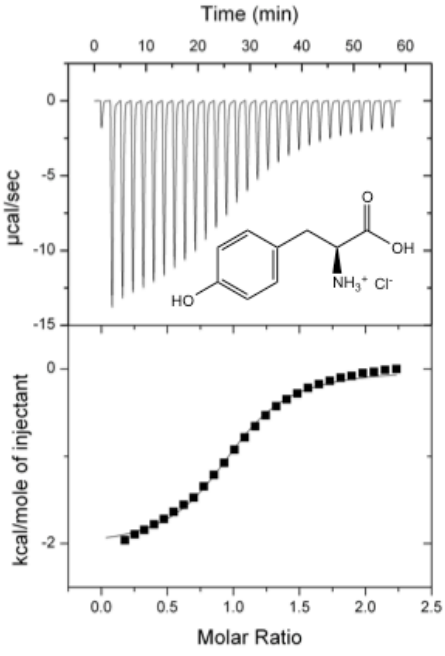
Time (min)
µcal/sec
kcal/mole of injectant
Molar Ratio
O
OH
HO
NH3+ Cl-

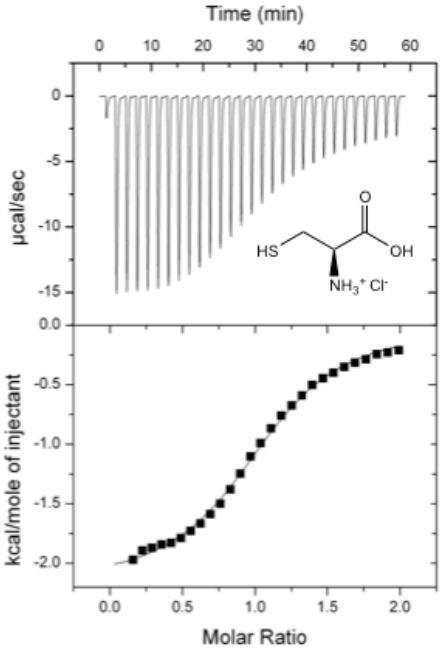

Figure 16 *ITC titrations (MeOH, 298 K) of* **2** *with seven amino acids (reported as inserts).*

The author

Born in Crema (Italy) on July 1st, 1988

July 2007	**High School Diploma** Liceo Scientifico "L. da Vinci" Crema, Italy
October 2010	**Bachelor in Industrial Chemistry** University of Parma, Italy Supervisor: Prof. E. Dalcanale
October 2012	**Master in Industrial Chemistry** University of Parma, Italy Supervisor: Prof. E. Dalcanale
January 2013-December 2015	**Doctoral Research** University of Parma, Italy Supervisor: Prof. E. Dalcanale
March 2015-August 2015	**Research exchange** Massachusetts Institute of Technology, Cambridge, MA, USA Supervisor: Prof. T. M. Swager